Critical load effects on bridges using heavy vehicle weigh-in-motion data

by
Tyron Ian Stap

This Thesis presented in fulfilment of the requirements for the degree of Master of Engineering in Civil Engineering in the Faculty of Engineering at Stellenbosch University

Supervisor: Prof Nico De Koker
Co-supervisor: Prof Roman Lenner

April 2022

Plagiaatverklaring / Plagiarism Declaration

1 Plagiaat is die oorneem en gebruik Van die idees, materiaal en, ander intellektuele eiendom Van, ander persone asof dit jou eie werk is.

Plagiarism is using ideas, material, and other intellectual property of another's work, and presenting it as my own.

2 Ek erken dat die pleeg Van plagiaat 'n strafbare oortreding is aangesien dit 'n vorm Van diefstal is.

I agree that plagiarism is a punishable offence because it constitutes theft.

3 Ek verstaan ook dat direkte vertalings plagiaat is.

I also understand, and that direct translations are plagiarism.

4 Dienooreenkomstig is alle aanhalings en bydraes Vanuit enige bron (ingesluit die internet) volledig verwys (erken). Ek erken dat die woordelikse aanhaal Van teks sonder aanhalingstekens (selfs al word die bron volledig erken) plagiaat is. *Accordingly, all quotations, and contributions from any source whatsoever (including the internet) have been cited fully. I underst, and that the reproduction of text without quotation marks (even when the source is cited) is plagiarism.*

5 Ek verklaar dat die werk in hierdie skryfstuk vervat, behalwe waar, anders aangedui, my eie oorspronklike werk is en dat ek dit nie Vantevore in die geheel, of gedeeltelik, ingeh, andig het om enige kwaifikasie te verwerf nie.

I declare that the work contained in this thesis/dissertation, except where otherwise stated, is my original work, and that I have not previously in its entirety, or in part, submitted this thesis/dissertation to obtain any qualification.

April 2022

Abstract

This study forms part of a set of research working towards updating South Africa's bridge design codes. According to literature, Weigh-In-Motion (WIM) data is commonly used to develop traffic load models. Using traffic load models in conjunction with statistical distribution families, the future critical load effects (LE) for a bridge are predicted for the design life, i.e., characteristic values. Previous authors have typically grouped vehicles within the WIM data set as "mixed-axle vehicle groups" while characteristic values are determined using the Extreme Value (EV) distribution family. However, it is argued that using a mixed-axle vehicle group violates the identically and independently distributed (iid) requirements of EV theory. The aim of this thesis is to determine whether the vehicle subsets from the data are in better agreement with the requirements of EV theory as opposed to the mixed-axle vehicle group.

In this study, three splitting levels were investigated to determine if the iid nature of the data sets would improve by sub-dividing the vehicles in the WIM data files. At the first level, no splitting took place, hence, the data sets on this level represented the mixed-axle vehicle groups commonly used in literature. At this point in the study, it was decided to limit the study to focus on normal traffic loading caused by single-vehicle events. On the second splitting level, the vehicles recorded in the WIM data files were separated into different groups based on the number of axles each group had. The groups on this level were referred to as the "sub-axle groups". The final splitting level involved grouping the vehicles into groups based on the geometry of the vehicles found within each sub-axle group. These groups were referred to as the "sub-categories of sub-axle groups".

The cause of the underlying distributions found in the previous level could be identified within each splitting level. By splitting the WIM data set more *iid* and non-*iid* data sets were introduced into the study. This led to an overall increase in the percentage of data sets with an underlying Fréchet distribution. Splitting had led to obtaining multiple vehicle subsets some of which were in better agreement with EV theory requirements than the mixed-axle vehicle group and while others were not. However, splitting had allowed for the identification of erroneous vehicle records which improved the *iid* nature of the mixed-axle vehicles data sets. In the end, splitting had resulted in the mixed-axle groups' data sets better adhering to the requirements of EV theory.

Overall, splitting the vehicle data sets allowed for a better understanding of the causes of the underlying distributions and improved the *iid* nature of the LE data sets for the mixed-axle group. However, splitting is not recommended for the sole purpose of predicting characteristic values for bridges. Instead, it is better suited for identifying potential erroneous vehicle records to allow additions to the filtration used during the cleaning of the WIM data file.

Opsomming

Hierdie studie vorm deel van 'n stel navorsing om Suid-Afrika se brugontwerpkodes te opdateer. Volgens literatuur word Weeg-In-Beweging (WIB) data algemeen gebruik om verkeerslasmodelle te ontwikkel. Deur gebruik te maak van verkeerslasmodelle in samewerking met statistiese verspreidingsfamilies, word die toekomstige kritieke laseffekte (LE) vir 'n brug vir die ontwerplewe voorspel, dit wil sê kenmerkende waardes. Vorige skrywers het gewoonlik voertuie binne die WIB-datastel as "gemengde-asvoertuiggroepe" gegroepeer, terwyl kenmerkende waardes bepaal word deur gebruik te maak van die Ekstreem Waarde (EW) verspreidingsfamilie. Daar word egter aangevoer dat die gebruik van 'n gemengde-as voertuiggroep die identies en onafhanklik verspreide (iov) vereistes van EW teorie oortree. Die doel van hierdie tesis is om te bepaal of die voertuigsubversamelings uit die data beter ooreenstem met die vereistes van EW-teorie in teenstelling met die gemengde-as voertuiggroep.

In hierdie studie is drie splitsingsvlakke ondersoek om te bepaal of die iov aard van die datastelle sal verbeter deur die voertuie in die WIB datalêers te onderverdeel. Op die eerste vlak het geen splitsing plaasgevind nie, dus het die datastelle op hierdie vlak die gemengde-as voertuiggroepe verteenwoordig wat algemeen in literatuur gebruik word. Op hierdie stadium van die studie is 'n besluit geneem om die studie te beperk om te fokus op normale verkeerslading wat veroorsaak word deur enkelvoertuiggebeure. Op die tweede splitsingsvlak is die voertuie wat in die WIB-datalêers aangeteken is, in verskillende groepe geskei gebaseer op die aantal asse wat elke groep gehad het. Die groepe op die vlak word verwys na as "sub-asgroepe". Die finale splitsingvlak het die voertuie gegropeer gebaseer op die geometrie van die voertuie wat binne elke sub-asgroep gevind word. Hierdie groepe bestaan bekend as die "subkategorieë van sub-asgroepe".

Die oorsaak van die onderliggende verdelings wat in die vorige vlak gevind is, kon binne elke splitsingsvlak geïdentifiseer word. Deur die WIM-datastel te verdeel, is meer iid- en nie-iid-datastelle in die studie ingebring. Dit het gelei tot 'n algehele toename in die persentasie datastelle met 'n onderliggende Fréchet-verspreiding. Splitsing het gelei tot die verkryging van veelvuldige voertuigsubstelle waarvan sommige beter ooreenstem met EV-teorievereistes as die gemengde-asvoertuiggroep en terwyl ander nie. Splitsing het egter voorsiening gemaak vir die identifikasie van foutiewe voertuigrekords wat die iid aard van die gemengde-asvoertuie se datastelle verbeter het. Op die ou end het splitsing daartoe gelei dat gemengde-as groepe se datastelle beter voldoen het aan die vereistes van EV teorie

Oor die algemeen het die verdeling van die voertuigdatastelle 'n beter begrip van die oorsake van die onderliggende verspreidings moontlik gemaak en die iid-aard van die LE-datastelle vir gemengde-asgroepe verbeter. Splitting word egter nie aanbeveel vir die uitsluitlike doel om kenmerkende waardes vir brûe te voorspel nie. In plaas daarvan is dit beter geskik om potensiële foutiewe voertuigrekords te identifiseer om toevoegings tot die filtrasie wat tydens die skoonmaak van die WIM-datalêer gebruik word, toe te laat.

Acknowledgements

I want to express my sincere gratitude to the following people:

- My supervisors Professor De Koker and Professor Lenner, thank you for your patience and guidance throughout this thesis.
- Dr Van der Spuy thank you for all the advice and assistance.
- My family thank you for always being there to provide support and motivation, especially my parents, thank you for always being there for me.
- My friends for all the memorable moments you have given me during my time in Stellenbosch, I will always treasure them.

Contents

List of figures

List of tables

Abbreviations

BM	Block Maxima
C1-4	Category 1-4
CDF	Cumulative Distribution Function
GPP	Gumbel Probability paper
GVM	Gross Vehicle Mass
iid	Independently and identically distributed
LE/s	Load Effect/s
LS	Least Square
MLE	Maximum Likelihood Estimation
PP	Probability Paper
PDF	Probability Density Function
POT	Peak Over Threshold
PWM	Probability of Weighted Moments
RMA	Restricted mixed axle
TT	Truck-Tractor
ULS	Ultimate Limit State
UMA	Unrestricted mixed axle
WIM	Weigh-in-Motion

List of Symbols

$F(x)$	Cumulative distribution function
$f(x)$	Probability density function
i	Index of an item in a list
L	Span length
n	Number of items in a data set
X	Random variable
x_i	i^{th} value in a list
x_L	The value below which left censoring takes place
x_U	The value above which right censoring takes place
γ	Euler constant
ω	Scale parameter
μ	Mean
σ	Standard deviation
θ	Location parameter
σ^2	Population variance
β	Shape parameter

1. Introduction

For centuries, bridges have been built to provide passage to traverse rugged terrain and avoid obstacles. Over time the design of bridging structures has been improved to allow for the construction of bridges with longer span lengths and the ability to support heavier loads. The Romans were the first true bridge engineers in history who had a profound influence on bridge-building technology. They discovered that timber structures, especially when submerged in water, were liable to decay or be damaged by fires or insects. To improve the life span of bridges, the Romans developed methods of treating the wood before using it and discovered alternative construction materials. As a result of the research done on volcanic clay found in the village of Puzzoli, the Romans discovered lime mortar and pozzolanic cement. They used this material to lay bricks and stones or create waterproof concrete (Bennet, 2008). With the discovery of cement, the Romans could construct bridges that would withstand the test of time. For instance, the oldest reliably dated bridge still used today, the Caravan bridge, was built close to 3000 years ago in 850 B.C by the Romans in Izmir, Turkey (Nagy, 2013).

Since the days of the Roman empire, the design of bridges has continuously improved to incorporate the heavier loads created with the development of the transportation industry. In addition, the creation of design codes and safety regulations for bridges ensured that these structures were safe and could withstand the loads applied to them without collapse (Bennet, 2008).

The design codes used for bridges incorporate three categories of loads. First, the loads applied to the structure that do not have significant daily variations are permanent loads. These loads include the self-weight of the bridge construction material, any superimposed dead load, the loads created due to the pre-stressing of the steel reinforcement and the creep and shrinkage of the Concrete. Second, loads involving the utilisation of a structure are variable loads. These mainly include traffic loads caused by vehicles, trains, people, or some combination of them. Finally, the third category refers to the temporary loads created due to the environmental factors generated in the bridges' area. These include loads generated by environmental pressure (earth, water, wind), earthquakes, settlement and temperature (Lenner, 2021).

In this study, the main bridge loads considered are those created by the variable loads' category. As the name implies, these temporary loads vary from day-to-day and bridge-to-bridge depending on the traffic experienced—for instance, a pedestrian bridge experiences much lower live loads than a bridge built to transport vehicles. Even with bridges designed to transport vehicles only, a wide range of different vehicles have to be responsible for the variable loads. For example, bridges located along with a country’s import and export routes experience much heavier traffic loads than most of the country’s bridges. Therefore, the bridge design codes should incorporate the appropriate load effects (LEs). Furthermore, these bridge design codes must be continuously updated with ever-changing traffic loads.

1.1. Background

Since 1981, South African Engineers have relied on the Technical Methods for Highways 7 (TMH-7) manual to design bridges. Unfortunately, these codes for bridge design have not been thoroughly updated since the year of its publication, even though the traffic load that these bridges experience have changed significantly. Thus, the TMH7 is considered outdated. Furthermore, the methods described in the TMH-7 are somewhat complex to apply, which further motivates the derivation of a new traffic load model for designing bridges in South Africa.

Van der Spuy (2019) set out to derive a new preliminary traffic load model aimed at designing bridges in South Africa. First, a bridge traffic loading analysis was performed to determine what LEs bridges in South Africa experienced. Then, using the information on different truck speeds, geometries, and loading patterns recorded in Weigh in Motion (WIM) files, convoys of vehicles were created and used to perform the bridge traffic loading analysis. From the analysis, the daily maxima LEs were determined and were used in conjunction with the Extreme Value (EV) distributions to predict the future critical LEs, a bridge in South Africa might encounter.

1.2. Problem statement and motivation

In the Van der Spuy (2019) study, the data set used consisted of multiple different types of trucks. The trucks within the data set ranged in length and the number of axles they had. From a glance at the WIM data files, multiple different sub-axle vehicle groups, which differed based on the number of axles, could be observed. This meant that the data set used in Van der Spuy (2019) was a mixed-axle vehicle data set. A requirement of using EV distributions to predict characteristic values is that the data in the sample data set must be independently and identically distributed (*iid*). Using a mixed-axle vehicle data set consisting of different vehicle types would mean using data with different probability distributions. Using the entire data set to make predictions violates the *iid* condition. Hence, Van der Spuy (2019) fitted the distribution to the tail of the data set instead, as the tail is be said to be more *iid* as it provides a better representation of the extreme LEs caused by the heaviest vehicles in the data set. Although the tail of data is more *iid* than the entire data set, it is still composed of different vehicle subsets.

1.3. Objectives

This study falls into a set of research working towards updating the South African bridge design codes. The study completed by Van der Spuy (2019) provides the backbone for the research done in this study. The bridge traffic loading analysis follows a similar approach to Van der Spuy (2019) in this study, except focusing on normal traffic loads. As stated in Section 1.2, even though the tail of the mixed-axle vehicle data set is considered more *iid* than the entire data set, it still contains different sub-axle vehicle groups. The main question and goal of this investigation is to determine whether the vehicle subsets from the data can be found

to better adhere to the requirements of EV theory. Accomplishing the primary goal of this thesis requires the following to be addressed:

1. Create a vehicle data set to represent the mixed-axle vehicle group
2. Determine the characteristic values and underlying distributions
3. Investigate the vehicle subsets within the mixed-axle vehicle group
4. Generate the LEs created by each sub-axle vehicle group
5. Predict the characteristic values for each sub-axle vehicle group
6. Compare the underlying distributions found for the mixed-axle vehicles to the sub-axle vehicle groups
7. Investigate if further splitting is required and can be done
8. After each split, compare the *iid* nature of the data sets

1.4. Basic assumptions

As is the nature of research, various constraints and limitations are encountered during this study. The limitations and constraints encountered in this investigation, as well as any assumptions made, are listed below:

- In this study, the vehicle data sets created were compared to the mixed-axle group used by Van der Spuy (2019). For a fair comparison, the WIM data had to come from the same WIM station. If the WIM data from another station were used, an entirely different data set would be obtained.

- Although the WIM data contains information on a vehicles' speed, there is no information on said vehicles' acceleration or deceleration afterwards. Therefore, with no acceleration values, the vehicles will need to be assumed to travel at a constant speed after they were recorded.

- Even though splitting the vehicles into the sub-axle groups might result in a data set that would contain similar vehicles, it does not mean that the data set would be *iid*. There is still a large amount of variation in sub-axle groups. For instance, even though each vehicle in a sub-axle group has the same number of axles, they have varying vehicle lengths and axle spacings. In addition, there are some sub-populations of vehicles that exist within the sub-axle groups as well. This variability makes it unlikely that the traffic loads will ever be completely *iid*. Regardless, a prediction must be made for data sets.

- Splitting the mixed-axle vehicle group reduces the size of the data sets analysed. However, if a data set is split too far, there may be too few data points to predict.

1.5. Thesis outline

Chapter 1: Introduction

In the first chapter, the topic of this study is introduced. First, background on the TMH-7 is provided. Then the work done to develop a new traffic load model for South Africa is discussed. After that, the problem statement, motivation and objectives of this study are mentioned and some basic assumptions for the study going forward.

Chapter 2: Background knowledge

This chapter provides background knowledge of the concepts and methods used in this study. First, a literature review is provided for previous traffic load modelling studies. After that, the relevant statistical theory and the methods to conduct the traffic load analysis is discussed.

Chapter 3: Methodology

In Chapter 3, the general methods followed to determine the characteristic values and underlying distributions for the different vehicle groups used in this study are shown. The methods covered include cleaning and calibrating the WIM data, creating a convoy of vehicles, and determining the bridge LEs. Lastly, the methods followed to determine the parameters required to perform statistical extrapolation are discussed.

Chapter 4: Mixed-axle vehicles

In chapter 4, a replica of the mixed-axle vehicle group used by Van der Spuy (2019) is created. Some restrictions for the mixed-axle vehicle group are then recommended. From there, a breakdown analysis of the vehicles responsible for the LEs is done, and motivation is provided for splitting the mixed-vehicle group into separate vehicle groups.

Chapter 5: Vehicle subsets

This chapter investigates the underlying distributions found for the sub-axle groups and the subsets of vehicles within the WIM data files. In addition, the extent to which the data sets fit the requirements of EV theory is discussed.

Chapter 6: Conclusion

Chapter 6 summarises the work and outcomes of this study. Some concluding remarks and recommendations for future research are also included in the chapter.

2. Background knowledge

2.1. Chapter introduction

In this chapter, the background knowledge required to understand better the content in this thesis is discussed. These discussions include the explanation of the key concepts and relevant information.

There are three main discussion topics in this chapter. This first topic involves a brief review of previous literature that focused on traffic loading analysis which provides the foundation for the investigation done in this study. The second discussion point is on the relevant statistical theory required to perform extrapolations and predict future critical LEs. Finally, the third discussion point is on the background knowledge required to perform a traffic loading analysis, which includes information on WIM traffic data, the LEs investigated and the categorisation of the different trucks seen on the roads of South Africa.

2.2. Traffic load modelling literature

It is common to find bridge design codes that have been developed using measured data and statistical extrapolations. For example, in O'Connor (2001), an outline of various design codes is given. The codes analysed included the United Kingdom bridge design codes, the Ontario Highway Bridge Design Code (OHBDC), the Canadian Highway Bridge Design Code (CHBDC), the American Association of State Highway and Transportation Officials (AASHTO) Standard Specification for American Highway Bridges and the Eurocode for bridge traffic loading, Eurocode 1: Part 3, Traffic Actions on Bridges. Each of these codes has been developed and calibrated by considering the LEs generated from the statistical analyses of the LEs created from the respective developed traffic models (Caprani, 2005).

Before WIM technology was developed, static weigh scales were used to estimate vehicle properties for traffic studies. However, the results obtained from these static weighing stations were considered biased (Caprani, 2005). With the introduction of WIM technology, engineers now had a method available to collect unbiased vehicle traffic, which allowed for creating more accurate traffic load models (Caprani, 2005; Van der Spuy, 2019).

The current bridge design code used in South Africa is the TMH7. In this design code, the variable loading due to traffic is separated into Normal Loading (NA), Abnormal Loading (NB) and Super Loading (NC). In Basson (2020), a performance reliability analysis was done for the TMH-7's traffic load model for normal traffic conditions, i.e. the NA loading. The study checked the reliability of a bridge designed according to the NA loading conditions against actual traffic loading recorded in WIM data. In one of the two case studies investigated in the thesis, the NA loading generally performed well for typical highway bridges, especially for the longer span lengths of 30 m to 50 m. However, a poor reliability performance was found for short narrow span bridges, especially for span lengths of 5 m and 10 m.

In the Road Traffic Act, 1996 (Act No 93 of 1996), the single axle unit limits for South Africa was increased from 8.2 t to 9 t and an overall loading limit of 56 t was introduced. This change had a significant impact on axle loading in the country. This motivated the need for a new traffic load model, and with the availability of WIM technology, it became possible to create a more accurate traffic load model (Lenner, De Wet and Viljoen, 2017; Van der Spuy, 2019).

In Van der Spuy (2019), WIM data from 2010 to 2016 was acquired from the local Roosboom WIM station to derive a new preliminary traffic load model. In the study, the acquired WIM data was used to create vehicle convoys which were iterated across a theoretical bridge to determine the hogging moments, sagging moments and shear forces experienced by the bridge. A censored GEV distribution containing the upper $2\sqrt{N}$, was fitted to the LE data sets, and the characteristic values were predicted for a 5% probability of exceedance in a 50-year reference period, similar to the Eurocode and South African building design codes. The values predicted in Van der Spuy (2019) were recorded in Table 2.1. In general, the new model developed by Van der Spuy (2019) exceeded the NA and NB loading in TMH-7 at the characteristic and Ultimate Limit State (ULS) levels.

Table 2.1 Roosboom characteristic load effects obtained from Table 8 in Van der Spuy (2019)

Span Length [m]	Hog [kNm]	Sag [kNm]	Shear [kN]
5	250	401	336
10	841	1 269	485
15	1 779	2 034	566
20	2 490	3 315	722
25	3 160	4 729	819
30	3 178	6 121	890
35	3 907	7 808	976
40	4 547	9 461	1 045
45	5 557	11 459	1 130
50	6 749	13 061	1 151

2.3. Statistical analysis

Statistical analysis plays a vital role in the development of traffic load models. Statistical analysis helps draw conclusions from large quantities of data and allows for predicting future critical LEs.

This section provides information on the probability distributions commonly used for traffic load analyses and the methods used to estimate their required parameters. The methods generally used to predict the future critical LEs that a bridge can be exposed to is then discussed.

2.3.1. Probability distributions

In the statistical analysis used to develop traffic load models, probability distributions are used to display the probabilities of the LEs recorded occurring. The probability distributions commonly used are the Gaussian/normal distribution (Nowak, 1993; Sivakumar, Ghosn and Moses, 2008; Soriano, Casas and Ghosn, 2017; Anitori, Casas and Ghosn, 2018), the log-normal distributions (Basson, 2020), the Weibull distribution (O'Connor, 2001; O'Connor, Caprani and Belay, 2002; O'Brien and Enright, 2011), the Gumbel distribution (O'Connor, Caprani and Belay, 2002; Caprani, 2005; Caprani and O'Brien, 2010; Soriano, Casas and Ghosn, 2017) and the GEV distributions (Caprani, 2005; Caprani and O'Brien, 2010; O'Brien and Enright, 2011; Zhou, 2013; O'Brien *et al.*, 2015; Van der Spuy, 2019).

The Weibull, Gumbel and the GEV distributions form part of the same family of distributions, the EV family distributions. The use of EV distributions for the predictions of LEs has become the more common distribution in recent years, according to Caprani and O'Brien (2010).

Extreme Value (EV) distributions

The EV distributions are used to predict extreme minima and maxima values of random variables. Three types of EV distributions are used for extrapolation, namely the Type 1 EV, Type 2 EV, and Type 3 EV, known as the Gumbel, the Fréchet, and the Weibull distribution, respectively (Allen, Singh and Powell, 2011).

Type I EV – Gumbel distribution

The first type of EV distribution is known as the Gumbel distribution. Two versions of the Gumbel distribution exist; one is used to predict extreme minimum values while the other is used to predict extreme maxima values. Due to the nature of this study, only the maxima version is essential. Thus, the minima version will not be discussed further. The Probability Density Function (PDF) and the Cumulative Distribution Function (CDF) of the Gumbel distribution are defined using two parameters: the scale parameter (ω) and the location parameter (θ). The PDF and CDF can be determined using the Equations $(2.1)$and (2.2) respectively (Castillo et al., 2005).

$$f(x) = \frac{1}{\omega}\exp\left(\frac{x-\theta}{\omega} - \exp\left(\frac{x-\theta}{\omega}\right)\right) \qquad (2.1)$$

$$F(x) = \exp\left(-\exp\left(\frac{x-\theta}{\omega}\right)\right) \quad (2.2)$$

Population mean:

$$\mu = \theta - \gamma\omega \quad (2.3)$$

Population Variance:

$$\sigma^2 = \frac{1}{6}\pi^2\omega^2 \quad (2.4)$$

Where:

γ Euler constant with a value of approximately 0.57722

Type II EV – Fréchet distribution

The second type of EV distribution is known as the Fréchet distribution. The PDF and CDF of the Fréchet distribution are defined using the three parameters: the scale parameter (ω), the location parameter (θ), and the shape parameter (β). The PDF and CDF can be determined using the Equations (2.5) and (2.6). (Castillo *et al.*, 2005).

$$f(x) = \frac{\beta\omega}{(\theta-x)^2}\left(\frac{\omega}{x-\theta}\right)^{\beta-1} e^{-\left(\frac{\omega}{x-\theta}\right)^{\beta}} \quad (2.5)$$

$$F(x) = e^{-\left(\frac{x-\theta}{\omega}\right)^{\beta}} \quad (2.6)$$

Population mean:

$$\mu = \theta - \omega\Gamma\left(1-\frac{1}{\beta}\right), \qquad for\ \beta > 1 \quad (2.7)$$

Population variance:

$$\sigma^2 = \omega^2\left[\Gamma\left(1-\frac{2}{\beta}\right) - \Gamma^2\left(1-\frac{1}{\beta}\right)\right], \qquad for\ \beta > 2 \quad (2.8)$$

Where:

$\Gamma(y)$ Gamma function evaluated at y

The tail of a Fréchet distribution has an unbounded nature, which can lead to non-plausible predictions. Due to its unbounded nature, Fréchet distributions are considered unsuitable for traffic load modelling (OBrien et al., 2015).

Type III EV – Weibull distribution

The third type of EV distribution is known as the Weibull distribution. The Weibull distribution has a bounded nature and is defined using the three parameters: the scale parameter (ω), the location parameter (θ) and the shape parameter (β). The PDF and CDF can be determined using Equations (2.9)and (2.10) respectively (Castillo et al., 2005).

$$f(x) = \frac{\beta}{\omega}\left(\frac{x-\theta}{\omega}\right)^{\beta-1} \exp\left(-\left(\frac{x-\theta}{\omega}\right)^{\beta}\right), \qquad x < \theta \tag{2.9}$$

$$F(x) = 1 - \exp\left(-\left(\frac{x-\theta}{\omega}\right)^{\beta}\right), \qquad x \leq \theta \tag{2.10}$$

Population mean:

$$\mu = \omega\Gamma\left(1+\frac{1}{\beta}\right) \tag{2.11}$$

Population variance:

$$\sigma^2 = \omega^2\left[\Gamma\left(1-\frac{2}{\beta}\right) - \Gamma^2\left(1-\frac{1}{\beta}\right)\right] \tag{2.12}$$

According to EV theory, the Weibull distribution has a finite upper bound (Coles, 2001). This makes the Weibull distribution well suited for traffic load modelling. Furthermore, it provides a realistic prediction since traffic loads are considered to have a finite upper bound. In practice, there is a limited number of vehicles that can fit on a bridge at once. In addition, trucks are limited to how much weight they can carry before a mechanical failure occurs (Bailey and Hirt, 1996; O'Connor, Caprani and Belay, 2002; O'Brien *et al.*, 2015).

Generalized Extreme Value distribution

In the early applications of EV theory, one of the three distributions had to be chosen and used to estimate the relevant parameters. However, in more recent studies, the Generalized Extreme Value (GEV) distribution, which combines the three types of EV distribution, is preferred to be used as it does not require a predetermined choice (Coles, 2001).

Like the EV distributions, the GEV distribution is described using a scale parameter, a location parameter and a shape parameter. For this study, the symbols ω, θ and β are used in the GEV scale, location and shape parameters, respectively.

For the GEV distribution, the shape parameter found will decide which EV distribution the data fits. The EV distribution used is Gumbel for ($\beta = 0$), Fréchet for ($\beta > 0$) and Weibull for ($\beta < 0$). In some publications, the sign of the shape parameter is switched in the GEV formula. In these publications, the distribution fits Gumbel for ($\beta = 0$), Fréchet for ($\beta < 0$) and Weibull for ($\beta > 0$) (Castillo *et al.*, 2005).

$$g(x) = \begin{cases} \frac{1}{\omega}[1+\beta\left(\frac{\mathrm{x}-\theta}{\omega}\right)]^{1-1/\beta}\exp\left[-\left[1+\beta\left(\frac{\mathrm{x}-\theta}{\omega}\right)\right]^{-\frac{1}{\beta}}\right], & \beta \neq 0 \\ \frac{1}{\omega}\exp\left(\frac{\mathrm{x}-\theta}{\omega}\right)\exp\left\{-\exp\left(\frac{\mathrm{x}-\theta}{\omega}\right)\right\}, & \beta = 0 \end{cases} \quad (2.13)$$

$$G(x) = \begin{cases} exp\left\{-\left[1+\beta\left(\frac{\mathrm{x}-\theta}{\omega}\right)^{-\frac{1}{\beta}}\right]\right\}, & \beta \neq 0 \\ \exp\left\{-\exp\left(\frac{\mathrm{x}-\theta}{\omega}\right)\right\}, & \beta = 0 \end{cases} \quad (2.14)$$

Independently and identically distributed requirement

A prior requirement to using the Extreme value theory is that the random variables must be independently and identically distributed (*iid*). For the independently distributed condition to be met, each random variable in the data set needs to have the same probability distribution and no connection to each other. Thus, no overall trends can exist in the data set (Castillo *et al.*, 2005; Caprani and O'Brien, 2010; Messervey, Frangopol and Casciati, 2011; Zhou, 2013).

There are plenty of pitfalls that can lead to a violation of the iid condition. One of these pitfalls relating specifically to analysing the LEs generated by the vehicles in the data set is when multiple vehicles are on the bridge simultaneously, i.e., a multi-vehicle event. The distribution of these multi-vehicle events would differ from single-vehicle events, and therefore cannot be compared to each other. Another example would be that sub-populations of vehicles could exist for single-vehicle events, which means that different distributions can exist for even the single-vehicle events.

Tail fitting

For studies on extreme traffic loading, it is common to censor the LE data sets to isolate the more critical values caused by the heavier vehicles. In addition, by censoring the data sets, a better representation of the extreme LEs is obtained, thus improving the *iid* nature of the data set.

In general, either the data sets' lower or upper tail is censored, otherwise referred to as left-censoring and right censoring, respectively. The number of data points removed during the censoring depends on the censoring done. In Phien & Fang (1989), the two types of censoring used are described. The first censoring type, type I, is defined as censoring above or below some known data point in the data set, where the total values removed is a random variable. The second type of censoring, type II, refers to when the total values removed is known, but the data point above or below which the censoring takes place is a random variable. Both types of censoring can be used to perform either single (left-censoring or right-censoring) or double censoring (left-censoring and right-censoring).

Consider a random sample with *N* values available. Before any censoring occurs, the random variable *x* in the sample has fallen into the range $-\infty < x < \infty$. If the data set is censored to the left, then *x* falls into the range

of $x_L < x < \infty$, where x_L is the lowest value in the censored sample. If the data set is censored to the right, then *x* falls into the range of $-\infty < x < x_U$, where x_U is the value right of which censoring takes place. Where the number of values removed from the left of x_L and from the right of x_L are *m* and *k*, respectively. In the case of double censoring, *x* falls into the range of $x_L < x < x_U$ and the censored sample size (*n*) is determined by $n = N - m - k$.

The exact length of the tail (*n*) of data varies from study to study. Some of the different tail lengths investigated include the upper 30% used by Enright (2010), the upper 5% used by Anitori, Casas and Ghosn (2018) and the upper $2\sqrt{n}$, where n being the number of datapoints of values in the data set suggested by Castillo (1988).

There are two commonly used tail fitting techniques used for traffic load modelling. These two methods are known as Peaks-Over-Threshold (POT) method and the Block Maxima (BM) method (O'Brien *et al.*, 2015).

Block Maxima method

The block maxima (BM) method involves selecting the maximum LEs from equal-size, non-overlapping block periods. The size of these block periods varies based on the period selected, i.e., daily maxima, weekly maxima. Once the size of the block period has been decided upon, a distribution can then be fitted to either the entire set of BM LEs or to the right tail of BM and extrapolated to obtain the maximum LEs for a specific return period. The decision of block size is depended on what block size can represent the extreme LEs or not. Thus, the size of the block is critical. If the block size is too small, it results in a data set that contains less critical LEs, which leads to a lower extrapolated result. Conversely, if the block size is too large, the data set may be too small, and valuable data points describing critical LEs may be left out (O'Brien et al., 2015). An illustration of the BM method is shown in Figure 2.1

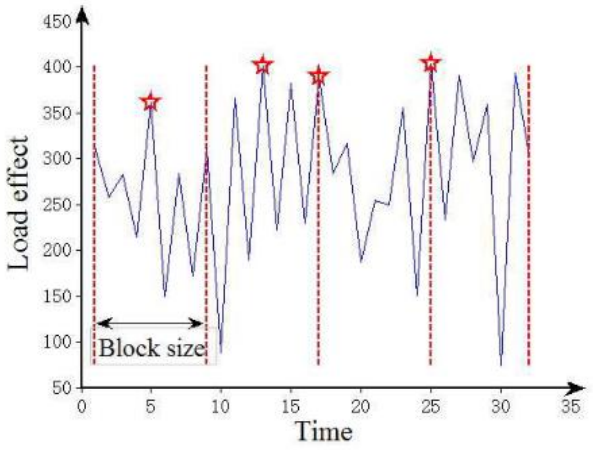

Figure 2.1 Illustration of the BM method shown in Zhou (2013)

Peak Over Threshold method

The POT method involves choosing a threshold point above which the data is fitted to a generalized Pareto distribution (GPD). The disadvantage of this method is that it is difficult to determine the threshold point to be used. If the threshold chosen is too low, too many non-critical extreme events may be included, resulting in an

incorrect prediction. On the other hand, if the threshold is too high, the data set predicted will contain too few data points, which will result in high variance and unreliable predictions (O'Brien et al., 2015). An illustration of the POT method is shown in Figure 2.2 Illustration of the POT method shown in Zhou (2013)Figure 2.2

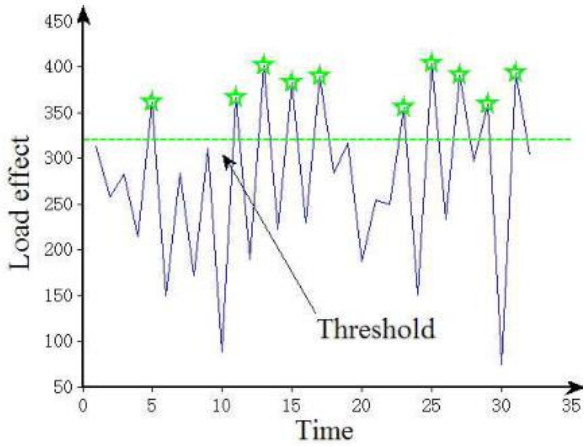

Figure 2.2 Illustration of the POT method shown in Zhou (2013)

Probability paper

An initial assumption as to what distribution a data set would potentially fit needs to be made to perform a prediction. After assuming a distribution type, a graphical check can be performed to see if the data fits the assumed distribution using probability paper (PP). This graphical check method involves plotting the assumed distributions CDF on probability paper after a linear transformation. The linear transformation scales the CDF so that if the correct distribution is chosen, the resulting plot will yield a straight line instead of an S-curve (Snell, Montgomery and Runger, 1995; Nowak and Collins, 2000).

To create the probability plots, the data is rearranged into ascending order then the empirical probability of each data is determined with Equation (2.15), where *i* represents the index of the variable in the ordered data set and *n* represents the number of data points in the complete data set.

$$\hat{G}(x_i) = \frac{i}{n+i} \tag{2.15}$$

The ordinate drawn because of the scaling of a distribution CDF is referred to as the Standard Extremal Variate (SEV). The SEV values are determined using Equation (2.16)

$$SEV(z) = -\ln[-\ln(G(z))] \tag{2.16}$$

Where:

z The value obtained because of an experiment, i.e., the event or LE in this case

$G(z)$ Probability function

In extreme value statistics, a Gumbel probability paper (GPP) is often used. The SEV values for the GPP plot are determined using the CDF for the GEV distribution in conjunction with Equation (2.16). The Gumbel

distribution is plotted as a straight line by scaling the GEV distribution, hence the name GPP (Bissell, Ang and Tang, 1979). By inspecting the tail resulting plot, it can be seen as to which type of EV the data set fits. Figure 2.3 shows a clear distinction between the tail behaviours of the Fréchet, Gumbel and Weibull distributions.

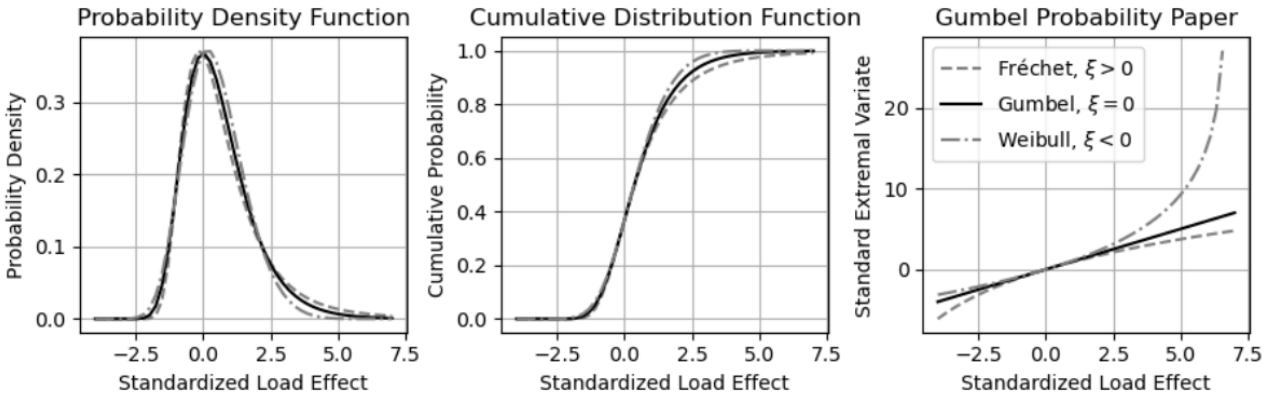

Figure 2.3 PDF, CDF, and probability paper plot for the GEV distribution (Caprani and Lenner, no date)

2.3.2. Parameter estimation methods

In the theory of large samples, the parameters (mean, standard deviation, shape) for the sample are assumed to be reasonable estimates of the parameters that belong to the population. There are several methods to use to estimate the parameters of the population from the sample, such as the method of least squares (LS), the probability of weighted moments (PWN) and maximum likelihood estimation (MLE) (Phien and Fang, 1989; Kendall and Stuart, 2010). Of these parameter estimation methods, the MLE method is preferred in literature (Coles, 2001).

MLE method

The general statistics problem encountered in probability theory is described by probability density *f (x; θ)*, which allows for information to be gleaned about the distribution of a model given a known parameter (*θ*). However, if the goal is to determine the value of *θ* given a known distribution, it would be represented by *f (θ; x).* This is known as an 'inverse probability problem'(King, 1998).

The MLE method, developed by R. A. Fisher (1912), allows for the estimation of the parameter *θ,* which maximizes the likelihood equation (L), shown in Equation (2.17), if each value each value x_i is independent. The log-likelihood equation (*l*), shown in (2.18), is generally used instead as it is simpler to work with (Söderbom *et al.*, 2014).

$$L(\hat{\theta}) = \prod_{i=1}^{n} f(x_i|\hat{\theta}) \tag{2.17}$$

$$l(\hat{\theta}) = \ln L(\hat{\theta}) = \sum_{i=1}^{n} \ln f(x_i|\hat{\theta}) \tag{2.18}$$

Where:

$\hat{\theta}$ The parameter the maximizes $L(\hat{\theta})$ and $l(\hat{\theta})$

The likelihood equation is shown in Equation (2.17) can be considered as the general likelihood equation. Equations (2.19) and (2.20) respectively, describe the likelihood and log-likelihood equations for the uncensored GEV distribution (Caprani, 2005).

$$L(\hat{\theta}, \hat{\omega}, \hat{\beta}) = \prod_{i=1}^{n} f(x_i|\hat{\theta}, \hat{\omega}, \hat{\beta}) \tag{2.19}$$

$$l(\hat{\theta}, \hat{\omega}, \hat{\beta}|x_i) = -n \ln \hat{\omega} \ - \left(1 - \frac{1}{\hat{\beta}}\right) \sum_{i=1}^{n} f(x_i|\hat{\theta}, \hat{\omega}, \hat{\beta}) - \sum_{i=1}^{n} f(x_i|\hat{\theta}, \hat{\omega}, \hat{\beta})^{\frac{1}{\hat{\beta}}} \tag{2.20}$$

In Phien and Fang (1989), equations (2.21) and (2.22) respectively describe the likelihood and log-likelihood equation for the censored GEV distribution

$$L(\hat{\theta}, \hat{\omega}, \hat{\beta}) = \left[\int_{-\infty}^{x_L} f(x_i|\hat{\theta}, \hat{\omega}, \hat{\beta}) dx\right]^m \times \prod_{i=1}^{n} f(x_i|\hat{\theta}, \hat{\omega}, \hat{\beta}) \ \times \left[\int_{x_u}^{\infty} f(x_i|\hat{\theta}, \hat{\omega}, \hat{\beta}) dx\right]^k \tag{2.21}$$

$$l = \ln(N!) - \ln(k!) - \ln(m!) + m \ln F(x_L|\hat{\theta}, \hat{\omega}, \hat{\beta}) + \sum_{i=1}^{n} \ln f(x_i|\hat{\theta}, \hat{\omega}, \hat{\beta}) + k \ln\left[1 - F(\ln(x_U|\hat{\theta}, \hat{\omega}, \hat{\beta}))\right] \tag{2.22}$$

Where:

N The number of data points in the complete data set

n The number of data points in the censored data set, $n = N - m - k$

m The number of data points removed from below the tail

k The number of data points removed from the top of the tail of the data set

x_L The lowest value in the tail of the data below which left censoring is applied

x_U The highest value in the tail of the data above which right censoring is applied

$F(x)$ The CDF for the standard GEV distribution

$f(x)$ The PDF for the standard GEV distribution

2.3.3. Statistical Extrapolation

Statistical extrapolation is needed to predict extreme traffic LEs for a specified return period. Statistical extrapolation involves fitting a probability distribution to either a whole data set of LEs or only the upper portion. The fitted data is then extrapolated, and a characteristic load effect corresponding to a specified return period is obtained.

2.3.3.1. Probability of exceedance and return period

In statistics, the return period, otherwise known as the reoccurrence interval, is used to describe the time between repeat occurrences of events of similar intensity. The relationship between an events' return period, and its' probability of exceedance in one period, can be represented by Equation (2.23).

$$R(z) = \frac{1}{p} \tag{2.23}$$

Where:

p The probability that an event of similar magnitude is obtained or exceeded.

Return periods are used in many industries as a means of expressing extremely low probabilities of exceedance comprehensively. In the engineering code of practices, the design of structures uses the return period to represent the probability of exceedance for a LE that the structure might experience during its design life (T). The relationship between the return period, design life and probability of exceedance is represented by Equation (2.24) (Ang and Tang 1975).

$$R(z) = \frac{1}{1-(1-p)^{\frac{1}{T}}} \approx \frac{T}{p} \tag{2.24}$$

2.4. Traffic load analysis

This section gives some background information on WIM technology and its uses in traffic load modelling. Firstly, a breakdown of a WIM data structure used in South Africa is shown, and methods of cleaning and calibrating the WIM data to remove errors is discussed. Furthermore, in this section, the relevant LEs commonly determined during a traffic load analysis are discussed. The final discussion point in this section relates to classifying the different types of heavy vehicles seen on the road.

2.4.1. Weigh-in-Motion data

2.4.1.1. What is WIM data

Weigh-in-Motion (WIM) technology allows for an undetected measurement of information about the heavy vehicles that are travelling along a road. WIM technology is practical for traffic load modelling studies because it allows for the data collection on heavy-vehicle characteristics such as axle loads, axle spacings, and the number of axles while the vehicle is still in motion. Furthermore, the fact that the WIM sensors are usually undetected by the drivers is considered helpful as it allows for the recordings of overloaded trucks whose drivers would have purposefully avoided a weigh station (Enright, 2010; Jacob and Feypell-de La Bemaumell, 2010; O'Brien *et al.*, 2015; Soriano, Casas and Ghosn, 2017; Anitori, Casas and Ghosn, 2018).

Depending on the application and information required, various sensors or devices may be combined into a WIM system, allowing for the recording of further relevant vehicle parameters. For instance, by including a camera it becomes possible to collect images of the vehicles, including those that are overloaded. Independent of the sensing technology used, various methods of vehicle data recording are available. Two commonly used methods of data recording are known as low-speed and high-speed WIM (van Loo and Žnidarič, 2019).

For low-speed WIM, the weighing is done in a dedicated controlled area which is usually outside of the main traffic lane. An advantage of low-speed WIM is the elimination of the dynamic effects of vehicles by limiting the velocity of the passing vehicles to between 5 to 15 km/h. This ensures that the tyre impact forces obtained closely resemble static wheel loads. The low-speed WIM sensors are reported by Jacob & Feypell-de La Bemaumell (2010) to have an accuracy of 3% to 5% when measuring data related to the axle units.

In contrast to low-speed WIM, High-Speed WIM allows for measurements at normal traffic speeds. This makes the measurements more vulnerable to dynamic effects (Jacob and Feypell-de La Bemaumell, 2010). In general, a good high-speed WIM system will have an inaccuracy of ±5 to ±10% for GVM measurements recorded on a smooth roadway. The accuracy of a high-speed WIM system depends on factors such as the evenness of the road surface, the trucks suspension performance and even the truck drivers driving behaviour (van Loo and Žnidarič, 2019).

2.4.1.2. Location of South Africa's WIM data stations

In South Africa, there is a surplus of WIM data available for traffic studies. South Africa has reportedly 100 WIM sensors installed alongside its National and Provincial roads, according to De Wet (2010). Figure 2.4, obtained from Van der Spuy (2019), shows the location of the different WIM sensors that can be found locally.

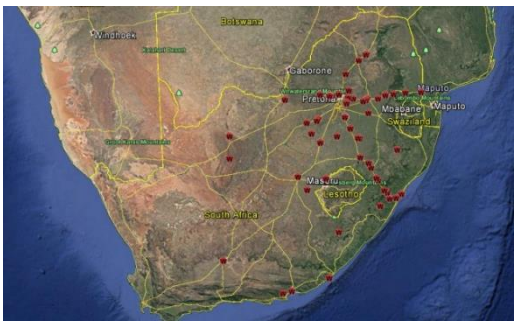

Figure 2.4 WIM sensors installed across South Africa (Van der Spuy, 2019, figure 26)

2.4.1.3. WIM data structure

The vehicle characteristics recorded using the WIM sensors are stored as a string of numbers. Each number in the string represents a different characteristic of the truck. Unfortunately, every manufacturer responsible for constructing the various traffic loggers available in South Africa had a unique output format, making it challenging to compare traffic data from different traffic loggers. Therefore, a national standard data format was created to solve this problem. The most recent South African standard data format (RSA3) was defined in COTO (2019). However, data obtained before the release of the RSA3 format, follow older versions such as the RSA2 data formats specified in SANRAL (2006). There are serval Vehicle Data formats in SANRAL (2006) which differ depending on the truck characteristics measurements taken. For example, in Table 2.2, a breakdown description of the string of numbers representing one vehicle that passed the WIM sensor at Roosboom station in 2018 was recorded. The string of numbers was stored according to the Vehicle data record 13 format, which recorded information on an individual vehicle's axle mass and spacings.

Table 2.2 Breakdown description of a heavy vehicle recorded at Roosboom WIM station

Code	Description	Code	Description
13	Vehicle Data Record ID code	13	Vehicle Class Code I
0	Edit Code	3	Vehicle Class Code II
180101	Departure Date (YYMMDD)	6	Number of Axles
3355930	Departure Time (hhmmsscc)	61	Weight on Axle 1 (100xkg)
4	Logical Lane Number	329	Axle Spacing 1 (cm)
4	Physical Lane Number	65	Weight on Axle 2 (100xkg)
1	Direction Code	136	Axle Spacing 2 (cm)
82	Speed (km/hr)	62	Weight on Axle 3 (100xkg)
1620	Length (cm)	718	Axle Spacing 3 (cm)
999	Bumper-to-1st Axle spacing	79	Weight on Axle 4 (100xkg)
1	Chassis Height Code	138	Axle Spacing 4 (cm)
0	Tag Code	64	Weight on Axle 5 (100xkg)
1	Following Vehicle Code	133	Axle Spacing 5 (cm)
0	Failure Code	50	Weight on Axle 6 (100xkg)

2.4.1.4. Cleaning of WIM data

Although WIM technology is helpful for civil engineering applications, the data recorded may contain gross errors that need to be addressed before it is used for any analysis. These errors are corrected by first cleaning the data set and then calibrating the values recorded. In Table 2.3, the cleaning criteria used to exclude vehicles from WIM data sets developed by O'Brien and Enright (2011), Sivakumar, Ghosn and Moses (2008), Zhou (2013) recorded as well as the data processing software used by Van der Spuy (2019) known as Golem. Of all the cleaning criteria, only Golem, developed by a South African transportation engineer known as M Slavik, was designed to be used locally. However, the derivation of it remains unpublished (Van der Spuy, 2019).

Table 2.3 Cleaning criteria used to exclude vehicles from a WIM data set

Criteria	O'Brien and Enright (2011)	Sivakumar, Ghosn and Moses (2008)	Zhou (2013)	Golem (not published)
Axle limit	Less than two	Less than three or more than 12	Less than two or more than eight	Less than two
Speed limit	Travelling less than 40 km/h or more than 120 km/h	Travelling less than 16 km/h or more than 160 km/h	Travelling less than 40 km/h or more than 120 km/h	Travelling less than 5 km/h or more than 150 km/h
Vehicle length limit	Wheelbase length of less than 1 m	Longer than 36 m	Longer than 30 m and GVM greater than 20 t	Shorter than 4 m or longer than 26 m
Individual axle spacing limit	Less than 0.4 m or greater than 20 m	First axle spacing less than 1.5 m or any axle spacings less than 1 m	-	Less than 0.53 m or more than 10 m
Sum of axle spacings check	Different wheelbase length to the sum of axles	The sum of axles spacings greater than vehicle length	The sum of axles spacings greater than vehicle length or less than 65% of the vehicle length	-
GVM limit	Less than 3.5 t	Less than 5.4 t	-	Less than 3.5 t
Individual axle mass	Greater than 40 t or greater than 15 t and responsible for more than 85% of the GVM	Less than 1 t or more than 32 t	Axle mass of 0.6 t or less or an axle mass responsible for more than 85% of the GVM	Greater than 16 t
Sum of axles check	Different GVM to the sum of their axles	The sum of axle masses differed from GVM by more than 10%	The sum of axle masses differed from GVM by more than 10%	
Axle inconsistence check	Inconsistent number of axles, axle spacing and axle masses	-	-	-
Steering axle masses	-	Less than 2.7 t or greater than 11.3 t	-	-
Lateral position	-	-	Lateral position outside of the notional lane	-

2.4.1.5. Calibrating of WIM data

Once the WIM data is cleaned, the next objective is to address the errors found in the data. Two errors can be found in the WIM data, the random error and the systematic error. The random error is caused due to intrinsic properties of the WIM, while the systematic error occurs because of the WIM system being improperly calibrated. Both errors can lead to inaccurate estimations being made.

In South Africa, a post-calibration method was developed by De Wet (2010) to suppress the systematic error. This method, known as the Truck Tractor (TT) method, has been approved by the South African National Road Authority (SANRAL) and included in the TMH-8. In the TT method, a portion of "eligible trucks" in the WIM data set was used to perform quality checks on collected WIM data. These eligible trucks referred to six and seven axle trucks with a single steering axle and double driving axle. These eligible trucks were used to generate a k-factor by comparing them to the target monthly average TT loads of 21.8 t. This k-factor could then be applied to adjust the axle weights of each vehicle in the WIM data set.

2.4.2. Determining the LEs

A truck can be viewed as a series of point loads placed one after the other in a line. In the WIM data files, the magnitude of these point loads is determined by the axle weights, while the axle-spacings determine the relative location of these point loads. Figure 2.5 shows an example of how a truck can be broken down into a series of point loads.

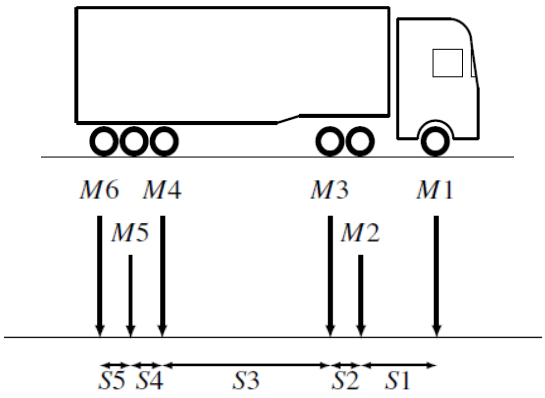

Figure 2.5: Point load representation of axle-masses and axle-spacings

To represent the truck moving across the bridge, these point loads can be incremented across a bridge slowly. After each increment, the different LEs experienced by the bridge can be calculated. By summing the LEs created by each point load on the bridge, the total LEs experienced by the bridge can be determined. Using the WIM data files, any LE can be investigated, though, for the purpose of this study, only the moments and shears are necessary, namely the hogging moments, sagging moments and the shear forces.

The first LE commonly investigated is known as the hogging moments. The maxima hogging moments are measured at the support between two spans. Figure 2.6 shows a visual representation of the axle point load being applied to a two-span bridge. Using Equations (2.25), and (2.26), the hogging moments can be calculated for when the point is in the first or second span length, respectively (Van der Spuy, 2019).

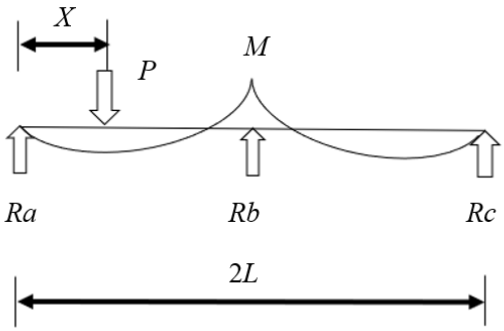

Figure 2.6 Resulting hogging moments for a two-span bridge

$$M = \frac{P(L^2 - x^2)x}{4L^2} \; for \; 0 < x < L \tag{2.25}$$

$$M = \frac{P(L^2 - (2L - x)^2)(2L - x)}{4L^2} \; for \; L < x < 2L \tag{2.26}$$

Where:

M	The hogging moments measured at support B
P	The applied point load P
L	The bridge span length
X	The distance along the span where P is applied
Ra, Rb, Rc	The reaction forces at supports A, B, and C

The second load effect determined is the sagging moment. The maximum sagging moments are recorded at the centre of a simply supported beam at its centre. Figure 2.7 shows a visual representation of the axle point load being applied to a single-span bridge. Using Equations (2.27), and (2.28), the sagging moments can be calculated for when the point is in the first or second half of the span length, respectively (Van der Spuy, 2019).

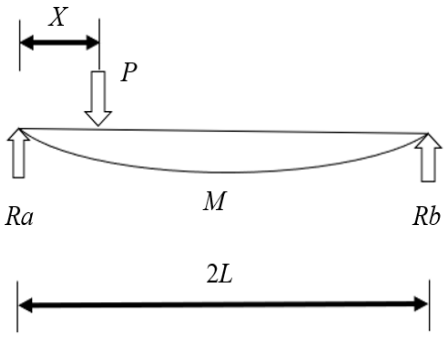

Figure 2.7 Resulting sagging moments for a single-span bridge

$$M = \frac{Px}{2} \; for \; x \leq \frac{L}{2} \tag{2.27}$$

$$M = -\frac{Px}{2} + \frac{PL}{2} \; for \; x > \frac{L}{2} \tag{2.28}$$

Where:

M The sagging moments measured at mid-span

The third load effect determined is the shear forces. Similarly, to the sagging moments, the shear forces are calculated for a single span between two supports. Figure 2.8 shows a visual representation of the axle point load being applied to a single-span bridge. Using Equation (2.29), the shear force can be calculated for when the point is in the first or second half of the span length.

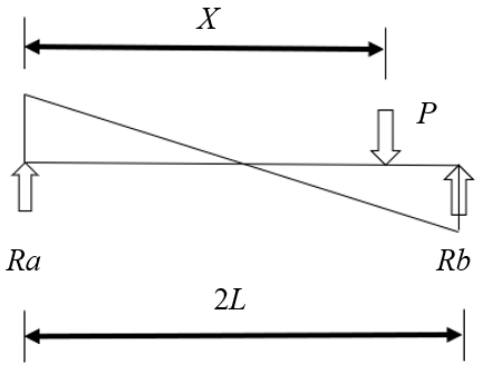

Figure 2.8 Resulting shear force for a single-span bridge

$$V = P(1 - \frac{x}{L}) \qquad (2.29)$$

Where:

V The shear force recorded

In literature, it is preferred to create a convoy of vehicles to determine the bridge LEs. A convoy allows for multiple vehicle events to be accounted for, which have been shown to occasionally produce higher LEs than single-vehicle events (Caprani, 2005). When creating a convoy, the appropriate spacings and gaps should be used to ensure that vehicles do not approach too close to each other. In literature, the principal terms used when referring to the spacings between two vehicles are the "gap" and "headway" terms. In C. C. Caprani (2005), the gap term refers to the distance between the rear axle of the leading vehicle and the front axle of the following vehicle, while the headway is defined as the gap distance plus the lead trucks length.

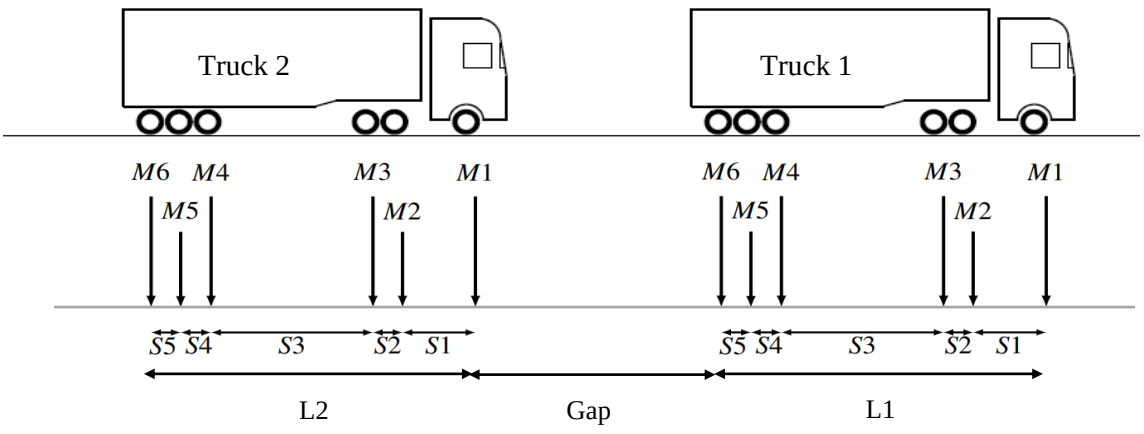

Figure 2.9 Example of trucks in a convoy

In literature, various gap lengths have been investigated. For example, in Nowak A.S. (1993), headway distances of 5 m to 30m were investigated, where five meters implies bumper to bumper traffic. In C. C. Caprani (2005), minimum gap distances of 5 m, 10m, 0.5s and 1.0s were investigated, while in O'Connor (2001), a minimum gap of 5 m was investigated.

Since a single vehicle can be regarded as a series of point loads and a convoy is just a series of vehicles, a convoy represents a series of point loads as well. This means that the same iterative process can be used to simulate the vehicles crossing over the bridge. Then after each iteration, the point loads on the bridge can be used to determine the total Hogging moments, sagging moments and Shear forces experienced by the bridge.

2.4.3. Truck type classification

In design codes, it is typical to split the traffic loads into separate classes. For instance, in the TMH-7, three different vehicle loading components are used to define different types of traffic, namely the NA loading for normal traffic, NB loading for abnormal traffic, and NC for super loading (CSRA, 1981).

In this study, only the normal traffic loads and the abnormal traffic loads are discussed. The main difference between these two categories is if a vehicle violates specific loads or dimension regulations given by a country's traffic regulation. In general, a vehicle that complies with the regulation falls into the normal traffic loading category, while a vehicle that violates the regulations falls into the abnormal traffic loading category and require a permit to travel. In South Africa, vehicles with a combination of abnormal masses or dimensions that does not comply with the National Road Traffic Regulations (NRTR) are classified as abnormal vehicles. Regulation 284 of the NRTR defines an abnormal or permit vehicle as: "Any vehicle which is operated under a written exemption granted in terms of Section 81 of the Act and any motor vehicle accompanying such abnormal vehicle as a condition for operation". Due to the abnormal loads or dimensions of permit vehicles, they fall outside of the geometrical and structural design criteria used for road infrastructure. These abnormalities result in additional risks to the safety of other road users or the damages caused to the road infrastructure (COTO, 2017). There are guidelines available for the granting of permits, such as the one given by DoT (2000).

Despite the GVM restriction, there are still vehicles found on the road which are heavier than 56 t. Some of which, violate the grace given before prosecution and some which do not. These vehicles are known as overloaded vehicles, and they do not carry permits. Since overloaded vehicles are non-permit carrying vehicles, they are part of NA loading.

The data provided in the WIM data file allows for both the normal and abnormal categories to be further classified according to the different features and dimensions are given for each vehicle. For instance, vehicles can be collected into separate groups according to the number of axles each vehicle has. Even these "sub-axle" groups can be further separated into different sub-categories based on the different combinations of axle-groups that a vehicle is made up of. The main axle groups are the single-axle, the tandem-axle and the tridem-axle, and the quad-axle groups. Most design specifications have their version of what classifies as a tandem,

tridem, and quad-axle group. The general definitions were found to classify the groups according to the number of equally spaced consecutive axles. The tandem axle group consists of two consecutively equal spaced axles. Tridem and quad-axle groups are composed of three and four consecutively equal spaced axles, respectively. The main difference between the axle group definitions used by different countries is the exact dimensions used.

- In the Motor vehicle Act Regulations for British Columbia, a tandem axle was defined as "two or more equally spaced consecutive axles, having an axle spread of not less than 1.0 m nor more than 1.85 m" (British Columbia, 1999).
- In Ireland, the Road Safety Authority defined a tandem axle as "two successive axles, not being part of a triaxle or a four-axle bogie, which are spaced at a distance apart of not more than 2.5 m". A tridem is defined as "three successive axles, not being part of a four-axle bogie, which are spaced at a distance apart of not more than 3.25 m". Finally, a four-axle bogie/quad-axle is "four successive axles the outermost of which are spaced at a distance apart of less than 4.3 m" (RSA., 2015).
- In New South Wales, a tandem axle group is defined as "a group of two or more axles in which the distance 'D' between centrelines of the outermost axles is at least 1 m, but not more than 2 m.". A tri-axle group/ tridem group is defined as "A group of three or more axles in which the distance 'D' between centrelines of the outermost axles is more than 2 m, but not more than 3.2 m". Finally, a quad-axle is defined as "A group of four axles in which the distance 'D' between centrelines of the outermost axles is more than 3.2 m, but not more than 4.9 m"(Transport for NSW, 2012).
- In the Motor Traffic Act of 1936 for Australia (2006), a "quad-axle group" was defined as a group of four axles with a distance of more than 3.2 m and less than 4.9 m between the centrelines of the outermost axles.

In South Africa, the same general definition is used to define the different axle groups, however, the legislation does not cater for quad-axle groups. Therefore, any axle group combinations that include a quad-axle group on South African roads are part of Abnormal vehicles and thus require a permit (DOT, 2000a). The dimensions used in South Africa to classify an axle group are given in COTO (2019), where it states that an axle forms part of an axle group when the spacing between any two axles fall within 200 cm to 250 cm of each other or less. This is an appropriate definition to use as it can be seen by the mean axle spacings for tandem and tridem axle groups in South Africa noted by Lenner et al. (2017) and Bosman (2004).

- In Lenner et al. (2017), a comparison was made between South African traffic data obtained from the Roosboom WIM station and the traffic data used to develop the Eurocodes load model. A mean axle spacing of 1.2 m was found in the study for the tandem axles and tridem axle groups recorded at the Roosboom station.
- In a study done by Bosman (2004), an investigation into the characteristics of South African heavy vehicles was done. The average axle spacings for the different heavy vehicle classes found in South

Africa were recorded in the study. In the study, the average axle spacings between the tandem axles and tridem axles ranged from 1.2 m to 1.4 m

In traffic loading analyses, the vehicle data sets are typically not split into separate vehicle groups. Instead, it is common for mixed-axle vehicle data sets to be used (Nowak, 1993; Caprani, 2005; Van der Spuy, 2019). In addition, distinctions are not always made between the normal and abnormal vehicles during these bridge loading analyses. The reason for this is that there is no way to prove that a vehicle does have a permit from the WIM data or is just travelling illegally without one (Enright, 2010; Van der Spuy, 2019).

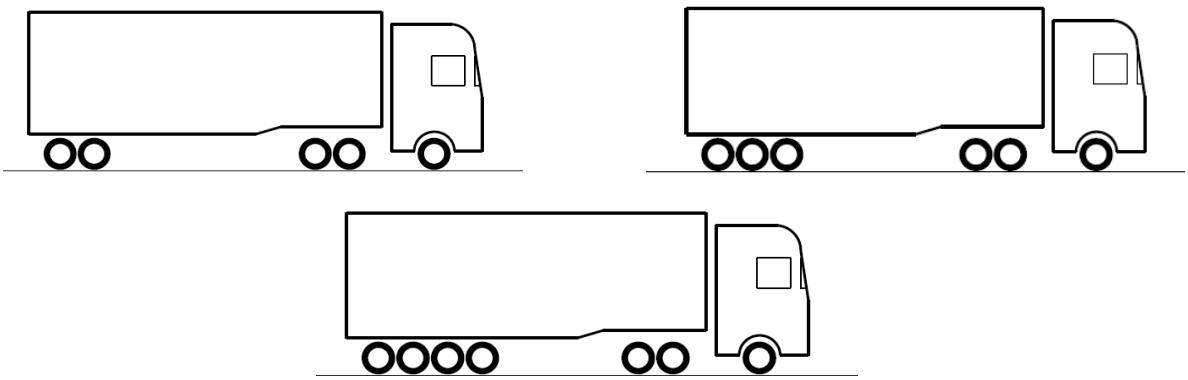

Figure 2.10 Examples of trucks with a tandem axle, tridem axle and a quad-axle group

3. Methodology

This section discusses the general steps followed for each of the vehicle groups created in this study. The methods discussed herein include the cleaning and calibration of the WIM data, the creation of a convoy of vehicles, determining the bridge LEs, the parameter estimation method used. Finally, the generation of GPP plots and the extrapolation to a characteristic return period to determine a characteristic value are also discussed.

The same variables used in Van der Spuy (2019) were used for this study unless otherwise stated. These variables include the span lengths, incrementation distance, tail length, bridge design life, and exceedance probability.

3.1. Raw data adjustment

In this study, the WIM data from the Roosboom WIM station located along the N3 between Johannesburg and Durban was used, as this was the same station that was used in Van der Spuy (2019). The Roosboom WIM station measures traffic travelling in both directions in the slow lanes along the N3. As combining two different lanes of traffic would violate the *iid* condition, only the slow lane travelling from Durban to Johannesburg was used in this study. This slow lane was chosen as it was said to have heavier vehicles than those travelling in the other slow lane from Johannesburg to Durban (Van der Spuy, 2019).

After removing the vehicles in the WIM data file from the other slow lane, the next step was to clean and calibrate the data to remove the gross and systematic errors from the data set. The gross errors were removed using Golem's rejection criteria described in Section 2.4.1.4, as the cleaning criteria used in Golem was created specifically for South African WIM data. In addition to the filters provided by Golem, two additional filters were investigated to clean the WIM data.

The first additional filter was a check to see if the wheelbase length was greater than the vehicle length. In the check, vehicles were removed if the sum of axles was greater than the vehicle length. The reason for this check was that in SANRAL (2006), the vehicle length value recorded in the WIM data files was said to be inaccurate as the magnetic influence of the vehicles was used to determine vehicle length value. Although it was not explicitly stated this filter was included in the Java program used to perform the bridge loading analysis in Van der Spuy (2019).

The second additional filter used was a failure code filter. This filter was included to remove any vehicle that had a none zero failure code value. Although SANRAL (2006), did not explicitly state that any vehicle with a none zero failure code value should be removed, it did state this in COTO (2019). This filter was not included in Van der Spuy (2019).

The WIM data was then calibrated to remove the systematic errors using the TT method described in Section 2.4.1.5 as SANRAL had approved this method. Both methods were used by Van der Spuy (2019), except the

sum of axle spacing check, to remove the gross and systematic errors as well, which further motivated their use in this study.

3.2. Vehicle convoys and load effect determination

After obtaining the "cleaned WIM data file", the heavy vehicles recorded were grouped into a convoy of vehicles described in section 2.4.2. As mentioned in section 2.4.2, since one vehicle represented a series of point loads and the convoy was a series of vehicles, it also represented a series of point loads. The magnitude of these point loads was determined by the axle masses *M1, M2…Mn,* multiplied by the gravitational acceleration ($g = 9.81$). The coordinates of the point loads were determined by the axle-spacings *S1, S2…Sn* and the gaps between each vehicle. The WIM data provided the axle masses and spacings, so all that needed to be determined was the gap between each heavy vehicle.

Since there was no data recorded on the acceleration or deceleration of the vehicle, the speed was assumed constant when calculating the gap between vehicles. The gap was determined using either Equation (3.1) . This equation consisted of two parts. The first part of Equation (3.1) determined the distance between the front axle of the leading vehicle (Truck 1 in Figure 2.9) and the front axle of the following vehicle (Truck 2 in Figure 2.9) based on the leading vehicle's speed and the time gap between the two vehicles. This distance was otherwise referred to as the headway distance. The second part of Equation (3.1) removed the length of the leading vehicle to ensure that the gap between the vehicles was the measured distance between the rear axle of the leading vehicle to the front axle of the following vehicle.

$$Gap = \frac{v_1(t_2 - t_1)}{3.6} - L_1 \tag{3.1}$$

Where:

$\frac{v_1(t_2-t_1)}{3.6}$ Distance-based on vehicle speed and time gap

v_1 Speed of the leading vehicle in km/h

t_1 The time that the leading vehicle leaves the WIM station in seconds

t_2 The time that the following vehicle leaves the WIM station in seconds

L_1 The length of the leading vehicle in meters

Once the convoy had been created, the analysis of the bridge traffic loads began. The point loads were then shifted forward by a constant incrementation distance, determined by the distance covered by a vehicle travelling at 80km/h in 0.02 seconds. (i.e., 0.44m). Although various travelling speeds were recorded for the different vehicles within the convoy, the same incrementation distance was used for each vehicle to ensure that the gaps remained constant. With a constant incrementation distance, less computing power was required for the programme. Furthermore, it was assumed that there would be enough variability in the spacings already, removing the need for relative vehicle movement.

The incrementation process was repeated until the entire convoy had crossed over the theoretical bridges specified span length. Then, the axle loads on the bridge were used at each incrementation point to determine the LEs using the Equations in Sections 2.4.2. An example of the analytical method used to determine the Sagging moments for a bridge with a span length of 30 m is shown in Figure 3.1 and Table 3.1.

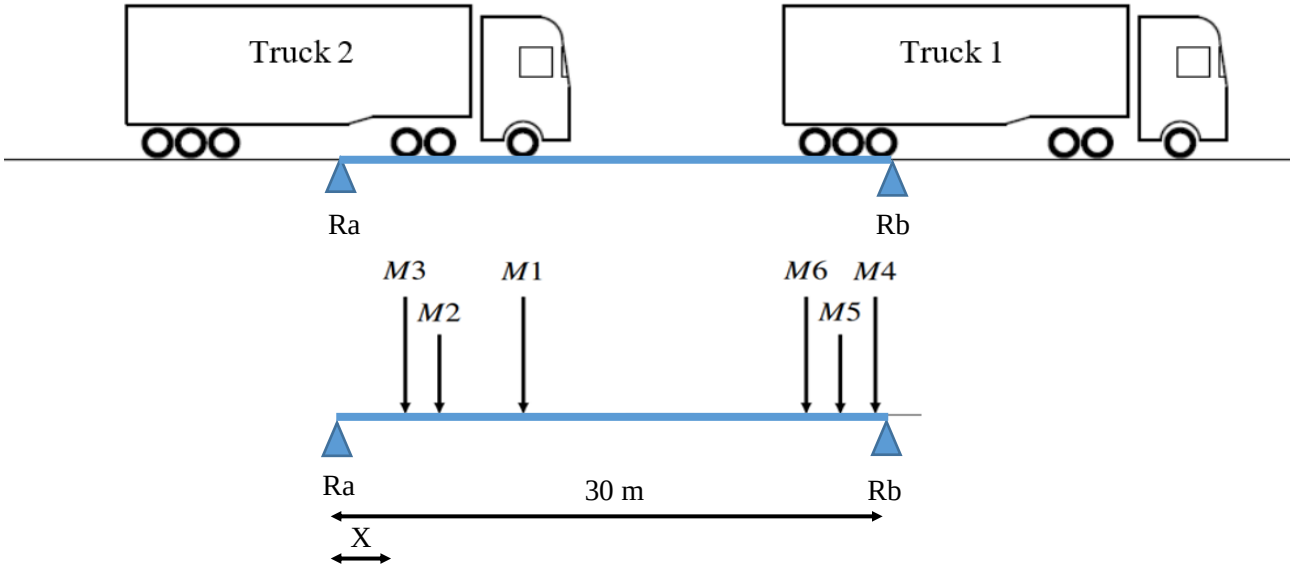

Figure 3.1 Example of axle-loads on a single-span bridge

Table 3.1 Example of the sagging moments determined for two trucks on a 30m span

	Truck 1			Truck 2		
	Axle 4	Axle 5	Axle 6	Axle 1	Axle 2	Axle 3
Axle-masses [t]	10.7	11.7	12.1	6.5	11.4	11.5
Axle-weights [kN]	104.8	115.1	118.9	64.2	112.3	113.3
Axle-coordinates [m]	29.6	28.2	26.9	7.5	4.4	3.0
Sagging moments [kNm]	23.0	101.9	184.3	239.2	246.3	168.5
Total sagging moments [kNm]	963.3					

3.3. Distribution type and parameter prediction

In this study, the EV family of distribution was used to fit the data as it has been the preferred distribution used by various authors for traffic loading analysis (C. C. Caprani, 2005; Colin Caprani & O'Brien, 2010; Enright, 2010; O'Brien et al., 2015; O'Brien & Enright, 2011; Zhou, 2013). The GEV distribution was chosen as it does not require a predetermined choice between the three types of EV distributions (Caprani, 2005).

As discussed in Section 2.3.1, fitting the distribution solely to the tail of the data is considered the standard practise as it ensures that the more critical populations are analysed. In this study, a tail length of $2\sqrt{n}$ is used where *n* represents the number of daily maxima LEs recorded. For ease of reference, the data set which contains these upper $2\sqrt{n}$ values is otherwise referred to as the censored data set, while the complete data set is

otherwise referred to as the uncensored data set. Once the uncensored and censored data sets are obtained, the next objective is to determine the parameters required to use the GEV CDF equation shown in Equation (2.14).

It was decided to use the MLE parameter estimation method over the PWM method as the PWM method was found to produce unreasonable results when working with a censored sample by Phien & Fang (1989). An R-script was used to solve the log-likelihood equation for the censored GEV shown in Equation (2.22) was used to determine the location, scale, and shape parameters. As the upper values in the tail were important critical LEs, only left censoring was used, i.e., $k = 0$.

A set of initial starting parameters was required for the MLE method to start estimating the required parameters. When working with a censored data set, it was recommended to use the MLE estimates obtained for the uncensored data set as the starting parameters for the censored data set by Phien & Fang (1989). However, this meant that the MLE method had to be used to solve the parameters for the uncensored data set first, which meant that the uncensored data set had to be given a set of starting parameters first. For the uncensored data set, the starting location was set to the mean of the uncensored data set. The starting scale was set to the standard deviation of the uncensored data set, and the starting shape was set to -0.05, which was found to be a good starting position through trial and error. These parameter estimates were then used to estimate the parameters for the censored data set.

3.4. GPP plotting and characteristic value prediction

After obtaining the parameters for the censored and uncensored data sets, the next step is to plot these LEs on a GPP plot. The LEs are rearranged into ascending order then the empirical probability of each LE is determined with Equation (2.15).

Once the empirical probabilities for the LEs have been obtained, they are used to determine the GPP plotting coordinates of each data point using Equation (2.16). Now that the GPP plotting coordinates have been acquired, the next step is to determine the return period for a bridge with a 50-year design life and a 5% probability of exceedance. The return period is calculated with Equation (2.24) and is determined to be 975 years. As heavy vehicles in South Africa are allowed to travel every day in a year, the probability of non-exceedance (p) is calculated for 365 days a year for 975 years, as shown in Equation (3.3).

$$p = 1 - \frac{1}{975 \times 365} = 0.999997 \tag{3.2}$$

After obtaining the return period, the censored data set is plotted out by determining the GPP coordinates using the GEV CDF Equation (2.14) and the SEV Equation (2.24). The censored data set is then extrapolated to the return periods SEV value and using Equation (3.3), the characteristic LEs are determined.

$$x = \begin{cases} \theta + \frac{\omega}{\beta} * \left[\frac{1}{\log\left(\frac{1}{G(x)}\right)^{\beta}} - 1 \right], & \beta \in (-0.5; 0.5), \quad \beta \neq 0 \\ \theta + \omega * \log\left(\frac{1}{\log\left(\frac{1}{G(x)}\right)} \right), & \beta = 0 \end{cases} \tag{3.3}$$

An example of the sagging moment GPP plot for a Mixed-axle vehicle group is shown in Figure 3.2. The y-coordinates are the SEV values, while the x-coordinates are the LEs. From an inspection of the tail, it is seen that the plot has an underlying Weibull distribution as the tail curves to the left. The x-coordinate at the intersection between the censored fit and return period lines represents the characteristic sagging moments for a span length of 5 m. As can be seen in Figure 3.2, the characteristic sagging moments is just over 400 kNm.

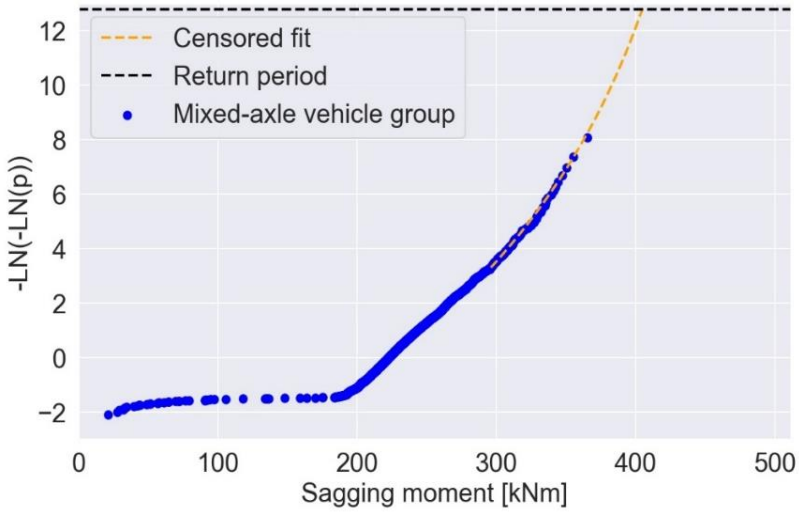

Figure 3.2 Sagging moments GPP plot for the mixed-axle vehicle group at a span of 5 m

4. Mixed-axle vehicle groups

4.1. Chapter introduction

Chapter 3 provided the general methodology used to perform a bridge loading analysis. This chapter focuses on using the methods described in chapter 3 to create a mixed-axle vehicle group to show that it can violate the *iid* condition of EV theory.

In this chapter, using the methods described in chapter 3, the WIM data is cleaned and calibrated. Then, using the cleaned WIM data, an imitation of the mixed-axle vehicle group used in Van der Spuy (2019) is created. Finally, a bridge traffic loading analysis is performed using the mixed-axle vehicle group from which the LEs experienced by the different span lengths is obtained.

After analysing the vehicles responsible for the LEs generated by this imitation group, two restrictions are recommended. These restrictions result in the formation of three new mixed-axle groups. First, a bridge traffic loading analysis is performed using all three from which their respective LEs and characteristic values are determined. From there, a breakdown analysis is performed for the imitation group and one of the three new mixed axle groups to reveal the different sub-populations of vehicles that form each mixed-axle group. Lastly, the underlying distributions found for each mixed-axle vehicle group are discussed, and motivation is provided for splitting the vehicle data sets into different sub-populations to improve the *iid* nature of the data sets.

4.2. Cleaning of raw WIM data

At the beginning of the Van der Spuy (2019) study, only the WIM data from 2010 to 2016 were available for analysis. These WIM files measured over 12.5 million vehicles within them. However, at the beginning of this study, the WIM data for 2017 and 2018 were also obtained. These two years of WIM data added around four million more vehicles into the sample size. Even though this led to more LEs, this was assumed not to be a problem. In O'Brien et al. (2015), more data was said to improve the accuracy of predictions made but does not eliminate the uncertainty associated with extrapolations.

There were 16 517 997 trucks recorded within the nine years of WIM data files from Roosboom station. Of the 16.5 million trucks, 54% of them were in the slow lane travelling from Johannesburg to Durban, which as mentioned in Section 3.1 was not the slow lane this study focused on; hence these vehicles were removed from the WIM data file. This left a total of 7 568 549 vehicles that required cleaning still.

Table 4.1 records the number of heavy vehicles found in the WIM data before and after applying the Golem cleaning criteria. As a result of the cleaning criteria specified by Golem, a total of 354 253 vehicles were removed.

Table 4.1 Number of vehicles recorded in the WIM data before and after applying Golem's cleaning criteria

Year	Total number	After cleaning
2010	755 237	722 663
2011	949 793	917 654
2012	800 213	764 602
2013	783 606	744 919
2014	861 054	816 918
2015	877 233	845 453
2016	859 896	826 042
2017	818 972	736 604
2018	862 545	829 441
Total:	7 568 549	7 204 296

Figure 4.1 records the percentage of the vehicles in the WIM data file that met the different cleaning criteria. As was seen, most vehicles removed during the cleaning were because of the axle limit. This meant that over 73% of the vehicles had either less than two axles or more than nine axles. The GVM limit was responsible for removing the second-highest number of vehicles with more than 16% of the vehicles having a GVM of less than 3.5 t.

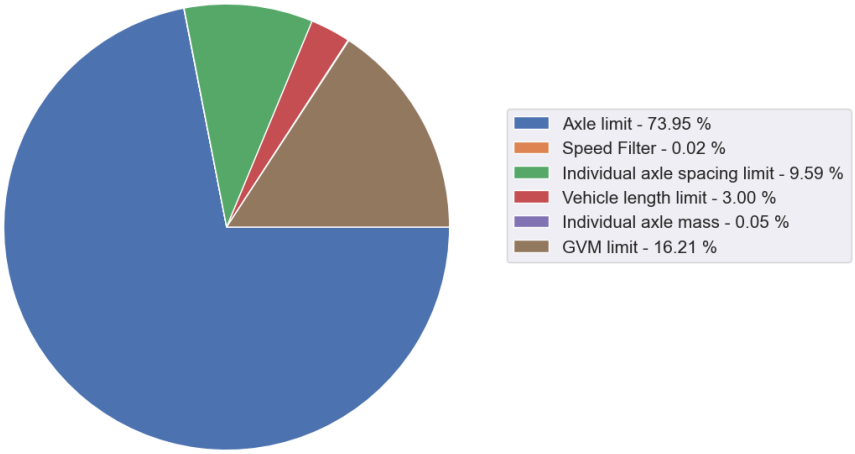

Figure 4.1 Percentage of WIM data which met the different Golem cleaning criteria

If the first additional filter discussed in Section 3.1 was included, then a further 84 372 vehicles would be removed. This meant that these vehicles had a greater wheelbase length than the vehicle length specified in the WIM file. This would leave 7 119 924 vehicles.

If the second additional filter discussed in Section 3.1 was included, then a further 623 573 vehicles would be removed. This meant that these vehicles all had a non-zero failure code. As this filter was not included in Van der Spuy (2019), it was decided to exclude this filter. This was done because the initial intent for the Chapter 4 was to attempt to imitate the data set used in Van der Spuy (2019).

After the cleaning, the TT method was used to address the systematic error within the WIM data. After cleaning and calibrating the WIM data, the traffic load modelling analysis could begin.

4.3. Vehicle convoys and load effect determination

Using the cleaned WIM data file, the vehicles were grouped into a convoy, with the gap between each vehicle being determined using Equation (3.1). This resulted in a mixed-axle vehicles group which was then iterated across the theoretical bridge as described in section 3.2 to determine the LEs for the span lengths of 5 m to 50m in span increments of 5 m.

The distribution of the mixed-axle vehicle groups' GVMs, vehicle lengths and the hogging moments for a span length of 20 m was shown in Figure 4.2. Similar figures were recorded for each LE at each span length in Figure A.1, Figure A.2 and Figure A.3 in Appendix A.

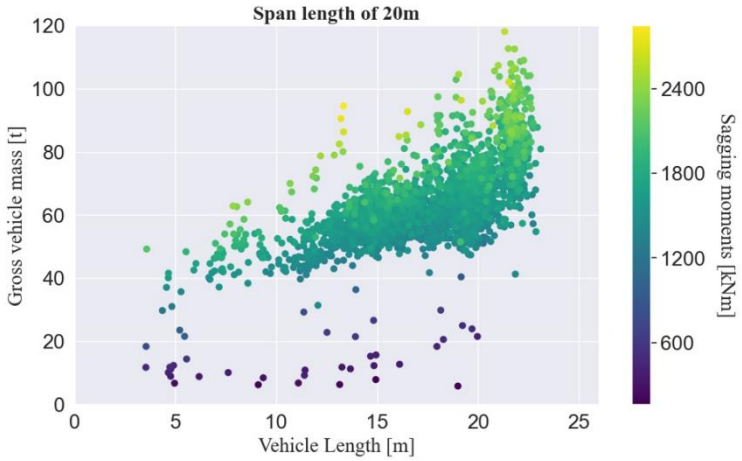

Figure 4.2 Distribution of mixed-axle groups GVM, vehicle length and sagging moments at 20 m

4.4. Characteristic values

The methods described in Sections 3.3 and 3.4 were used to determine the parameters for the censored GEV distribution. The statistical extrapolation was then performed to predict the characteristic values depicted in Table 4.2. The highlighted values represent the data set distributions for which the MLE method estimated a positive shape factor. This means that these data sets had an underlying Fréchet distribution and had an unbounded nature. Since this went against the theory that traffic should have a physical bound, the shape factor for these distributions was limited to zero. The characteristic values were then predicted using the Gumbel distribution to obtain more plausible LEs, which was the same procedure Van der Spuy (2019) followed when an underlying Fréchet distribution was obtained.

Table 4.2 Characteristic values obtained from result replication attempt

Span length [m]	Hog [kNm]	Sag [kNm]	Shear [kN]
5	262	405	344
10	868	1 281	481
15	1 825	1 960	541
20	2 451	3 441	759
25	2 927	4 948	807
30	3 306	6 298	881
35	4 060	7 902	972
40	4 858	9 299	1 041
45	5 764	11 012	1 107
50	6 868	12 900	1 149

In Figure 4.3, the characteristic values in Table 4.2 and Table 2.1 were drawn. As was seen by the two plots, the characteristic values obtained by the imitation group were similar to those obtained by Van der Spuy (2019) at each span. Although a slight difference of less than 7% was noticed, it was assumed to be within an acceptable range. The most probable cause for the difference was the two additional years of WIM data.

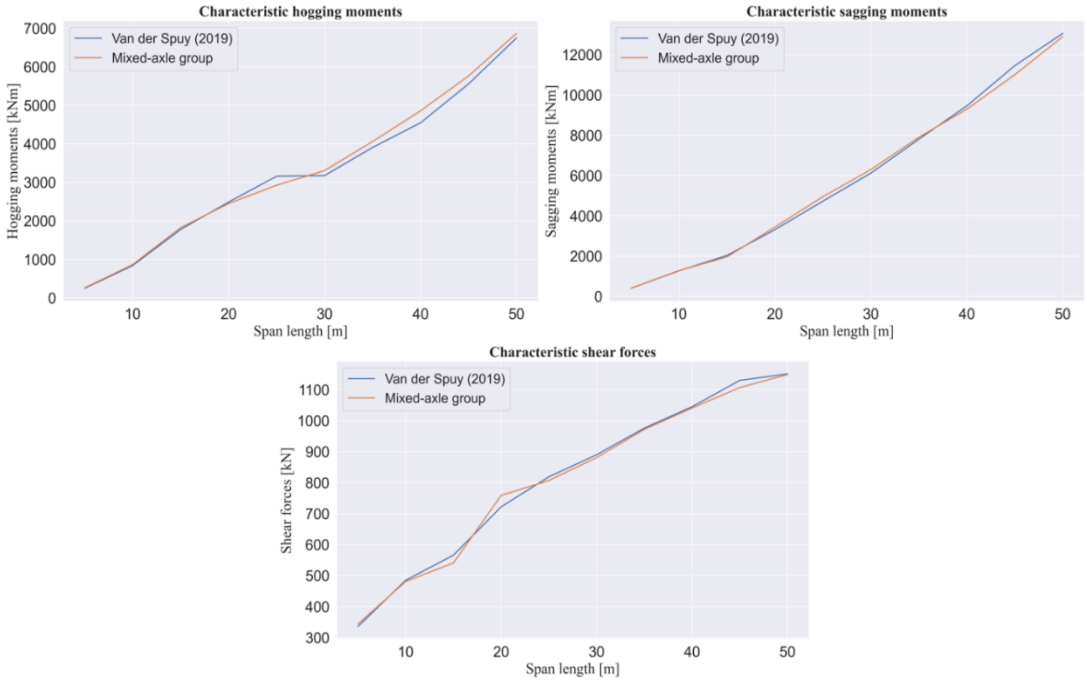

Figure 4.3 Characteristic values predicted by Van der Spuy (2019) and the mixed-axle vehicle group

4.5. Vehicles responsible for highest LEs

During the analysis of LEs created by the mixed-axle vehicle group, two types of extremities were noticed. The first extremity was related to the heavily overloaded vehicles noticed in the dataset, while the second extremity was related to the gaps found between vehicles. These two extremities were directly related to the LEs recorded in the tail of the data set.

4.5.1. Overloaded vehicles

In Figure 4.2, the GVMs of the vehicles in the mixed-axle vehicle groups at 20 m is recorded. Even though the legal limit for GVM in South Africa is 56 t, the majority of the vehicles responsible for the daily maximums LEs were observed to have GVMs greater than this (Lenner, 2021). Some of the vehicles were even more than double the legal limit. As was seen in the figure, the heavier vehicles tended to produce some of the highest LEs experienced by the bridge. A similar situation was seen for each span for each LE in Figure A.1, Figure A.2 and Figure A.3.

In Table 4.3, the axle masses and axle spacings for the vehicle with the highest GVM of 118 t. As can be seen, by the axle spacings, this vehicle would be classified as a quad-axle vehicle according to the axle group definition given in COTO (2019). As mentioned in Section 2.4.3, South African legislation does not cater for quad-axle groups, hence this vehicle would be regarded as an abnormal vehicle and would require a permit.

Table 4.3 Axle masses and spacings for the heaviest vehicle recorded in the data set

Index	Axle masses [t]	Axle spacing [m]
1	7.7	3.1
2	15.3	1.3
3	15.7	2.2
4	13.9	1.4
5	13.6	9.2
6	13.0	1.3
7	13.0	1.4
8	12.6	1.4
9	13.0	-

The percentage of vehicles that contained a quad-axle group or above in the censored LE data sets were quantified and represented in Figure 4.4. Most of the vehicles responsible for the sagging moments and shear forces at each span contained a quad-axle group or above. The hogging moments, however, only recorded large numbers of these vehicles up until span lengths of 25 m. Meaning the quad-axle vehicles dominated the tail of the sagging moments and shear forces for at each span but only dominated the tail of the hogging moments up to span lengths of 25 m.

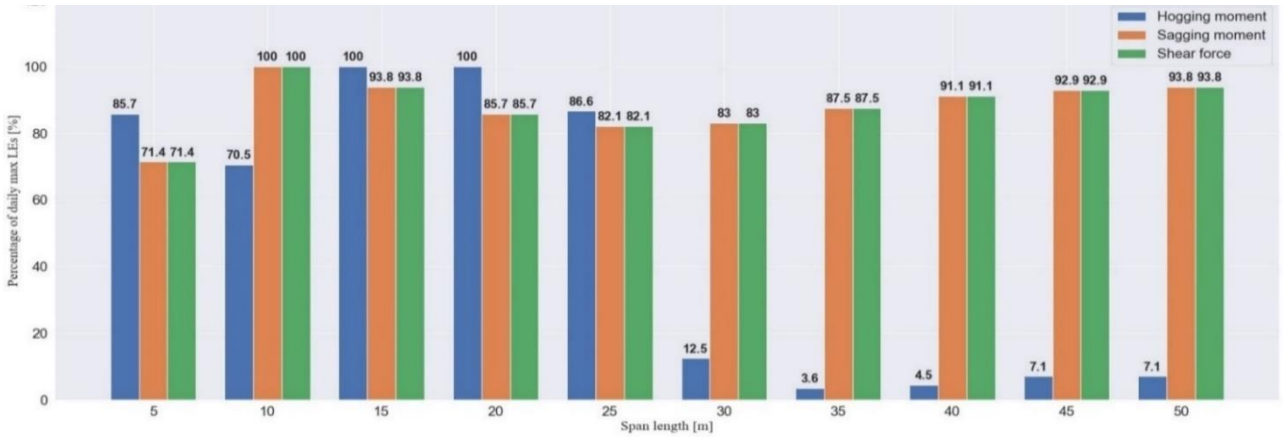

Figure 4.4 Percentage of censored LEs caused by a vehicle with a quad-axle group or above

4.5.2. Gaps between vehicles in the convoy

During the steps followed to replicate the characteristic values obtained by Van der Spuy (2019), an oversight was noticed in the gap calculation method in Equation (3.1). This method did not include a limiting gap size between the vehicles. From Figure 4.5, it was seen that the lack of a limiting gap size led to two vehicles on the bridge simultaneously, at the shortest span length investigated. For the sagging moments and shear forces at the 5 m span, 0.1% of the daily maxima LEs were caused by multiple vehicles on the bridge simultaneously, i.e., multi-vehicle events. Therefore, a multi-vehicle event on a span of 5 m meant that the gap between these vehicles was less than 5 m. Furthermore, the gap between vehicles was based on the axle to axle spacings and did not account for the overhang distance in the WIM data file, as it was said to be inaccurate by SANRAL (2006). Therefore, it was considered unlikely that vehicles should be closer than 5 m even in bumper-to-bumper traffic.

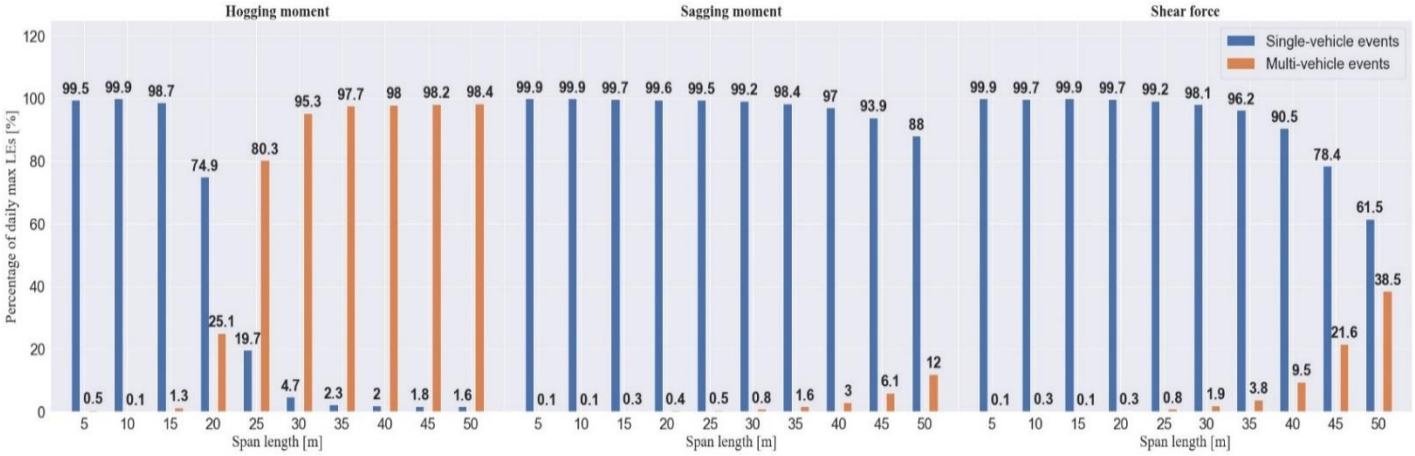

Figure 4.5 Percentage of censored LEs caused by single and multi-vehicle events

From an analysis of the gaps between the different vehicles in the convoy, the cause of the multi-vehicle events at the shorter span lengths of 5 m to 15 m was revealed due to negative gap spacings. Table 4.4 shows such an example, where two vehicles were travelling with a gap of - 6 m between them. These two vehicles were responsible for one of the multi-vehicle events that occurred at a span length of 10 m for the shear force analysis.

Table 4.4 Example of a multi-vehicle event with a negative gap

Date [yymmdd]	Time [hhmmsscc]	No. of axles	Speed [km/h]	Speed [m/s]	Length [m]
140808	12135450	7	81	22.5	19.5
140808	12135510	2	77	21.4	5.8

It is assumed that these negative gaps were caused because of an error in the recording of the vehicles. A possible cause of the negative gap would be if a vehicle had been split into two separate vehicles. Resulting in two extremely close vehicles, travelling at similar speeds and ultimately leading to a negative gap being calculated. As negative gaps are practically impossible, an absolute lower limit gap is required to prevent this from occurring. Both vehicles responsible for any negative gap should be removed from the data sets as the WIM data available for them are assumed to not be of good quality.

4.6. Restricted mixed-axle groups

It was decided to include three restrictions on the cleaned WIM data set to remove the extremities. These restrictions resulted in three new mixed-axle groups being created. These three groups were referred to as the restricted mixed-axle (RMA) groups 1, 2 and 3 respectively. In contrast, the original mixed-axle group was referred to as the unrestricted mixed-axle (UMA) group henceforth. After applying the restrictions, the LEs for the RMA groups were determined following the methods described in Chapter 3. The restrictions put into place and the results thereof were discussed below.

4.6.1. Failure code filter

The first restriction enforced, for all of the RMA groups, was the removal of all vehicles that contained a non-zero failure code. As mentioned previously in Section 4.2, there were a total of 623 573 vehicles that met this filter. This left a total of 6 506 351 vehicles to do the analysis.

4.6.2. Axle-group restriction

The second restriction enforced, was the removal of vehicles that contained a quad-axle group and above. As mentioned previously in Section 2.4.3, South Africa has no legislation allowing for quad-axle vehicles and they would hence be regarded as permit vehicles. For this study, which focused on normal traffic, these vehicles were excluded.

There were 7 463 vehicles that met the axle-group restriction criteria and were removed from the cleaned WIM data, less than 0.12% of all the vehicles recorded. As shown in Figure 4.6, the restriction placed has resulted in a decrease in the GVM encountered during the bridge traffic loading analysis. A similar occurrence was seen for each RMA group at each span length in Figure A.4 to Figure A.12 in Appendix A.

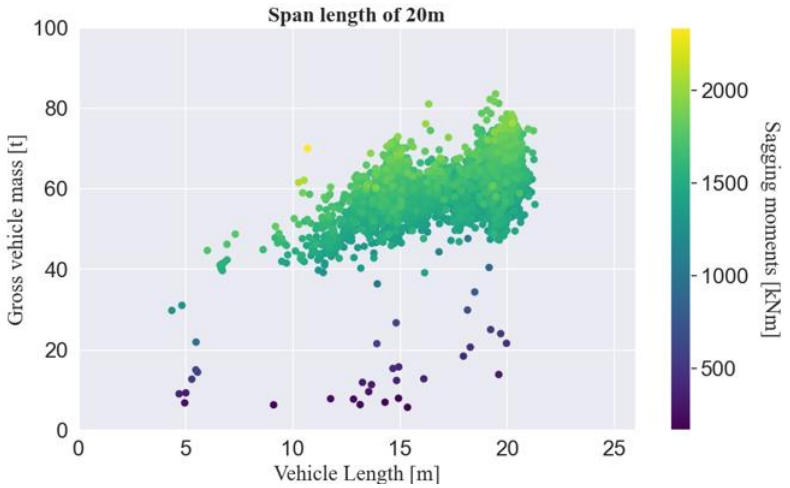

Figure 4.6 Distribution of RMA group 3's GVM, vehicle length and sagging moments at 20 m

4.6.3. Gap restriction

Similar to the UMA, the process described in Section 3.2 was followed to determine the gaps between the RMA groups too, but with the inclusion of a limiting gap between the vehicles. After considering the headway limits used by Nowak (1993), an absolute lower gap limit of 5 m was chosen. If a gap of lower than 5 m was found, the two vehicles responsible were removed from the data set. This was done under the assumption that a small gap was caused by the WIM sensor splitting a vehicle into two separate vehicles. This limiting gap prevented any negative gaps from appearing in the data set.

After implementing an absolute lower gap limit, three separate limiting gaps were to investigate the effect of different gap sizes. Based on Caprani (2005) and Arrive Alive (2020), these three limiting gaps were chosen to investigate the spacing size's effect on the LEs found. From Caprani (2005), it was decided that RMA group 1 would contain a limiting gap of one second. From the "2-3 Second Rule" for safe following distance proposed by Arrive Alive (2020), it was decided to use a limiting gap of two seconds for RMA group 2. Even though Arrive Alive (2020) recommended adjusting the "2-3 Second Rule" to five to six seconds when considering trucks, a time gap of 3.6 seconds and upwards results in only single-vehicle events occurring at a travelling speed of 100 km/h. Hence it was decided to use a limiting time gap of 3.6 seconds at a constant speed of 100 km/h, equivalent to 100 m, for the RMA group 3 to force a convoy that contained only single-vehicle events. A summary of the restrictions applied to the mixed-axle groups was recorded in Table 4.5.

Table 4.5 Summary of restrictions applied to RMA groups

Mixed-axle group	Failure code filter	Axle-group restriction	Limiting gap restriction
RMA group 1	Vehicles with a non-zero failure code	Vehicles with a quad-axle group or above	Limiting gap of one second and the removal of vehicles with less than 5 m gaps found.
RMA group 2	Vehicles with a non-zero failure code	Vehicles with a quad-axle group or above	Limiting gap of two seconds and the removal of vehicles with less than 5 m gaps found.
RMA group 3	Vehicles with a non-zero failure code	Vehicles with a quad-axle group or above	Limiting gap of 100 m and the removal of vehicles with less than 5 m gaps found.

The resulting single and multi-vehicle events encountered in the tail of the recorded LEs due to the different limiting-gap restrictions enforced on RMA groups 1, 2 and 3 are recorded in Figure 4.7, Figure 4.8 and Figure 4.9, respectively. The limiting-gap restrictions have resulted in a decrease in multi-vehicle events occurring with none occurring at the shorter span lengths of 5 m and 10 m for all LEs. It can be seen in Figure 4.7 that the multi-vehicle events start being the dominant cause of the daily maxima Hogging moments from around 25 m onwards.

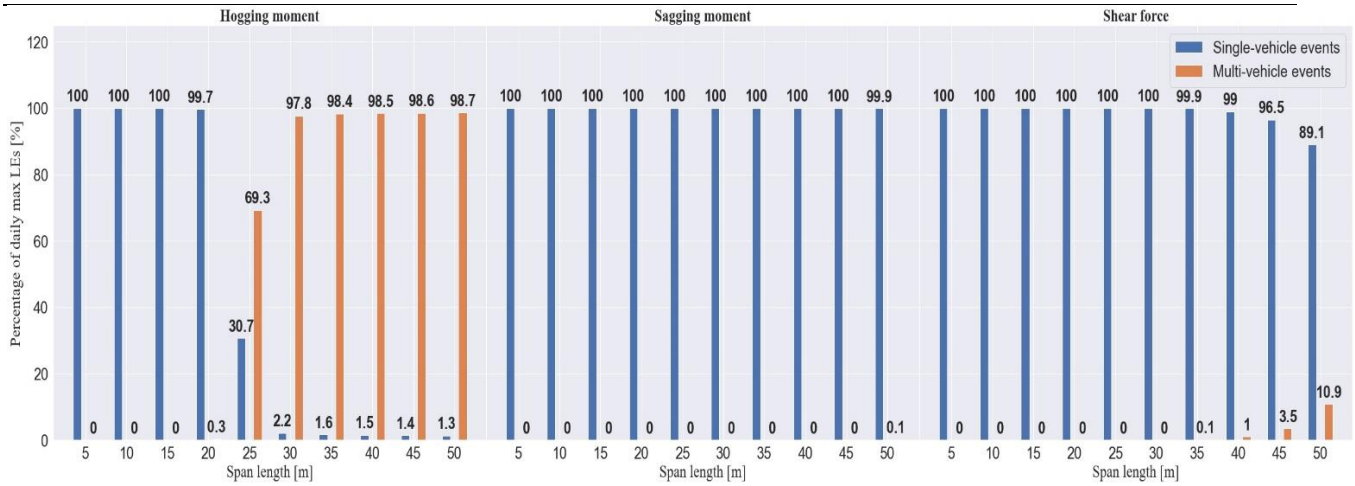

Figure 4.7 Percentage of RMA group 1's censored LEs caused by single and multi-vehicle events

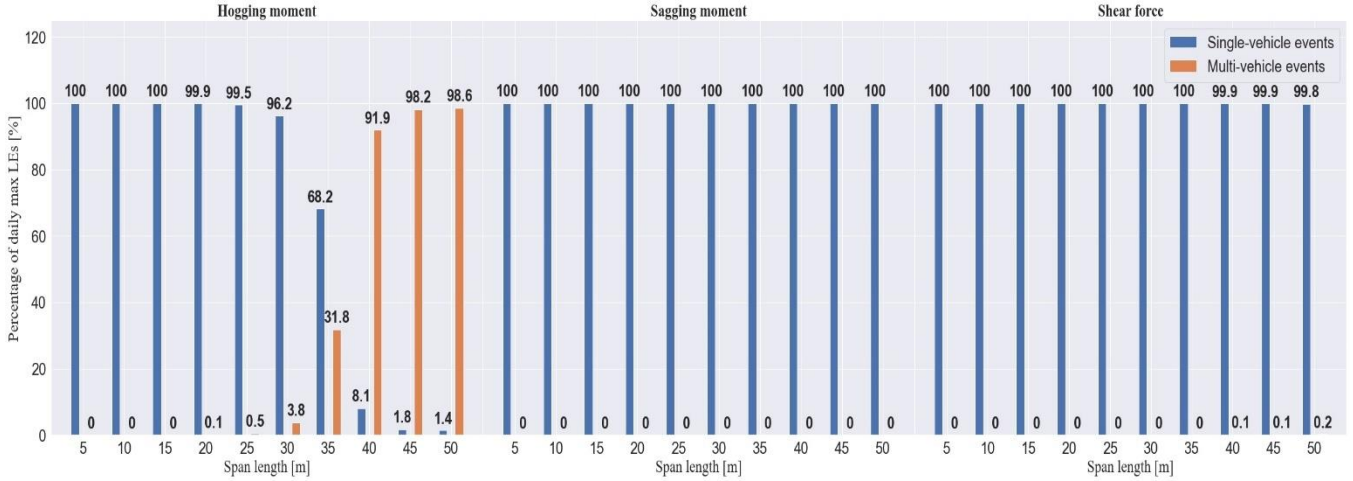

Figure 4.8 Percentage of RMA group 2's censored LEs caused by single and multi-vehicle events

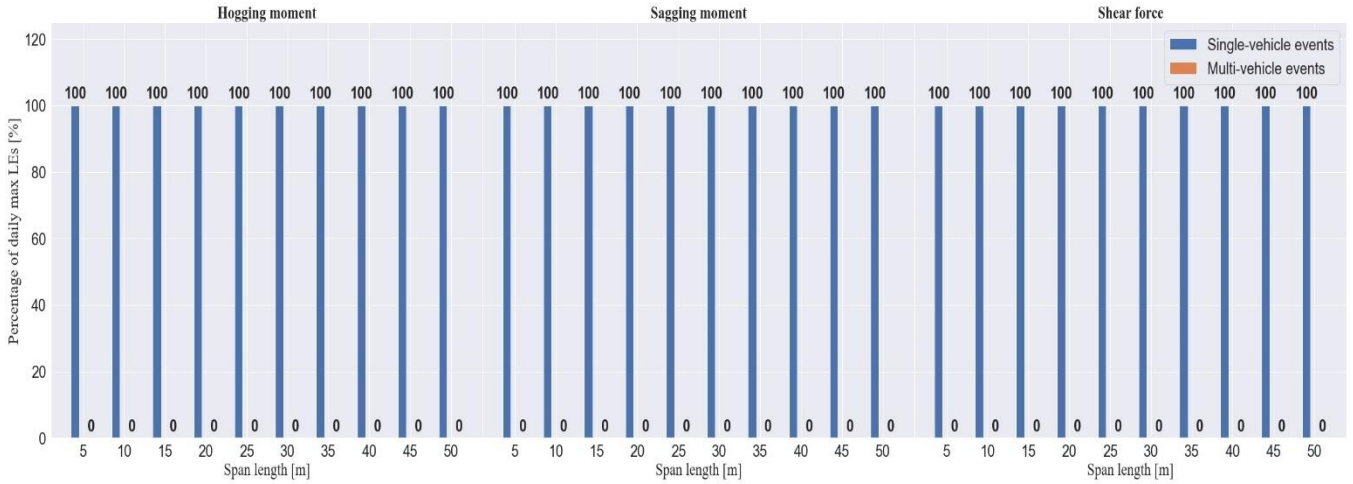

Figure 4.9 Percentage of RMA group 3's censored LEs caused by single and multi-vehicle events

4.7. Mixed axle vehicles LE comparison

4.7.1. GPP plots

In Figure 4.10, the hogging moments GPP plots for each mixed-axle vehicle group at span lengths of 5 m, 20 m, 25 m and 50 m are recorded. The hogging moments GPP plots for all the spans are recorded in Figure B.1. In general, the RMA groups have almost identical plots for 5 m to 20 m. However, from around 25 m onwards, the RMA groups 1 and 2 start to deviate away from the RMA group 3 plot. This means that multi-vehicle events start to dominate from around span lengths of 25 m, which correlates well with what is seen in Figure 4.7 and Figure 4.8. At 50 m, the distinction between the hogging moments produced by single-vehicle and multi-vehicle events is even more apparent. At this span, the highest values produced by the RMA groups 1 and 2 are close to 2000 kNm greater than the highest values produced by the RMA group 3. Overall, the UMA group produces higher hogging moments than the RMA groups, though as the span lengths increase, RMA group 1 produces similar values to the UMA group. The difference between them is a result of axle-group and failure-code restrictions.

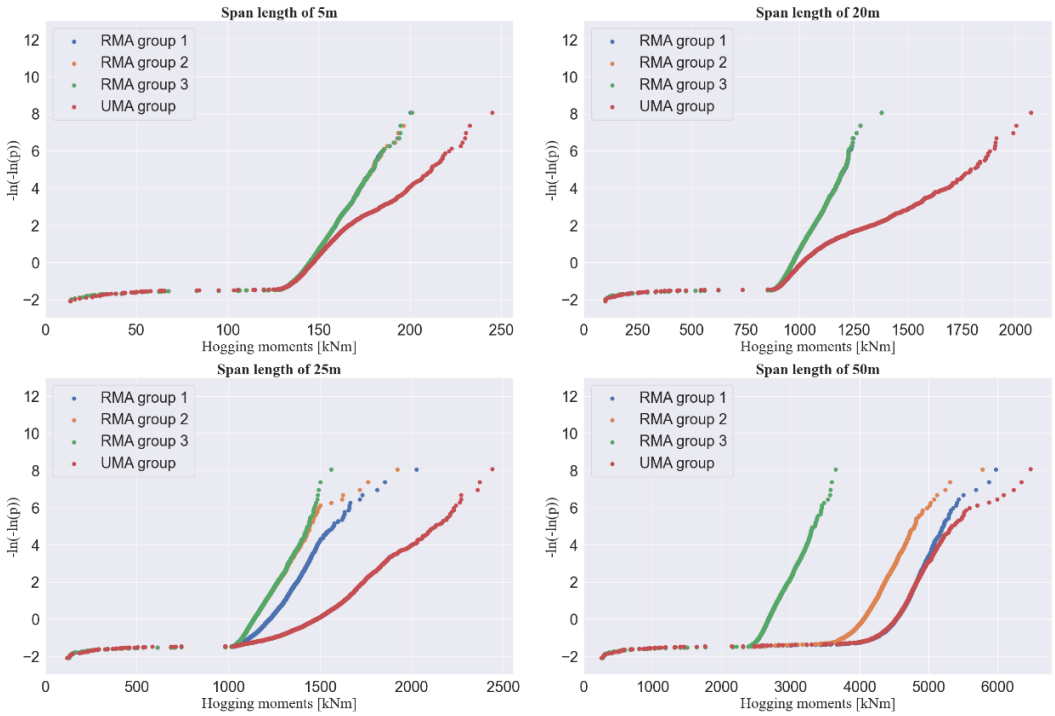

Figure 4.10 Hogging moments GPP plots for the different mixed-axle groups

In Figure 4.11, the sagging moments GPP plots for each mixed-axle vehicle group at span lengths of 5 m, 20 m, 25 m and 50 m is recorded. The GPP plots for all the span lengths investigated are recorded in Figure B.2 in Appendix B. At each span, the different RMA groups can be seen to have almost identical plots. This means that there are too few multi-vehicle events for any significant difference, which correlates well with what is seen in Figure 4.7. Overall, the RMA groups produce lower sagging moments than the UMA group, directly resulting from the enforced axle-group restriction, which reduced the GVMs encountered.

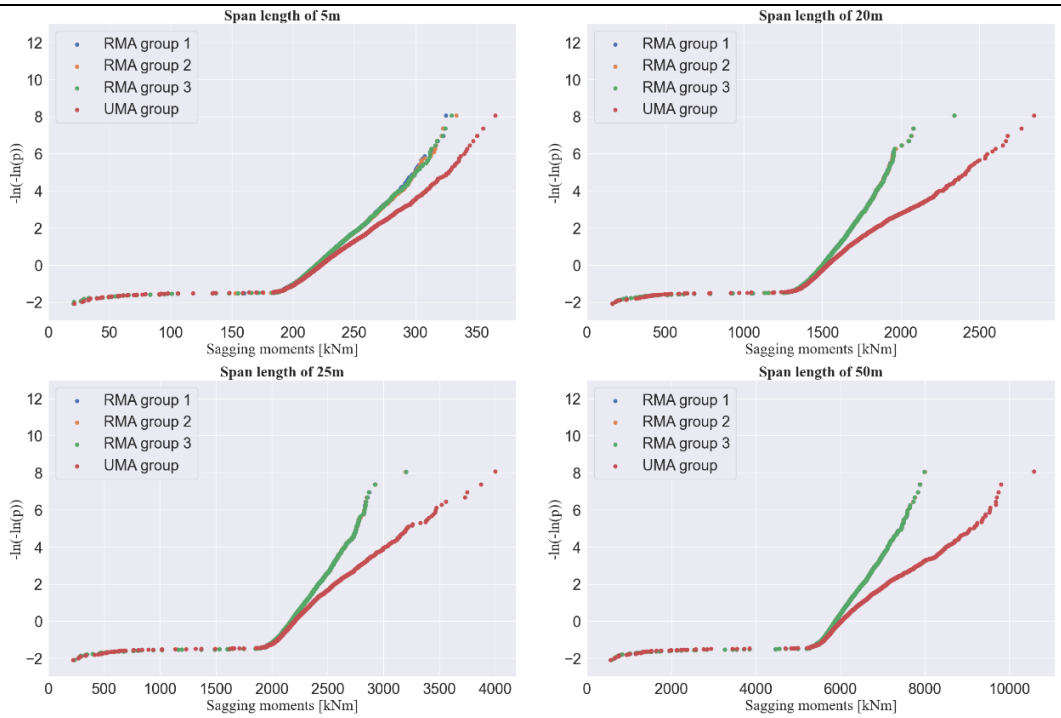

Figure 4.11 Sagging moments GPP plots for the different mixed-axle groups

In Figure 4.12, the shear force GPP plots for each mixed-axle vehicle group at span lengths of 5 m, 20 m, 25 m, and 50 m is recorded. The GPP plots for all span lengths investigated are recorded in Figure B.3 in Appendix B. A similar situation to the sagging moments GPP plots can be seen for the shear force GPP plots. There is no significant difference that can be seen between the different RMA groups, and they are producing lower shear forces than the UMA group due to the axle-group restrictions.

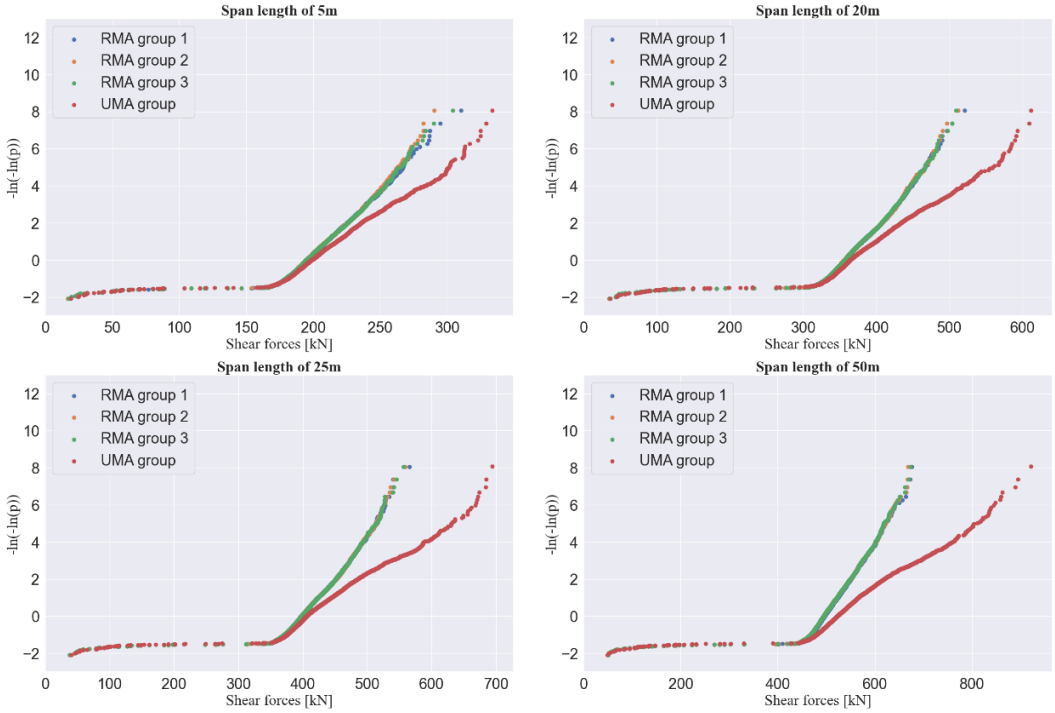

Figure 4.12 Shear forces GPP plots for the different mixed-axle groups

4.7.2. . Characteristic LEs and underlying distributions

Table 4.6 records the characteristic values predicted for the RMA groups. The data sets with an underlying Fréchet distribution were represented by the cells shaded in grey. All the data sets for the sagging moments and shear forces had an underlying Weibull distribution, while 47% of the hogging moments' data sets had an underlying Fréchet distribution.

Table 4.6 RMA groups characteristic values

Span length [m]	RMA group 1			RMA group 2			RMA group 3		
	Hog [kNm]	Sag [kNm]	Shear [kN]	Hog [kNm]	Sag [kNm]	Shear [kN]	Hog [kNm]	Sag [kNm]	Shear [kN]
5	225	336	337	225	349	305	225	344	317
10	678	916	394	679	931	385	677	902	389
15	1162	1565	502	1162	1591	487	1162	1559	506
20	1466	2440	558	1458	2442	569	1460	2479	553
25	2116	3360	588	1959	3346	575	1697	3358	581
30	2830	4334	630	2836	4379	601	2075	4325	606
35	3491	5399	638	4187	5397	637	2560	5390	641
40	4322	6578	667	5013	6576	660	3045	6535	689
45	5385	7649	693	5494	7680	685	3512	7651	693
50	6306	8760	748	5940	8783	705	3966	8784	712

Figure 4.13 depicts the percentage of data sets that contained an underlying Weibull and Fréchet distribution for the different mixed-axle groups. As a result of the three restrictions enforced on the vehicle data sets, the RMA groups 1 and 2 had more underlying Fréchet distributions and fewer underlying Weibull distributions than the UMA group. While the data sets for the RMA group 3 had the same percentage of underlying Weibull distributions as the UMA group.

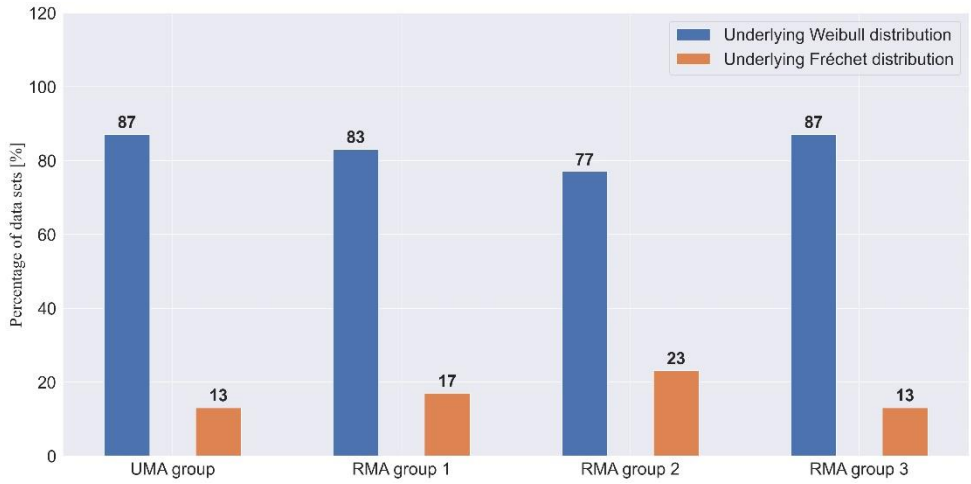

Figure 4.13 Percentage of mixed-axle group data sets with an underlying Weibull and Fréchet distribution

As done in Section 4.4, the data sets for which an underlying Fréchet distribution was found were limited to Gumbel, and new characteristic values were predicted. These new characteristic values were recorded in Table 4.7. Again, by limiting to Gumbel, lower characteristic values were predicted.

Table 4.7 RMA groups limited characteristic values

Span length [m]	RMA group 1			RMA group 2			RMA group 3		
	Hog [kNm]	Sag [kNm]	Shear [kN]	Hog [kNm]	Sag [kNm]	Shear [kN]	Hog [kNm]	Sag [kNm]	Shear [kN]
5	225	336	337	225	349	305	225	344	317
10	678	916	394	679	931	385	677	902	389
15	1162	1565	502	1162	1591	487	1162	1559	505
20	1466	2440	558	1458	2442	569	1460	2452	553
25	2116	3360	588	1959	3346	575	1697	3358	581
30	2830	4334	630	2836	4379	601	2075	4325	606
35	3491	5399	638	4187	5397	637	2560	5390	641
40	4322	6578	667	5013	6576	660	3045	6535	689
45	5385	7649	693	5494	7680	685	3512	7651	693
50	6306	8760	748	5940	8783	705	3966	8784	712

In Figure 4.14, graphical representations of the characteristic values in Table 4.2 and Table 4.7 are shown. The UMA group generally predicts the highest characteristic LEs of all the groups except at 30 m to 40 m for the hogging moments. At span lengths of 30 m to 40 m, the RMA group 2 predicts the highest characteristic hogging moments even though it does not produce the highest hogging moments of all the mixed-axle vehicle groups. From the hogging moments GPP plots in Figure B.1, the reason the RMA group 2 predicts higher characteristic hogging moments can be seen. At span lengths of 30 m to 40 m, the RMA group 2 appears to have a more extreme unbounded nature than the other groups at these spans. This is due to RMA group 2 being less *iid* due to the mix of single-vehicle and multi-vehicle events, as seen in Figure 4.8.

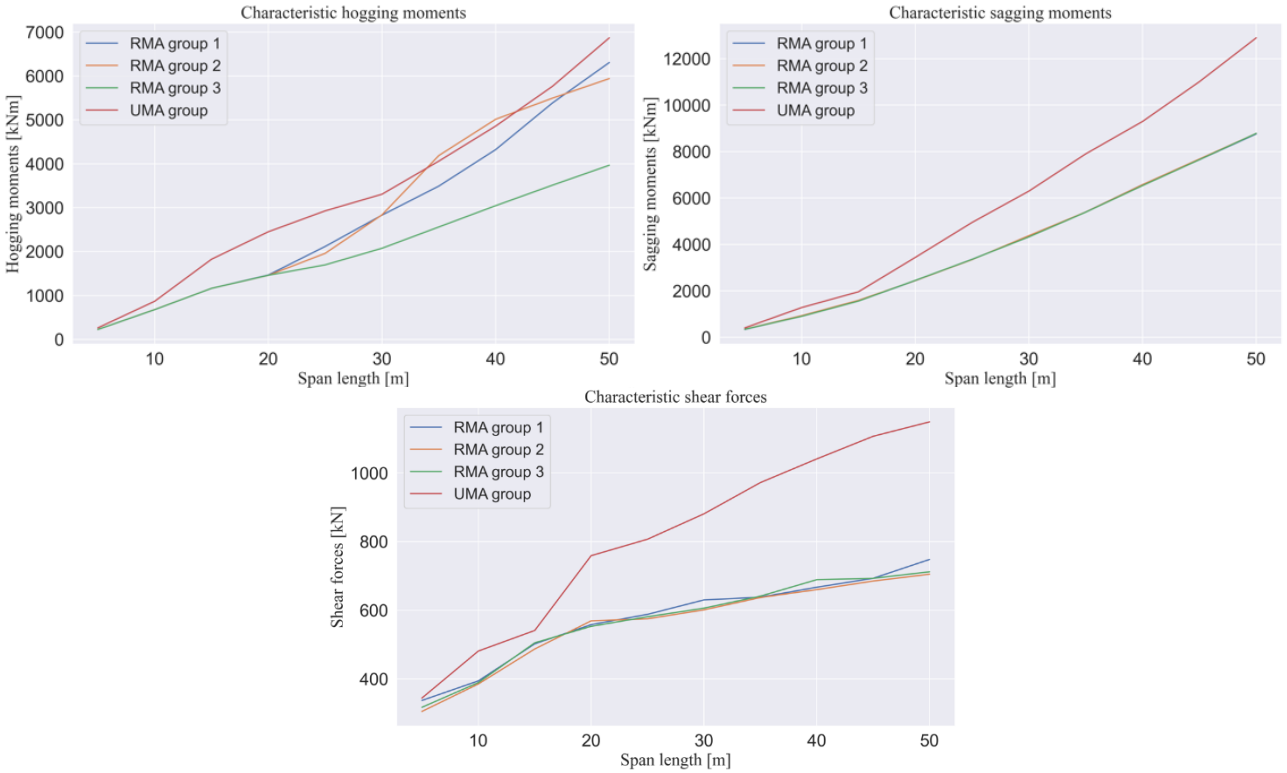

Figure 4.14 Comparison plot for the characteristic values predicted by the UMA and RMA groups

Overall, only the hogging moments for the RMA groups 1 and 2 produced data sets with an underlying Fréchet distribution, while the RMA group 3 had at least one data set for each LE with an underlying Fréchet distribution. Between the different RMA groups, the RMA group 3 had the least number of data sets with an underlying Fréchet distribution. Considering that the only difference between the different RMA groups was the limiting gap spacing used, it was concluded that the multi-vehicle events caused the RMA groups 1 and 2 to be less *iid* than the RMA group 3 for the hogging moments specifically. Although the sagging moments and shear forces GPP plots for the RMA groups appeared to closely follow each other, they were not the same. There were slight differences in the LEs generated by the different RMA groups. These slight differences resulted in a sagging moment and shear force data set for the RMA group 3 having an underlying Fréchet distribution despite the other two RMA groups not having one. Nevertheless, a data set showing an underlying Fréchet distribution was an indication that there was an issue with the data set because, as mentioned in Section 2.3.1, traffic loads are argued to be bounded in nature. To determine a possible cause of the underlying distributions, a breakdown analysis of the different contributing vehicle groups was required.

4.8. Breakdown analysis of the mixed-axle groups

It is already known that vehicles with a quad-axle or above dominate the UMA groups' tail LEs. However, it is not known what types of vehicles these are. Therefore, the contributing vehicle to these groups is investigated to show what the possible cause of the underlying distributions are for the UMA and RMA groups.

4.8.1. UMA group

After analysing the different types of vehicles that formed up the UMA vehicle data set, the main difference between the vehicles noticed was the number of axles each vehicle had. The vehicles in the UMA vehicle group were made up of a minimum of two axles and a maximum of nine axles. This meant there were a total of eight different "sub-axle" vehicle groups within the UMA vehicle data set. Figure 4.15 shows the percentage of sub-axle vehicles that form the entire UMA vehicle data set. Most of the vehicles recorded in the UMA vehicle data set were the 7-axle vehicles which made up over 43%. The second most common vehicle was the 6-axle vehicle making up over 32% of the vehicles. The 9-axle vehicles were the rarest sub-axle group. The 9-axle vehicles made up only 0.03% of all 7 119 924 UMA vehicles, only 2 316 vehicles. The 8-axle vehicles were the second rarest sub-axle vehicles, making up close to 1.4 % of all the vehicles.

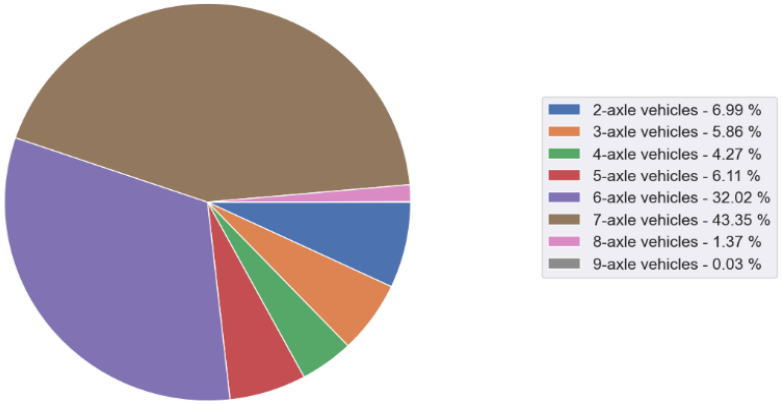

Figure 4.15 Percentage of each sub-axle vehicle group recorded in the UMA vehicle data set

In Figure 4.16, a breakdown of the tail of the UMA hogging moments at 5 m and 30 m is shown. The figure shows that the 9-axle vehicles dominate the tail and are responsible for over 73% of the hogging moments at 5 m. As shown in Figure C.4, the 9-axle vehicles dominate the tail for each span from 5 m up to 30 m. As these are the same type of vehicle and the *iid* criteria is likely met. However, from span lengths of 30 m onwards, the 7-axle vehicles start to dominate the tail, as shown in Figure 4.16 and Figure C.1. This is because, from around 25 m to 30 m, the multi-vehicle events dominate the span. It should be noted that these plots only account for one of the vehicles that show up in a multi-vehicle event.

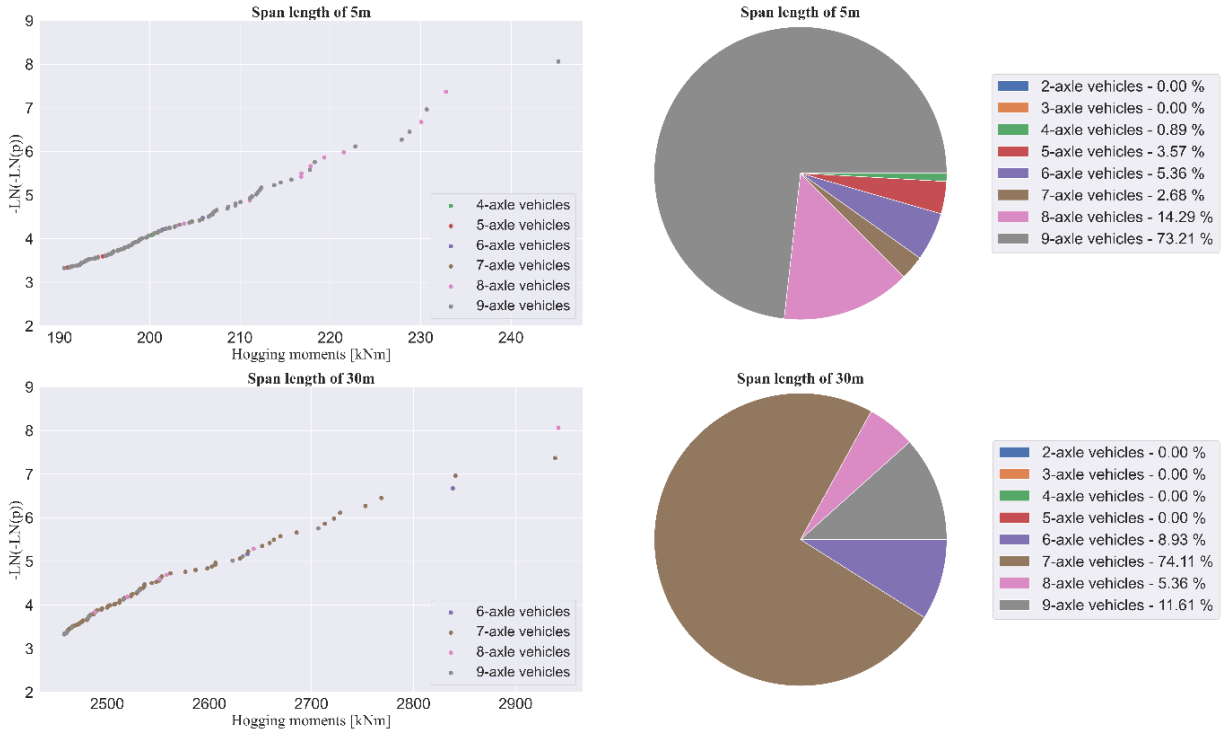

Figure 4.16 Breakdown of the sub-axle vehicles in the tail of the UMA HM data set at 5 m and 30 m

Figure 4.17 shows a breakdown of the tail of the UMA sagging moments and shear forces data set for a 5 m span length. Again, like the hogging moments, the 9-axle vehicles were the dominant vehicle group in the tail of the sagging moments and shear forces plots. This sub-axle group was responsible for over 53% and 66% of the tail of the sagging moments and shear forces. Similarly, the 9-axle vehicles dominated the rest of the spans lengths, as shown in Figure C.2, Figure C.3, Figure D.2 and Figure D.3.

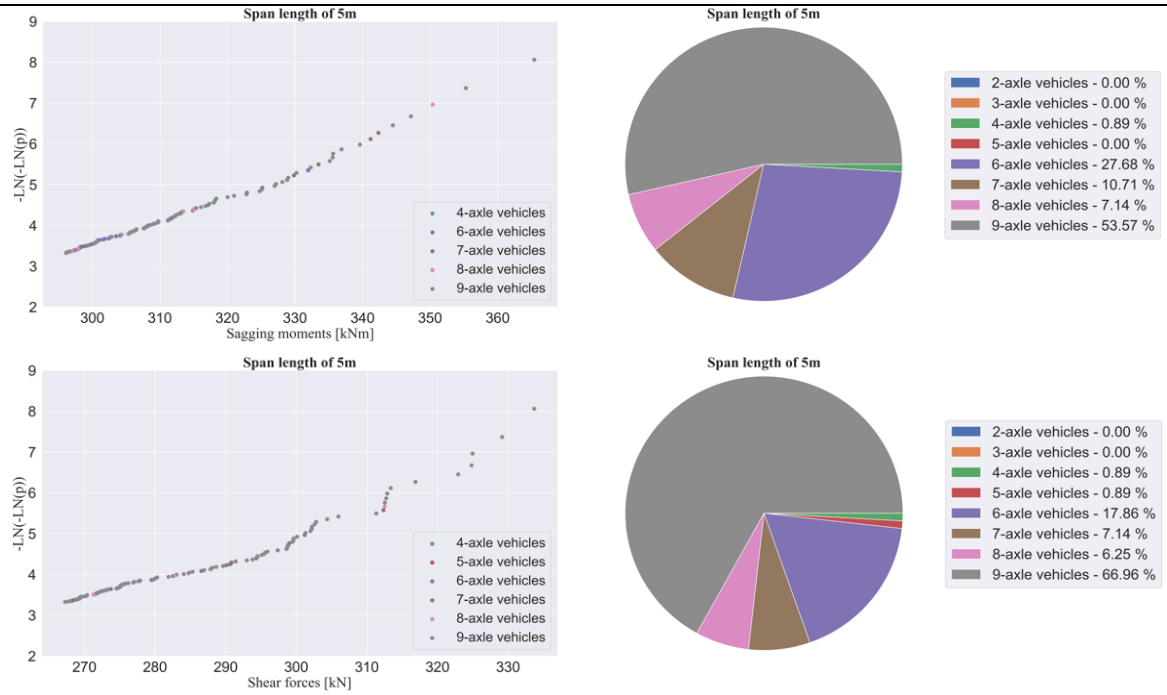

Figure 4.17 Breakdown of the sub-axle vehicles in the tail of the UMA SMs and SFs data set at 5 m

Once multi-vehicle events started dominating the tail, it became difficult to identify any possible causes of the non-iid nature of the data. This was because there were too many combinations found for any notable information to be acquired. Hence, from this point onwards, the study was limited to single-vehicle events and no breakdown analysis into multi-vehicle events was done. This was because the objective of this study was to investigate if splitting the data set into its respective data set would be a better fit to the requirements of EV theory and multi-vehicle events have a lot more sub-sets than single-vehicle events.

4.8.2. RMA group 3

As mentioned previously, the study has been limited to single-vehicle events, so out of all the RMA groups, only RMA group 3 was analysed. The percentage of each sub-axle vehicle group that contributed to the RMA group 3 was recorded in Figure 4.18. The 6-axle and 7-axle vehicles were the most common type of trucks found. They made up over 31% and 43% of the RMA group 3 vehicles, respectively. The 9-axle vehicle group contained the lowest number of vehicles, with only 474 vehicles being found.

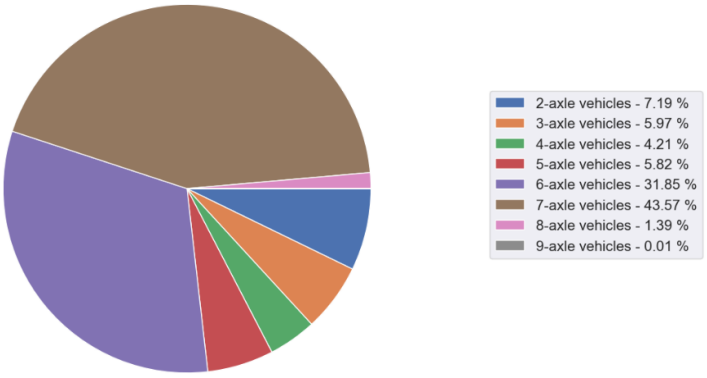

Figure 4.18 Percentage of each sub-axle vehicle group recorded in the RMA group 3 vehicle data set

In Figure 4.19, a breakdown of the 623 573 vehicles that were removed because of the failure code filter was shown. Most of the vehicles removed were 7-axle vehicles accounting for over 40% of them. The 9-axle vehicles had the least number of vehicles had a non-zero failure code resulting in 623 vehicles being removed. Since RMA group 3 had 1 842 fewer 9-axle vehicles than the UMA group, this meant that 34% of the 9-axle vehicles were removed because of the non-zero failure code, while 66% were removed because of the axle-group filter.

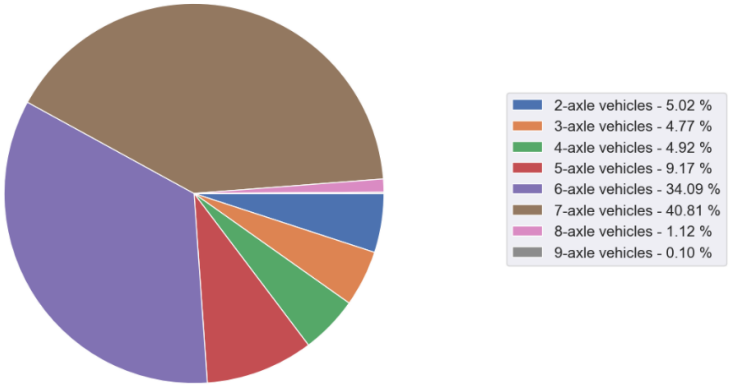

Figure 4.19 Percentage of each sub-axle vehicle group removed because of the failure code filter

Figure 4.20 shows the breakdown of the tail of the hogging moments for the RMA group 3 at span lengths of 5 m and 10 m. At 5 m, an underlying Fréchet distribution was obtained. From the pie graph, it was seen that over 56% of the tail hogging moments were occupied by 8-axle vehicles. Similarly, as seen in Figure C.4 and Figure D.4, the 8-axle vehicles dominated the rest of the span lengths, too, except for the span lengths of 10 m and 15 m. At these span lengths, the 6-axle vehicles dominated the tail, where it occupied over 91% and 60% of the tail at 10 m and 15 m, respectively. At 10 m, an underlying Weibull distribution had been found.

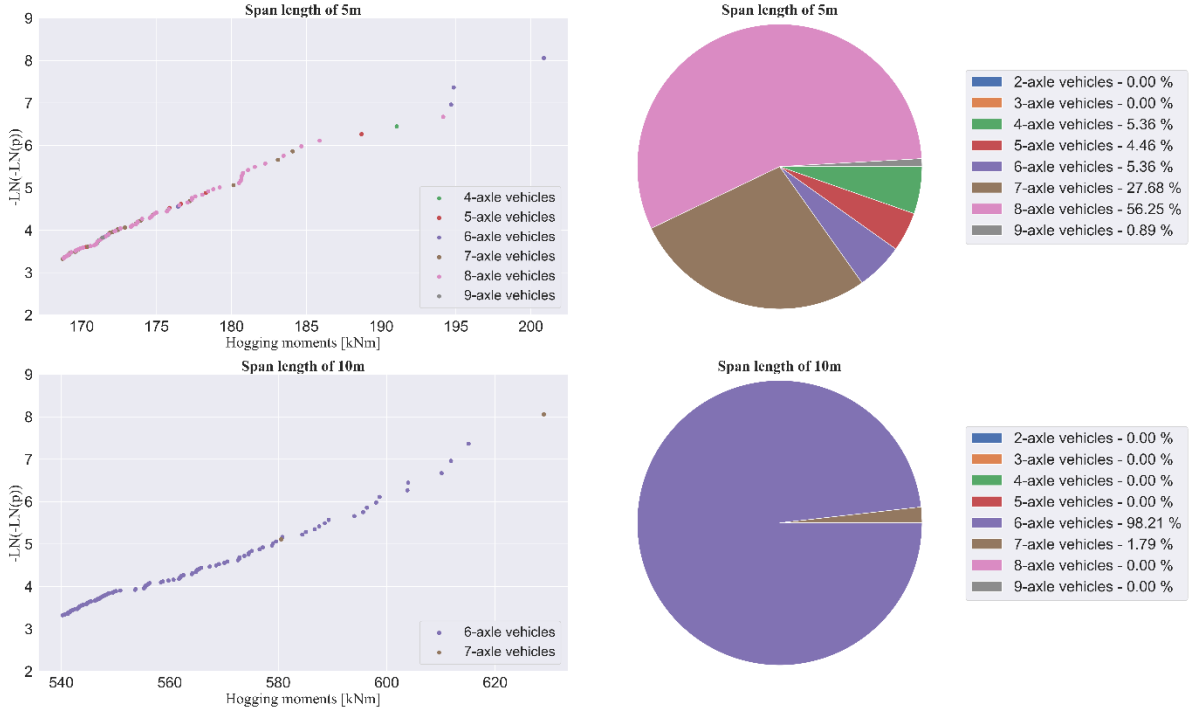

Figure 4.20 Breakdown of the sub-axle vehicles in the tail of the RMA group 3's hogging moments at 5 m and 10 m

In Figure 4.21, the breakdown plots at 5 m and 20 m was shown. At 5 m an underlying Weibull distribution was obtained. As shown by the pie graphs, over 95% of the tail was occupied by 6-axle vehicles, while at 20 m, where an underlying Fréchet distribution was found, they produced only 34% of the tail sagging moments. At 20 m, the 8-axle vehicles were responsible for most of the tail sagging moments and produced 50% of them. Figure C.5 and Figure D.5 shows the breakdown plots for the RMA group 3 sagging moments. For the shorter spans of 5 m to 15 m, the 6-axle vehicles were the dominant sub-axle vehicle group. From spans of 20 m onwards, the 8-axle vehicles dominated the tail.

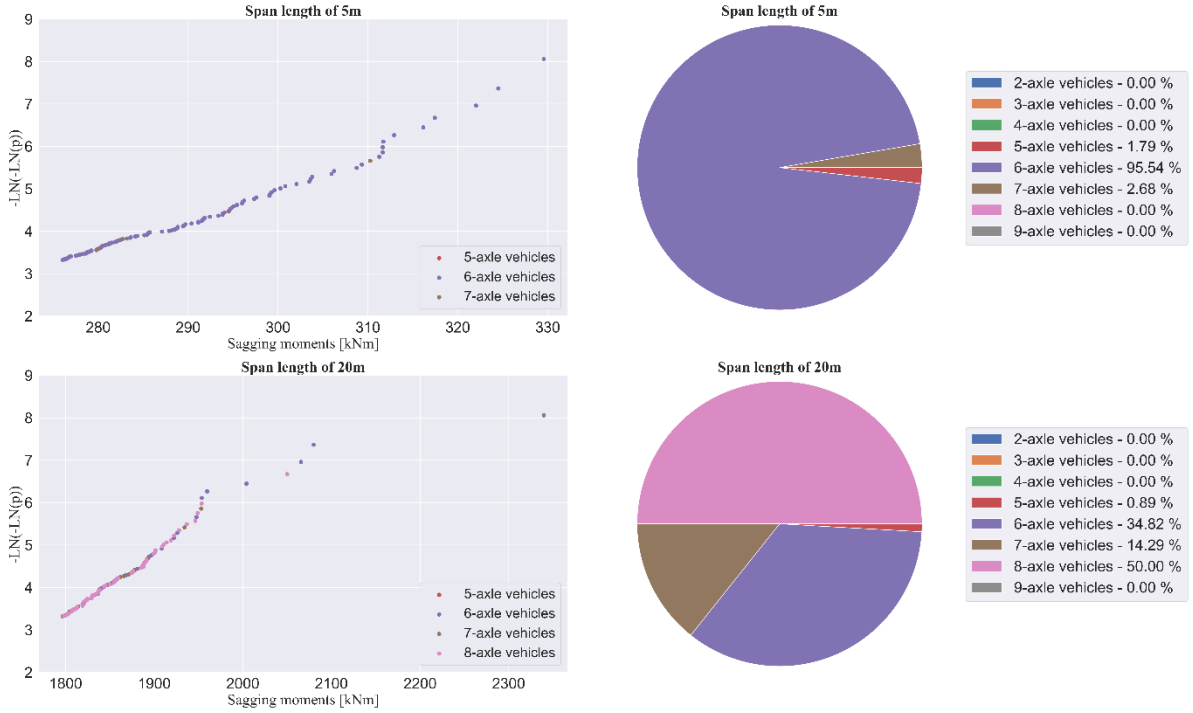

Figure 4.21 Breakdown of the sub-axle vehicles in the tail of the RMA group 3's sagging moments at 5 m and 20 m

In Figure 4.22, the breakdown plots at 5 m and 15 m was shown. At 5 m an underlying Weibull distribution had been obtained. As shown by the pie graph, the 6-axle vehicles occupied over 96% of the tail, while at 15 m, where an underlying Fréchet distribution was found, the 6-axle vehicles produced over 92% of the tail shear forces. Figures C.6 and D.6 recorded the breakdown plots for the RMA group 3 shear forces. The 6-axle vehicles were the dominant sub-axle vehicle group for spans of 5 m to 30 m. Between spans of 30 m and 35 m, the 8-axle vehicles became the dominant sub-axle group for the rest of the span lengths investigated.

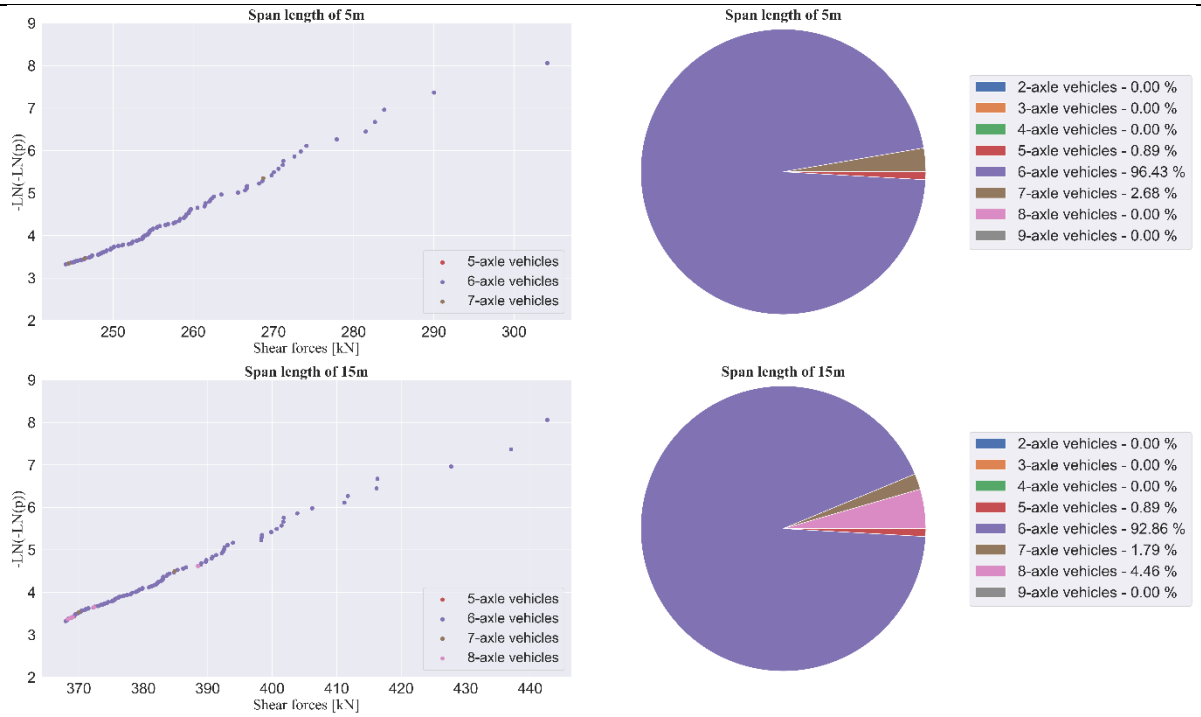

Figure 4.22 Breakdown of the sub-axle vehicles in the tail of the RMA group 3's shear forces at 5 m and 30 m

4.9. Discussion

The breakdown analysis showed that the mixed-axle groups were composed of different subsets of vehicles. In addition, the subsets had varying population sizes, as was evident by Figure 4.15 and Figure 4.18. Furthermore, each subset was seen to be responsible for a different percentage of the tail LEs.

For the UMA group, the 9-axle vehicles dominated the tail LEs, except for the spans where multi-vehicle events dominated. As shown in Figure 4.4, more than 70% of the tail LEs for the UMA group were caused by quad-axle vehicles. This meant that most of the 9-axle vehicles had a quad-axle group or above, which was proved by the axle-group restriction which removed 53% of the 9-axle vehicles recorded in the WIM data.

As a result of the axle-group restriction, the 6-axle or 8-axle vehicle groups dominated the tail of the LEs for the RMA group 3 instead of the 9-axle vehicles. For the RMA group 3, the 6-axle vehicle group was responsible for the majority of the LEs at the shorter span lengths of 5 m to 15 m except for the tail hogging moments at 5 m, where the 8-axle group was responsible for 56% of the hogging moments instead. At the longer span lengths, the 8-axle vehicles were responsible for the majority of the LEs. While the 6-axle and 8-axle vehicle groups occupied most of the LEs at the different spans, they did not always produce the highest LEs. The 7-axle vehicle group started to produce the highest hogging moments, sagging moments and shear forces recorded from span lengths of 15 m, 35 m and 35 m onwards respectively.

At 10 m for each LE, the 6-axle vehicles could be seen to be the clear dominating vehicle group occupying more than 90% of the tail LEs. At this span, an underlying Weibull distribution was found for each LE data set, which indicated that the data sets at 10 m were *iid.*

Although the data sets at 10 m had a clear dominating vehicle group, it was seen that an underlying Fréchet distribution could be obtained despite there being a clear dominating vehicle group. For instance, at 15 m an underlying Fréchet distribution was obtained for the RMA group 3 despite the 6-axle vehicles being responsible for over 92% of the tail shear forces. This, along with the fact that there were data sets without such a clear dominating sub-axle group (E.g., hogging moments at 35 m in Figure C.4) for which an underlying Weibull distribution had still been obtained, indicated it was not necessary to have a clear dominating sub-axle group to obtain an underlying Weibull distribution. Instead, it was more likely that the underlying distribution of the contributing sub-axle groups influenced the underlying distribution found for the parent mixed-axle group. This motivated an investigation into the underlying distributions of the sub-axle groups as it would help understand the cause of the underlying Weibull and Fréchet distributions found for the mixed-axle group data sets. In theory, by splitting the WIM data into separate sub-axle groups, the *iid* nature of the data sets should improve and the Fréchet distributions should be decreased. Furthermore, as multi-vehicle events were inherently non-iid, it was decided to limit this study to single-vehicle events only.

4.10. Summary

The methods described in chapter 3 were used to clean and calibrate the WIM data. Then, using cleaned WIM data, an imitation of the mixed-axle vehicle group used in Van der Spuy (2019) was created. Finally, after performing a bridge traffic loading analysis, the LEs experienced by the different span lengths was obtained, and the characteristic values for the imitation group were determined. These values were seen to be within 7% of the characteristic values predicted by Van der Spuy (2019), which was assumed to be within an acceptable range.

After analysing the vehicles responsible for the LEs generated by this imitation group, two restrictions were recommended. These restrictions resulted in forming the three restricted mixed-axle (RMA) groups 1, 2 and 3. The characteristic values for all three groups were determined, and the underlying distributions for the LE data sets at each span were noted.

A breakdown analysis of vehicles responsible for the tail LEs generated by the UMA group and the RMA group 3 revealed the different subsets that composed each group. Furthermore, these subsets were seen to different population sizes and were each responsible for only a portion of the tail of the daily maxima LEs recorded. As a result, the *iid* condition of EV theory had been violated and yet 87% of the data sets for the RMA group 3 had an underlying Weibull distribution. Splitting the WIM data set was recommended to determine how the underlying distribution of the sub-axle groups affected the underlying distribution found for the parent mixed-axle group. This would help understand the cause of the underlying Weibull and Fréchet distributions found and would show if splitting the WIM data set would better adhere to the requirements of EV theory.

5. Vehicle subsets

5.1. Chapter introduction

In chapter 4, it was shown that the mixed-axle groups were composed of eight different subsets of vehicles, each with varying population sizes. Furthermore, each of these sub-axle groups was responsible for a different portion of the LEs produced by the mixed-axle group. As a result, using the mixed-axle group to perform a traffic loading analysis could violate the *iid* requirement of EV theory.

In this chapter, the WIM vehicle data set is split into eight different sub-axle groups. Through this, an understanding of how the underlying distributions of the sub-axle groups affect the parent mixed axle group is obtained and it is investigated if splitting improves the *iid* nature of the data sets to better adhere to the requirements of EV theory.

As it was decided to limit this study to single-vehicle events, each of the sub-axle groups had the same restrictions placed on it that the RMA group 3 had, i.e., failure code filter, axle-group restriction and limiting gap of 100 m. After that, the incrementation process, described in section 3.2, is used to determine the LEs for each sub-axle group. A comparison is then made for GPP plots and the characteristic values. Finally, the underlying distributions of the different sub-axle groups' data sets and possible causes are discussed.

5.2. Sub-axle groups

As shown before in Section 4.8, eight different sub-axle groups were in the cleaned WIM data set. For each sub-axle group, a convoy was created with the same restrictions placed on RMA group 3. This was to ensure that only single-vehicle events took place.

5.2.1. GPP plots

Figure 5.1 shows the hogging moments GPP plots for the span lengths of 5 m, 10 m, and 15 m. The hogging moments GPP plots for the rest of the spans were recorded in Figure E.1.

At a span length of 5 m, the RMA group 3's hogging moments data set had an underlying Fréchet distribution. In the GPP plot, the RMA group 3's plot followed the 7-axle vehicles plot at first, then deviated away from it because of the 8-axle vehicles from which it deviated away right at the end of the tail because of a 4-axle and a 5-axle vehicle and three 6-axle vehicles. From the GPP plot, it was seen that the last three hogging moments created by 6-axle vehicles caused the RMA group 3 plot to have an unbounded nature resulting in an underlying Fréchet distribution being found.

At a span length of 10 m, the RMA group 3 hogging moments data set had an underlying Weibull distribution. In the GPP plot, the RMA group 3's plot followed the 6-axle vehicles plot until the last four hogging moments, where one 7-axle vehicle caused the RMA group 3 plot to deviate slightly. In the figure, the 6-axle vehicles

plot appeared to have a bounded nature, and since it was the dominant sub-axle group at 10 m, it makes sense that an underlying Weibull distribution was found for the RMA group 3 at this span.

At a span length of 15 m, the RMA group 3's hogging moments data set had an underlying Frechet distribution. From the GPP plot, the 7-axle vehicles plot was seen to cause the RMA group 3 plot to deviate away from the 6-axle vehicles plot near the end of the tail. This resulted in the RMA group 3 plot having an unbounded nature and the underlying Frechet distribution being found.

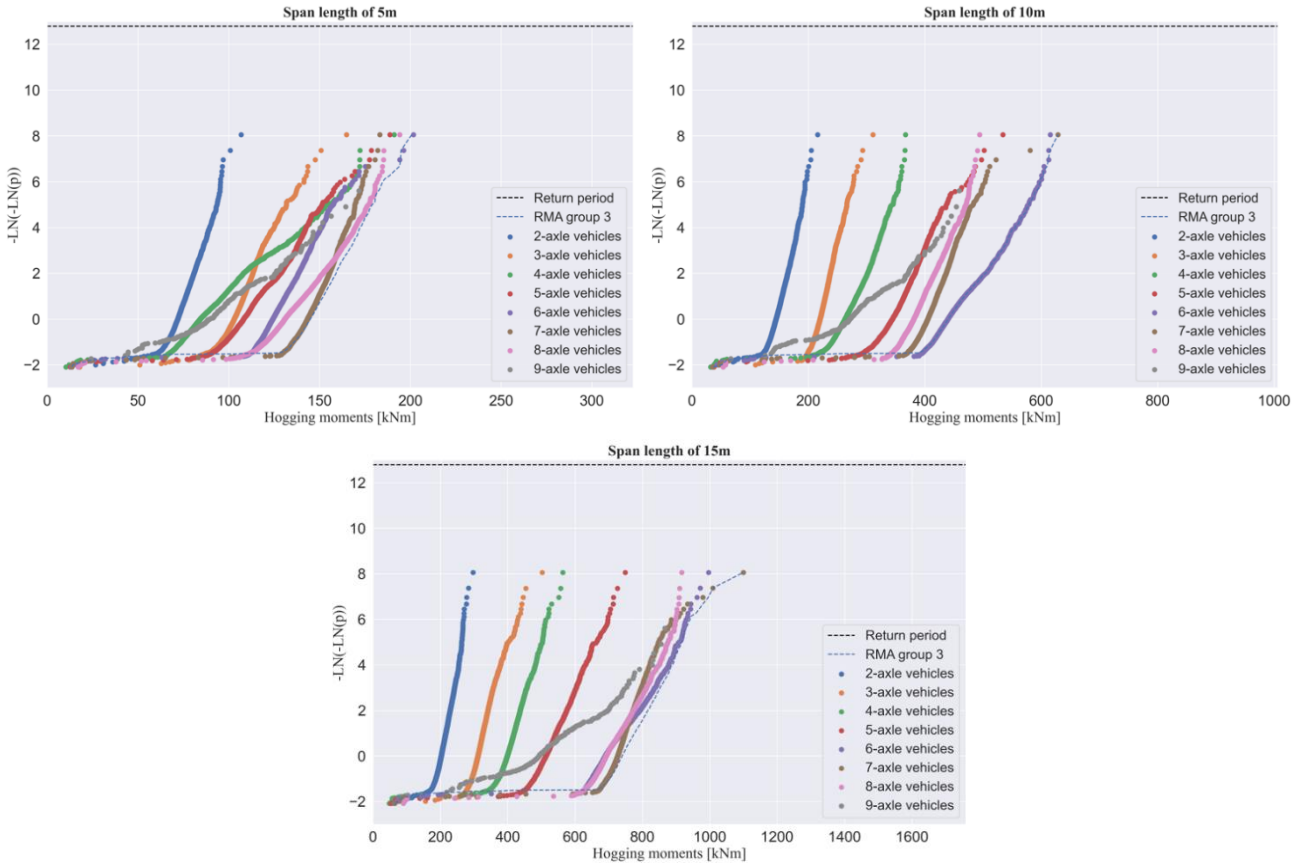

Figure 5.1 Hogging moments GPP plots for the sub-axle groups and RMA group 3 at 5 m, 10 m, and 15 m

Figure 5.2 shows the sagging moments GPP plots for the span lengths of 15 m and 20 m. The sagging moments GPP plots for the rest of the spans were recorded in Figure E.2.

At 15 m an underlying Weibull distribution was found for the RMA group 3's. In the figure, the RMA group 3's plot was be seen to initially be made up of mainly the 6, 7 and 8-axle vehicles, while near the end of the RMA group 3's plot mainly follows the 6-axle vehicles plot. At 20 m, the RMA group 3 was found to have an underlying Fréchet distribution. From the GPP plot, the cause of this appeared to be the influence of the four 6-axle vehicles.

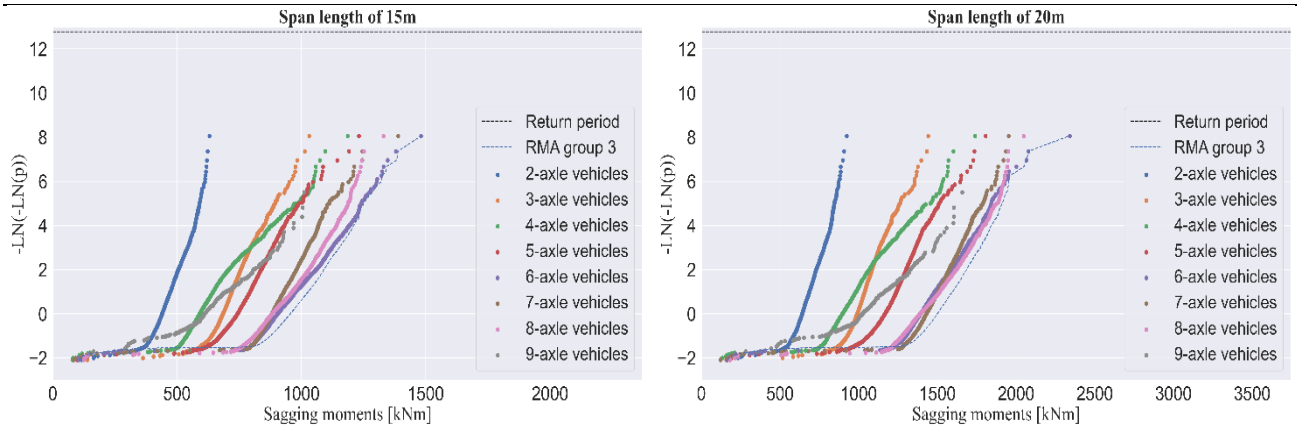

Figure 5.2 Sagging moments GPP plots for the sub-axle groups and RMA group 3 at 15 m and 20 m

Figure 5.3 shows the shear forces GPP plots for the span lengths of 10 m and 15 m. The shear force GPP plots for the rest of the spans were recorded in Figure E.3.

At a span length of 10 m, an underlying Weibull distribution was found for the RMA group 3's while an underlying Fréchet distribution was found at 15 m. At both spans, the RMA group 3 followed the 6-axle vehicles plot until the end of the tail. At 10 m, the 6-axle vehicle appeared to have a bounded nature and since it was the dominating sub-axle group, it resulted in the RMA group 3 obtaining an underlying Weibull distribution. At 15 m, the influence of the last four 6-axle vehicles was significant enough to result in the RMA group 3 appearing to have an unbounded nature, which resulted in an underlying Fréchet distribution being found.

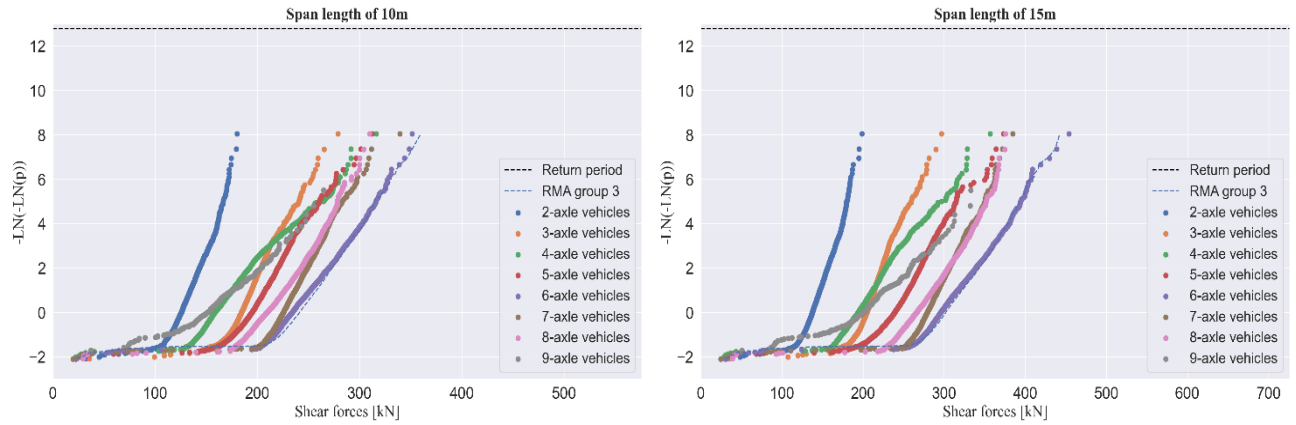

Figure 5.3 Shear forces GPP plots for the sub-axle groups and RMA group 3 at 10 m and 15 m

In general, when the dominant sub-axle vehicle groups appeared to display a bounded plot, an underlying Weibull distribution would be found for the RMA group 3. However, if the interference from other sub-axle groups was significant enough or the dominant vehicle group had an unbounded nature, an underlying Fréchet distribution would be found instead.

5.2.2. Characteristic values and underlying distributions

In Chapter 4, when a Fréchet distribution was encountered for a data set, it was limited to Gumbel. In this chapter, the characteristic values for the data sets that had underlying Fréchet distributions were left as is.

The characteristic hogging and sagging moments and shear forces for each sub-axle group were displayed in Table 5.1, Table 5.2 and Table 5.3, respectively. The data sets for which an underlying Fréchet distribution was found were shaded in grey. The unshaded cells represent the data sets for which an underlying Weibull distribution was obtained.

Table 5.1 Sub-axle vehicle groups characteristic hogging moments

Span length [m]	Characteristic hogging moments [kNm]								
	2-axle vehicles	3-axle vehicles	4-axle vehicles	5-axle vehicles	6-axle vehicles	7-axle vehicles	8-axle vehicles	9-axle vehicles	RMA group 3
5	110	216	223	302	483	191	198	192	242
10	234	343	379	764	633	1 100	502	489	677
15	303	639	660	869	1 030	1 320	956	950	1 208
20	440	950	1 033	1 014	1 296	1 682	1 302	1 198	1 460
25	571	1 116	1 290	1 567	1 533	1 715	1 558	1 545	1 697
30	697	1 331	1 545	1 992	1 982	2 355	1 884	1 695	2 075
35	823	1 664	1 814	2 327	2 358	2 784	2 324	2 130	2 560
40	953	1 848	1768	2 616	2 781	3 320	2 767	2 553	3 045
45	1071	2 088	2092	3 010	3 168	3 834	3 206	2 965	3 512
50	1183	2 385	2 475	3 338	3 556	4 359	3 641	3 378	3 966

Table 5.2 Sub-axle vehicle groups characteristic sagging moments

Span length [m]	Characteristic sagging moments [kNm]								
	2-axle vehicles	3-axle vehicles	4-axle vehicles	5-axle vehicles	6-axle vehicles	7-axle vehicles	8-axle vehicles	9-axle vehicles	RMA group 3
5	201	275	245	550	358	367	302	219	344
10	399	732	815	919	909	1 230	739	611	902
15	653	1 298	1 694	1 570	1 575	1 788	1 370	1 039	1 559
20	949	1 945	2 090	2 486	2 600	2 254	2 097	1 728	2 375
25	1 253	2 565	3 027	3 416	3 352	3 634	3 087	2 528	3 358
30	1 565	3 228	3 371	4 358	4 249	4 851	4 151	3 532	4 325
35	1 886	3 777	4 060	5 091	5 218	6 193	5 118	4 447	5 390
40	2 233	4 496	4 712	6 474	6 183	7 320	6 284	5 378	6 535
45	2 507	5 209	5 429	6 768	7 094	8 704	7 280	6 288	7 651
50	2 810	5 319	6 590	7 638	8 081	10 023	8 350	7 247	8 784

Table 5.3 Sub-axle vehicle groups characteristic shear forces

Span length [m]	Characteristic shear forces [kN]								
	2-axle vehicles	3-axle vehicles	4-axle vehicles	5-axle vehicles	6-axle vehicles	7-axle vehicles	8-axle vehicles	9-axle vehicles	RMA group 3
5	160	230	226	418	338	370	233	216	317
10	188	314	334	348	382	402	339	290	389
15	223	337	387	473	556	391	386	358	500
20	228	338	412	526	566	779	467	436	553
25	234	341	421	559	587	778	534	472	581
30	240	349	438	578	615	830	573	543	606
35	243	359	451	589	661	851	605	576	641
40	244	356	434	598	686	1001	629	579	689
45	244	361	435	603	696	958	660	625	693
50	246	377	440	614	704	977	663	621	712

Figure 5.4 depicts the percentage of data sets with an underlying Weibull or Fréchet distribution for the different sub-axle groups. As seen in the figure, most of the data sets for the 2-axle, 4-axle and 6-axle vehicle groups and all data sets for the 8-axle and 9-axle vehicle groups had an underlying Weibull distribution. In contrast, most data sets for the 3-axle, 5-axle and 7-axle vehicle groups had an underlying Fréchet distribution.

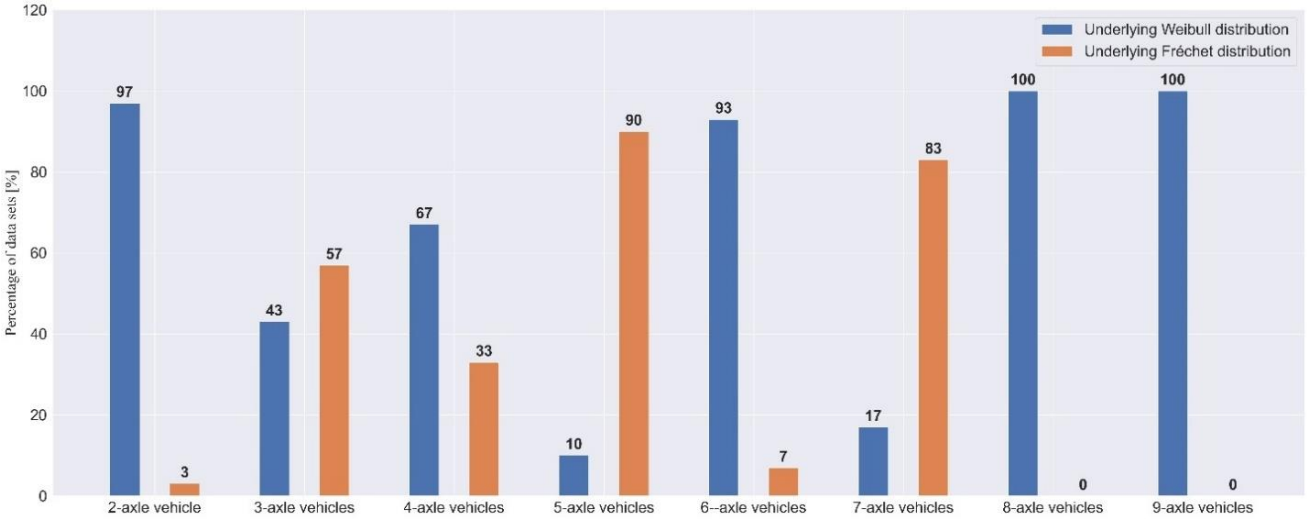

Figure 5.4 Percentage of sub-axle groups data sets found to have an underlying Weibull or Fréchet distribution

5.2.3. Discussions

In general, it could be seen that the underlying distribution found for the RMA group 3's data sets was related to the underlying distributions found for the tail dominating sub-axle groups. If the tail dominating sub-axle groups LE data set had an underlying Weibull distribution, so did the RMA group 3's LE data set. Whereas if the dominating sub-axle group had an underlying Fréchet distribution, so too did the RMA group 3's LE data set. For example, at 15 m the RMA group 3's shear force data sets had an underlying Fréchet distribution. At this span, the dominant sub-axle group was the 6-axle vehicles, which as shown in Table 5.3, had an underlying Fréchet distribution at 15 m as well.

Although it was generally seen that the underlying distribution of the dominant sub-axle groups determined the underlying distribution of the mixed-axle group, there was an exception. The exception was when the interference from the other sub-axle groups was significant enough that the tail of the RMA group 3's data set was pulled down, resulting in the data set fitting a Fréchet distribution. This was the cause of the underlying Fréchet distributions found for the RMA group 3's hogging moments data sets at 5 m and 15 m, and the sagging moment data sets at 20 m.

As displayed in Figure 5.1 at 5 m and 15 m for the hogging moments' data sets, the tails of RMA group 3 plots were sharply pulled down by the 6-axle and 7-axle vehicles respectively. The hogging moment data sets for the 6-axle and 7-axle vehicles had an underlying Fréchet distribution at 5 m and 15 m respectively.

In Figure 5.2, the RMA group 3's plot was pulled down by the 6-axle vehicles, which resulted in an underlying Fréchet distribution being obtained. At this span, the 6-axle vehicles sagging moment data set was found to have an underlying Fréchet distribution as well.

Overall, by subdividing the RMA group 3's LE data sets into the separate sub-axle groups a total of 240 LE data sets had been obtained. Of these sub-axle groups LE data sets, 35% of them had an underlying Fréchet distribution, while the other 65% had an underlying Weibull distribution. It appeared that splitting had a negative impact on the traffic loading analysis as there were now more data sets with an underlying Weibull distribution. However, splitting had allowed for an understanding of how the underlying distributions of the sub-axle groups affected the underlying distributions of the parent mixed-axle group. If the sub-axle groups are further sub-divided, then an understanding of the causes of the underlying Fréchet distributions found for the sub-axle groups could be obtained as well. Therefore, further investigation into the sub-categories of sub-axle groups was required to see if it was possible to make the data sets more *iid*.

5.3. Sub-categories of sub-axle vehicle groups

In this Section, an investigation into the sub-categories of the 5-axle to 8 axle vehicle groups was done. No investigation was done for the 2-axle, 3-axle, 4-axle, and 9-axle vehicles, as these sub-axle groups produced non-critical LEs, so any further breakdown analysis was considered unnecessary.

For the 5-axle to 8-axle vehicle groups, a similar naming convention to that used by Bosman (2004) was used to represent the sub-categories of each sub-axle vehicle group. For example, the two trucks shown in Figure 3.1 represent two 6-axle vehicles that contain a single driving axle, followed by a tandem axle group, which a tridem axle group followed. These two trucks would fall into the 6: 1-2-3 sub-category of 6-axle vehicles.

5.3.1. Different sub-categories found

To discover the different sub-categories, a breakdown analysis of the vehicles responsible for the tail of the Sagging moments recorded at 5 m, 25 m and 50 m for each sub-axle group considered, was done. In Tables Table 5.4, Table 5.5 and Table 5.6, information on the different sub-categories found was recorded. This information included the total number of vehicles recorded in the cleaned WIM data files, the number of vehicles that appeared in the tail of the daily maxima sagging moments and the mean and standard deviation for the sagging moments, GVMs and vehicle lengths. Four sub-categories were found within the 5-axle vehicle group, two in the 6-axle vehicle group, three in the 7-axle vehicle group and two in the 8-axle vehicle group.

Table 5.4 The sub-categories of sub-axle vehicles found at a span length of 5 m

Sub-category	Total vehicles	Vehicles in tail	Sag [kNm]		GVM [t]		Vehicle length [m]	
			μ	σ	μ	σ	μ	σ
5: 2-3	35 951	21	240.2	21.2	47.3	6.1	11.2	1.1
5: 1-2-2	238 951	73	227.7	7.8	45.8	4.9	13.4	2.2
5: 1-1-3	68 228	15	227.6	7.7	43.0	3.2	12.2	2.0
5: 1-2-1-1	39 712	3	222.9	3.2	48.8	1.4	18.0	0.1
6: 1-2-3	2 159 814	112	290.2	11.3	64.3	5.0	14.8	1.1
7: 1-3-3	580	13	260.5	17.9	65.3	6.7	17.0	2.0
7: 1-2-2-2	3 012 571	67	241.2	9.0	65.8	7.1	19.5	1.3
7: 1-2-3-1	36 538	32	238.2	4.6	53.9	1.6	17.9	0.7
8: 1-2-3-2	73 586	106	238.6	9.7	69.7	5.0	19.6	1.7
8: 1-2-2-3	21 137	6	232.1	2.4	63.2	10.9	19.7	1.1

Table 5.5 The sub-categories of sub-axle vehicles found at a span length of 25 m

Sub-category	Total vehicles	Vehicles in tail	Sag [kNm]		GVM [t]		Vehicle length [m]	
			μ	σ	μ	σ	μ	σ
5: 2-3	35 951	29	2 079.4	135.3	48.1	3.7	10.6	0.1
5: 1-2-2	238 951	65	2 024.2	114.9	46.0	4.0	11.3	2.2
5: 1-2-1-1	39 712	6	2 003.6	78.8	49.0	1.5	16.1	2.9
5: 1-1-3	68 228	12	1 992.6	54.9	43.2	2.8	10.8	1.7
6: 1-2-3	2 159 553	108	2 531.3	82.5	65.7	3.6	14.4	1.2
7: 1-3-3	580	2	2 666.8	120.4	77.8	3.3	16.4	0.1
7: 1-2-2-2	3 012 571	110	2 494.8	105.9	69.9	5.2	18.5	2.3
8: 1-2-2-3	21 137	2	2 697.3	50.7	78.2	3.0	19.1	0.5
8: 1-2-3-2	73 586	110	2 614.2	87.9	71.8	3.4	19.6	1.2

Table 5.6 The sub-categories of sub-axle vehicles found at a span length of 50 m

Sub-category	Total vehicles	Vehicles in tail	Sag [kNm]		GVM [t]		Vehicle length [m]	
			μ	σ	μ	σ	μ	σ
5: 2-3	35 951	27	5 079.1	321.9	49.0	3.2	10.8	0.9
5: 1-2-2	238 951	70	4 952.7	237.8	48.8	2.5	12.9	1.9
5: 1-2-1-1	39 712	10	4 915.3	158.2	48.5	1.4	16.2	3.4
5: 1-1-3	68 228	5	4 828.3	134.9	46.3	2.8	12.4	1.7
6: 2-2-2	71 188	3	6 910.4	410.96	64.6	3.9	10.5	0.2
6: 1-2-3	2 159 553	104	6 618.6	224.8	67.0	2.4	14.8	0.9
7: 1-3-3	580	3	7 160.8	471.4	76.3	3.4	17.3	1.3
7: 1-2-2-2	3 012 571	109	6 875.4	290.5	71.9	3.1	19.3	1.6
8: 1-2-2-3	21 137	2	7492.9	233.8	78.2	3.0	19.1	0.5
8: 1-2-3-2	73 586	110	7040.8	231.6	72.5	2.5	19.9	0.9

The axle masses and spacings recorded in Table 5.7 and Table 5.8, respectively, were based on all the vehicles of each sub-category that appeared in the entire WIM data set, not just the tail of their respective sub-axle groups. For the axle-groups found in the different sub-categories, the mean spacing between adjacent axles ranged from 0.8 m to 1.4 m.

Table 5.7 Axle masses recorded for each sub-category group

Sub-category	M1 [t]		M2 [t]		M3 [t]		M4 [t]		M5 [t]		M6 [t]		M7 [t]		M8 [t]	
	μ	σ	μ	σ	μ	σ	μ	σ	μ	σ	μ	σ	μ	σ	μ	σ
5: 2-3	6.1	1.8	6.1	1.8	4.1	1.8	4.0	1.8	4.2	1.8	-	-	-	-	-	-
5: 1-1-3	5.4	1.0	6.5	1.7	3.9	1.5	4.0	1.4	4.2	1.4	-	-	-	-	-	-
5: 1-2-2	5.7	1.2	6.1	2.1	5.1	1.6	5.1	2.0	5.5	2.0	-	-	-	-	-	-
5: 1-2-1-1	5.1	1.2	3.8	1.8	4.0	1.4	4.3	1.5	3.6	1.4	-	-	-	-	-	-
6: 1-2-3	5.9	1.0	6.5	1.8	6.5	1.8	5.3	1.9	5.4	1.8	5.7	1.9	-	-	-	-
6:2-2-2	6.3	1.8	6.2	1.7	5.4	1.8	5.5	1.9	4.9	1.8	4.9	1.8	-	-	-	-
7: 1-2-2-2	5.9	1.0	6.4	1.8	6.4	1.7	6.3	2.0	6.7	2.0	5.9	2.0	6.0	2.0	-	-
7:1-2-3-1	6.3	1.0	7.8	1.4	7.8	1.3	7.0	1.5	6.9	1.5	6.9	1.4	5.7	2.0	-	-
7:1-3-3	6.2	1.5	7.9	1.7	7.8	2.6	1.4	2.5	6.4	2.0	6.6	1.9	6.7	1.9	-	-
8: 1-2-2-3	5.6	1.0	5.5	1.7	5.7	1.7	5.6	1.8	6.0	1.8	4.6	1.7	4.4	1.5	4.4	1.6
8: 1-2-3-2	5.9	0.9	6.2	1.6	6.3	1.5	6.2	1.9	6.1	1.7	6.1	1.8	5.0	1.9	5.2	2.0

Table 5.8 Axle spacings recorded for each sub-category group

Sub-category	S1 [m]		S2 [m]		S3 [m]		S4 [m]		S5 [m]		S6 [m]		S7 [m]	
	μ	σ	μ	σ	μ	σ	μ	σ	μ	σ	μ	σ	μ	σ
5: 2-3	1.3	0.1	7.1	0.6	1.3	0.1	1.3	0.1	-	-	-	-	-	-
5: 1-1-3	3.6	0.2	6.8	1.1	1.3	0.1	1.3	0.1	-	-	-	-	-	-
5: 1-2-2	4.1	1.1	1.3	0.1	7.7	1.2	1.3	0.1	-	-	-	-	-	-
5: 1-2-1-1	3.8	0.9	1.3	0.1	6.8	1.4	5.9	1.3						
6: 1-2-3	3.3	0.4	1.3	0.1	7.2	0.6	1.3	0.0	1.3	0.0	-	-	-	-
6:2-2-2	1.3	0.1	6.0	0.8	1.3	0.0	5.7	0.9	1.3	0.0	-	-	-	-
7: 1-2-2-2	3.3	0.3	1.3	0.1	6.0	0.8	1.3	0.0	5.7	0.9	1.3	0.0	-	-
7:1-2-3-1	3.3	0.2	1.3	0.0	7.4	0.3	1.4	0.0	1.4	0.0	4.2	0.3	-	-
7:1-3-3	3.3	0.4	1.3	0.2	1.1	0.3	6.6	0.9	1.3	0.1	1.3	0.1	-	-
8: 1-2-2-3	3.2	0.3	1.3	0.1	5.1	0.8	1.3	0.0	5.9	0.6	1.3	0.1	1.3	0.1
8: 1-2-3-2	3.2	0.3	1.3	0.0	6.5	0.7	1.3	0.0	1.3	0.1	4.5	0.8	1.3	0.1

From this point onwards, a new naming convention was used to represent the different sub-categories for ease of reference. The different sub-categories were named according to the sub-axle group they formed apart of and numbered C1, C2 … Cn according to the number of sub-categories in the group. In this naming convention, C stood for "category".

In Table 5.9, the naming convention used in this study for the different sub-categories was recorded as well as a reference that confirmed that these vehicles exist. No reference was found for the 6: 2-2-2 vehicle group. It was assumed that the vehicles recorded in this group were because of an error with the WIM recording, hence their data were regarded as being erroneous records. While a record was found for a 7: 1-3-3 vehicle, it was not a local reference and since there were only 580 of these vehicles recorded, it might have been an erroneous vehicle record as well.

Table 5.9 Sub-categories naming convention

Category	Notation	Reference
5-axle C1	5: 2-3	(Volvo, 2016)
5-axle C2	5: 1-1-3	(Bosman, 2004)
5-axle C3	5: 1-2-2	(Bosman, 2004)
5-axle C4	5: 1-2-1-1	(Bosman, 2004)

Category	Notation	Reference
6-axle C1	6: 1-2-3	(Bosman, 2004)
6-axle C2	6:2-2-2	

Category	Notation	Reference
7-axle C1	7: 1-2-2-2	(Bosman, 2004)
7-axle C2	7:1-2-3-1	(Media Digital, 2017)
7-axle C3	7:1-3-3	(Province of Novascotia, 2015)

Category	Notation	Reference
8-axle C1	8: 1-2-2-3	(Bosman, 2004)
8-axle C2	8: 1-2-3-2	(Bosman, 2004)

Once the new naming convention was assigned to each sub-category, the next step was to create the GPP plots and determine the characteristic values for each sub-category. The GPP plots for all sub-categories at each span length were shown in Appendix F. In the following sections, each of these sub-categories was analysed, and possible causes of the underlying Fréchet distributions were discussed. The cells highlighted in grey in the characteristic value tables represent the data sets for which an underlying Fréchet distribution was obtained unless otherwise stated.

5.3.2. Five axle vehicles:

In this section, the different LEs produced by the different sub-categories of 5-axle vehicles are analysed. Furthermore, the different sub-categories' influence on the parent sub-axle group is noted, and underlying distributions of the sub-categories are investigated.

5.3.2.1. GPP plots

The GPP plots for the sub-categories at 5 m, 20 m, 25 m and 50 m were recorded in Figure 5.5, Figure 5.6 and Figure 5.7 for the hogging moments, sagging moment and shear forces, respectively. The GPP plots for the rest of the spans were recorded in Figure F.1, Figure F.2 and Figure F.3.

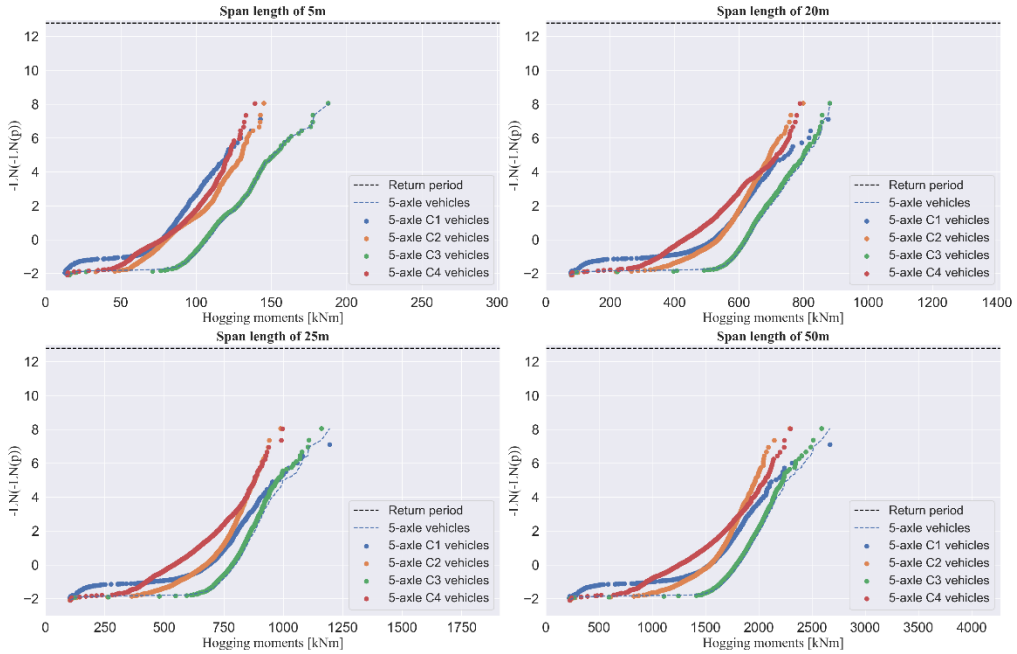

Figure 5.5 Hogging moments GPP plots for the 5-axle sub-categories

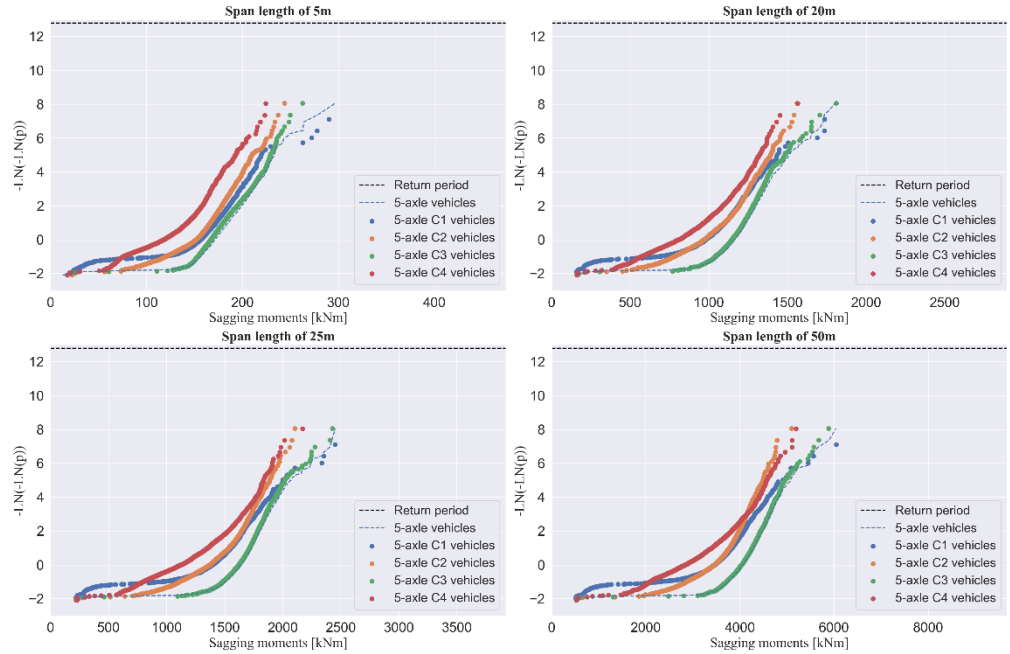

Figure 5.6 Sagging moments GPP plots for the 5-axle sub-categories

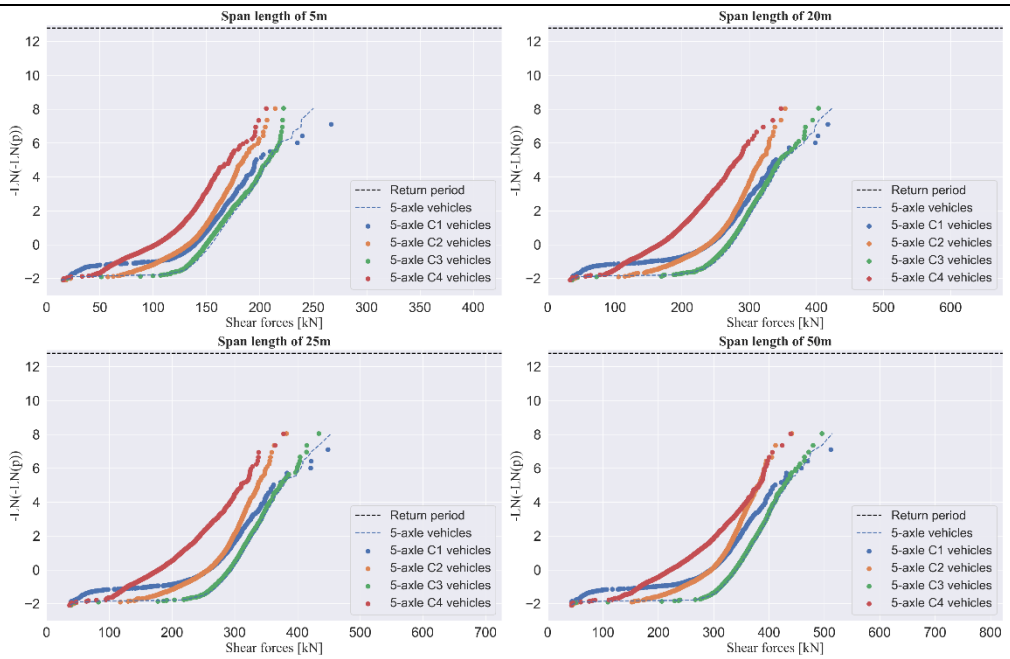

Figure 5.7 Shear forces GPP plots for the 5-axle sub-categories

In the GPP plots, the 5-axle vehicles plots were seen to closely follow the 5-axle C3 plots. This showed that the 5-axle C3 group was the dominant 5-axle sub-category. From the GPP plots, it was seen that the 5-axle C1 group influenced the 5-axle vehicles plots causing it to deviate away from the 5-axle C3 plots. This happened because the 5-axle C1 group was seen to produce the highest LEs at every span except for at 5 m and 20 m for the hogging moments and at 20 m for the sagging moments.

5.3.2.2. Characteristic LEs

After obtaining the GPP plots, the characteristic values were predicted for the 5-axle C1, C2, C3, and C4 groups and recorded in Table 5.10. As shown in Table 5.12, there were still plots with an underlying Fréchet distribution even after splitting the 5-axle vehicles into the different sub-categories. For the different sub-categories, 65%, 14%, 68% and 0% of the plots had an underlying Fréchet distribution for the 5-axle C1, C2, C3 and C4 vehicle groups, respectively. This meant that the 5-axle C2 group was the most *iid* of all the groups, and yet it was not wholly *iid*, as there were still plots that had an underlying Fréchet distribution being found. This went against the theory that traffic loads should fit a Weibull distribution. Overall, 57% of the plots had an underlying Weibull distribution, which was 47% more than what was found for the 5-axle group.

Table 5.10 Characteristic values for the 5-axle sub-categories

Span length [m]	5-axle C1 group			5-axle C2 group			5-axle C3 group			5-axle C4 group		
	Hog [kNm]	Sag [kNm]	Shear [kN]	Hog [kNm]	Sag [kNm]	Shear [kN]	Hog [kNm]	Sag [kNm]	Shear [kN]	Hog [kNm]	Sag [kNm]	Shear [kN]
5	200	592	489	156	292	250	377	277	249	105	169	143
10	707	2 170	837	496	755	314	697	680	430	301	388	184
15	1 097	2 783	618	718	1 186	352	871	2 070	748	522	706	231
20	1 397	2 163	576	854	1 700	392	988	2 227	561	668	1 002	260
25	1 329	2 932	618	1 077	2 268	429	1 329	2 992	610	822	1 484	291
30	1 750	4 319	674	1 321	2 774	472	1 633	3 714	598	981	1 999	322
35	2 094	4 742	677	1 567	3 367	480	3 015	4 714	654	1 221	2 518	337
40	2 321	5 471	697	1 844	4 225	436	2 220	5 609	730	1 426	3 104	348
45	2 643	6 814	665	2 113	4 612	466	2 546	6 811	706	1 648	3 557	354
50	2 972	7 334	699	2 377	5 100	505	2 888	7 872	755	1 870	4 103	360

5.3.2.3. Investigating underlying distributions

By removing various numbers of values from the end of the tail of the different sub-category data sets, it was seen that it was possible to obtain an underlying Weibull distribution. Figure 5.8 shows an example of how the extrapolation plots were affected by excluding values from the end tail of hogging moments for the 5-axle C1 group at 20 m. Extrapolation plot 1 was based on all the hogging moments in the tail and had an underlying Fréchet distribution. Extrapolation plot 2 was based on all the values in the tail except the last three and had an underlying Weibull distribution. This meant that a minimum of three values had to be excluded before an underlying Weibull distribution was found. Excluding more values still resulted in an underlying Weibull distribution.

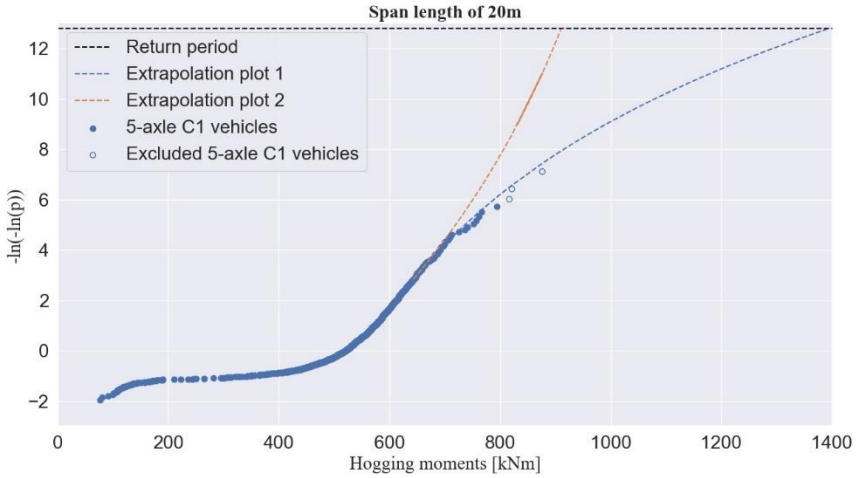

Figure 5.8 GPP plot predictions after removing LEs from tail of the 5-axle C1 group

In Table 5.11, Table 5.12 and Table 5.13, the minimum number of LEs that had to be excluded from the tail of the data sets for the different sub-categories to obtain an underlying Weibull distribution was recorded. In addition, the characteristic values predicted and the maximum LEs before any were removed, was also recorded. Note that the cells shaded in grey in these tables highlight occurrences where a lower characteristic value is predicted than the removed maximum LE. The importance of this is discussed at the end of this chapter in Section 5.3.6.

Table 5.11 Forced Weibull data sets for the 5-axle subcategories for the hogging moments

Span length [m]	Tail LEs removed				Characteristic value [kNm]				Maximum LE [kNm]			
	C1	C2	C3	C4	C1	C2	C3	C4	C1	C2	C3	C4
5	1	-	7	-	171	156	189	148	142	145	187	139
10	1	1	4	-	541	436	499	511	534	436	501	423
15	2	-	3	-	770	718	791	825	748	666	713	640
20	3	-	0	-	911	854	988	1036	876	798	881	788
25	-	-	8	-	1 329	1 077	1 148	1038	1 195	988	1 161	997
30	-	-	-	-	1 750	1 321	1 633	1299	1 501	1 261	1 458	1 266
35	-	-	2	-	2 094	1 567	1 824	1 571	1 799	1 525	1 747	1 531
40	-	-	-	-	2 321	1 844	2 220	1 847	2 092	1 785	2 031	1 790
45	-	-	-	-	2 643	2 113	2 546	2 135	2 381	2 040	2 311	2 045
50	-	-	-	-	2 972	2 377	2 888	2 398	2 668	2 292	2 589	2 298

Table 5.12 Forced Weibull data sets for the 5-axle subcategories for the sagging moments

Span length [m]	Tail LEs removed				Characteristic value [kNm]				Maximum LE [kNm]			
	C1	C2	C3	C4	C1	C2	C3	C4	C1	C2	C3	C4
5	3	-	-	3	290	292	277	263	290	243	262	224
10	3	1	-	-	267	709	680	608	767	629	617	544
15	2	-	3	-	1224	1186	1228	1062	1224	1048	1180	1005
20	-	-	3	-	1 736	1700	1 937	1588	1736	1560	1 810	1564
25	-	-	4	-	2 450	2 268	2 628	2197	2 450	2103	2 427	2 169
30	2	-	2	-	3 187	2 774	3 385	2904	3 168	2 629	3 102	2 766
35	1	-	2	-	4 236	3 367	4 029	3 561	3 893	3 228	3 793	3 377
40	-	-	1	-	5 471	4 225	4 855	4 213	4 601	3 847	4 497	3 976
45	1	-	1	-	5 521	4 612	5 605	4 766	5 326	4 477	5 190	4 579
50	1	-	1	-	6 372	5 100	6 316	5 427	6 047	5 343	5 884	5 190

Table 5.13 Forced Weibull data sets for the 5-axle subcategories for the shear forces

Span length [m]	Tail LEs removed				Characteristic value [kNm]				Maximum LE [kNm]			
	C1	C2	C3	C4	C1	C2	C3	C4	C1	C2	C3	C4
5	3	-	0	5	237	224	249	233	266	214	222	205
10	3	-	3	3	287	314	337	288	303	271	297	250
15	2	-	5	2	414	352	385	338	371	320	360	295
20	2	-	4	-	443	392	446	401	417	353	403	347
25	2	-	3	-	475	429	479	415	448	382	434	377
30	2	1	3	-	492	408	488	425	469	402	454	398
35	2	1	4	-	504	426	504	434	484	416	469	412
40	2	-	5	-	493	436	498	442	495	426	480	423
45	1	-	5	-	552	466	498	452	504	434	488	432
50	1	-	4	-	544	505	526	459	511	441	495	439

The vehicles were excluded from the tail as per Table 5.11, Table 5.12 and Table 5.13 were investigated for each LE. This was to identify possible causes for the variability found in the tail of the LEs.

For the 5-axle C1 groups' hogging moments a minimum of one and a maximum of three vehicles had to be removed before an underlying Weibull distribution could be obtained. In Figure 5.9, the distribution of the 5-

axle C1 vehicles sum of axles, spacing between outer axles and the hogging moments at 5 m and 10 m was shown. At 5 m, different loading combinations were found where a different number of axles were present on the bridge at the time the daily max hogging moment occurred. At 5 m, 22% of the daily max hogging moments were caused by two axles, 55% by three axles, 17% by four axles and 5% due to all five axles. From a span length of 10 m onwards, all the axles for each vehicle were present on the bridge at the time of daily maxima hogging moment recording. This meant that from 10 m onwards the GVM was an important feature to analyse.

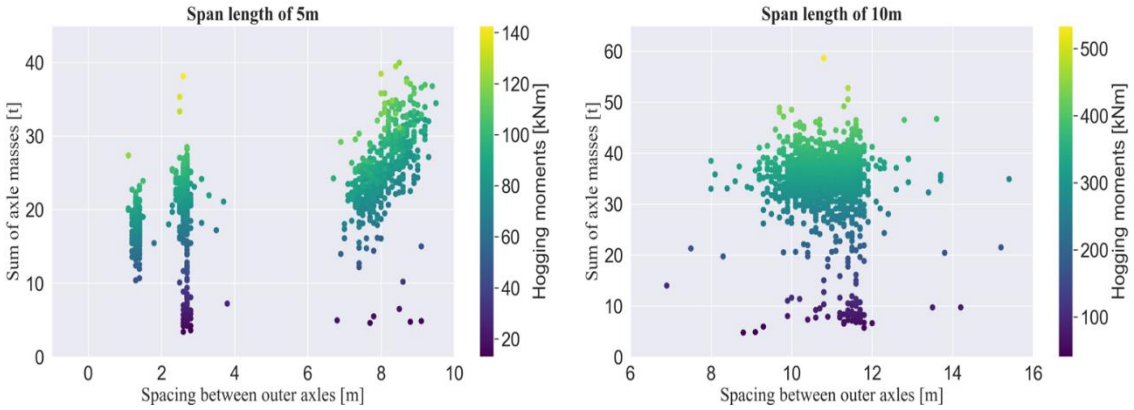

Figure 5.9 Distribution of the 5-axle C1 vehicles sum of axle masses, outer axle spacings and hogging moments at 5 m and 10 m

In Figure 5.10, the distribution of the 5-axle C1 vehicles sum of axles, spacing between outer axles and the tail hogging moments at 5 m was shown as well as a sum of axles versus hogging moment plot. Only 3% of the tail hogging moments were caused by only the tandem axle of the vehicle, while 25% was caused by only the tridem axles. The rest of the tail hogging moments were due to a combination of the axle groups, where 31% of them were due to there being four axles on the bridge, while 40% was caused by all five axles on the bridge. At 5 m only one tail hogging moment had to be removed for an underlying Weibull distribution to be obtained. The highest hogging moment was caused by only the tridem axle of a vehicle and yet it had the fourth-highest sum of axle masses of all the values in the tail.

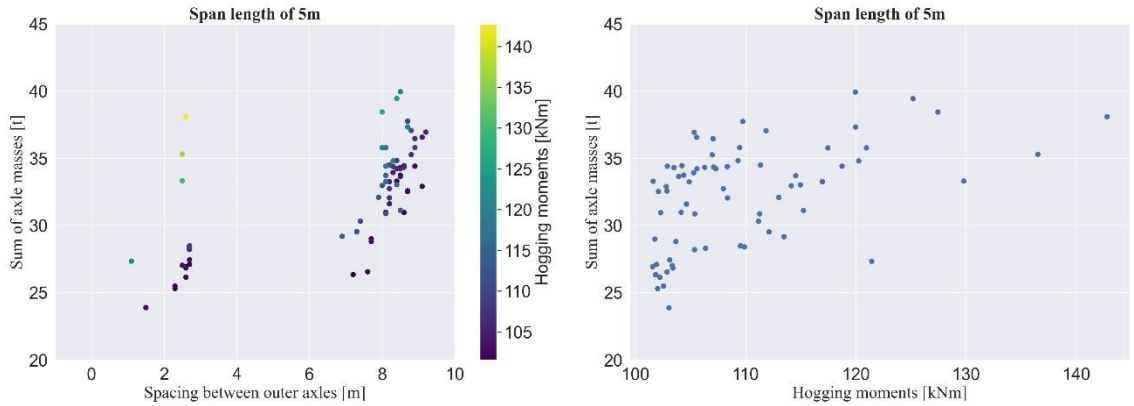

Figure 5.10 Graphs used for analysis of the 5-axle C1 vehicles responsible for the tail hogging moments at 5 m

In Figure 5.11, the distribution of the 5-axle C1 vehicles GVM, vehicle length and the tail hogging moments at 20 m was shown as well as a GVM versus hogging moment plot. At this span, a minimum of three values had to be removed for an underlying Weibull distribution to be obtained. In Table 5.14 and Table 5.15, the mean and standard deviation for the GVM, axle masses, vehicle length and axle spacings for 5-axle C1 vehicles

that were responsible for the tail hogging moments at 20 m were recorded. After analysing the top three vehicles, their mean GVM was found to be 23% heavier than the mean GVM for the other vehicles in the tail.

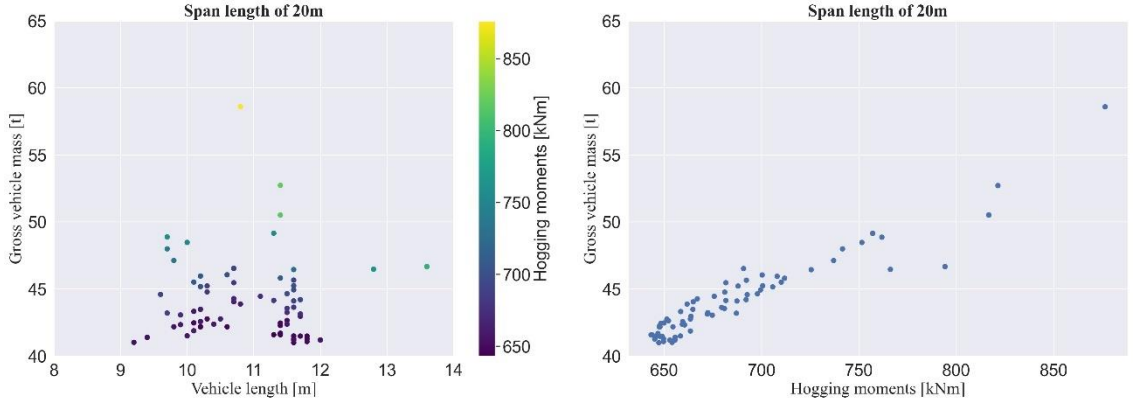

Figure 5.11 Graphs used for analysis of the 5-axle C1 vehicles responsible for the tail hogging moments at 20 m

Table 5.14 GVM and Axle masses comparison for the 5-axle C1 group hogging moments at 20 m

Tail region	GVM [t]		M1[t]		M2[t]		M3[t]		M4[t]		M5[t]	
	μ	σ	μ	σ	μ	σ	μ	σ	μ	σ	μ	σ
Top three	53.9	3.4	9.5	2.9	8.9	2.4	13.3	0.8	11.8	0.4	10.6	1.9
Rest of tail	43.8	2.1	9.7	1.3	9.3	1.2	8.2	1.4	8.3	1.2	8.3	1.3

Table 5.15 Vehicle length and axle-spacing comparison for the 5-axle C1 group hogging moments at 20 m

Tail region	Length[m]		S1[m]		S2[m]		S3[m]		S4[m]	
	μ	σ	μ	σ	μ	σ	μ	σ	μ	σ
Top three	11.2	0.3	1.3	0.1	7.4	0.2	1.3	0.1	1.3	0.1
Rest of tail	10.9	0.9	1.3	0.1	6.9	0.8	1.3	0.1	1.3	0.1

In Figure 5.12, the distribution of the 5-axle C1 vehicles GVM, vehicle length and the tail hogging moments at 25 m was shown as well as the GVM versus hogging moment plot. From this span onwards all the hogging moment data sets had underlying Weibull distribution. The same vehicles responsible for the top three hogging moments at 20 m caused the top three hogging moments at 25 m and yet an underlying Weibull distribution had still been obtained. From a comparison between Figure 5.11 and Figure 5.12, it was seen that the two circled values, no longer produced the fourth and fifth-highest hogging moments as they did at 20 m. With each span increment, the shorter vehicles started to produce higher hogging moments than longer vehicles with the same GVM.

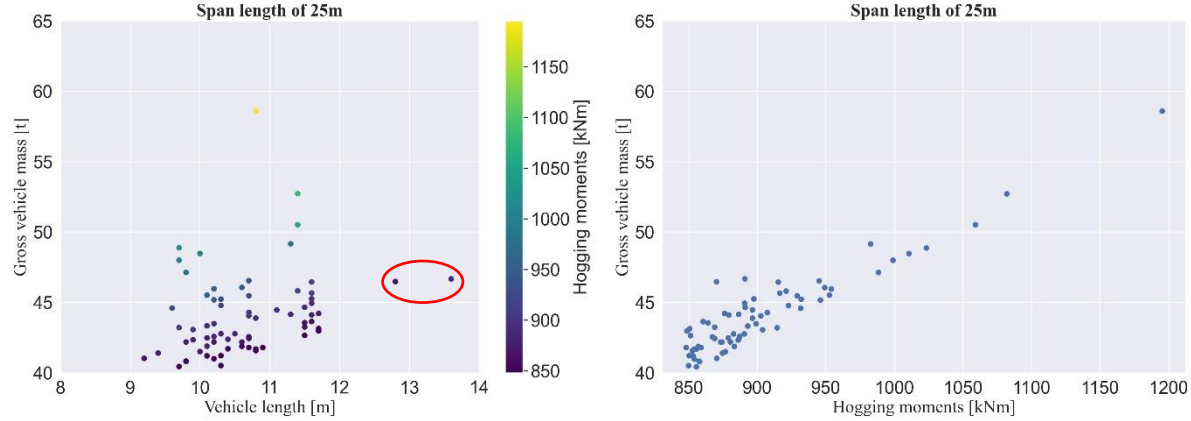

Figure 5.12 Graphs used for analysis of the 5-axle C1 vehicles responsible for the tail hogging moments at 25 m

For the 5-axle C1 groups' sagging moments a minimum of one and a maximum of three vehicles had to be removed before an underlying Weibull distribution could be obtained. In Figure 5.13, the distribution of the 5-axle C1 vehicles sum of axles, spacing between outer axles and the hogging moments at 5 m to 20 m was shown. At the shorter spans, the axle groups were the dominant cause of the daily sagging moments. As the span length increased more axles could fit on the bridge, shifting away from the axle groups being the dominant cause of the daily max sagging moments. At a span length of 20 m, 95% of the daily max sagging moments were caused by the entire vehicle being on the bridge. From 25 m, all the axles for each vehicle were present on the bridge at the time of daily maxima sagging moment recording. This meant that from 25 m onwards the GVM was an important feature to analyse.

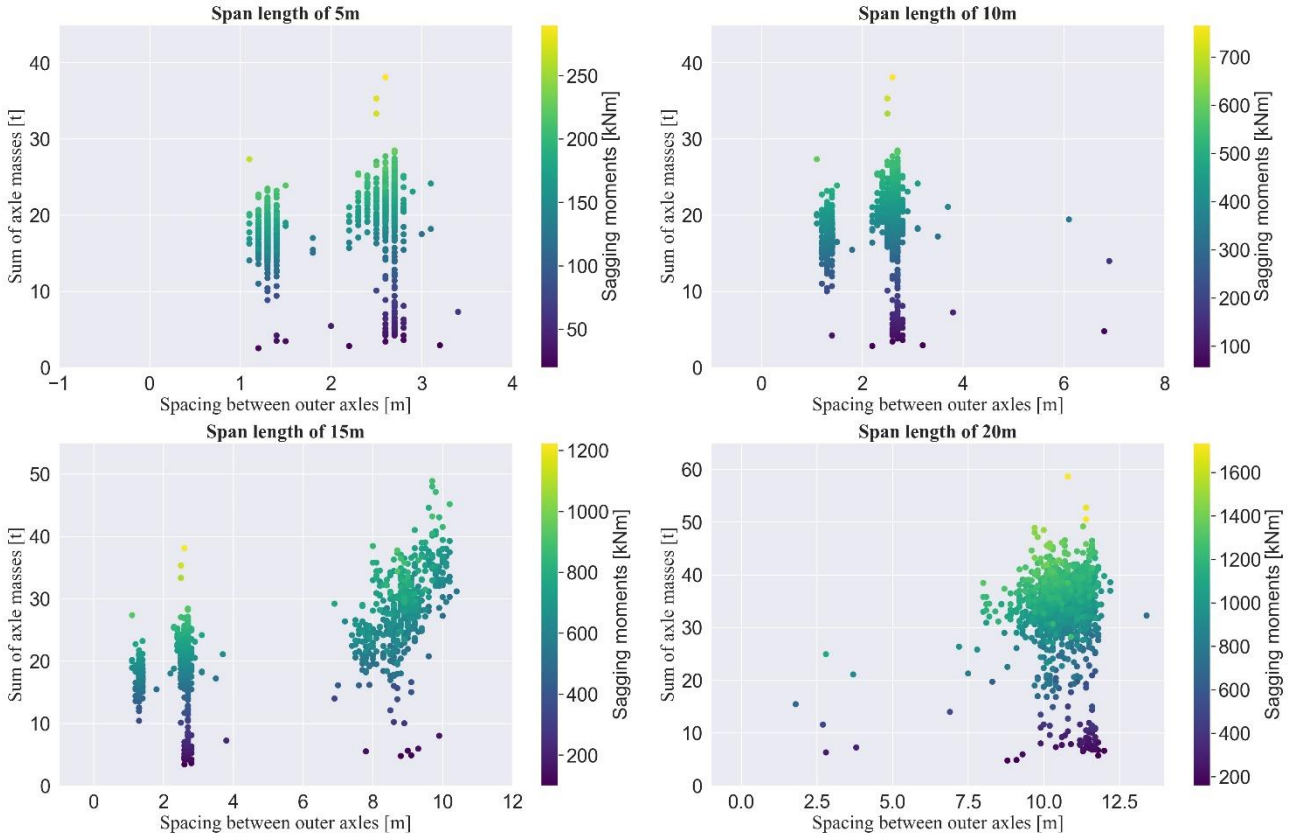

Figure 5.13 Distribution of the 5-axle C1 vehicles sum of axle masses, outer axle spacings and sagging moments from 5 m to 20 m

For the tail of the 5-axle C1 groups' sagging moments at 5 m and 10 m, the tridem axle group was the dominant cause of the daily max sagging moment. At 5 m 27% of the values in the tail were due to the tandem axle group, while the tridem axle group caused 73% of them. In Table 5.16 and Table 5.17, the mean and standard deviation for the GVM, axle masses, vehicle length and axle spacings for 5-axle C1 vehicles that were responsible for the tail sagging moments at 5 m were recorded. The top three vehicles were seen to be slightly heavier but had similar lengths to the other trucks in the tail. Since the tridem axle was responsible for most of the sagging moments, it was essential to analyse. The tridem axle group for the top three vehicles had a mean axle group mass of 35.3 t. In contrast, the tridem axle group for the rest of the tail produced a daily max sagging moment that had a mean axle-group mass of 25.9 t, which was over a 36% difference.

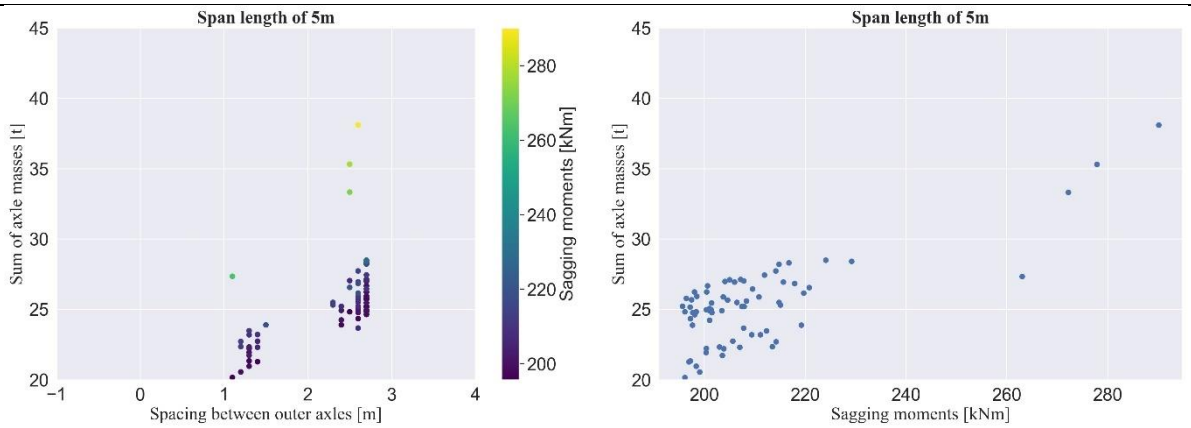

Figure 5.14 Graphs used for analysis of the 5-axle C1 vehicles responsible for the tail sagging moments at 5 m

Table 5.16 Vehicle GVM and axle-masses comparison for the 5-axle C1 group sagging moments at 5 m

Tail region	GVM [t]		M1[t]		M2[t]		M3[t]		M4[t]		M5[t]	
	μ	σ	μ	σ	μ	σ	μ	σ	μ	σ	μ	σ
Top three	53.9	4.2	9.5	3.6	8.9	2.9	13.3	1.0	11.8	0.5	10.6	2.3
Rest of tail	41.9	4.0	9.1	2.0	9.0	2.2	7.8	1.8	8.2	2.1	7.9	2.1

Table 5.17 Vehicle length and axle-spacing comparison for the 5-axle C1 group sagging moments at 5 m

Tail region	Length[m]		S1[m]		S2[m]		S3[m]		S4[m]	
	μ	σ	μ	σ	μ	σ	μ	σ	μ	σ
Top three	11.2	0.4	1.3	0.1	7.4	0.3	1.3	0.1	1.3	0.1
Rest of tail	10.9	0.9	1.3	0.1	7.0	0.9	1.3	0.1	1.3	0.1

In Figure 5.15, the distribution of the 5-axle C1 vehicles GVM, vehicle length and the tail sagging moments at 30 m was shown as well as a GVM versus sagging moment plot. At this span, a minimum of two values had to be removed for an underlying Weibull distribution to be obtained. As the entire vehicle contributed to the span, the most important component to consider was the GVM of these vehicles. The vehicles responsible for the top two tail sagging moments had a GVM of 58.6 t and 52.7 t respectively. The rest of the vehicles responsible for the tail sagging moments had a mean GVM of 43.6 t with a standard deviation of 2.4 t. This was a 34.4% and 20.9% difference. These were the same two vehicles responsible for the highest sagging moment from 30 m to 50 m. The highest of which had to be removed from the data sets at 35 m, 45 m and 50 m to obtain an underlying Weibull distribution.

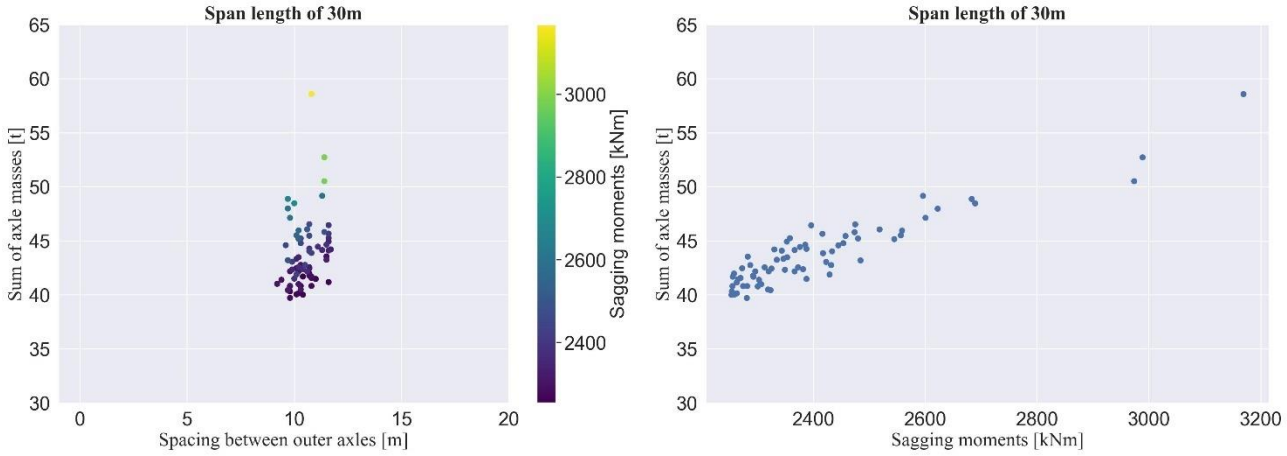

Figure 5.15 Graphs used for analysis of the 5-axle C1 vehicles responsible for the tail sagging moments at 30 m

For the 5-axle C1 groups' shear forces a minimum of one and a maximum of three vehicles had to be removed before an underlying Weibull distribution could be obtained. In Figure 5.16, the distribution of the 5-axle C1 vehicles sum of axles, spacing between outer axles and the shear forces at 5 m to 20 m was shown. For the tail of the 5-axle C1 groups' tail shear forces at 5 m` a total of 25% of the values were due to the tandem axle group, while the tridem axle group caused the other 75% of them. This was very similar to what was seen for the sagging moments. At 10 m only 4% and 19% of the tail shear forces were caused solely due to the tandem and tridem axle groups respectively. The other 52% and 24% of tail shear forces were due to there being four and five axles present on the bridge at the time of the daily max shear forces were recorded. From 15 m onwards, 99% of the daily max shear force were caused by all five axles of each vehicle.

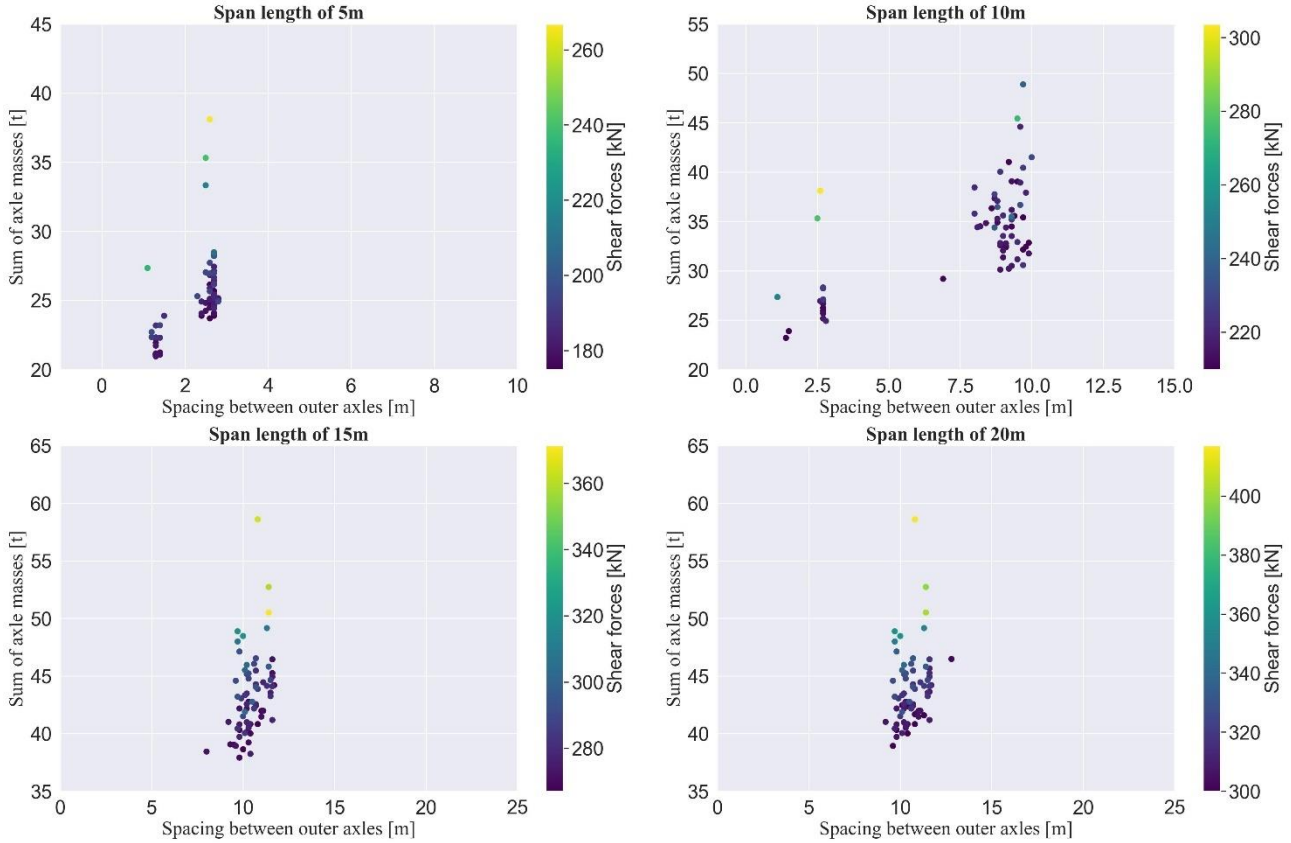

Figure 5.16 Distribution of the 5-axle C1 vehicles sum of axle masses, outer axle spacings and tail shear forces from 5 m to 20 m

At 5 m, three shear forces had to be removed to obtain an underlying Weibull distribution. The top two shear forces were caused by the tridem axle of each respective vehicle while the third-highest shear force recorded was caused by the tandem axle of a vehicle. An analysis of the axle group mass revealed that the top three shear forces had a mean axle group mass of 33.6 t with a standard deviation of 5.6 t. The rest of the vehicles in the tail had a mean axle group mass of 24.9 t with a standard deviation of 2.3 t.

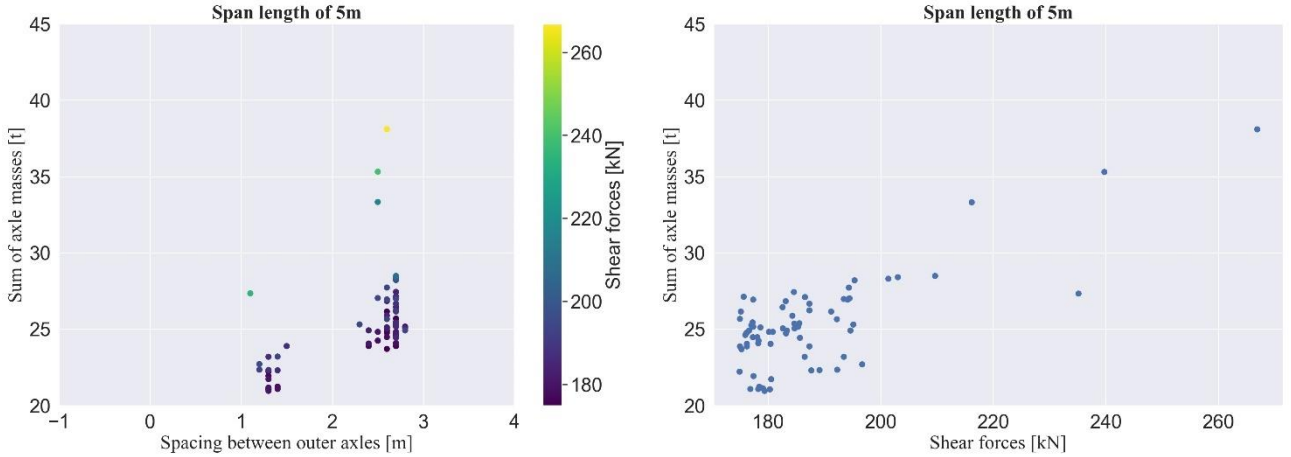

Figure 5.17 Graphs used for analysis of the 5-axle C1 vehicles responsible for the tail shear forces at 5 m

For the longer spans of 15 m onwards where the GVM of the 5-axle vehicles C1 became an important component to analysis. The vehicles that had to be removed to force an underlying Weibull distribution for the shear forces were the same vehicles seen for the sagging moments at 30 m. These vehicles had a mean GVM that was 30 % greater than the rest of the vehicles responsible for the tail shear forces.

Overall, after analysing the 5-axle C1 vehicles responsible for the tail LEs two distinct features were important to analyse. At the shorter span lengths, where the entire vehicle could not fit on the bridge, the different axle groups the critical feature contributing to the LEs found. At the longer span lengths, where the entire vehicle could fit on the bridge, the GVM of the vehicles started to become the most critical feature to analyse. From the analysis of the LEs at all the span lengths, it was seen that the mean difference found in axle masses and axle spacing resulted in significant LE differences. It was theorized that splitting had resulted in a collection of fewer critically loaded vehicles appearing near the end of the tail, which caused more significant LE gaps to be found. By excluding LEs from the end of the tail, the effect of these significant LE gaps was minimized, and after removing enough values, an underlying Weibull distribution could be obtained. A similar situation was seen for the data sets for the other sub-categories of 5-axle vehicles which had an underlying Fréchet distribution.

5.3.3. Six Axle vehicles:

In this section, the different LEs produced by the different sub-categories of 6-axle vehicles are analysed. Furthermore, the different sub-categories' influence on the parent sub-axle group is noted, and underlying distributions of the sub-categories are investigated.

5.3.3.1. GPP plots

The GPP plots for the sub-categories at 5 m, 25 m and 50 m were recorded in Figure 5.18, Figure 5.19 and Figure 5.20 for the hogging and sagging moments and shear forces, respectively. The GPP plots for the rest of the spans were recorded in Figure F.4, Figure F.5 and Figure F.6 in Appendix F.

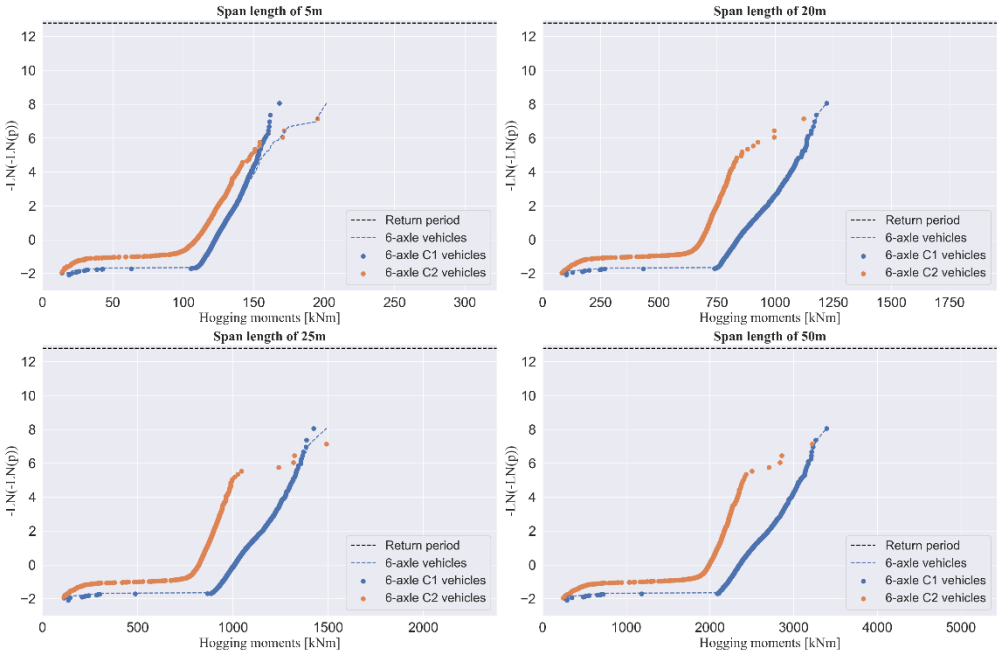

Figure 5.18 Hogging moments GPP plots for the 6-axle sub-categories

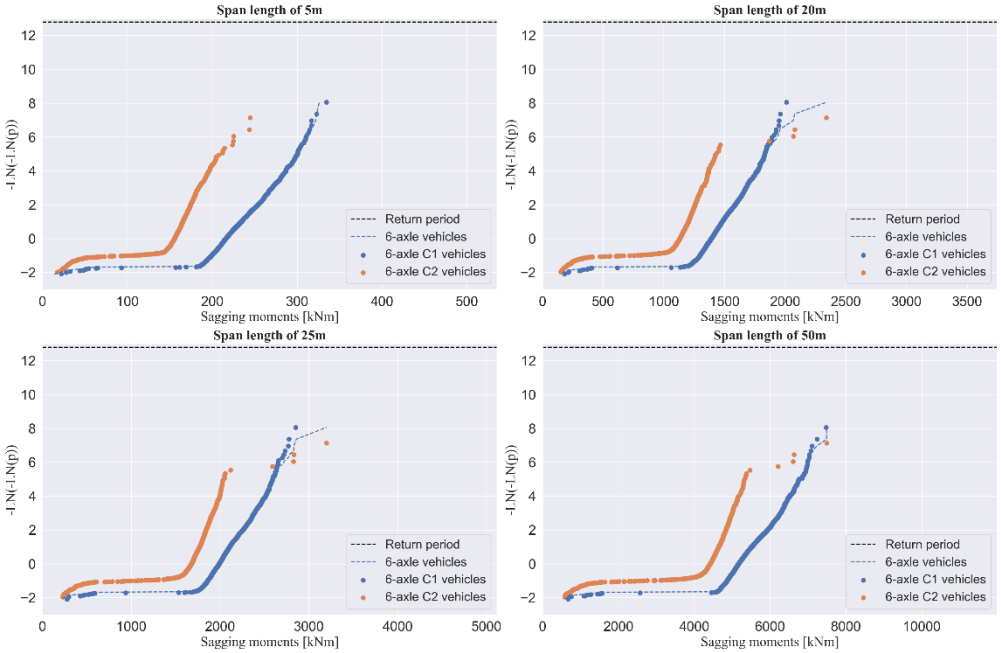

Figure 5.19 Sagging moments GPP plots for the 6-axle sub-categories

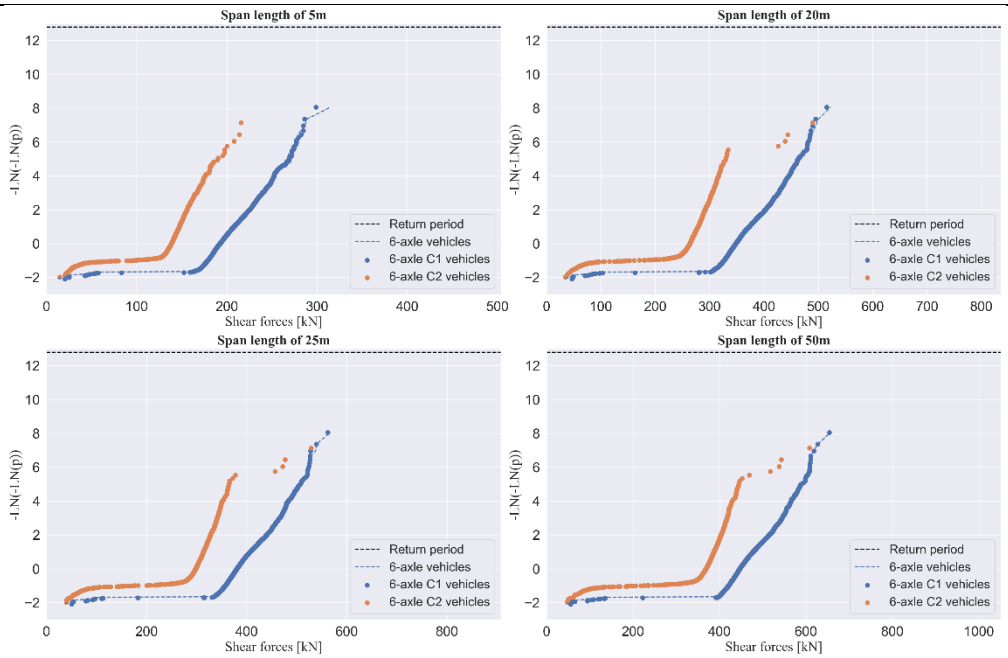

Figure 5.20 Shear forces GPP plots for the 6-axle sub-categories

In general, the 6-axle vehicles plot was seen to follow the same path as the 6-axle C1 groups' plot. However, the 6-axle C2 group occasionally caused the tail of the 6-axle vehicle group to deviate from the 6-axle C1 group. The influence of the 6-axle C2 group resulted in the 6-axle vehicles data sets having an underlying Fréchet distribution. This could be seen by the hogging moments' plot at 5 m, the sagging moments' plot at 20 m and the shear force plot at 15 m. If the 6-axle C2 vehicles were excluded from the WIM data set, then all the 6-axle vehicles LE data sets would have had an underlying Weibull distribution. The removal of the 6-axle C2 vehicles would also result in an underlying Weibull distribution being obtained for the RMA group 3's hogging moment data set at 5 m, the sagging moment data set at 20 m and the shear force data set at 15 m.

5.3.3.2. Characteristic LEs

The characteristic values predicted for the 6-axle C1 group were recorded in Table 5.18. Since the 6-axle C2 group was regarded as being erroneous records no further calculations were done for them. Every data set for the 6-axle C1 group was found to have an underlying Weibull distribution, which indicated that it was *iid*. Since the 6-axle C1 group was the dominant sub-category, it showed why 90% of the 6-axle vehicles' data sets had an underlying Weibull distribution as well.

Table 5.18 Characteristic values for the 6-axle sub-categories

Span length [m]	Hog [kNm]	Sag [kNm]	Shear [kN]
5	182	357	319
10	664	944	388
15	1 033	1 520	470
20	1 286	2 254	563
25	1 487	2 955	590
30	1 937	4 014	668
35	2 350	4 951	684
40	2 753	5 898	686
45	3 155	6 897	715
50	3 561	7 873	706

5.3.3.3. Investigating underlying distributions

In Figure 5.21, the distribution of the 6-axle C1 vehicles sum of axle masses, outer axle spacings and tail sagging moments at 5 m and 30 m was shown, as well as the sagging moments versus the sum of axle masses graphs. As could be seen in the figure, the sagging moments were closely concentrated which resulted in small LE gaps. As a result of the LEs being closely concentrated, an underlying Weibull distribution had been found. This was a similar scene seen for each LE at each span for the 6-axle C1 group, which indicated that the data sets were *iid*.

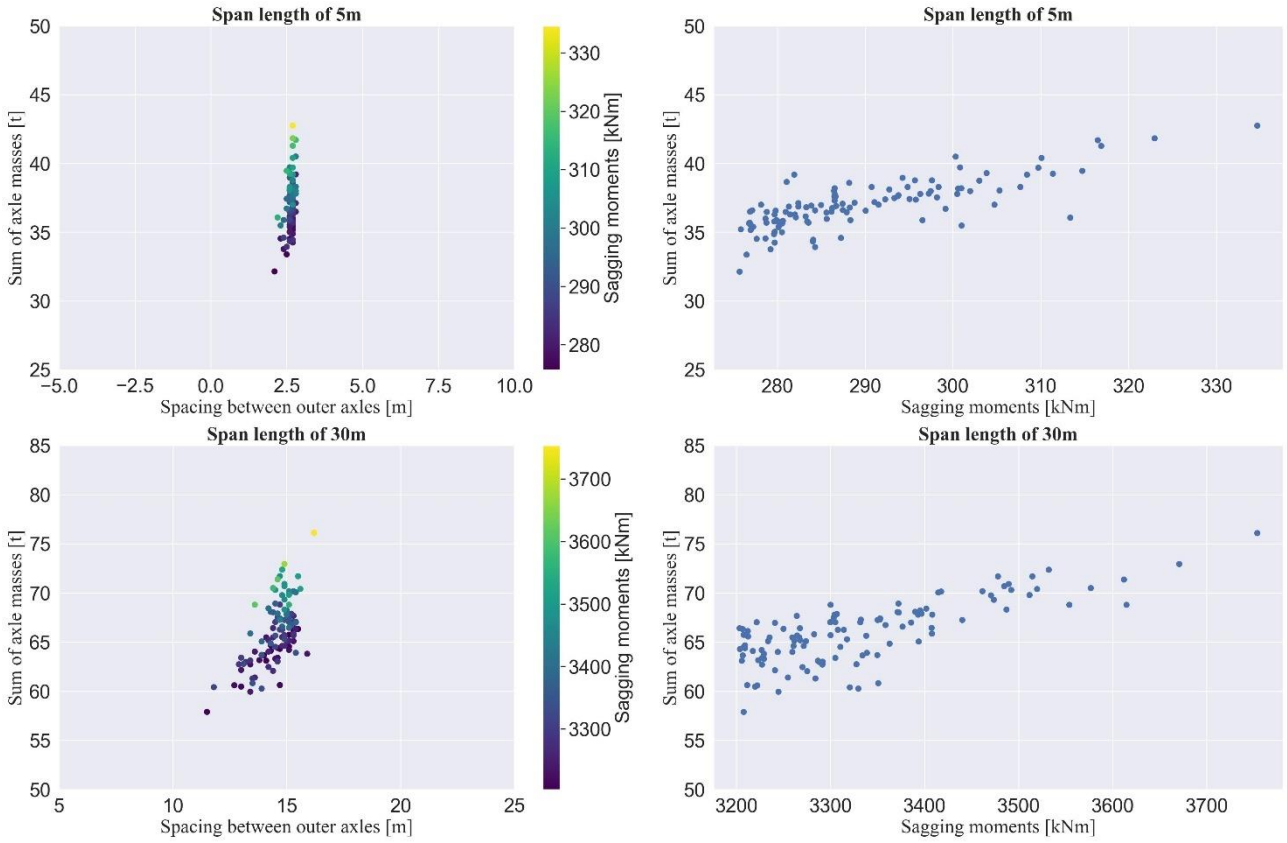

Figure 5.21 Graphs used for analysis of the 6-axle C1 vehicles responsible for the tail sagging moments at 5 m and 30 m

5.3.4. Seven Axle vehicles:

In this section, the different LEs produced by the different sub-categories of 7-axle vehicles are analysed. Furthermore, the different sub-categories' influence on the parent sub-axle group is noted, and underlying distributions of the sub-categories are investigated.

5.3.4.1. GPP plots

The GPP plots for the sub-categories at 5 m, 20 m, 25 m and 50 m were recorded in Figure 5.22, Figure 5.24 and Figure 5.23 for the hogging and sagging moments and shear forces, respectively. The GPP plots for the rest of the spans were recorded in Figure F.7, Figure F.8 and Figure F.9 in Appendix F.

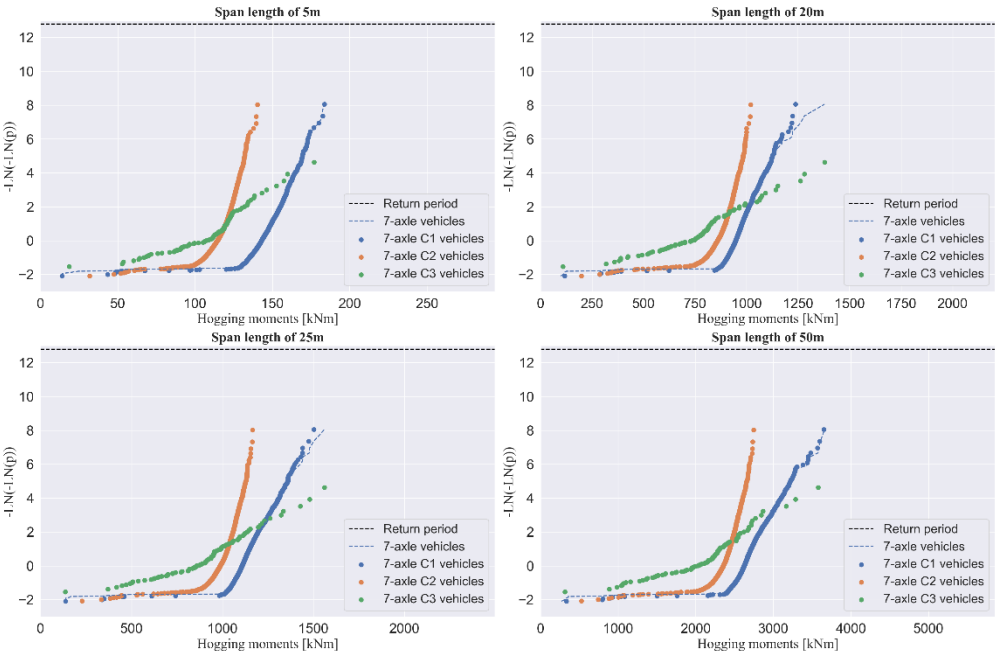

Figure 5.22 Hogging moments GPP plots for the 7-axle sub-categories

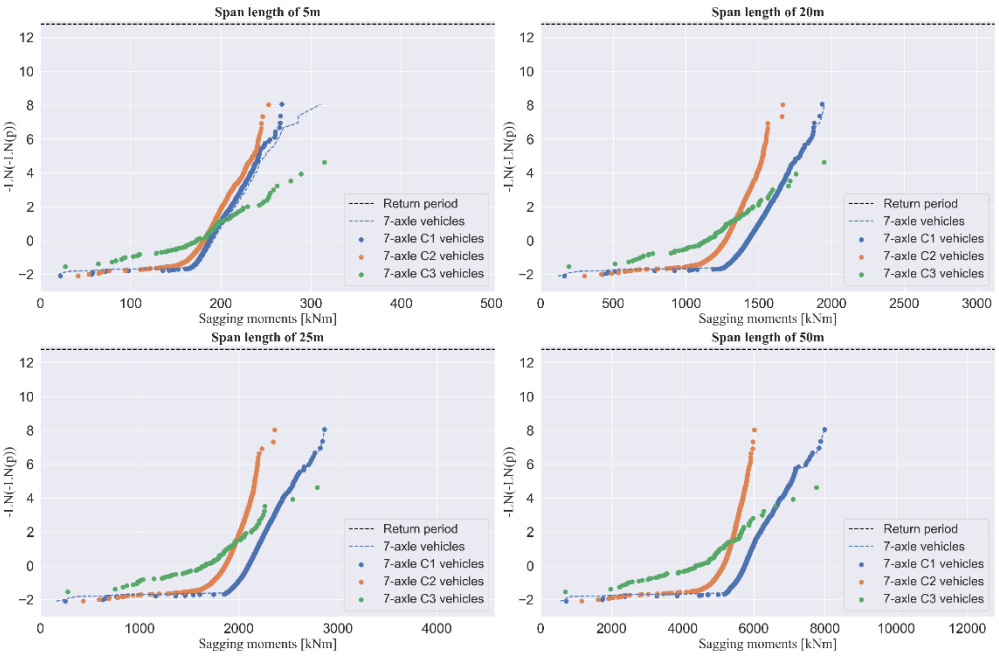

Figure 5.23 Sagging moments GPP plots for the 7-axle sub-categories

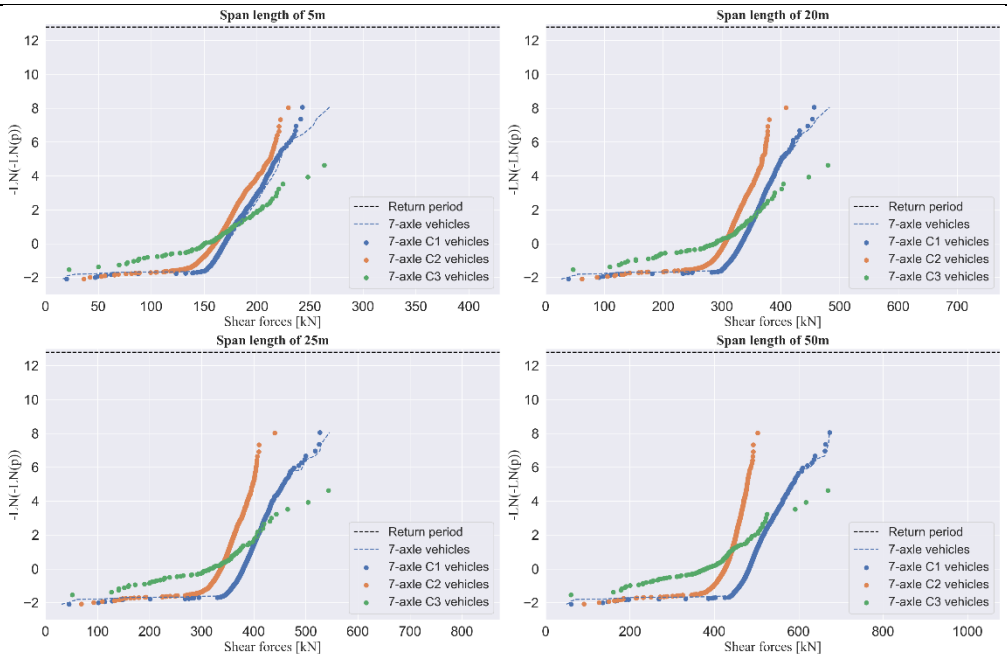

Figure 5.24 Shear forces GPP plots for the 7-axle sub-categories

In the GPP plots, the 7-axle vehicles plot followed the 7-axle C1 groups' plot closely. However, the 7-axle C3 group occasionally caused the 7-axle vehicles plot to deviate from the 7-axle C1 group. The 7-axle C1 group was seen to produce the highest hogging moment at 5m and from 35 m to 50 m, the highest sagging moment from 25 m to 50 m and the highest shear force at 50 m. At every other span for each respective LE, the 7-axle C3 group produced the highest LE.

5.3.4.2. Characteristic LEs

The characteristic values were predicted for the 7-axle C1 and recorded in Table 5.19. Unfortunately, no characteristic values were predicted for the 7-axle C3 group as there was less than a years' worth of data available for it. In general, at least one year of data was recommended for live traffic load modelling Sivakumar, Ghosn and Moses (2008). However, it should be noted that the three 7-axle vehicles seen in Figure 5.1 that caused the deviation of RMA group 3's hogging moment plot at 15 m belonged to the 7-axle C3 group. This meant that the 7-axle C3 group was the cause of the underlying Fréchet distribution found for the RMA group 3's hogging moment data set at 15 m.

Table 5.19 Characteristic values for the 7-axle C1 vehicle

Span length [m]	7-axle C1 group			7-axle C2 group		
	Hog [kNm]	Sag [kNm]	Shear [kN]	Hog [kNm]	Sag [kNm]	Shear [kN]
5	193	301	266	147	255	232
10	565	743	332	503	662	269
15	1 148	1 350	384	830	1 070	361
20	1 408	2 202	561	1 045	1 725	415
25	1 678	3 587	1 055	1 184	2 432	451
30	2 255	4 911	830	1 519	3 195	476
35	2 786	6 008	775	1 859	3 880	485
40	3 312	7 173	783	2 193	4 652	497
45	3 827	8 458	821	2 523	5 436	508
50	4 347	9 817	851	2 846	6 257	521

From Table 5.19, it was seen that all the LE data sets for the 7-axle C2 group had an underlying Weibull distribution, while an underlying Fréchet distribution was found for 63% of the 7-axle C1 LE data sets. A comparison between the data sets for the 7-axle group and the sub-categories of 7-axle vehicles reveals that there had been an increase in the data sets with an underlying Weibull distribution. At the sub-axle splitting level, only 13% of the data sets had an underlying Weibull distribution. At the sub-categories of sub-axle groups splitting level now 68% of all the data sets had an underlying Weibull distribution.

5.3.4.3. Investigating underlying distributions

Although the percentage of data sets with an underlying Weibull distribution had been improved due to splitting, it remained that 32% of all the data sets still had an underlying Fréchet distribution. This meant that splitting the 7-axle vehicle group into its respective sub-populations had not fixed the cause of the underlying Fréchet distribution. Therefore, there had to be some other underlying cause.

Similar to what was done for the sub-categories of 5-axle vehicles, the minimum number of vehicles that had to be removed from the different sub-categories to force a Weibull distribution was determined and recorded in Table 5.20, Table 5.21 and Table 5.22 for the hogging moments, sagging moments and shear forces respectively. In addition, the newly predicted characteristic values, and the maximum LEs recorded before excluding any values were also shown in these tables.

Table 5.20 Forced Weibull data sets for the 7-axle subcategories for the hogging moments

Span length [m]	Tail LEs removed		Characteristic value [kNm]		Maximum LE [kNm]	
	C1	C2	C1	C2	C1	C2
5	-	-	193	147	183	140
10	-	-	565	503	522	490
15	3	-	954	830	930	799
20	-	-	1 408	1 045	1 238	1 019
25	-	-	1 678	1 184	1 502	1 165
30	3	-	2 077	1 519	1 888	1 473
35	2	-	2 605	1 859	2 346	1 782
40	2	-	3 102	2 193	2 790	2 105
45	2	-	3 591	2 523	3 223	2 429
50	2	-	4 097	2 846	3 650	2 747

Table 5.21 Forced Weibull data sets for the 7-axle subcategories for the sagging moments

Span length [m]	Tail LEs removed		Characteristic value [kNm]		Maximum LE [kNm]	
	C1	C2	C1	C2	C1	C2
5	-	-	301	255	267	252
10	-	-	743	662	693	653
15	-	-	1 350	1 070	1 248	1 058
20	-	-	2 202	1 725	1 936	1 665
25	4	-	3 197	2 432	2 866	2 364
30	4	-	4 259	3 195	3 899	3 087
35	4	-	5 371	3 880	4 918	3 825
40	3	-	6 542	4 652	5 945	4 551
45	3	-	7 724	5 436	6 971	5 279
50	4	-	8 581	6 257	7 991	6 017

Table 5.22 Forced Weibull data sets for the 7-axle subcategories for the shear forces

Span length [m]	Tail LEs removed		Characteristic value [kNm]		Maximum LE [kNm]	
	C1	C2	C1	C2	C1	C2
5	-	-	266	232	242	229
10	-	-	332	269	302	267
15	-	-	384	361	373	356
20	2	-	492	415	456	408
25	6	-	533	451	527	440
30	4	-	617	476	575	461
35	3	-	651	485	610	475
40	3	-	670	497	636	487
45	3	-	685	508	657	495
50	3	-	707	521	673	502

The 7-axle C1 group started to have an underlying Fréchet distribution from around span lengths of 15 m to 25 m. where it was seen that a minimum of one to six vehicles had to be removed from the tail before an underlying Weibull distribution was found. After analysing the vehicles responsible for the LEs, a shift started to occur, where the vehicles with the heaviest GVMs started to become responsible for the highest LEs. For example, as seen by Figure 5.25, at a span length of 20 m, the vehicles that produced the top four sagging moments had a sum of axle mass of 55.4 t, 59.6 t, 54.6 t and 64.2 t respectively. From 25 m onwards, the

vehicles that produced the top four sagging moments had a sum of axles of 83.6 t, 82.2 t, 81.6 t and 79.5 t respectively.

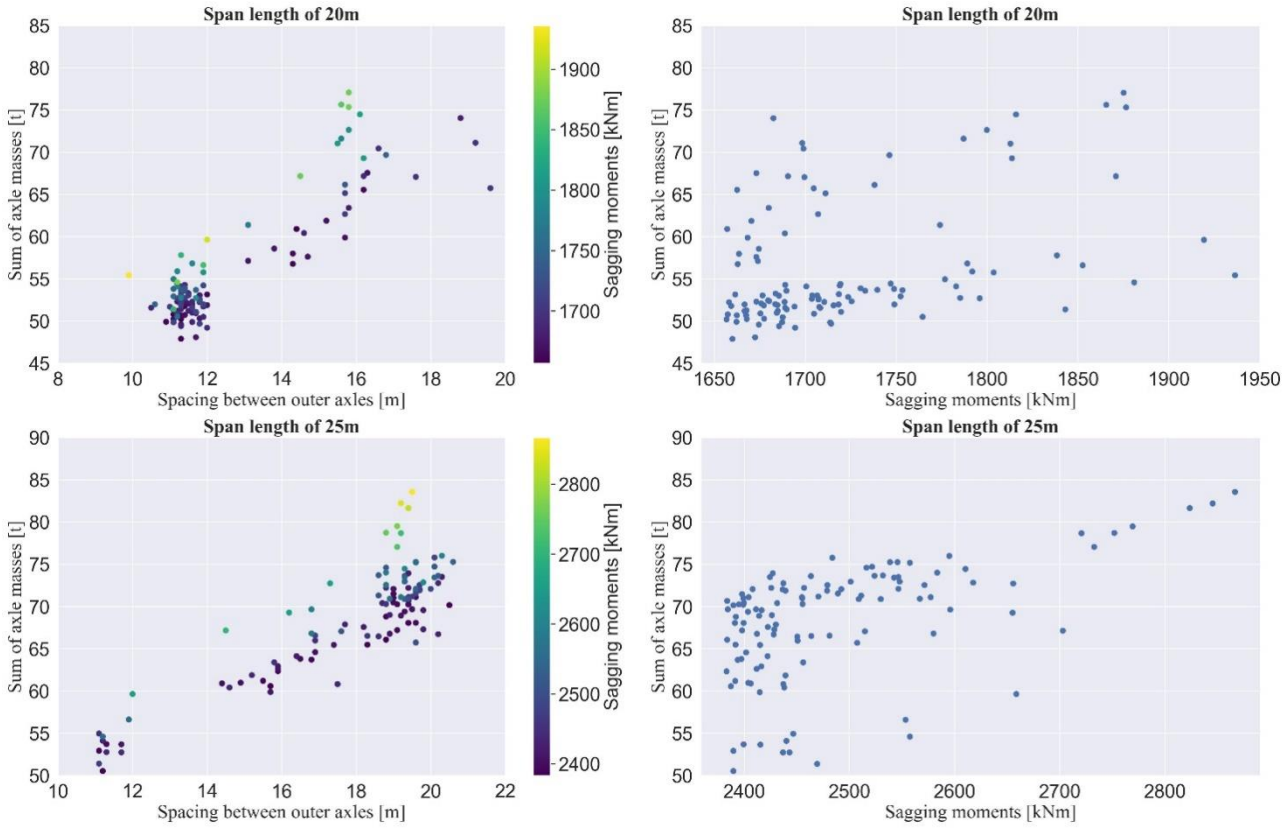

Figure 5.25 Graphs used for the analysis of the 7-axle C1 vehicles responsible for the tail sagging moments at 20 m and 25 m

In general, the vehicle's geometry had more influence than the GVM at the shorter spans. This made sense as the GVM would not come into full effect until the entire vehicle fitted on the bridge, which was between span lengths of 15 m to 20 m since the 7-axle C1 vehicles had a mean vehicle length of 18.5 m, according to Table 5.5. Therefore, the cause of the underlying Fréchet distribution being found was most likely due to insufficient critical values near the end of the tail. This, as previously mentioned for the 5-axle C1 group, most likely caused the tail to become more susceptible to influence from the LEs gaps near the end of the tail, which led to the underlying Fréchet distribution being found.

5.3.5. Eight Axle vehicles:

In this section, the LEs produced by the different sub-categories of 8-axle vehicles are analysed. In addition, the sub-categories' influence on the parent sub-axle group is noted, and their data sets underlying distributions are investigated.

5.3.5.1. GPP plots

The GPP plots for the sub-categories at 5 m, 25 m and 50 m were recorded in Figure 5.26, Figure 5.27 and Figure 5.28 for the hogging and sagging moments and shear forces, respectively. The GPP plots for the rest of the spans were recorded in Appendix F, in Figure F.10, Figure F.11 and Figure F.12.

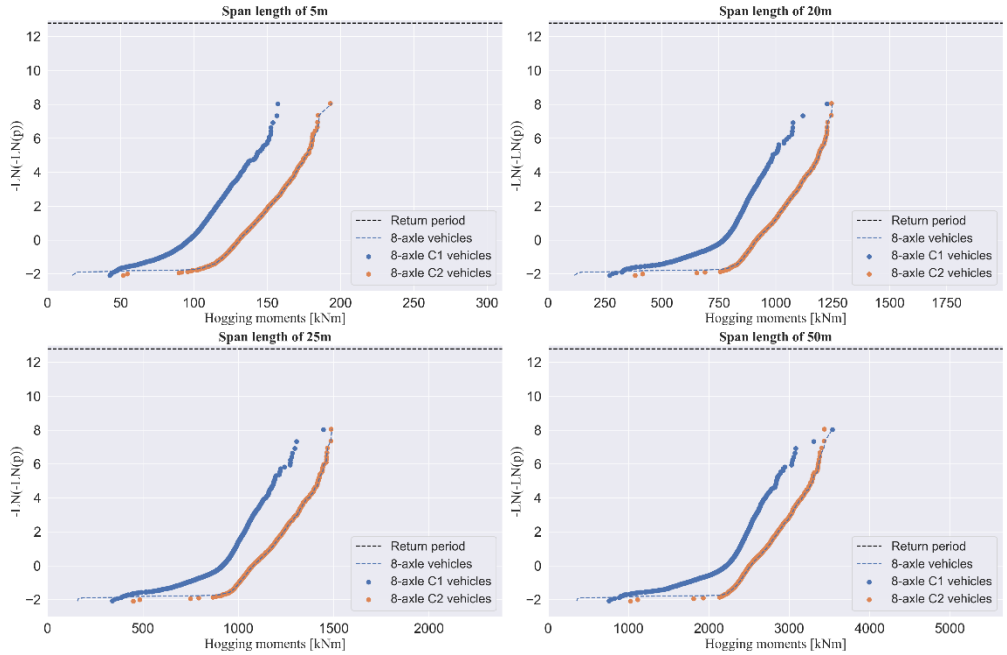

Figure 5.26 Hogging moments GPP plots for the 8-axle sub-categories

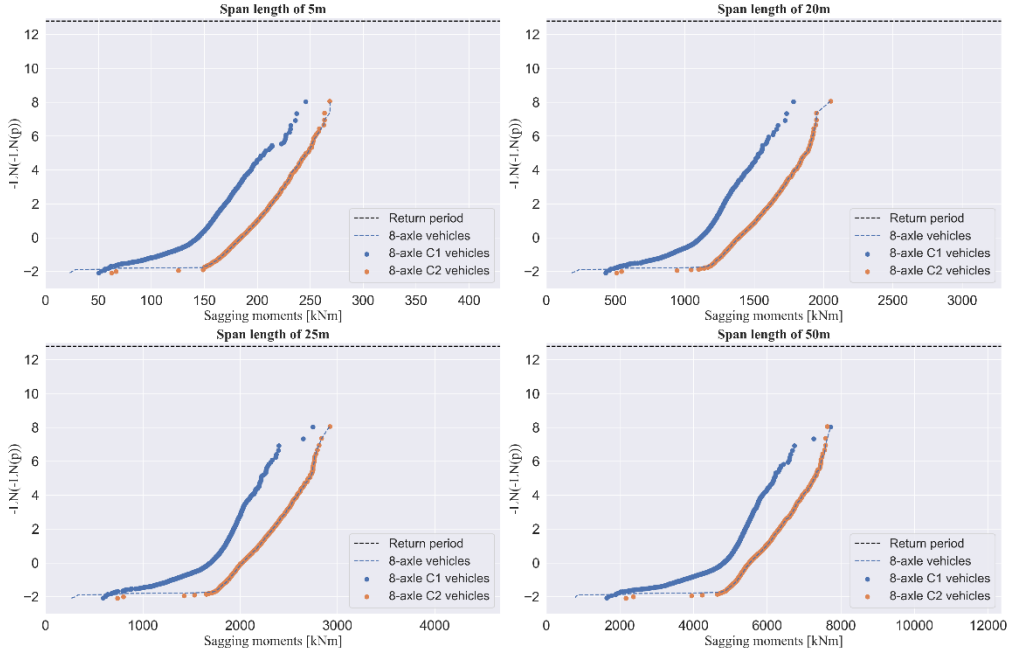

Figure 5.27 Sagging moments GPP plots for the 8-axle sub-categories

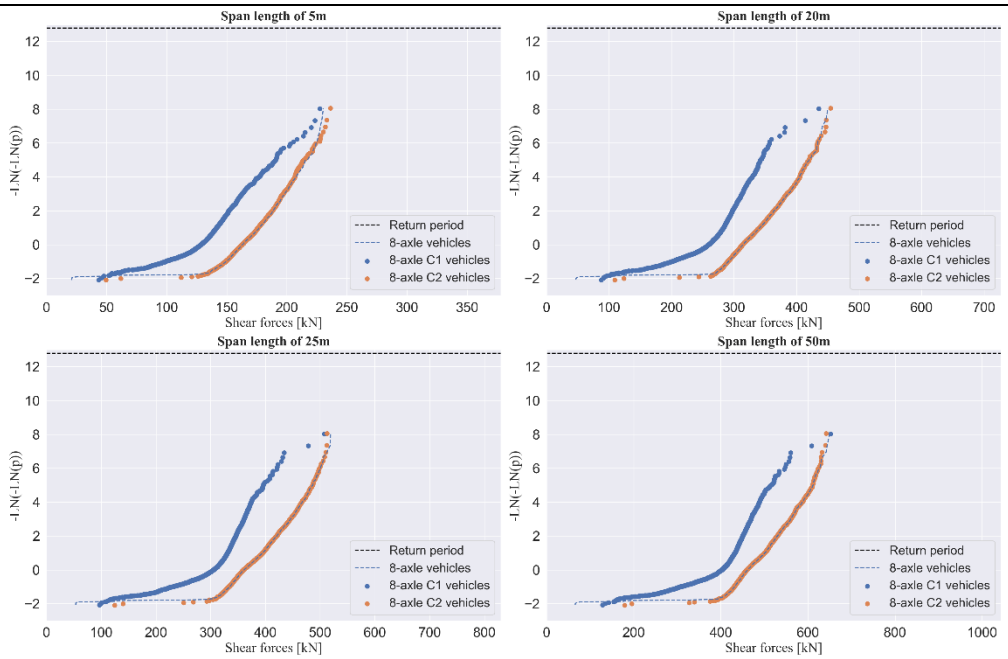

Figure 5.28 Shear forces GPP plots for the 8-axle sub-categories

In general, the 8-axle vehicle plot followed the same plot as the 8-axle C2 group. The 8-axle C2 was responsible for more than 94% of the 8-axle vehicles LEs at each span. In general, the 8-axle C2 produced the highest hogging moments from 5 m to 25 m, the highest sagging moments from 5 m to 40 m and the highest shear forces from spans of 5 m to 30 m. At the rest of the span lengths, the 8-axle C1 group produced the highest LEs.

5.3.5.2. Characteristic LEs

The characteristic values predicted for the 8-axle C1, and C2 groups were recorded in Table 5.23. A total of 33% of the data sets for the 8-axle C1 group had an underlying Fréchet distribution, while every data set for the 8-axle C2 group was found to have an underlying Weibull distribution. Since the 8-axle C2 group was the dominant sub-category, it showed why all the 8-axle vehicles data sets had an underlying Weibull distribution.

Table 5.23 Characteristic values for the 8-axle sub-categories

Span length [m]	8-axle C1 group			8-axle C2 group		
	Hog [kNm]	Sag [kNm]	Shear [kN]	Hog [kNm]	Sag [kNm]	Shear [kN]
5	170	361	268	196	295	268
10	589	802	371	507	766	341
15	1 125	1 353	371	938	1 397	394
20	1 287	2 104	455	1 336	2 177	484
25	1 544	3 013	464	1 616	3 096	531
30	1 973	4 587	491	1 990	4 139	571
35	2 440	5 075	551	2 425	5 070	603
40	3 018	7 553	618	2 739	6 289	623
45	3 333	7 355	636	3 355	7 326	642
50	3783	8 389	652	3 573	8 412	656

5.3.5.3. Investigating underlying distributions

Table 5.24, Table 5.25 and Table 5.26 shows the minimum number of values that had to be removed from the 8-axle sub-categories before an underlying Weibull distribution was obtained for the different LE data sets. In addition, the characteristic LEs predicted and the maximum LEs before any values were removed was also recorded.

Table 5.24 Forced Weibull data sets for the 8-axle subcategories for the hogging moments

Span length [m]	Tail LEs removed		Characteristic value [kNm]		Maximum LE [kNm]	
	C1	C2	C1	C2	C1	C2
5	-	-	170	196	157	193
10	1	-	538	507	490	492
15	1	-	945	938	908	914
20	-	-	1 287	1 336	1 224	1 244
25	-	-	1 544	1 616	1 446	1 486
30	-	-	1 973	1 990	1 820	1 797
35	-	-	2 440	2 425	2 268	2 221
40	1	-	2 733	2 739	2 700	2 634
45	-	-	3 333	3 355	3 122	3 038
50	-	-	3 783	3 573	3 537	3 436

Table 5.25 Forced Weibull data sets for the 8-axle subcategories for the sagging moments

Span length [m]	Tail LEs removed		Characteristic value [kNm]		Maximum LE [kNm]	
	C1	C2	C1	C2	C1	C2
5	3	-	292	295	245	268
10	-	-	802	766	634	704
15	-	-	1353	1397	1088	1323
20	-	-	2 104	2 177	1 783	2 051
25	-	-	3 013	3 096	2 747	2 924
30	1	-	3 874	4 139	3 743	3 832
35	-	-	5 075	5 070	4 739	4 778
40	1	-	5 812	6 289	5 734	5 712
45	-	-	7 355	7 326	6 732	6 667
50	-	-	8 389	8 412	7 726	7 631

Table 5.26 Forced Weibull data sets for the 8-axle subcategories for the shear forces

Span length [m]	Tail LEs removed		Characteristic value [kN]		Maximum LE [kN]	
	C1	C2	C1	C2	C1	C2
5	-	-	268	268	227	236
10	-	-	371	341	283	308
15	-	-	371	394	350	383
20	1	-	455	484	435	454
25	8	-	464	531	507	512
30	12	-	491	571	555	555
35	8	-	551	603	590	586
40	3	-	618	623	616	609
45	3	-	636	642	636	627
50	2	-	652	656	652	641

All the plots for the 8-axle C2 group had an underlying Weibull distribution, so none of the LEs had to be removed. For the 8-axle C1 group, the minimum number of LEs that had to be removed before an underlying Weibull distribution was obtained ranged from one to twelve, excluding the data sets that were already Weibull.

After removing one data point from the hogging moments 8-axle C1 data sets at 10m, 15 m and 40 m spans, an underlying Weibull distribution was found. This showed that the last data point caused the underlying Fréchet distribution for the 8-axle C1 data set. In Figure 5.29, this vehicle was seen to have the highest sum of axle masses at 15 m and 40 m. Although the vehicle that had to be removed at 10 m did not have the highest sum of axles, it was the same vehicle that had to be removed from the data sets at 15 m and 40 m.

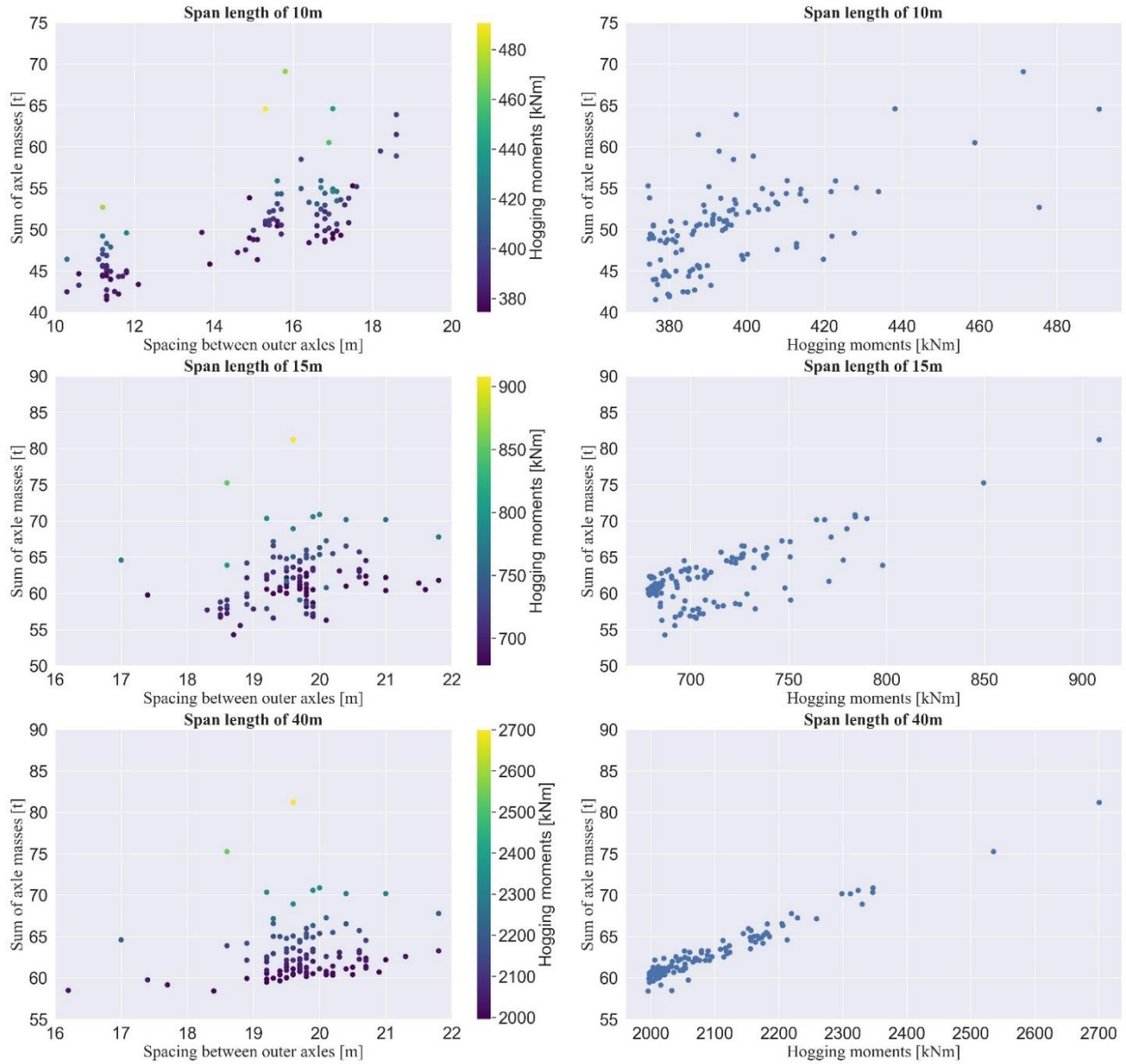

Figure 5.29 Graphs used for analysis of the 8-axle C1 vehicles responsible for the tail hogging moments at 10 m, 15 m, and 40 m

In Figure 5.30, the 8-axle C1 vehicles sum of axles masses, spacing between outer axles and the tail sagging moments at 5 m and 30 m were shown as well as the sum of axles versus sagging moment plots. At 5 m, 68% of the tail sagging moments were caused by only the tandem axle of the 8-axle C1 vehicle while the other 32%

were caused by only the tridem axle. After removing the top three data points from the 5 m sagging moments plot, an underlying Weibull distribution was found. The top two sagging moments were caused by only the tandem axle group, while the third-highest sagging moment was caused by only the tridem axle group. In contrast to the 8-axle C1 tail sagging moments at 5 m, all eight axles of each vehicle contributed to the tail sagging moments at 30 m. At 30 m a minimum of one vehicle had to be excluded from the data set to obtain an underlying Weibull distribution. This was seen to be the heaviest vehicle with a GVM of 81.2 t, which was 19.1 t heavier than the mean GVM of the rest of the tail. This was the same vehicle that had to be excluded at 40 m to obtain an underlying Weibull distribution.

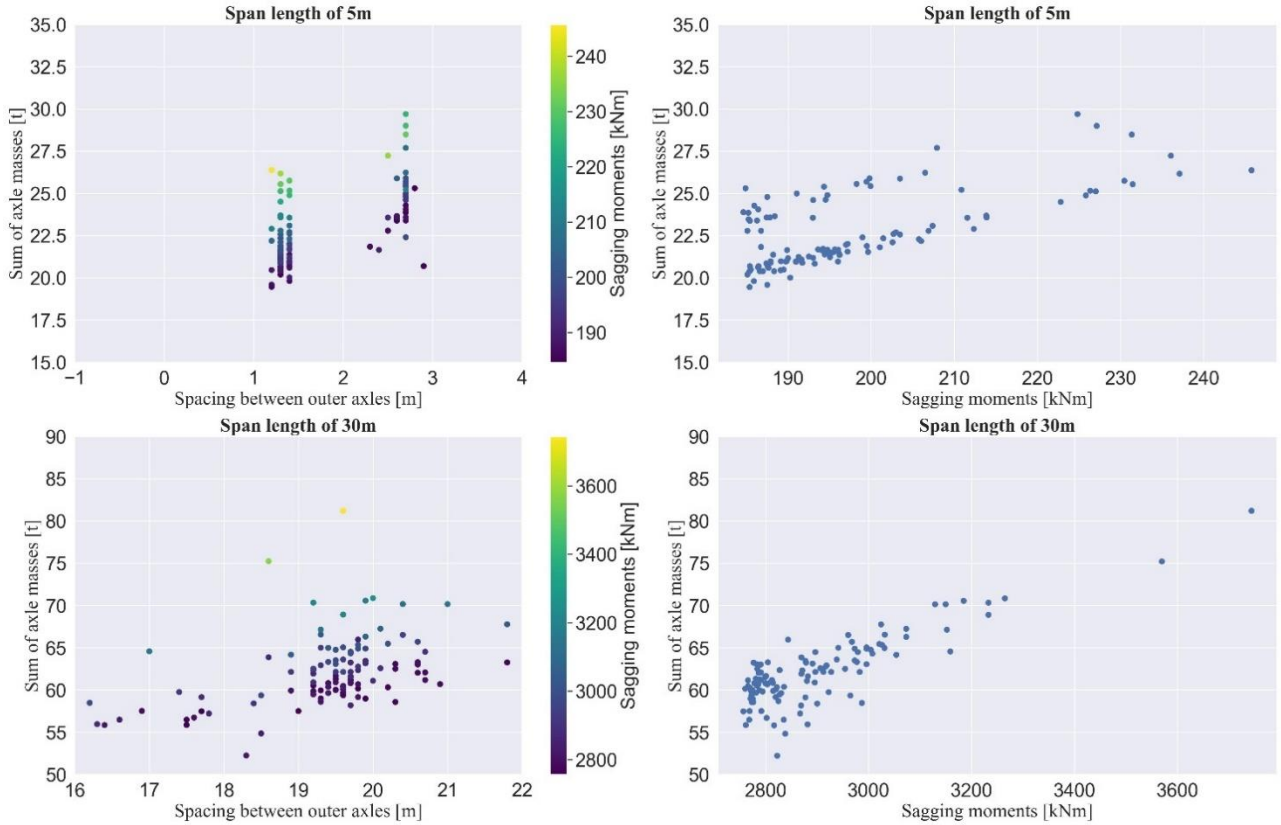

Figure 5.30 Graphs used for the analysis of the 8-axle C1 vehicles responsible for the tail sagging moments at 5 m and 30 m

In Figure 5.31, the 8-axle C1 vehicles sum of axles masses, spacing between outer axles and the tail shear forces at 20 m, 25 m and 30 m were shown as well as the sum of axles versus tail shear forces plots. The minimum number of values to be removed for the shear force data sets to obtain an underlying Weibull distribution ranged from one to ten. At 20 m, 35%, 21% and 44% of the tail shear forces were caused by five, seven and eight of the axles for each vehicle respectively. At this span, only one shear force had to be excluded to obtain an underlying Weibull distribution. The vehicle responsible for the top shear force was the same vehicle responsible for the top shear force at every span from 15 m onwards.

At 25 m and 30 m, 5%, 16% and 79% of the tail shear forces were caused by eight of the axles for each vehicle respectively. At these spans, a minimum of eight and twelve tail shear forces had to be excluded from the respective data sets for an underlying Weibull distribution to be obtained. At 25 m the top eight vehicles had a mean sum of axle masses of 70.8 t which was 10.9 t heavier than the rest of the tail. At 30 m the top twelve

vehicles had a mean sum of axles masses of 73.9 t which was only 0.8 t heavier than the rest of the vehicles in the tail.

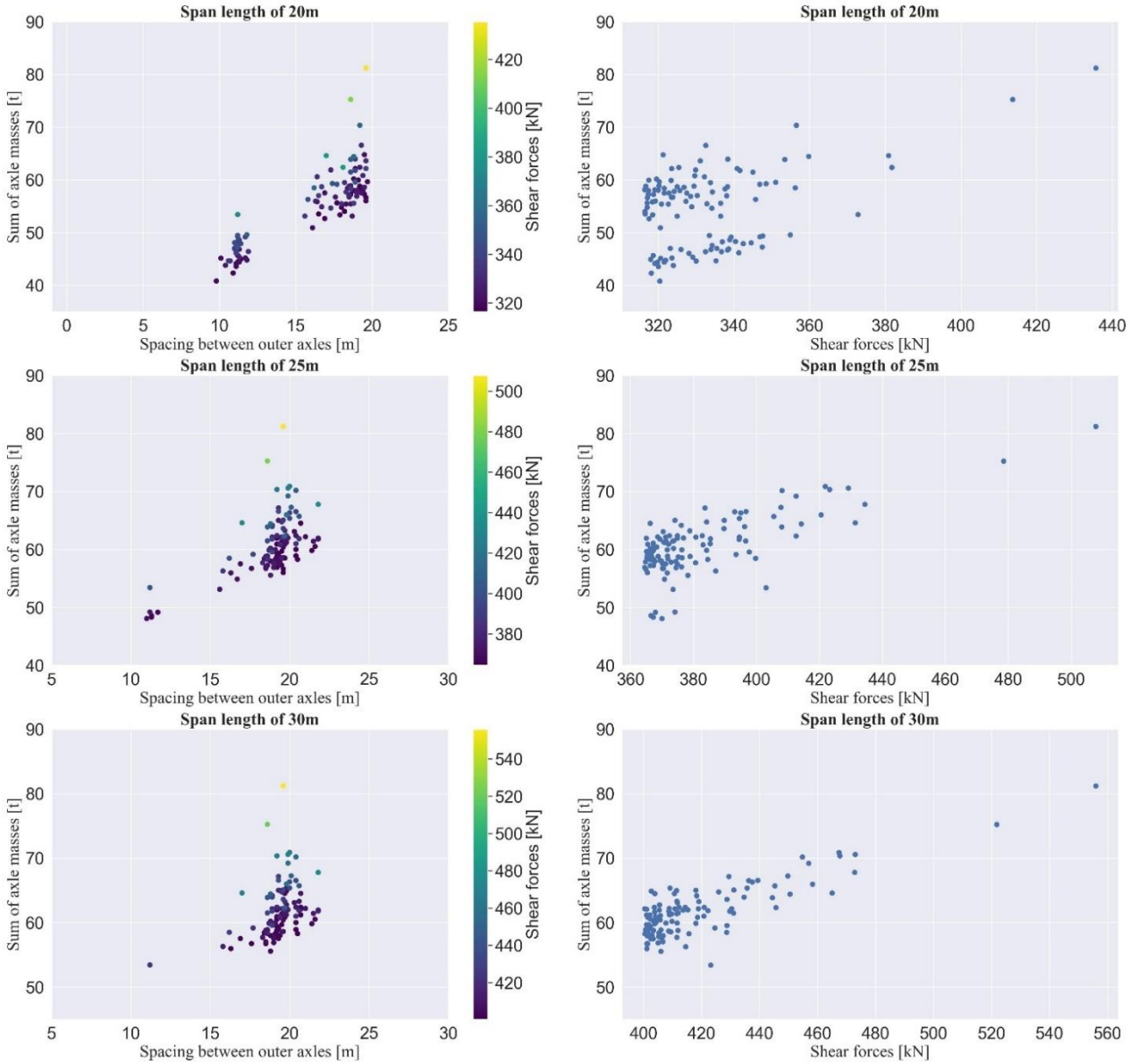

Figure 5.31 Graphs used for the analysis of the 8-axle C1 vehicles responsible for the tail shear forces at 20 m to 30

An alternative to removing 10 datapoints at 30 m to force a Weibull distribution was to decrease the tail length to be $\sqrt{N}$ instead of $2\sqrt{N}$ and then exclude the highest shear force. This resulted in an underlying Weibull distribution being obtained and a characteristic value of 588 kN being predicted. This was a 33 kN greater than the shear force produced by the vehicle that had to be removed, which was found to be the exact 81.2 t vehicle that had to be removed from the hogging moments' plots as well.

Overall, after splitting, 83.3% of the plots were found to have an underlying Weibull distribution, while the rest of the plots had an underlying Fréchet distribution. At the sub-axle splitting level, all the data sets for the 8-axle vehicles group had an underlying Weibull distribution. This meant that splitting had resulted in more data sets that had an underlying Fréchet distribution.

5.3.6. Discussions for the sub-categories

Even after splitting the sub-axle groups into the different sub-categories, data sets with an underlying Fréchet distribution were still found. Investigations into the vehicles responsible for the LEs in these data sets revealed possible causes of the underlying Fréchet distributions found.

At the shorter span lengths of around 5 m to 20 m, depending on each vehicle's length, the axle groups that made up each vehicle were the most important aspect to analyse. This meant that at the shorter span lengths there were different loading groups responsible for the LE data sets. It was seen that at the spans where there were different loading combinations, splitting the data sets into different sub-categories was not always effective in improving the *iid* nature of the data sets.

At the longer span lengths from 25 m onwards, all the axles for a vehicle were able to fit on the bridge and contribute to the daily max LE. At the longer span lengths, the GVM of a vehicle became an important aspect to analyse. By splitting the WIM data sets into the respective data sets it revealed that there were data sets that had too few critical LEs in the tail. Since there were too few critical values in the tail, significant LE gaps were formed which occasionally resulted in an underlying Fréchet distribution being found. By removing LEs from the upper end of the tail, it was possible to reduce the effect of the LE gaps and obtain an underlying Weibull distribution. However, it was not possible to justify removing vehicles from the data sets to force an underlying Weibull distribution. There was no point in excluding critical values to force a data set to fit the theory. All it led to was predicting lower characteristic values than the maximum LEs recorded, as was indicated by the cells shaded in grey in the Forced Weibull data sets in Table 5.11 and Table 5.26.

Overall splitting the sub-axle groups into the sub-categories resulted in an increased percentage of data sets with an underlying Weibull distribution. A total of 31% of all the data sets for the sub-categories of sub-axle groups had an underlying Weibull distribution.

5.4. Final discussion

In this study, Chapter 4 can be regarded as the first level of splitting investigated. At this level, no splitting of the WIM data set was done. Although there were four different mixed-axle groups investigated in Chapter 4, for this study, the most important one was the RMA group 3. RMA group 3 was the most important one because the LE data sets were created using only single-vehicle events. At this level of splitting, 13% of the LE data sets had an underlying Fréchet distribution. In comparison, 87% had an underlying Weibull distribution.

Section 5.2 of this study can be regarded as the second level of splitting investigated. The vehicles in the cleaned WIM data sets were separated into eight different sub-axle groups on this level. At this splitting level, 35% of all the data sets for the sub-axle groups had an underlying Fréchet distribution. In contrast, 65% had an underlying Weibull distribution.

Section 5.3 represents the final splitting level investigated in this study. On this level, the vehicles recorded in the cleaned WIM data set was divided into the different sub-categories of sub-axle vehicles identified in this section. As a result, 31% of the data sets had an underlying Fréchet distribution, while 69% had an underlying Weibull distribution.

Figure 5.32 shows the percentage of plots with an underlying Weibull or Fréchet distribution for the RMA group 3, the sub-axle groups, and the sub-categories of sub-axle groups. From a comparison between the graphs for RMA group 3 and the sub-categories of sub-axle groups data sets, it was evident that splitting had increased the percentage of data sets with an underlying Fréchet distribution. However, there was a decrease in the percentage of data sets with an underlying Fréchet distribution from the sub-axle groups to the sub-categories of sub-axle groups. This indicated that splitting the WIM data sets into separate vehicle categories had the potential to increase and decrease the number of data sets that an underlying Fréchet distribution.

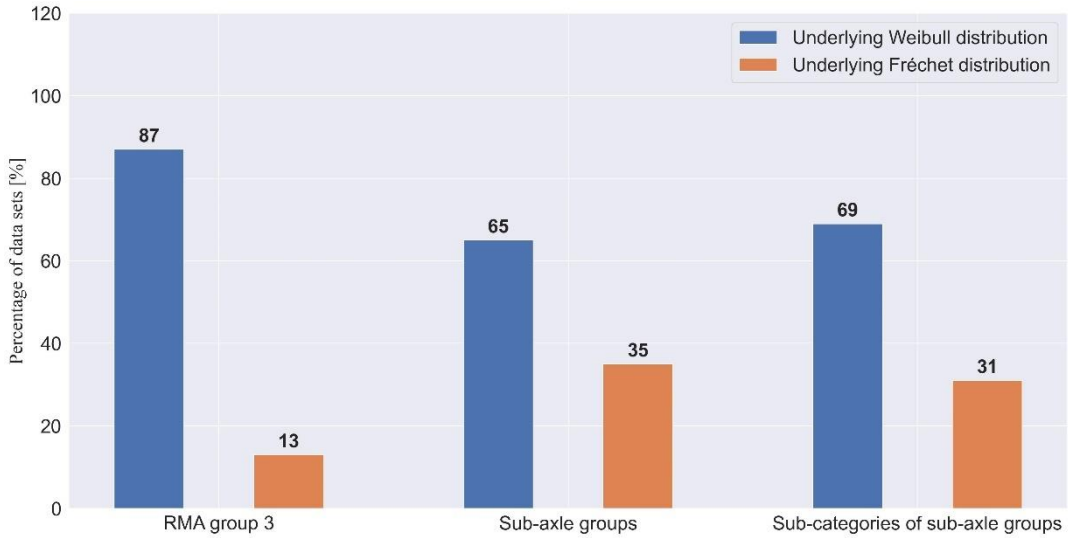

Figure 5.32 Percentage of underlying Weibull and Fréchet

At the mixed-axle level, 87% of the data sets had an underlying Weibull distribution because the dominant vehicle subsets had an underlying Weibull distribution too. This indicated that an underlying Weibull distribution was found at the mixed-axle level because the data sets for dominant vehicle subsets were *iid.* By splitting the WIM data sets, more data sets that were not *iid* were introduced. Hence, a higher percentage of data sets with an underlying Frechet distribution was found.

While splitting the WIM data set had overall increased the number of data sets with an underlying Frechet distribution, it had allowed for an understanding of the causes of the underlying distributions found for the parent groups to be obtained. Splitting the WIM data sets allowed for one to see the interaction between the different vehicle subsets and allowed for the identification of the different vehicle groups found in the WIM data. Through the identification of the different vehicle subsets, a vehicle group was found for which no reference could be obtained to prove that it existed. Splitting the WIM data set down to the third splitting level had allowed for the identification of a 6: 2-2-2 vehicle group, which was seen found to be the cause of 75% of underlying Frechet distributions found for the RMA group 3. By excluding this vehicle group from the WIM

data set, then only one data set for the RMA group 3 would have had an underlying Frechet distribution. The remaining data set, was due to the 7-axle C3 vehicle group, which as previously mentioned in Section 5.3.1, was potentially erroneous vehicle records as well. Therefore, splitting had in the end allowed for the improvement of the *iid* nature of the data sets at the mixed-axle level, resulting in only underlying Weibull distributions being obtained.

5.5. Chapter summary

In this chapter, the sub-axle groups identified in Chapter 4 were created with the same restrictions enforced on RMA group 3. The LEs for each span length was determined, the GPP plots were made, and the characteristic values were predicted. Splitting revealed the sub-axle groups responsible for the LEs recorded in the RMA group 3's LE data sets and allowed for illustration of each sub-axle group's influence on the mixed-axle groups' plot.

Even after splitting the WIM data sets into the sub-axle groups, data sets with an underlying Fréchet distribution were still found. To understand the possible causes of the underlying Fréchet distributions, the data sets were further subdivided. Each sub-axle group was divided into their respective separate subsets of vehicles, dubbed the sub-categories of the sub-axle vehicle groups.

After sub-dividing the vehicles in the cleaned Wim data sets into the different sub-categories, there were still data sets with an underlying Fréchet distribution being found. Investigations into the vehicles responsible for the LEs revealed two possible causes of the underlying Fréchet distributions. The first cause was due to the different axle loading combinations found at the shorter span lengths of 5 m to 20 m. The second cause of the underlying Fréchet distributions found for the sub-categories was too few critical values within the tail of the data sets after splitting. For both cases, it was possible to force an underlying Weibull distribution to be obtained by excluding vehicles from the upper tail of the LEs.

In the final discussion of the chapter, the percentage of data sets that had an underlying Weibull or Fréchet distribution for the RMA group 3, the sub-axle groups and the sub-categories of sub-axle groups were compared. Overall, splitting the vehicle data sets introduced more data sets that were non-*iid* leading to an increase in the percentage of data sets with an underlying Fréchet distribution. Splitting had however allowed for the understanding of the causes of the underlying distributions found for each parent group. Through splitting the WIM data set to the third splitting level, the cause of the underlying Fréchet distributions for the RMA group 3 was identified to be potential erroneous vehicle records. By excluding erroneous vehicle groups, the percentage of RMA group 3's data sets with an underlying Weibull distribution was increased, indicating an improved *iid* nature.

6. Conclusion and recommendation

6.1. Conclusion

This study aimed to investigate if vehicle data sets that better adhered to the independently and identically distributed (*iid*) requirements of Extreme Value (EV) theory could be obtained by splitting the vehicles into their respective subsets. Using Weigh-In-Motion (WIM) data from the Roosboom WIM station, three different splitting levels were investigated. With each level, the vehicles in the cleaned WIM data set were further sub-divided. On the first level, no splitting occurred, and vehicle groups were referred to as the mixed-axle groups. On the second level, the vehicles in the WIM data set were separated into different groups based on the number of axles each vehicle had. These vehicle groups were referred to as the sub-axle groups. On the final level of splitting investigated, the vehicles in the WIM data sets were further sub-divided into groups based on the axle groups that composed them. These vehicles groups were referred to as the sub-categories of sub-axle groups. With each splitting level, the causes of the underlying distribution found for the data sets on the previous level was seen. Generally, the underlying distributions found for the data sets on each splitting level was closely related to the underlying distributions of dominant vehicle subsets on the following splitting level. If the sub-axle groups responsible for most of the tail LEs at a span had an underlying Weibull distribution, then so too did the parent mixed-axle group. However, if the interference from another vehicle data set was significant enough, an underlying Fréchet distribution could be found.

At the mixed-axle level, 87% of the LE data sets had an underlying Weibull distribution while 13% of them had an underlying Fréchet distribution. Through splitting, potential erroneous vehicle records in the WIM data were identified. These erroneous records were seen to be the cause of the underlying Fréchet distributions. By removing the erroneous vehicle records, only an underlying Weibull distribution would be found for the mixed-axle vehicle groups data sets. This indicated that in the end, splitting had the potential to improve the *iid* nature of the mixed-axle vehicle data sets themselves.

In this study, it was seen that most of the mixed-axle vehicle group data sets had an underlying Weibull distribution because the vehicle subsets, which dominated the tail LEs, had an underlying Weibull distribution too. By splitting the WIM data into different vehicle subsets, more and more non-dominating vehicle data sets were introduced into the study. This led to an increased percentage of data sets with an underlying Fréchet distribution. Overall, splitting had increased the number of non-iid data sets available, which overcomplicated the study. If only the dominating vehicle groups were considered, then data sets that better fit the requirements of EV theory had been obtained. However, this was at the cost of critical LEs, which could result in lower characteristic values than what was found for the mixed-axle group being determined.

Ultimately, splitting a mixed-axle vehicle data set into its respective subsets should not solely be used to predict characteristic values. Instead, it would be better suited for identifying potential erroneous vehicle records to allow additions to the filtration used during the cleaning of the WIM data file.

6.2. Recommendations for future study

During this study, topics that warranted further research to develop an accurate bridge traffic loading model were identified. As a result, these topics have been discussed here:

- The LE datasets herein are formed by recording the maximum LE for each day. Further research is required to investigate the effects of splitting into LE data sets formed with larger block sizes. For example, suppose a larger block size than the daily maxima is used. In that case, it might decrease the percentage of data sets that had an underlying Fréchet distribution. An investigation of this sort can only be done for those groups with enough values.

- As a result of splitting, the data sets were seen to get smaller and smaller. It is possible that due to this, the tail length used for censoring in this study may no longer be suitable. Therefore, it is recommended to investigate alternative tail lengths when doing a study of a similar nature.

- The work done in this study focus on normal traffic loads. It is known. However, abnormal loads produce higher loads than regular traffic. Unfortunately, with the nature of WIM, identifying a vehicle with a permit to travel is not possible. Due to the axle-group restriction, the vehicles removed in this study were assumed permit vehicles based on their geometry and because South Africa has no legislation regarding quad-axle vehicles. Further research is recommended to develop a method to classify what vehicles in the WIM data files are permit vehicles to develop an abnormal load model.

7. References

Allen, D., Singh, A. and Powell, R. (2011) 'Extreme Market Risk-An Extreme Value Theory Approach', *Mathematics and Computers in Simulation*, 94(August), pp. 310–328.

Anitori, G., Casas, J. R. and Ghosn, M. (2018) 'Methodology for development of live load models for refined analysis of short and medium-span highway bridges', *Structure and Infrastructure Engineering*. Taylor & Francis, 14(4), pp. 477–490. doi: 10.1080/15732479.2017.1406961.

Australian Capital Territory (2006) *Motor Traffic Act, Black Hall Publication*. Available at: https://www.srilankalaw.lk/Volume-V/motor-traffic-act.html.

Bailey, S. F. and Hirt, M. A. (1996) 'Site specific models of traffic action effects for bridge evaluation', *Recent Advances in Bridge Engineering: Evaluation, Management and Repair*, pp. 404–425.

Basson, S. E. (2020) *An investigation into the reliability performance of bridges designed according to TMH-7*. Stellenbosch University.

Bennet, D. (2008) 'The History and Aesthetic Development of Bridges', in Parke, G. and Hewson, N. (eds) *ICE manual of bridge engineering*. Second edi. London: Thomas Telford Ltd., pp. 1–21. doi: 10.1680/mobe.34525.0001.

Bissell, D., Ang, A. H. S. and Tang, W. H. (1979) 'Probability Concepts in Engineering Planning and Design: Vol. I-Basic Principles.', *The Statistician*, 28(3), p. 226. doi: 10.2307/2987875.

Bosman, J. (2004) 'Traffic loading characteristics of South African heavy vehicles', *8th International Symposium on Heavy Vehicle Weights and Dimensions*.

British Columbia (1999) *Motor Vehicle Act Regulations*.

Caprani, C. C. (2005) *PROBABILISTIC ANALYSIS OF HIGHWAY BRIDGE TRAFFIC LOADING*. National University of Ireland.

Caprani, C. and O'Brien, E. J. (2010) 'Estimating Extreme Highway Bridge Traffic Load Effects', *Safety, reliability and risk of structures, infrastructures and engineering systems : proceedings of the Tenth International Conference on Structural Safety and Reliability (ICOSSAR2009), Osaka*, (October), pp. 3053–3060.

Castillo, E. (1988) *Extreme Value Theory in Engineering*. First edit, *The Statistician*. First edit. Academic Press Inc.

Castillo, E. *et al.* (2005) *Extreme value and related models with applications in engineering and science, A JOHN WILEY & SONS, INC. PUBLICATION*. Hoboken, N.J. : Wiley.

Coles, S. (2001) *An Introduction to Statistical Modeling of Extreme Values*. London: Springer-Verlag.

Committee of State Road Authorities (1981) *TMH7 Parts 1 and 2 : Code of Practice for the Design of Highway Bridges and Culverts in South Africa*.

Committee of Transport Officials (2017) *TRH11 - Administrative Guidelines for Granting of Exemption Permits for the Conveyance of Abnormal Loads*. 1st edn. Pretoria: Department of Transport.

Committee of Transport Officials (2019) *TMH 14 - South African Standard Automatic Traffic Data Collection Format*. Department of Transport.

Department of Transport (2000a) 'National Road Traffic Regulations', (March).

Department of Transport (2000b) *TRH11: Draft guidelines for granting of exemption permits for the conveyance of abnormal loads and for other events on public roads*. 7th edn. Bloemfontein: Committee of State Road Authorities.

Enright, B. (2010) *Simulation of traffic loading on highway bridges*, *Civil Engineering*. University College Dublin, Ireland.

Jacob, B. and Feypell-de La Bemaumell, V. (2010) 'Improving truck safety : Potential of weigh-in-motion technology', 34, pp. 9–15. doi: 10.1016/j.iatssr.2010.06.003.

Kendall, M. G. and Stuart, A. (2010) *The Advanced Theory of Statistics*, *Wiley*. New York: Hafner publishing compa.

King, G. (1998) *Unifying Political Methodology: The Likelihood Theory of Statistical Inference*. New York: Cambridge University Press.

Lenner, R. (2021) 'Advanced concrete design MT13 Lecture 16: Loading'. Stellenbosch.

Lenner, R., De Wet, D. P. G. and Viljoen, C. (2017) 'Traffic characteristics and bridge loading in South Africa', *Journal of the South African Institution of Civil Engineering*, 59(4), pp. 34–46. doi: 10.17159/2309-8775/2017/v59n4a4.

van Loo, H. and Žnidarič, A. (2019) 'Guide for Users of Weigh-In-Motion', *International Society for Weigh in Motion*. International Society for Weigh in Motion.

Media Digital (2017) *Local Bulk Haulage*.

Messervey, T. B., Frangopol, D. M. and Casciati, S. (2011) 'Application of the statistics of extremes to the reliability assessment and performance prediction of monitored highway bridges', *Structure and Infrastructure Engineering*, 7(1), pp. 87–99. doi: 10.1080/15732471003588619.

Nagy, A. (2013) *17 of the Oldest Man-Made Structures On Earth Still In Use*, *Gizmodo*. Available at: https://gizmodo.com/17-of-the-oldest-man-made-structures-on-earth-still-in-508293601#replies (Accessed: 28 October 2021).

Nowak, A. S. (1993) 'Live load model for highway bridges', *Structural Safety*, 93(June 1994), pp. 53–66.

Nowak, A. S. and Collins, K. R. (2000) *Reliability of Structures.* 1st edn, *MCGraw-Hill Higher Education*. 1st edn. Edited by M. Jones. United States of America: Casson, Thomas.

O'Brien, E. J. *et al.* (2015) 'A review of probabilistic methods of assessment of load effects in bridges', *Structural Safety*. Elsevier Ltd, 53, pp. 44–56. doi: 10.1016/j.strusafe.2015.01.002.

O'Brien, E. J. and Enright, B. (2011) 'Modeling same-direction two-lane traffic for bridge loading', *Structural Safety*. Elsevier Ltd, 33(4–5), pp. 296–304. doi: 10.1016/j.strusafe.2011.04.004.

O'Connor, A. J. (2001) *Probabilistic Traffic Modelling for Highway bridges*. University of Dublin.

O'Connor, A. J., Caprani, C. C. and Belay, A. (2002) 'Site-Specific Probabilistic Load Modelling for Bridge Reliability', *Assessment of Bridges and Highway Infrastructure*, pp. 97–104.

Phien, H. N. and Fang, E. (1989) 'Parameter estimation for the general extreme value distribution', *Water SA*, 1(5), p. 2.

Province of Novascotia (2015) 'Figure: Weights and Dimensions of Vehicles Regulations made under Section 191 of the Motor Vehicle Act'. Available at: https://www.novascotia.ca/just/regulations/regs/mvwd.htm.

Road Safety Authority. (2015) 'Guidelines on Maximum Weights and Dimensions of Mechanically Propelled Vehicles and Trailers , Including Manoeuvrability Criteria Road Safety Authority', (March).

SANRAL (2006) *Rsa Vehicle Data Collection Format*.

Sivakumar, B., Ghosn, M. and Moses, F. (2008) *Protocols for Collecting and Using Traffic Data in Bridge Design Prepared for National Cooperative Highway Research Program*.

Snell, J., Montgomery, D. C. and Runger, G. C. (1995) *Applied Statistics and Probability for Engineers.*, *Journal of the Royal Statistical Society. Series A (Statistics in Society)*. doi: 10.2307/2983314.

Söderbom, M. *et al.* (2014) 'Maximum likelihood estimation', in *Empirical Development Economics*. Routledge, pp. 237–253. doi: 10.4324/9780203070925-30.

Soriano, M., Casas, J. R. and Ghosn, M. (2017) 'Simplified probabilistic model for maximum traffic load from weigh-in-motion data', *Structure and Infrastructure Engineering*. Taylor & Francis, 13(4), pp. 454–467. doi: 10.1080/15732479.2016.1164728.

Van der Spuy, P. F. (2019) *Derivation of a traffic load model for the structural design of highway bridges in South Africa by Pierre Francois van der Spuy Dissertation presented for the degree of Doctor of Philosophy in the Faculty of Engineering at Stellenbosch University Supervis*. Stellenbosch University.

Transport for NSW (2012) *Vehicle standards information (VSI)*.

Volvo (2016) *Volvo Trucks releases five new features for rough terrain*. Available at: https://forestry.co.za/volvo-trucks-releases-five-new-features-for-rough-terrain/ (Accessed: 27 January 2020).

De Wet, D. P. G. (2010) *Post-calibration and quality management of Weigh-In-Motion Data*. Stellenbosch

University.

Zhou, X. Y. (2013) *Statistical analysis of traffic loads and traffic load effects on bridges*. Universite Paris Est.

Appendix A: Distribution of the different mixed-axle vehicle groups GVMs, vehicle lengths and LEs

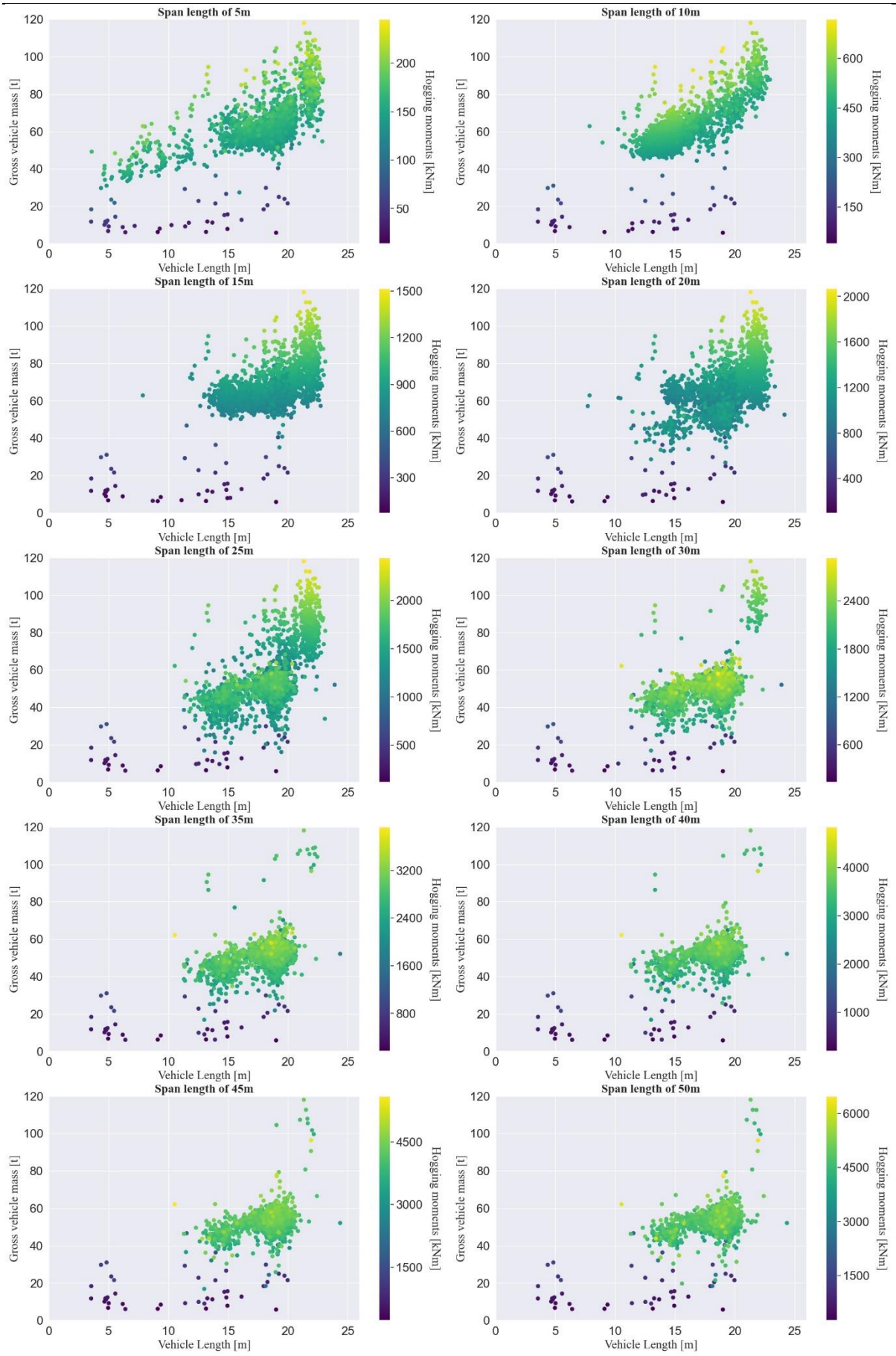

Figure A.1 Distribution of UMA group's GVM, vehicle length and hogging moments

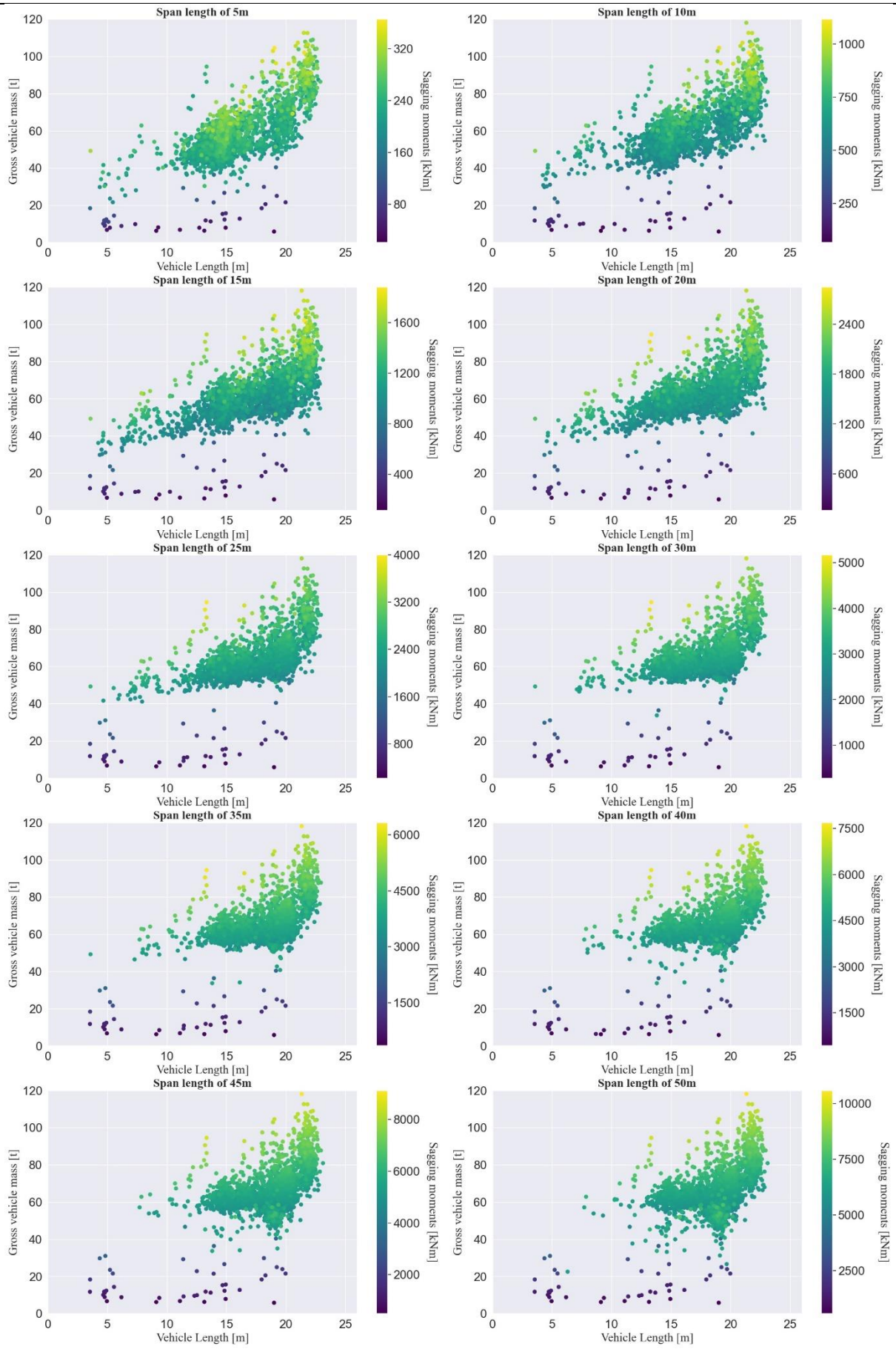

Figure A.2 Distribution of UMA group's GVM, vehicle length and sagging momnets

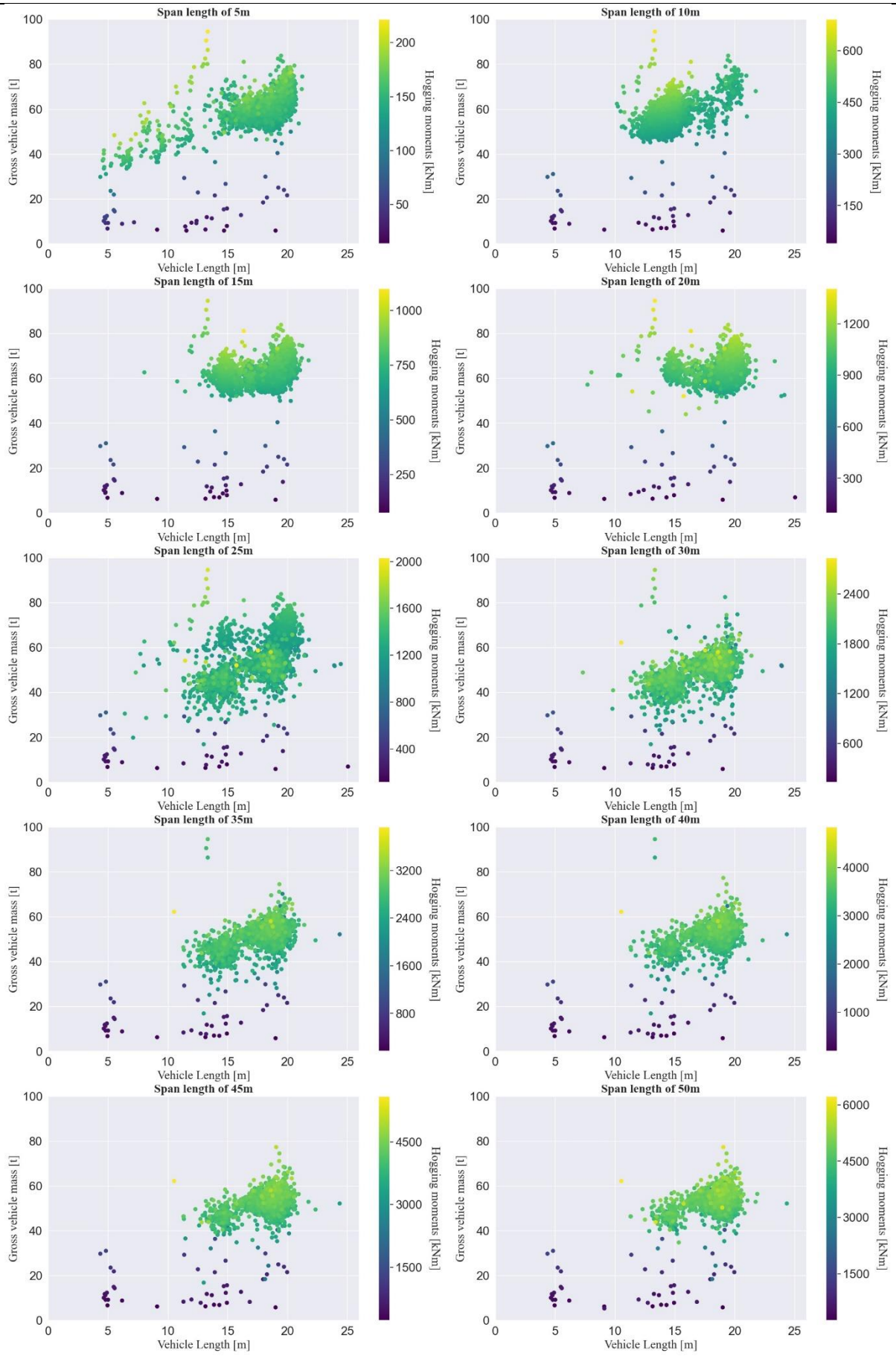

Figure A.3 Distribution of UMA group's GVM, vehicle length and shear forces

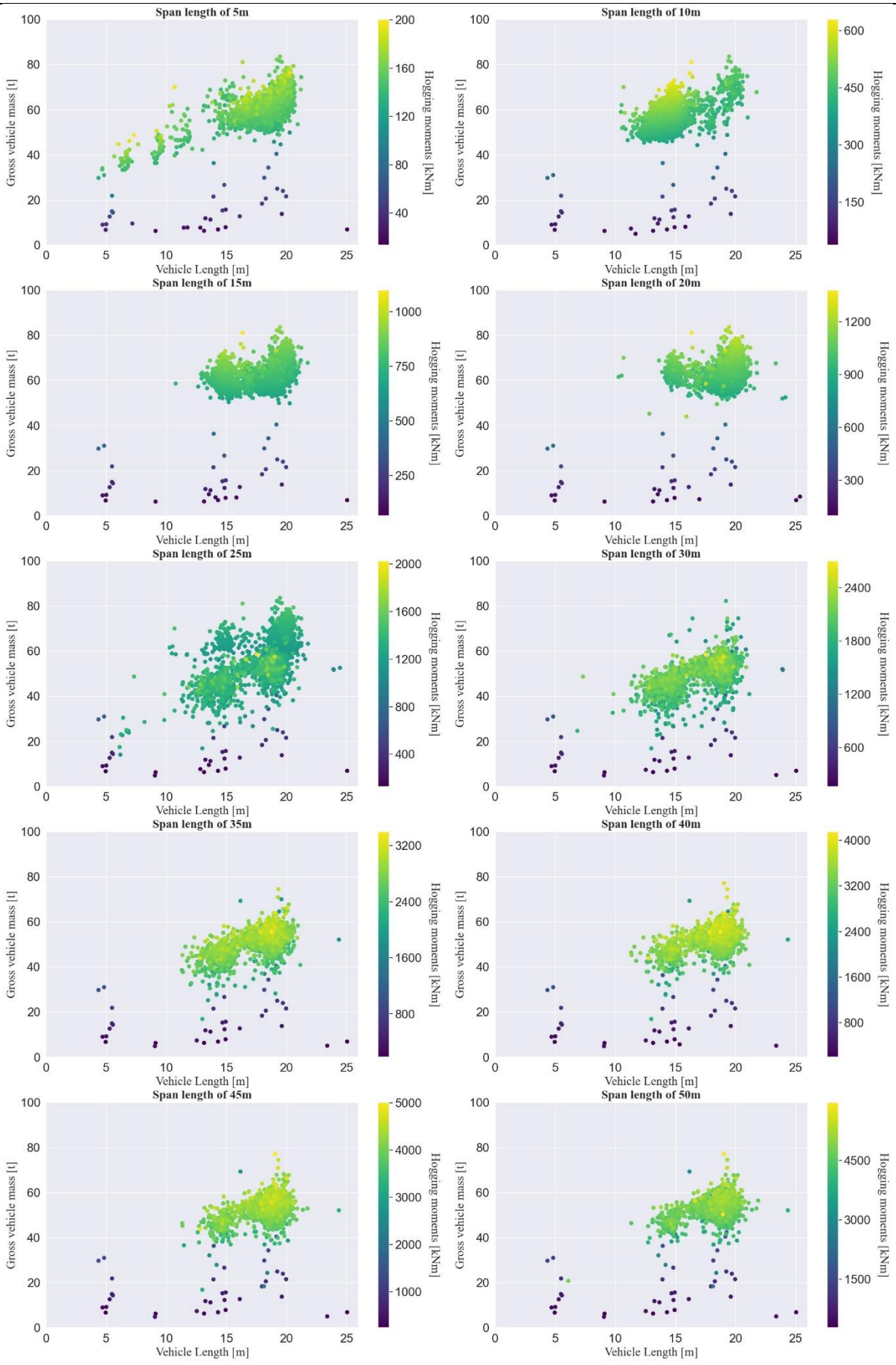

Figure A.4 Distribution of RMA group 1's GVM, vehicle length and hogging moments

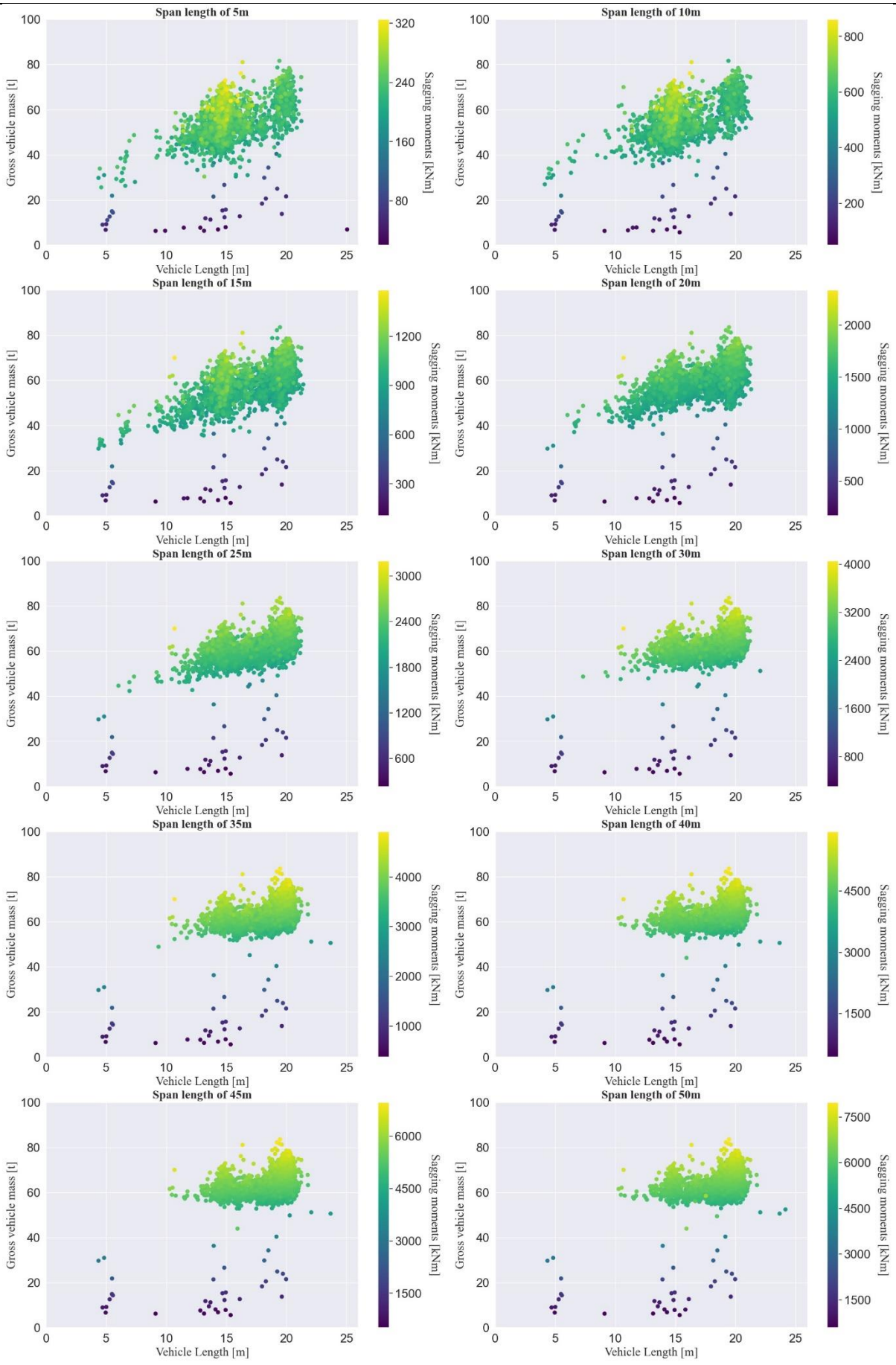

Figure A.5 Distribution of RMA group 1's GVM, vehicle length and sagging moments

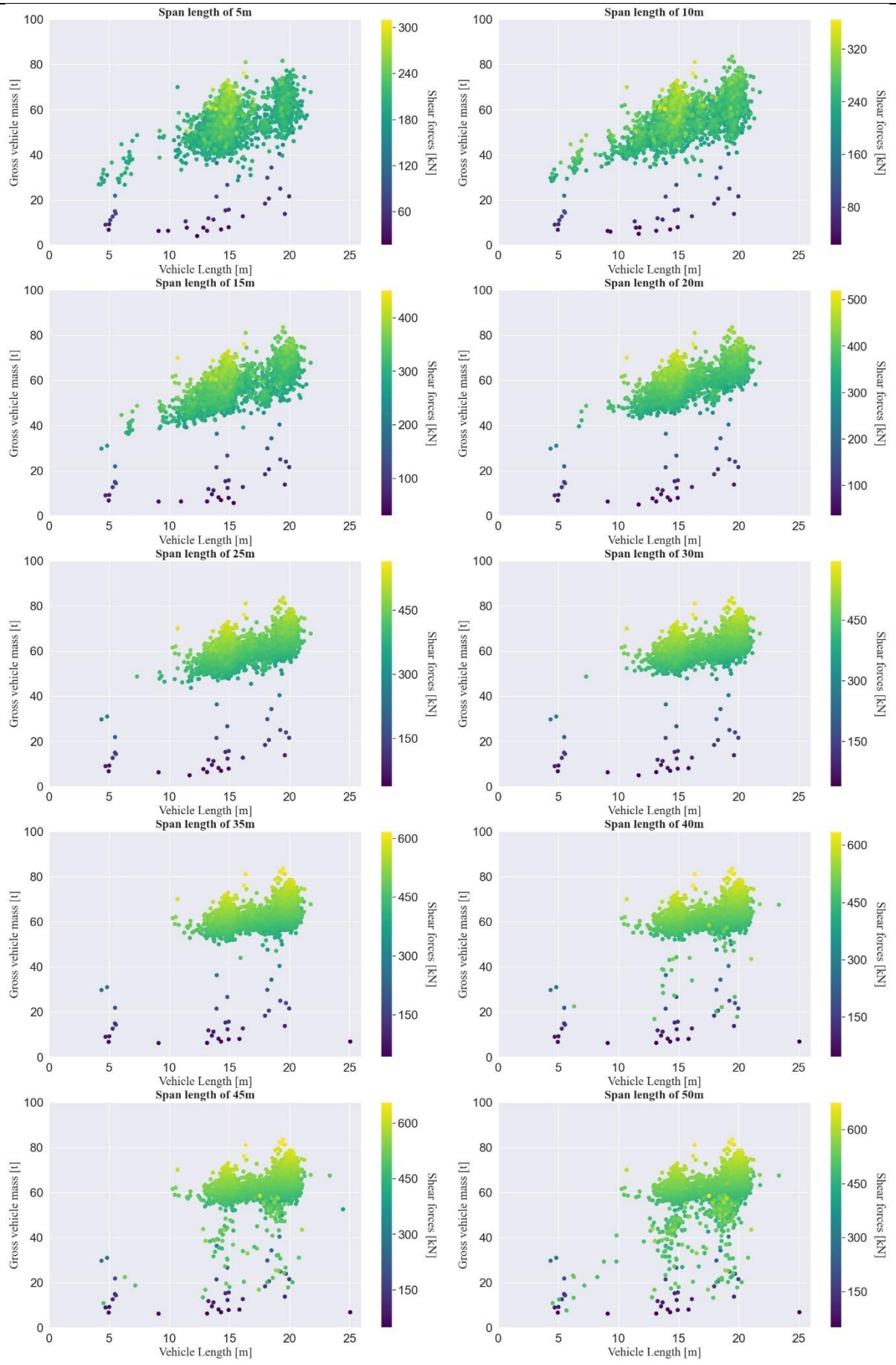

Figure A.6 Distribution of RMA group 1's GVM, vehicle length and shear forces

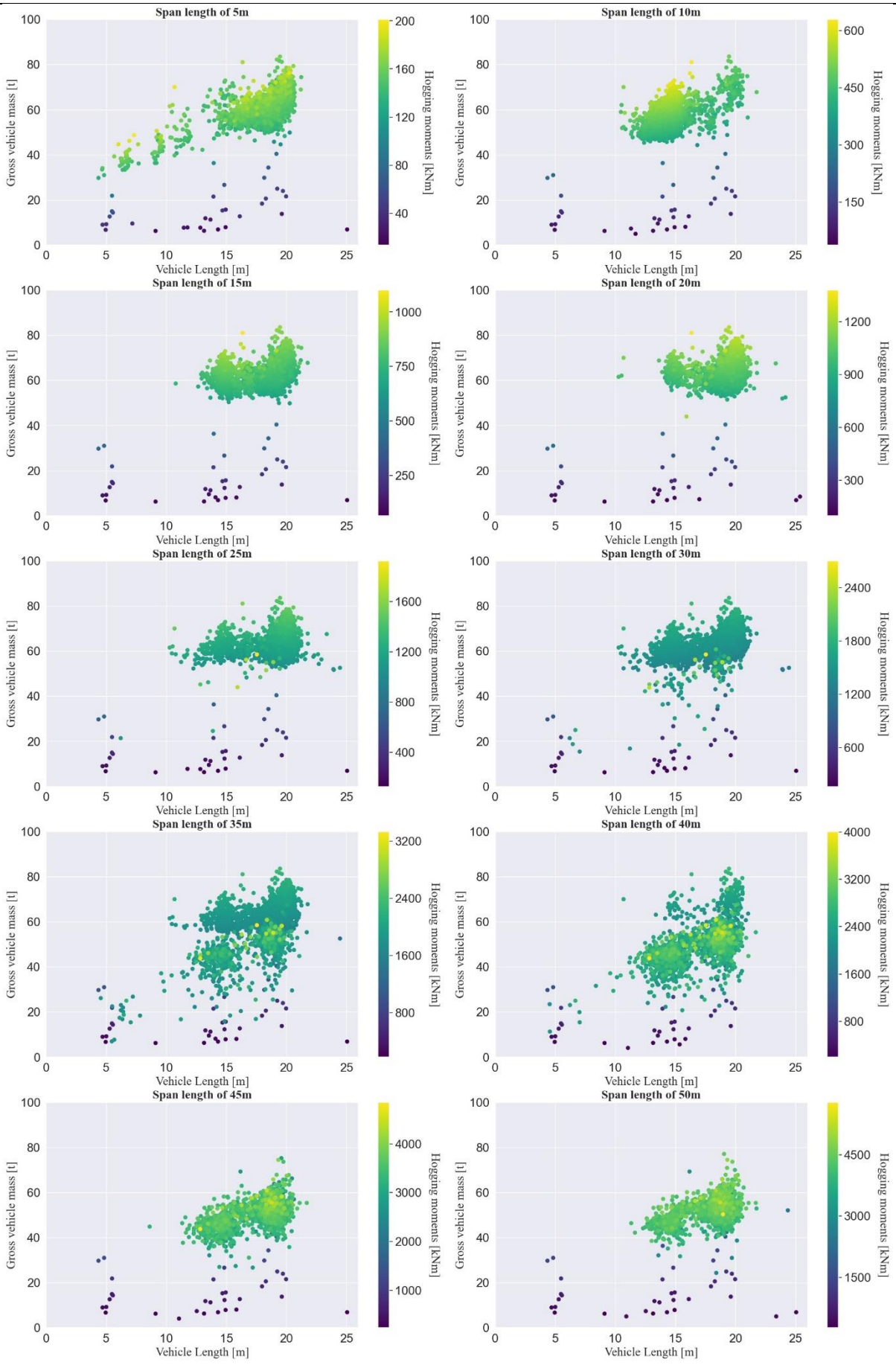

Figure A.7 Distribution of RMA group 2's GVM, vehicle length and hogging moments

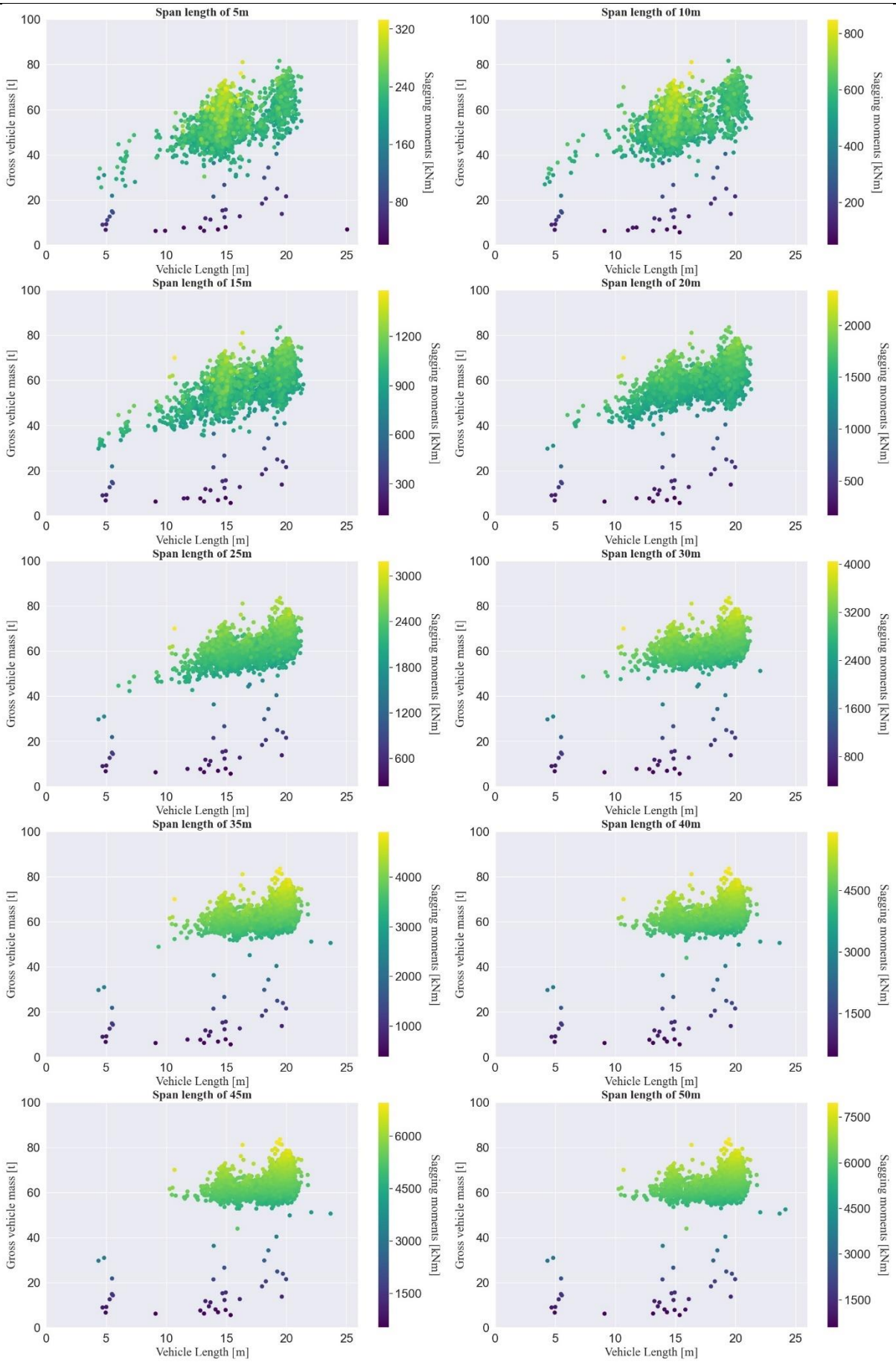

Figure A.8 Distribution of RMA group 2's GVM, vehicle length and sagging moments

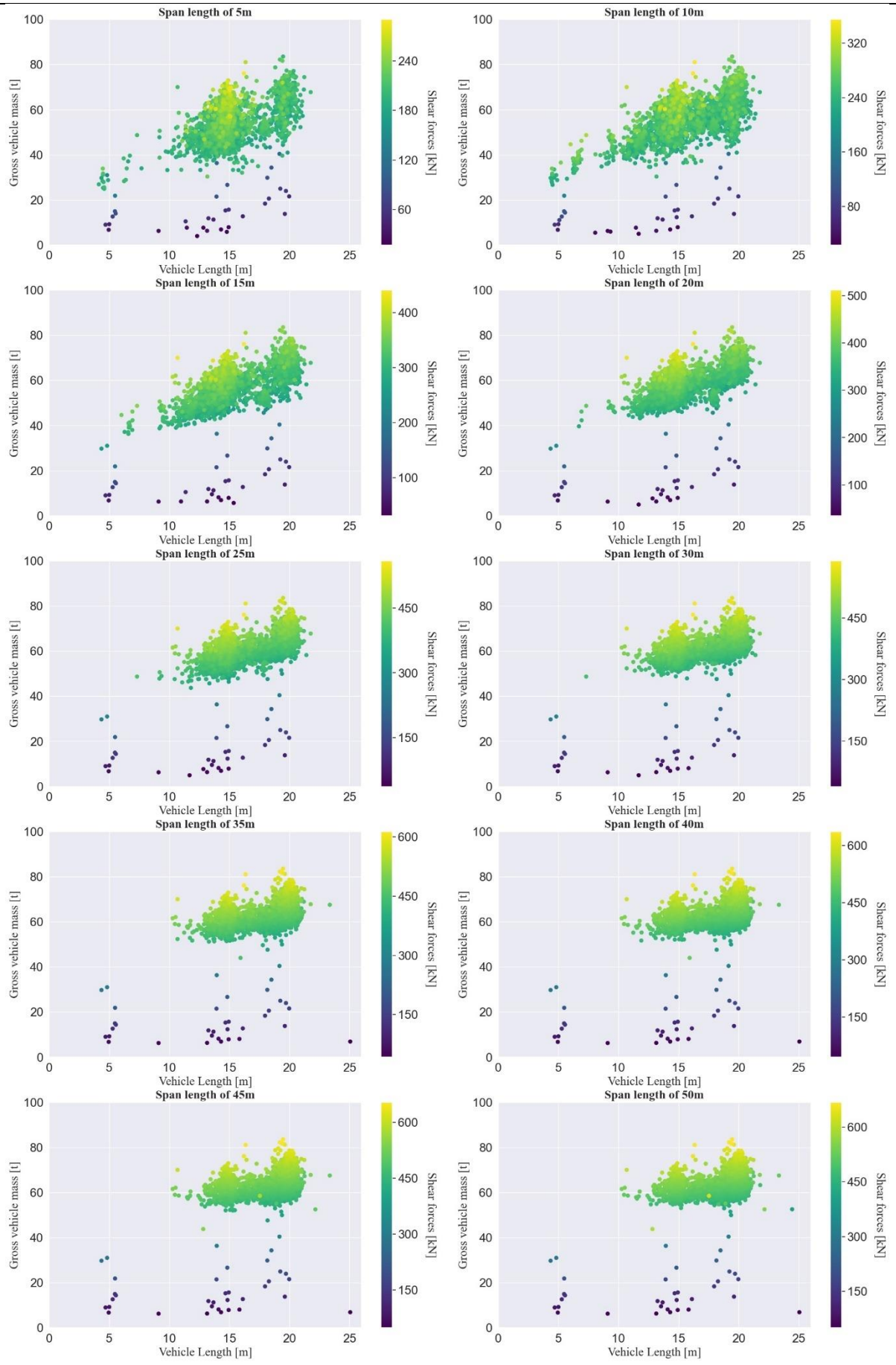

Figure A.9 Distribution of RMA group 2's GVM, vehicle length and shear forces

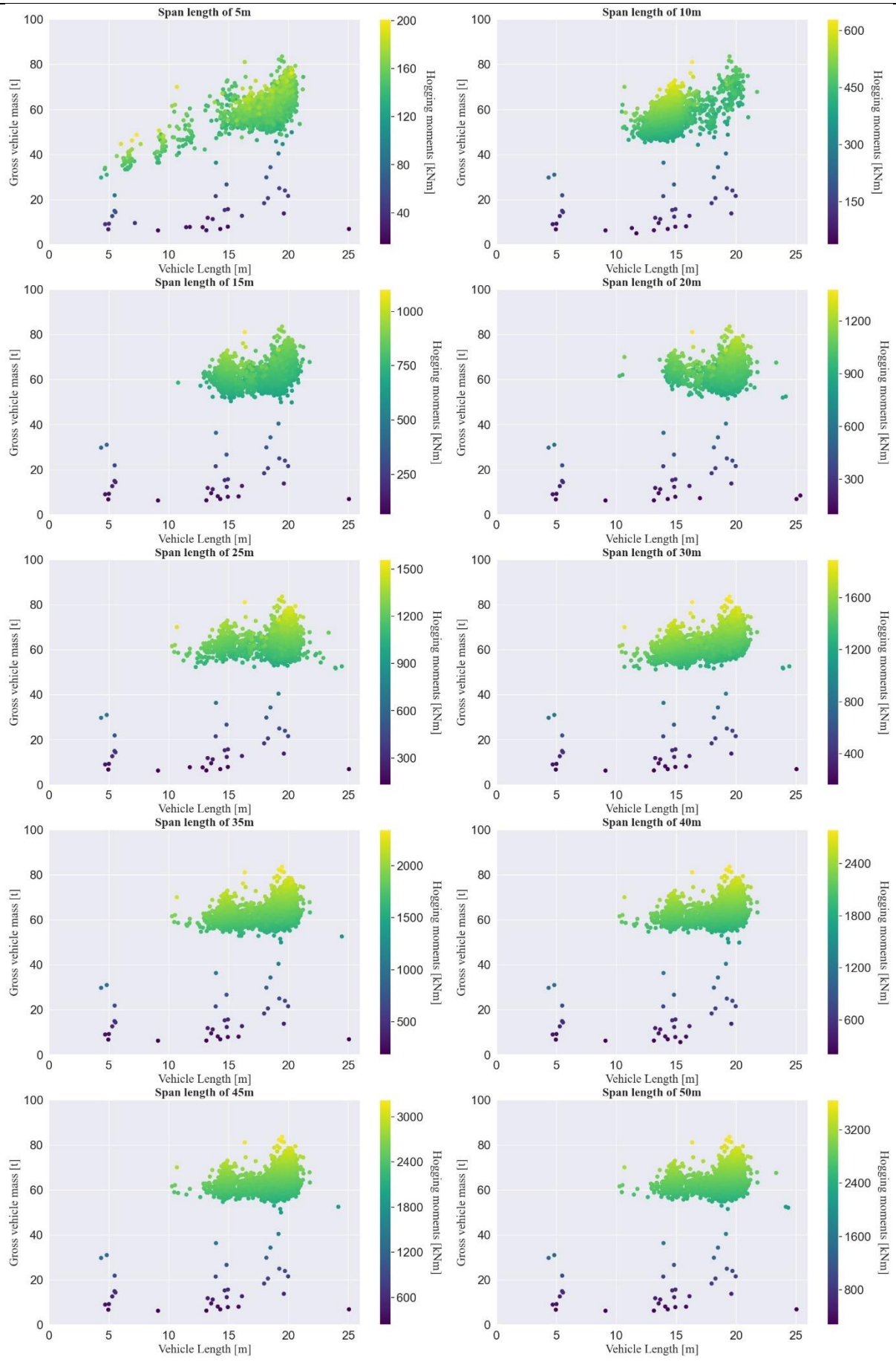

Figure A.10 Distribution of RMA group 3's GVM, vehicle length and hogging moments

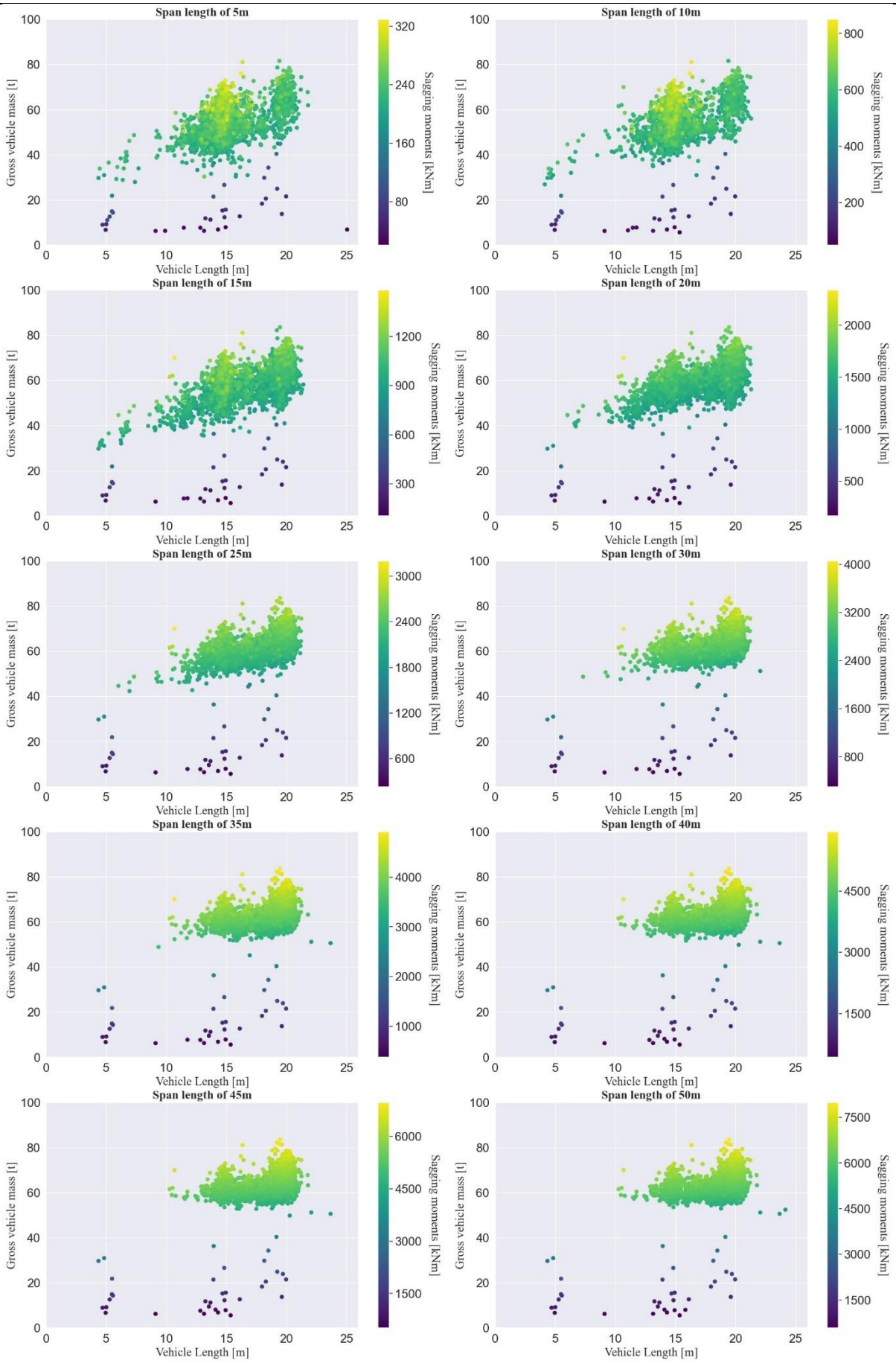

Figure A.11 Distribution of RMA group 3's GVM, vehicle length and sagging moments

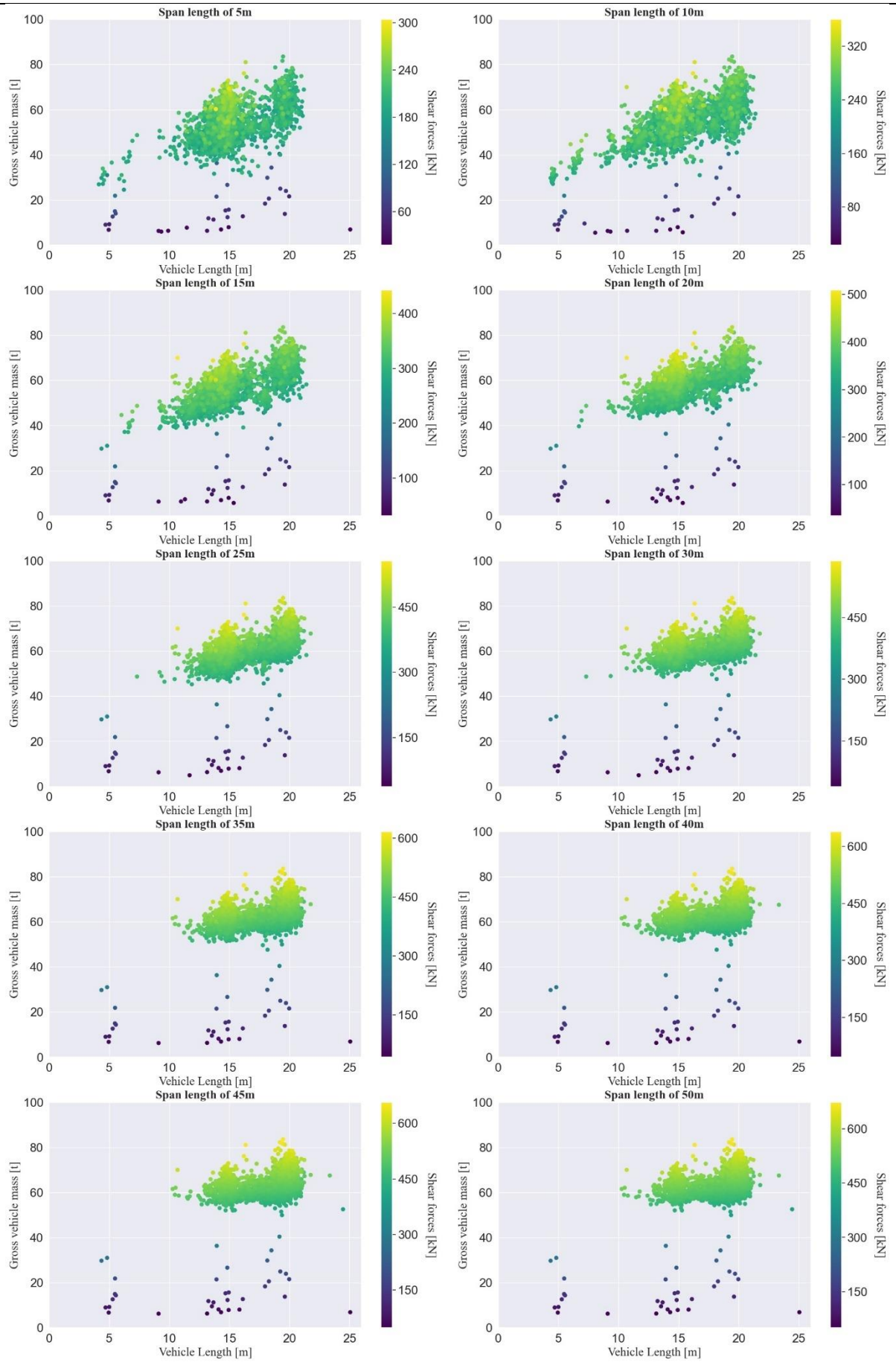

Figure A.12 Distribution of RMA group 3's GVM, vehicle length and shear forces

Appendix B: Mixed-axle vehicle groups GPP plots

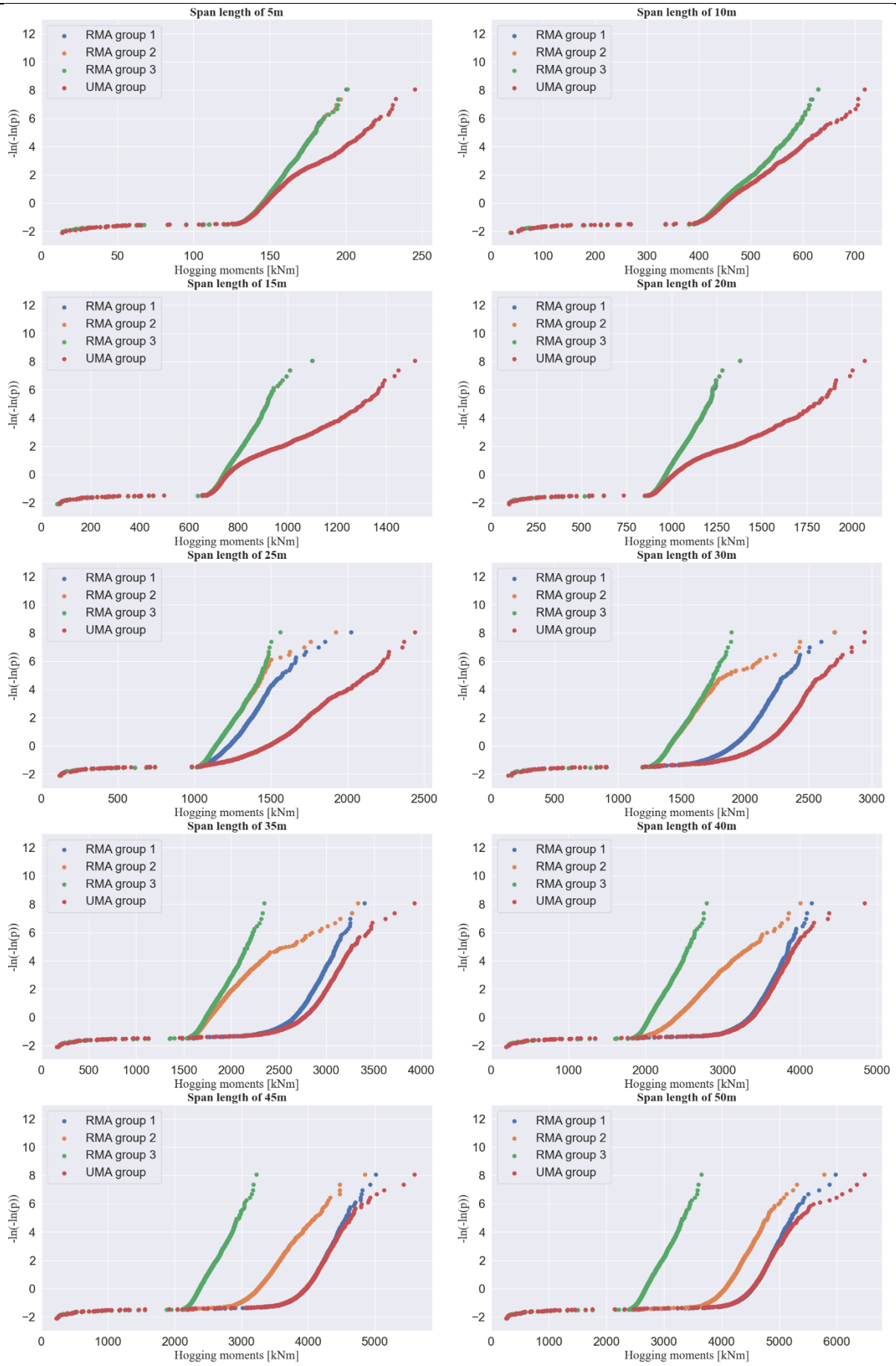

Figure B.1 Comparison of mixed axle groups hogging moments GPP plots

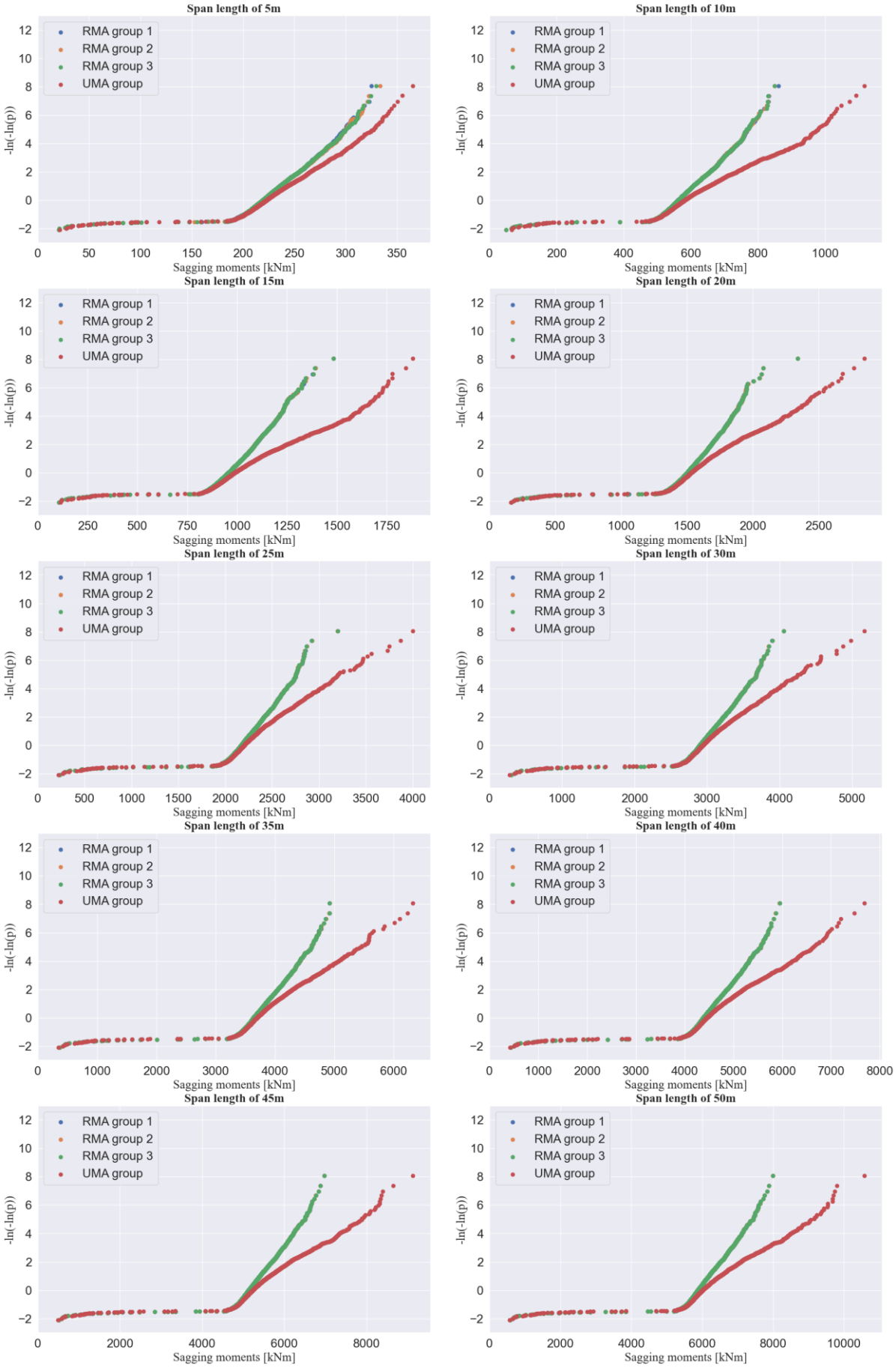

Figure B.2 Comparison of mixed axle groups sagging moments GPP plots

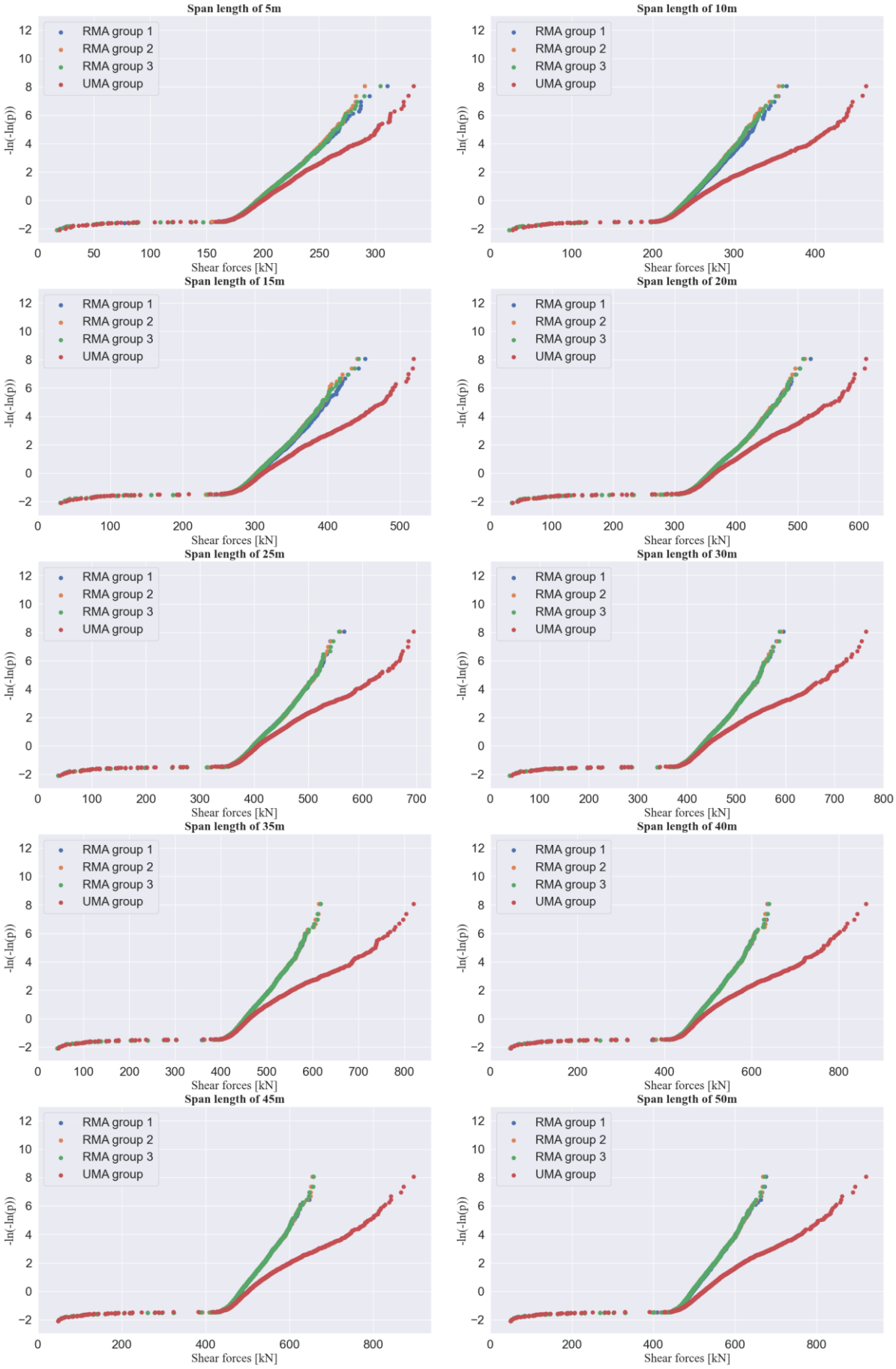

Figure B.3 Comparison of mixed axle groups shear forces GPP plots

Appendix C: Sub-axle groups in the tail of the UMA group and RMA group 3

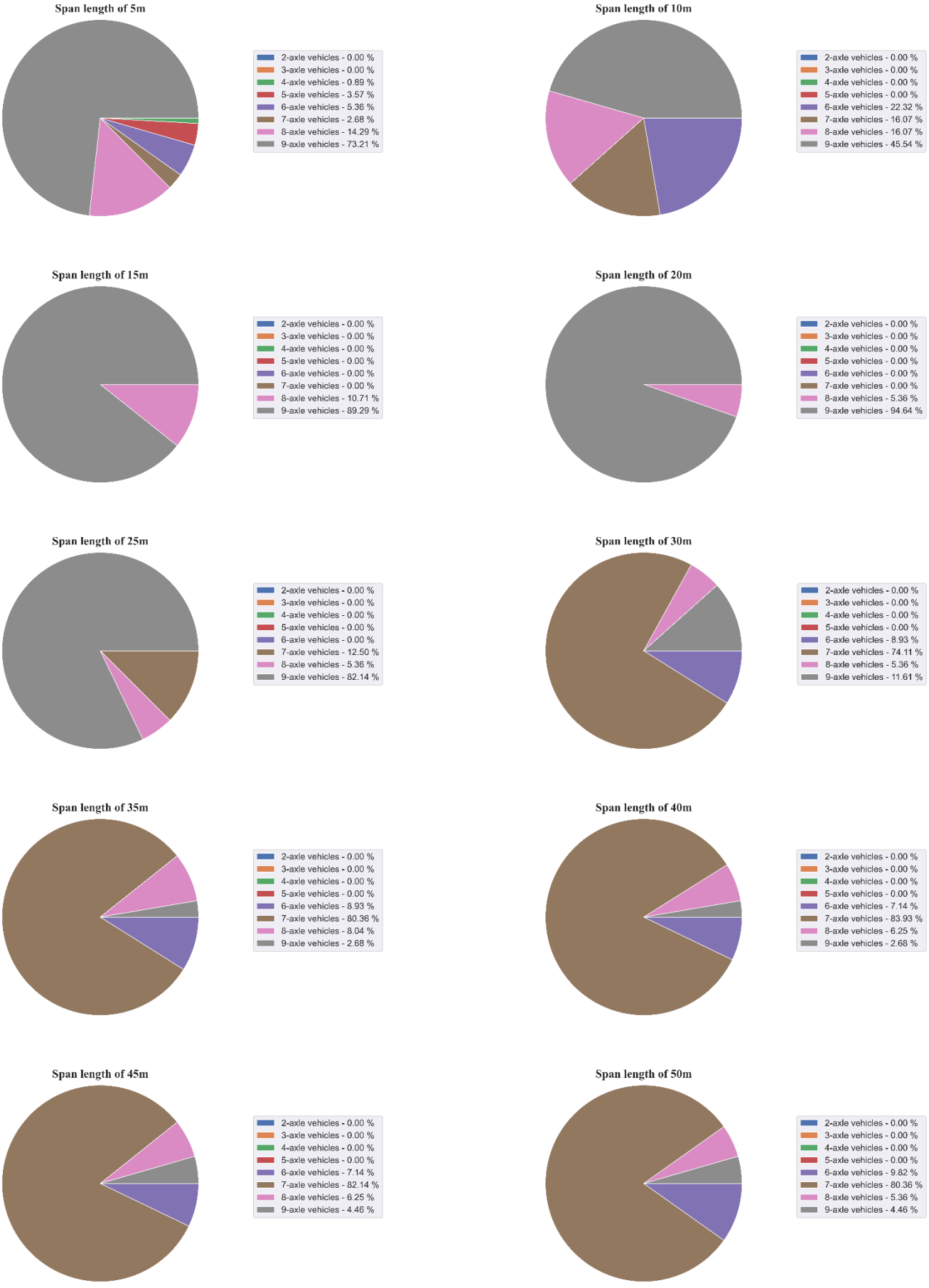

Figure C.1 Contributing sub-axle vehicles in the tail of daily maxima hogging moments for the UMA group

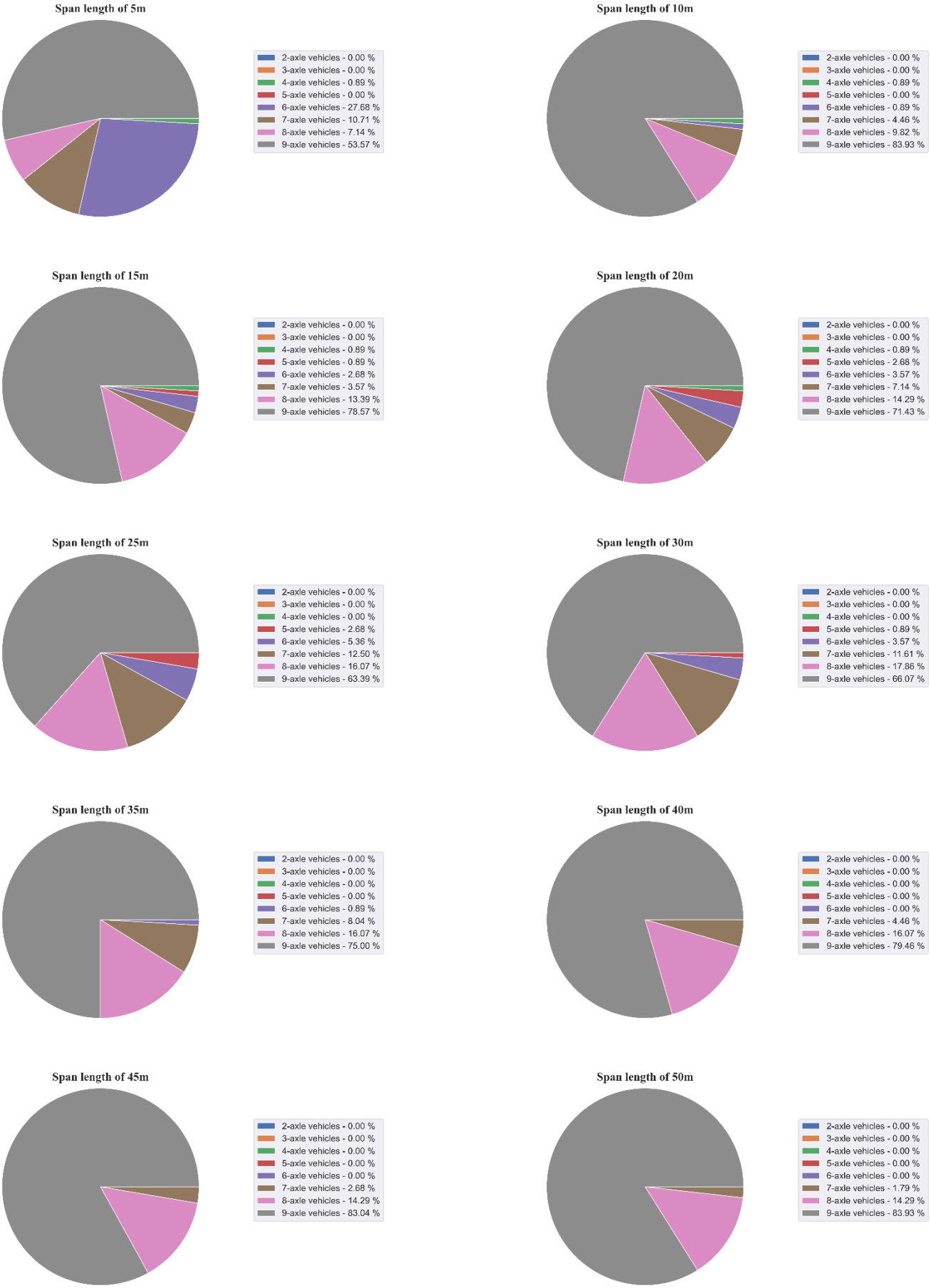

Figure C.2 Contributing sub-axle vehicles in the tail of daily maxima sagging moments for the UMA group

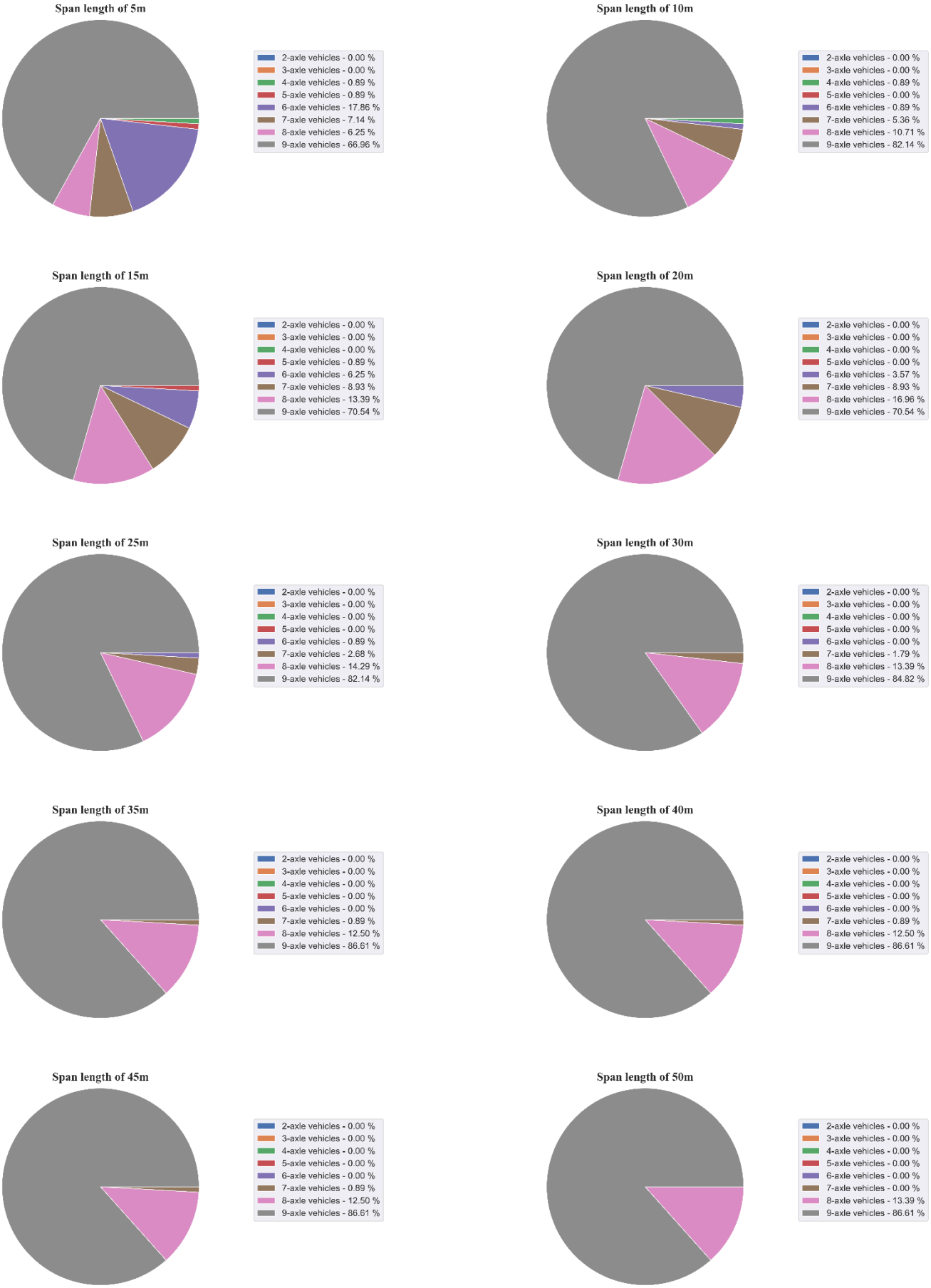

Figure C.3 Contributing sub-axle vehicles in the tail of daily maxima shear forces for the UMA group

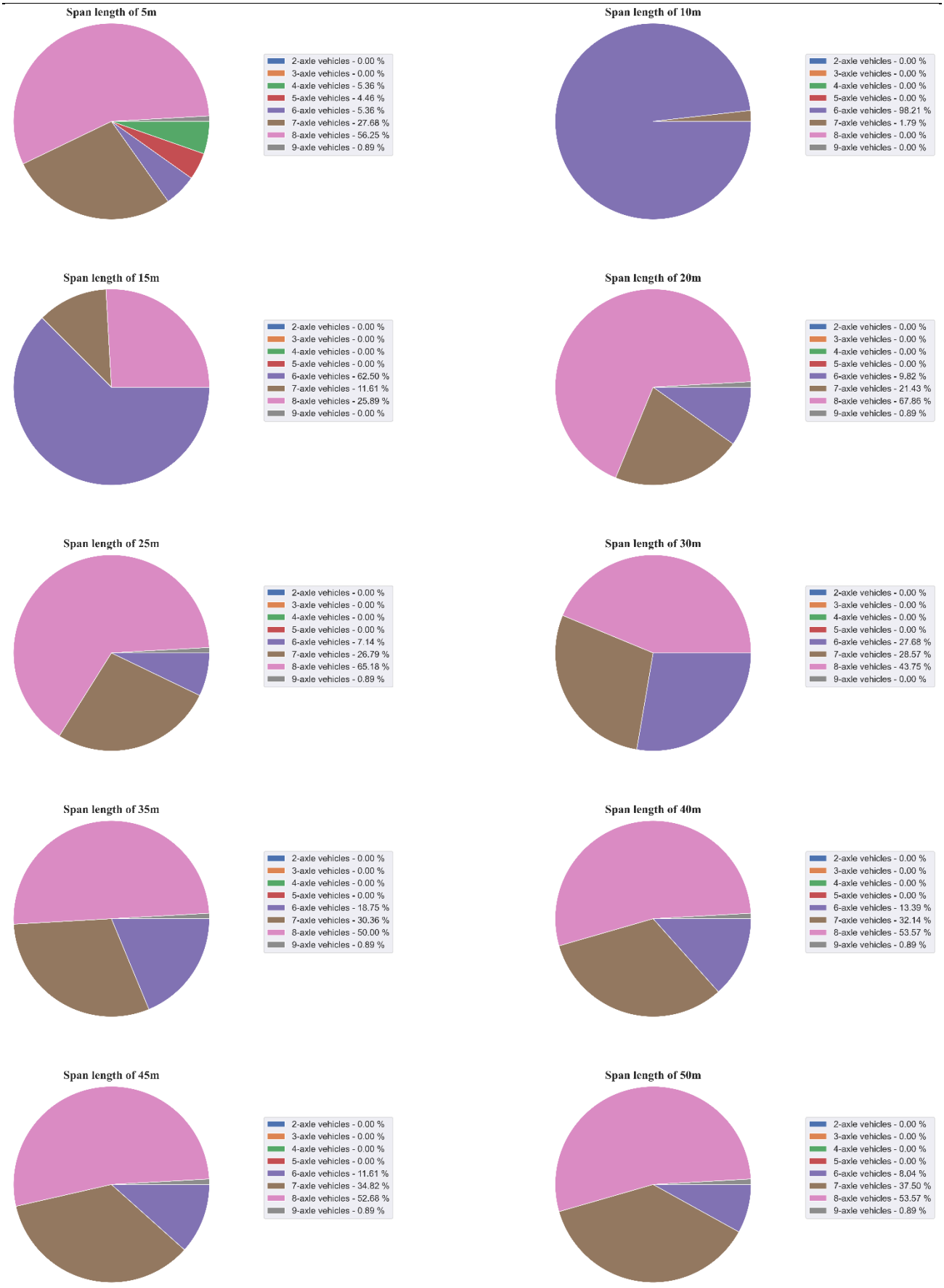

Figure C.4 Contributing sub-axle vehicles in the tail of daily maxima hogging moments for the RMA group 3

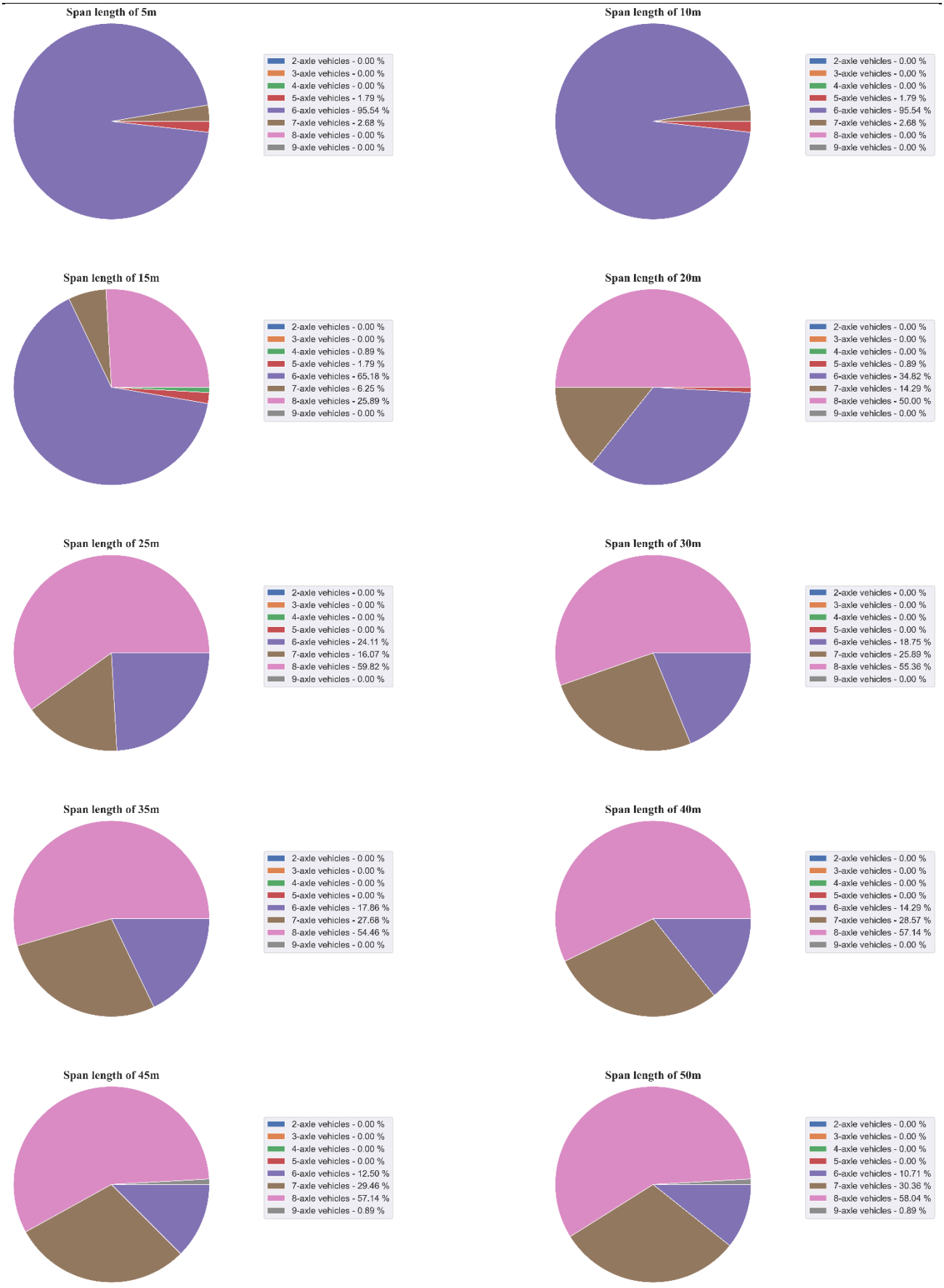

Figure C.5 Contributing sub-axle vehicles in the tail of daily maxima sagging moments for the RMA group 3

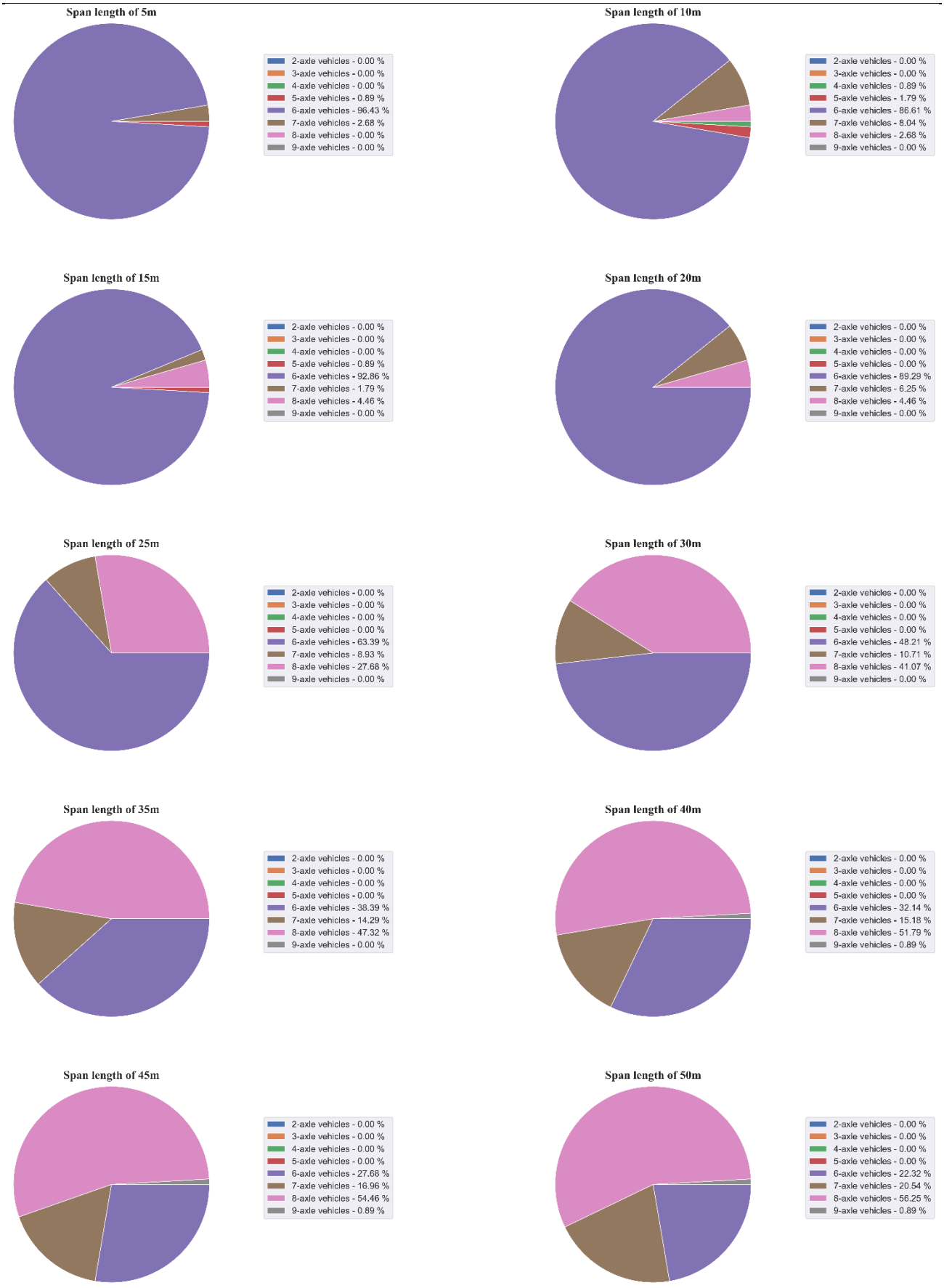

Figure C.6 Contributing sub-axle vehicles in the tail of daily maxima shear forces for the RMA group 3

Appendix D: UMA group and RMA group 3 GPP plot breakdown

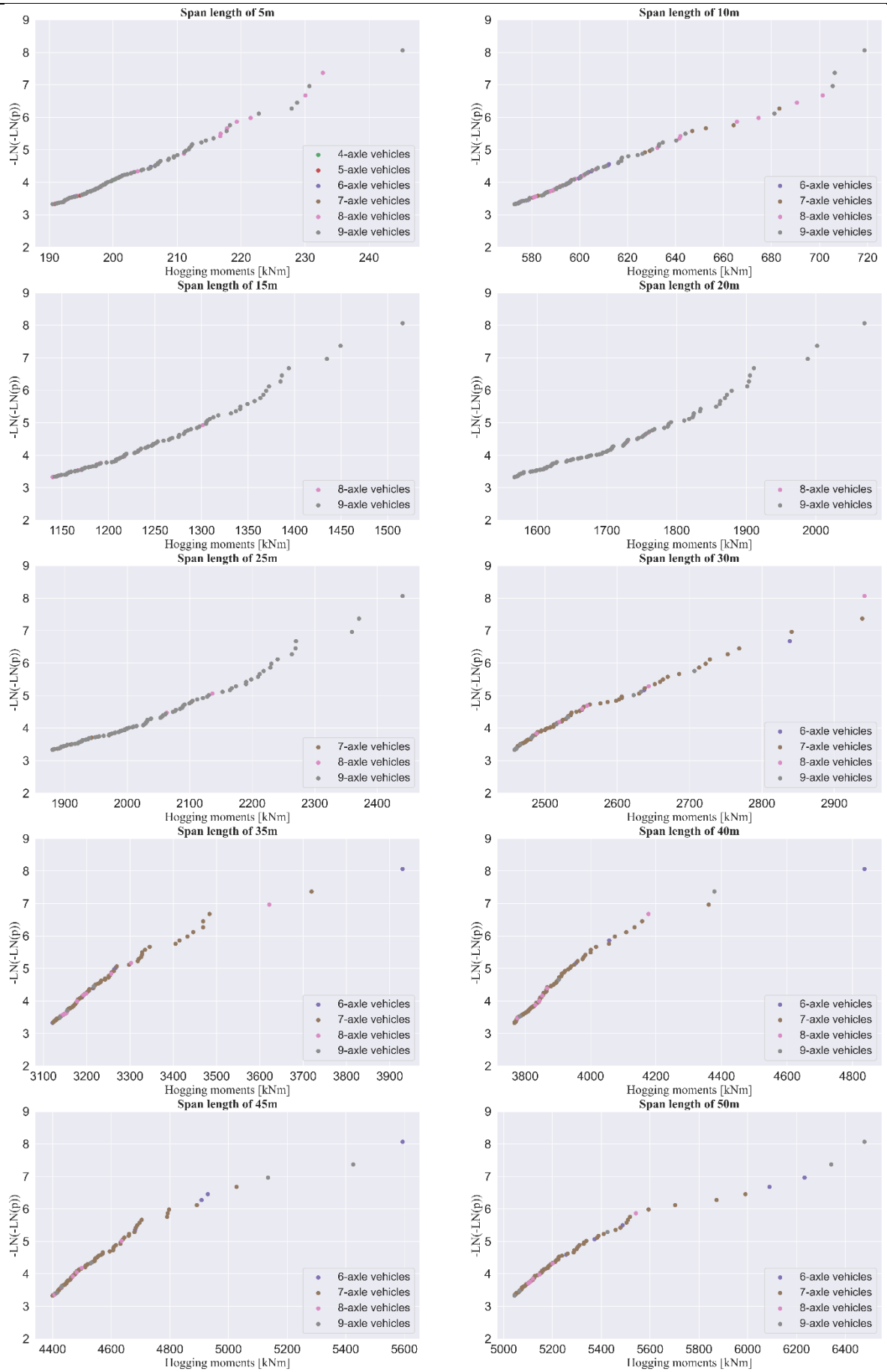

Figure D.1 Breakdown of the hogging moments GPP plots for the UMA group

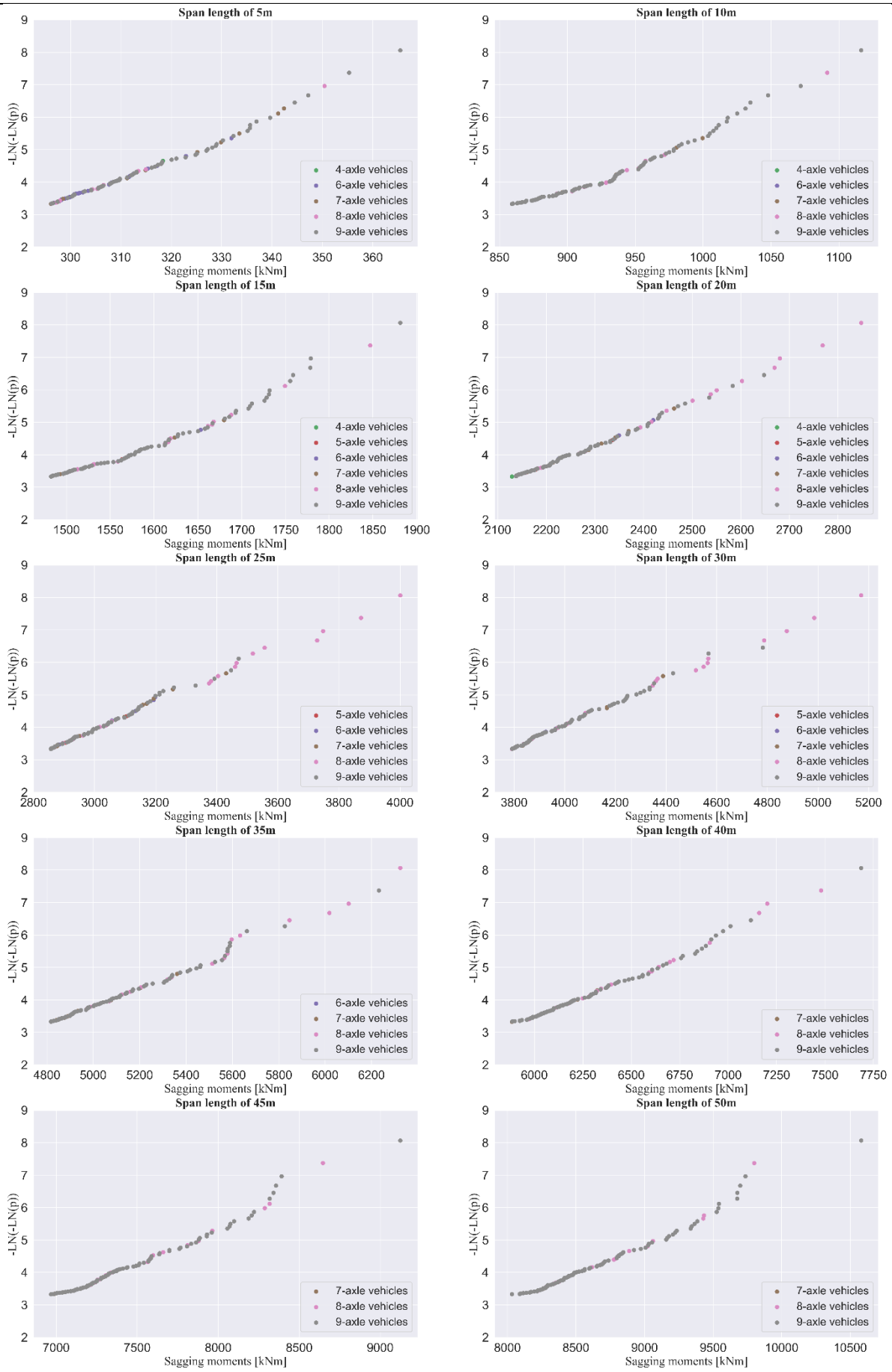

Figure D.2 Breakdown of the sagging moments GPP plots for the UMA group

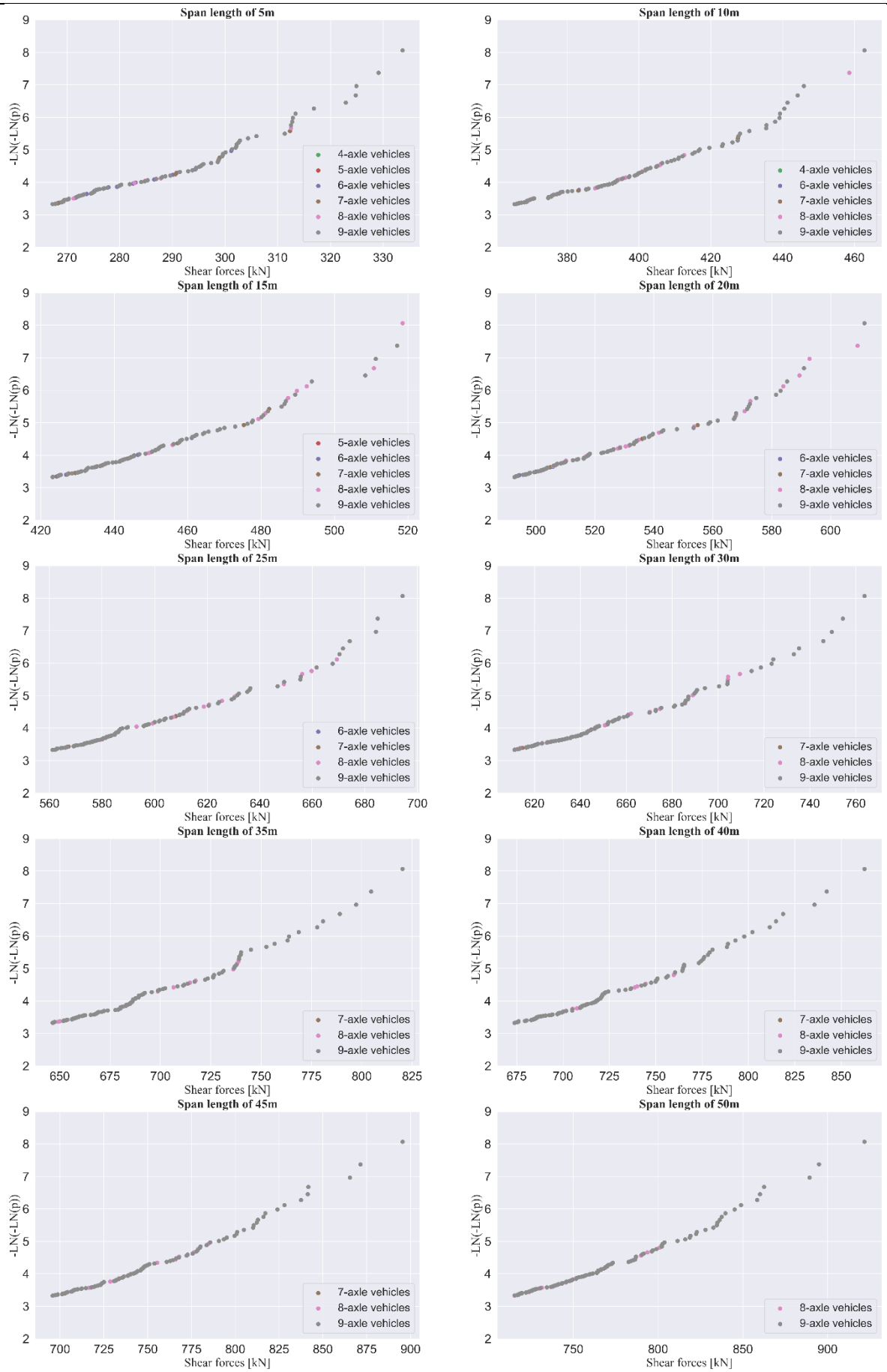

Figure D.3 Breakdown of the shear forces GPP plots for the UMA group

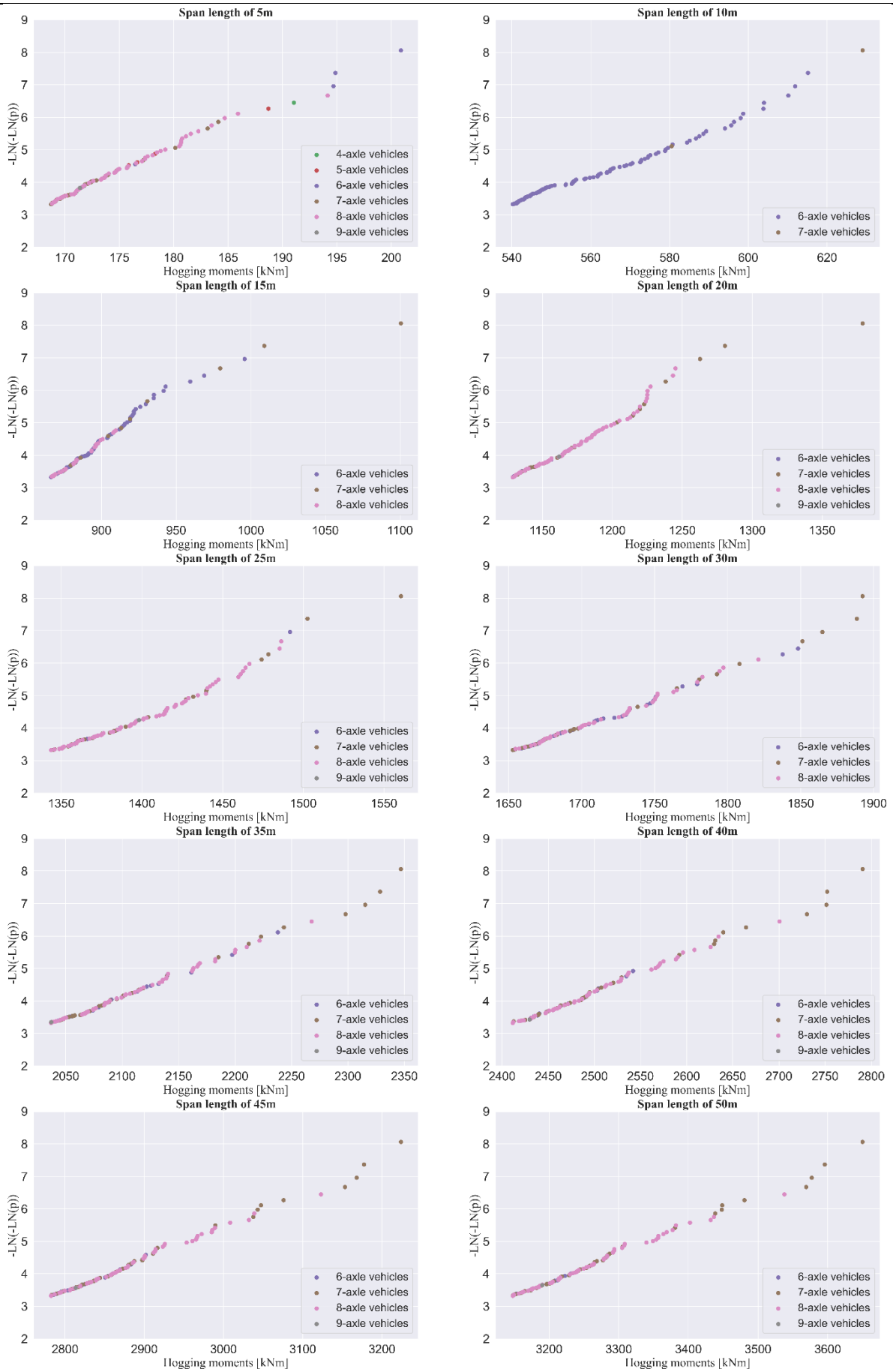

Figure D.4 Breakdown of the hogging moments GPP plots for the RMA group 3

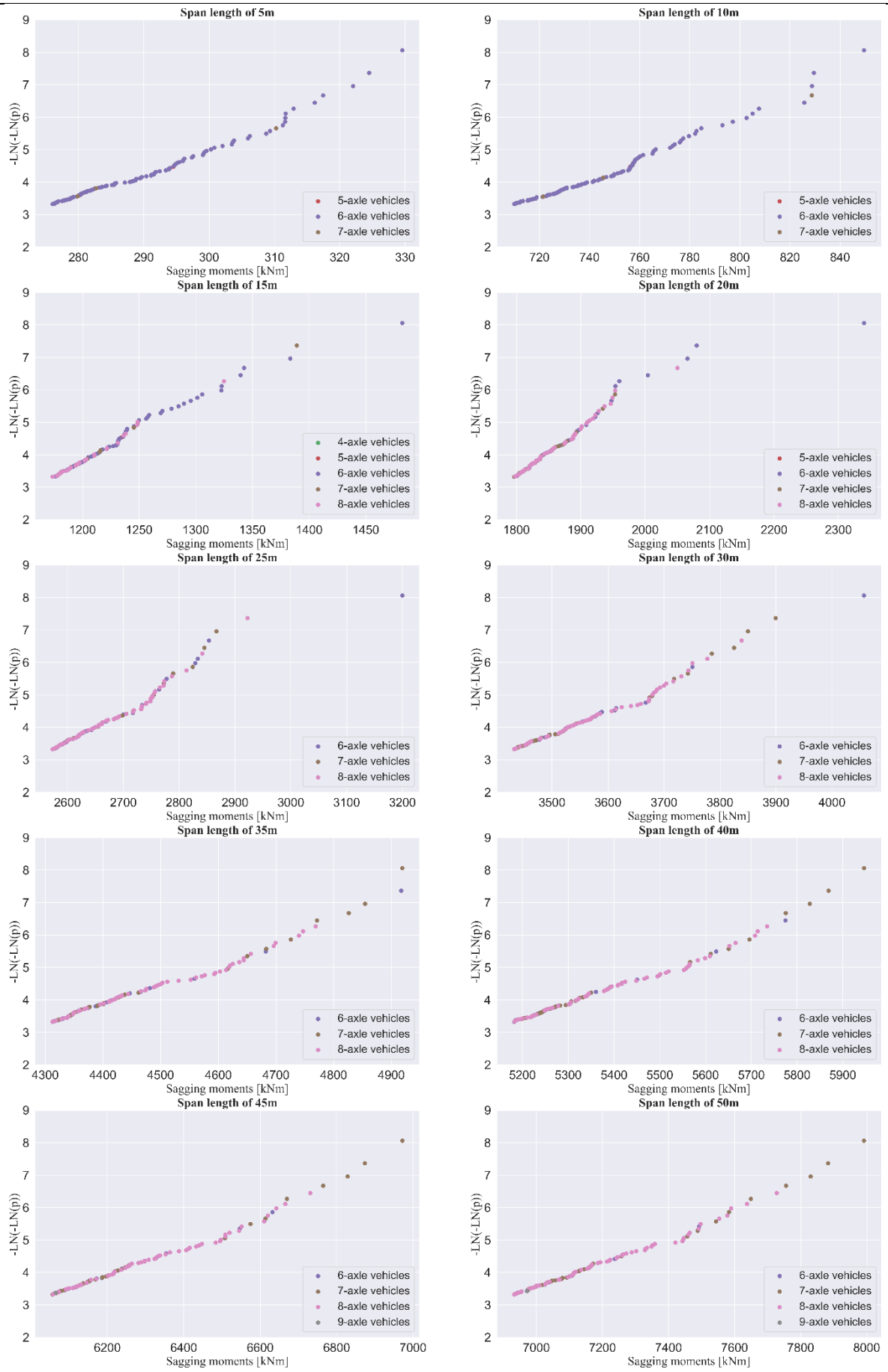

Figure D.5 Breakdown of the sagging moments GPP plots for the RMA group 3

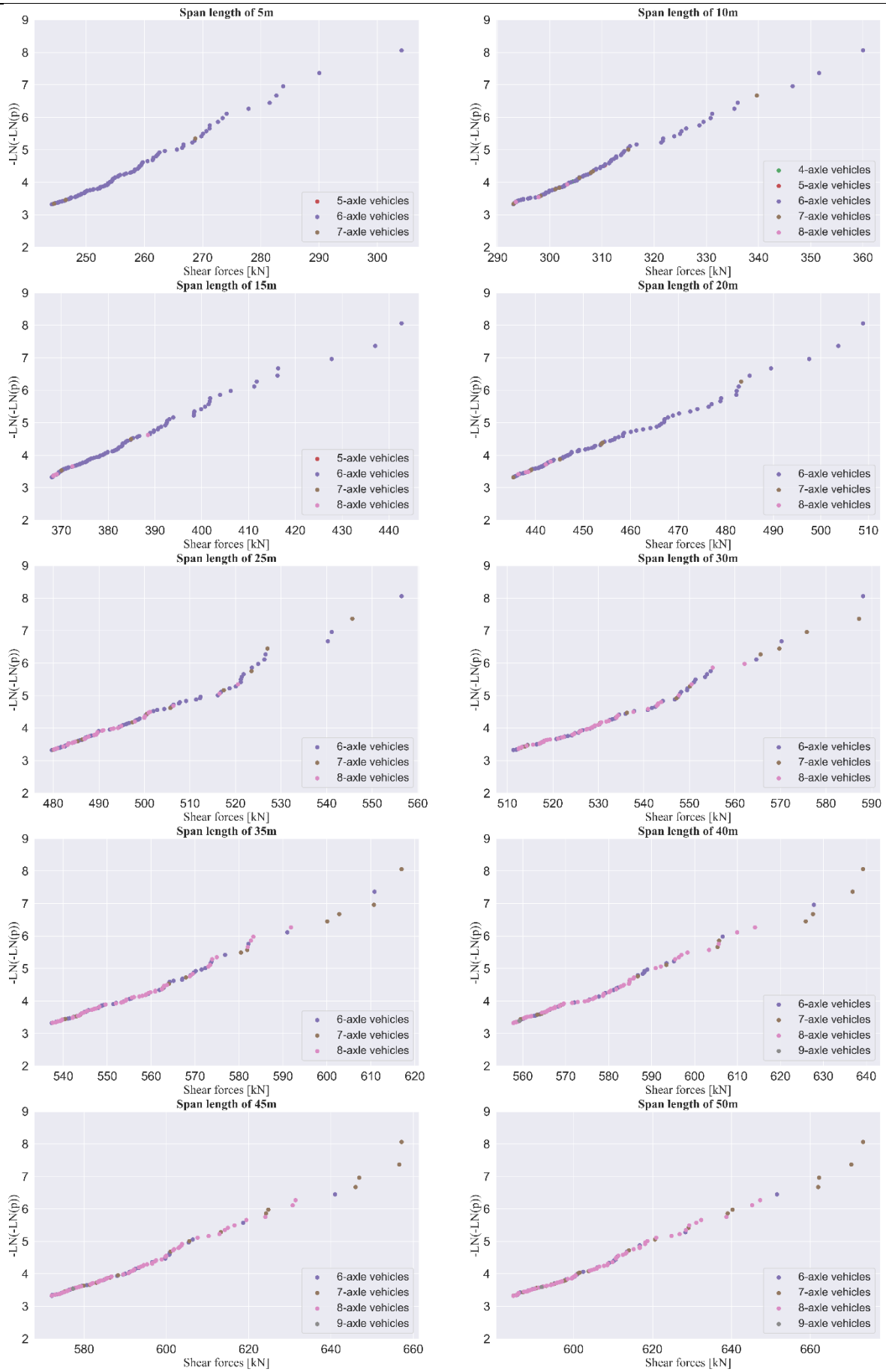

Figure D.6 Breakdown of the shear forces GPP plots for the RMA group 3

Appendix E: GPP plots for the sub-axle vehicle groups

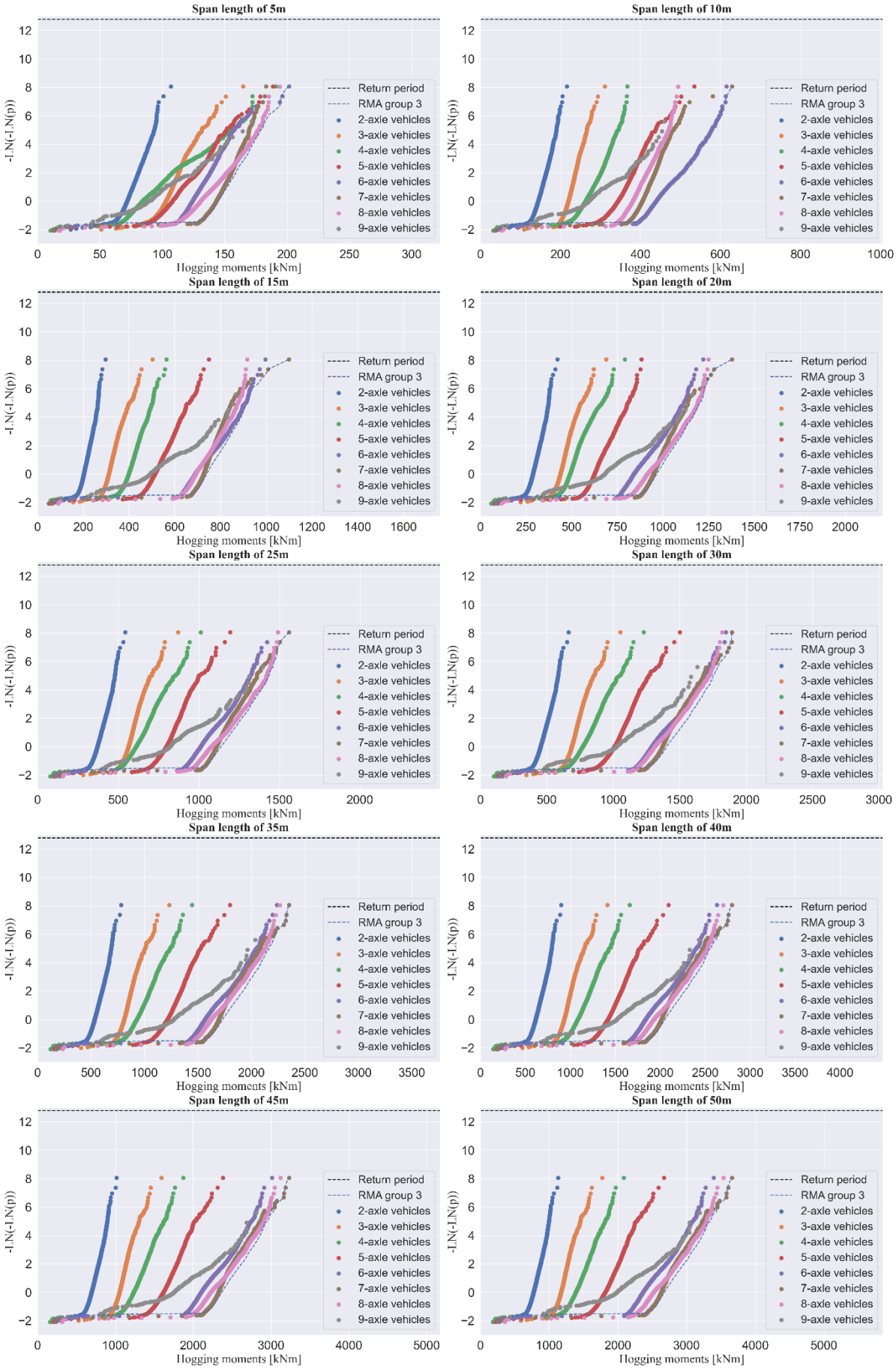

Figure E.1 Hogging moments GPP comparison for the sub-axle groups and RMA group 3

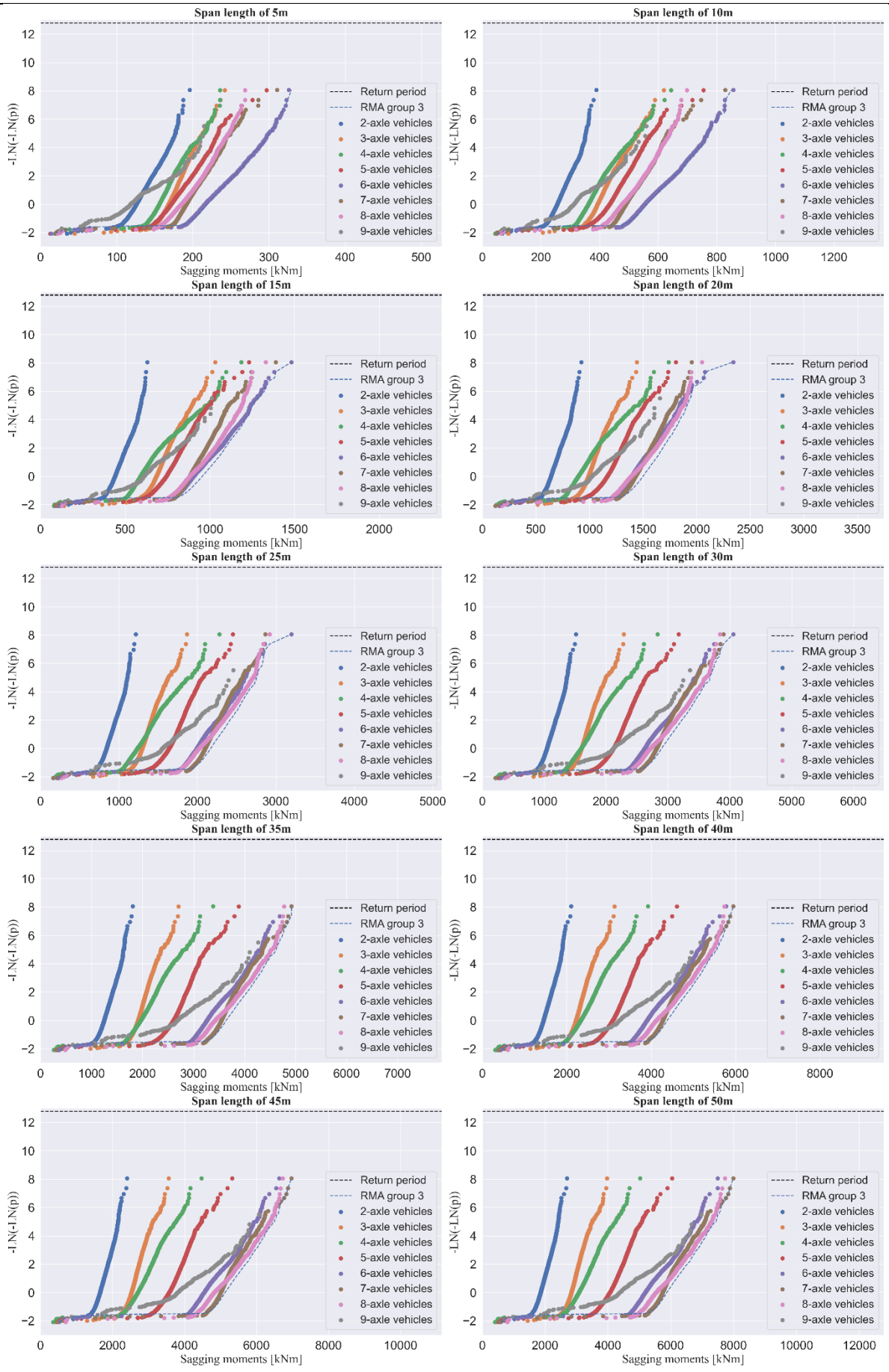

Figure E.2 Sagging moments GPP comparison for the sub-axle groups and RMA group 3

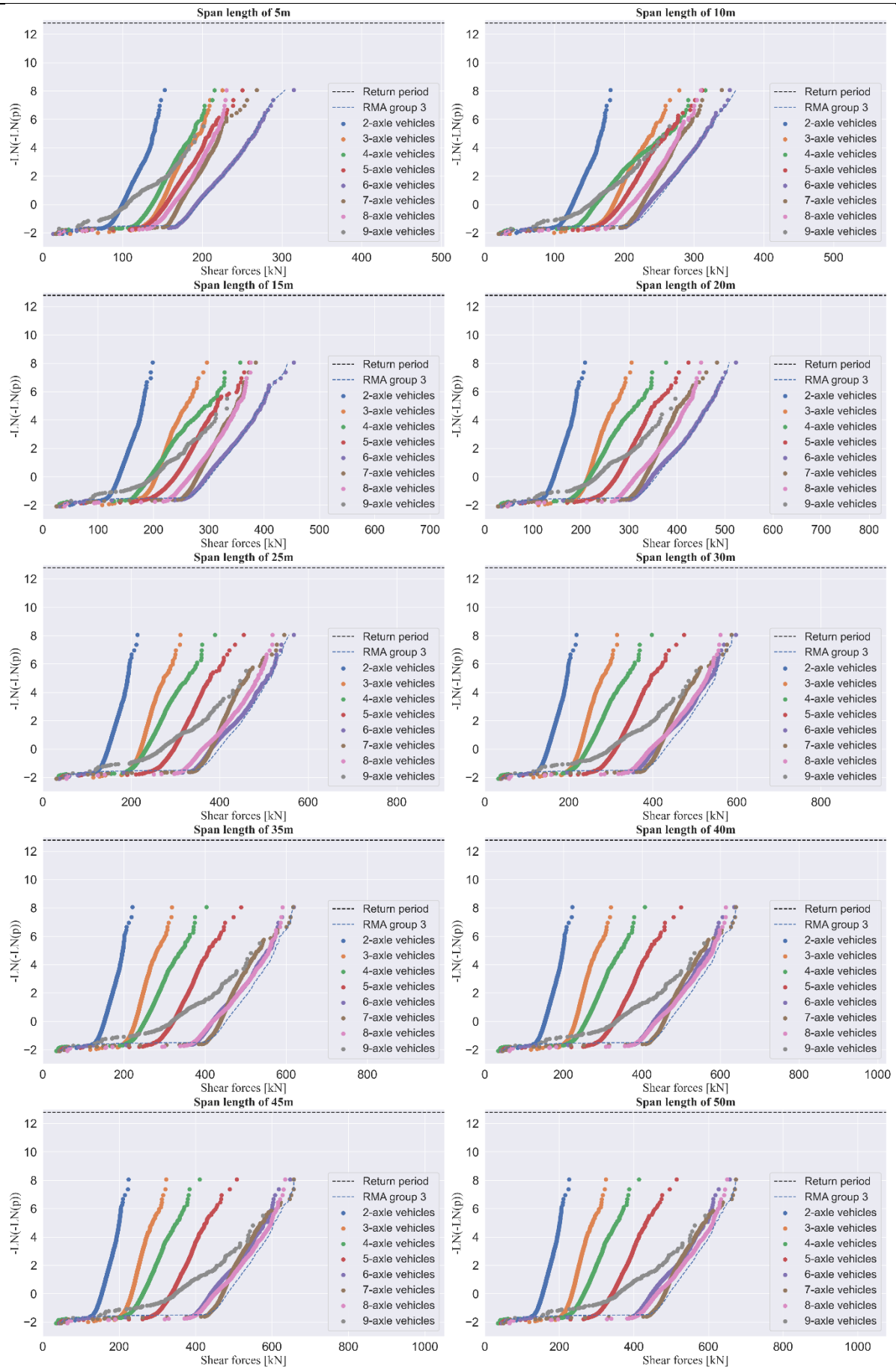

Figure E.3 Shear force GPP comparison for the sub-axle groups and RMA group 3

Appendix F: Sub-populations of sub-axle vehicle groups probability plots

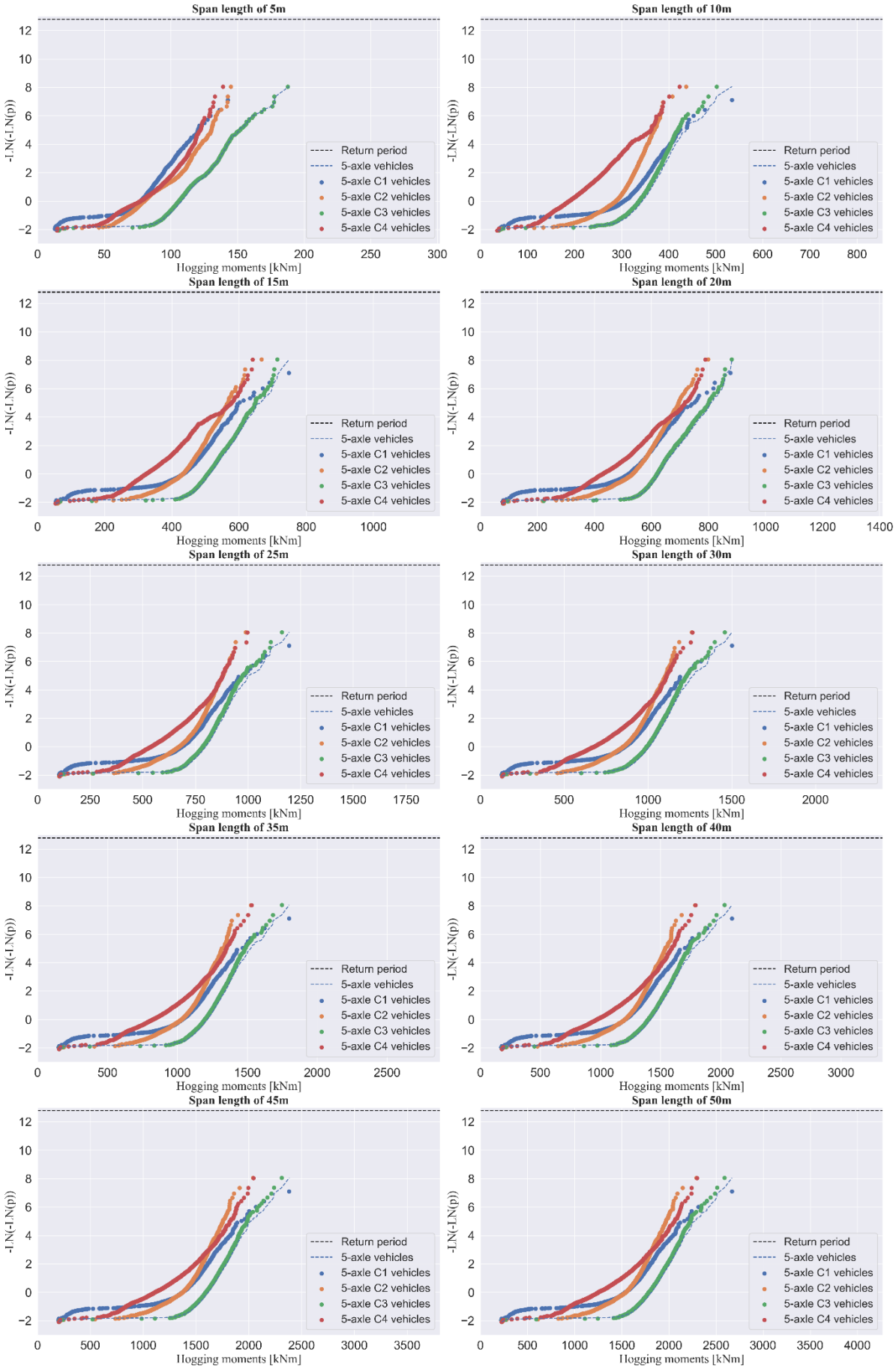

Figure F.1 Hogging moment GPP comparison for the sub-categories of 5-axle vehicles

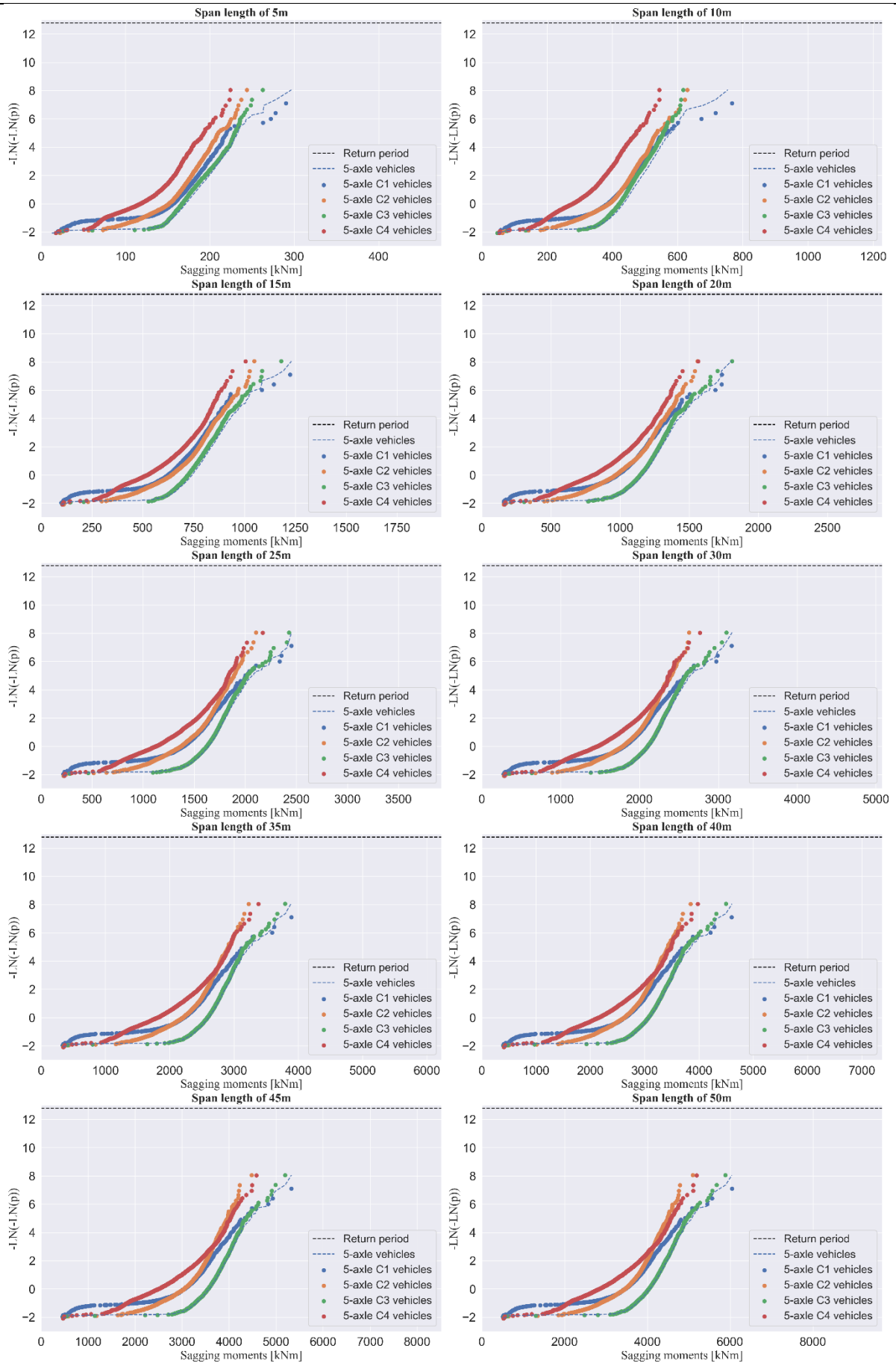

Figure F.2 Sagging moment GPP comparison for the sub-categories of 5-axle vehicles

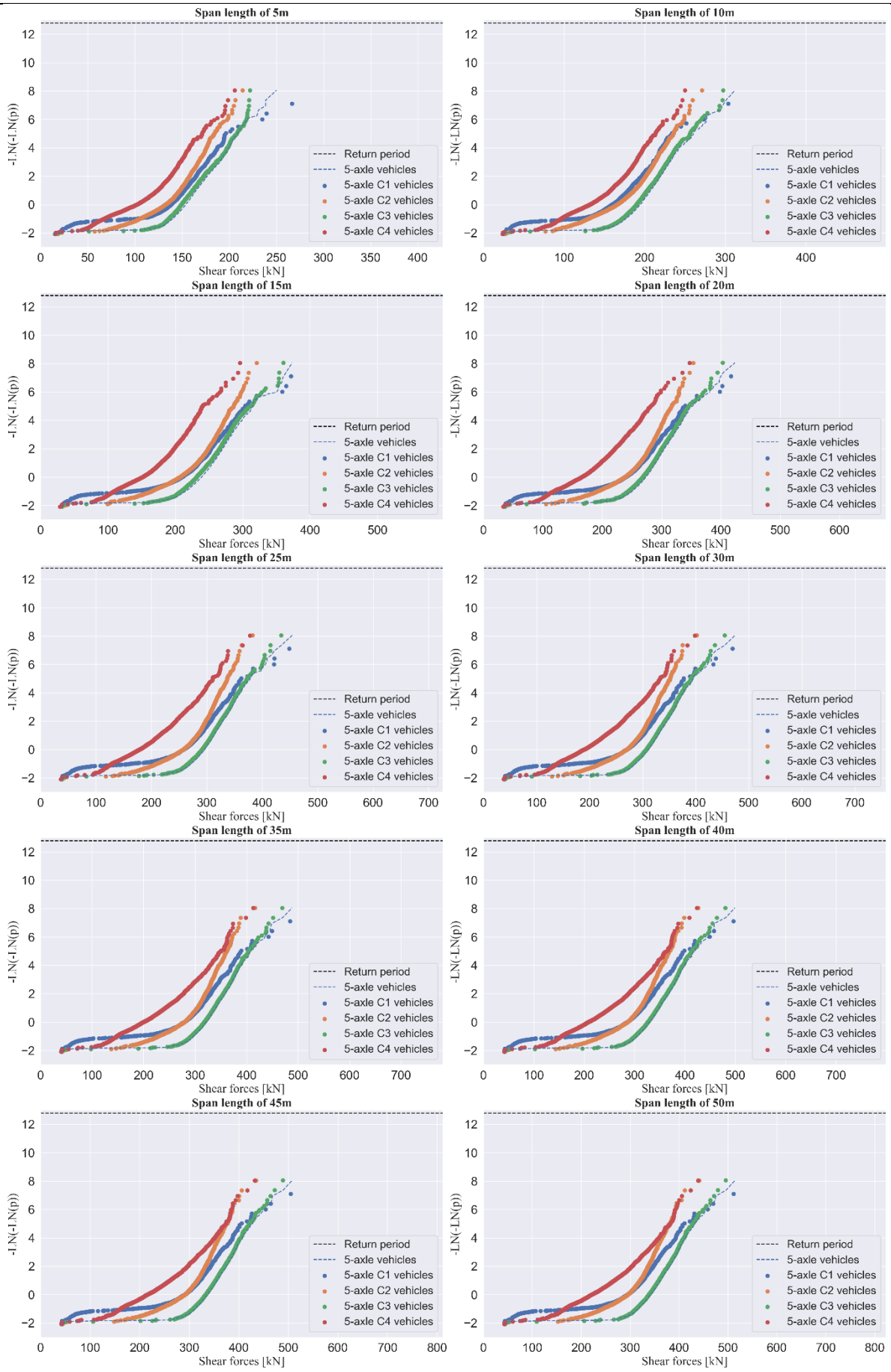

Figure F.3 Shear force GPP comparison for the sub-categories of 5- axle vehicles

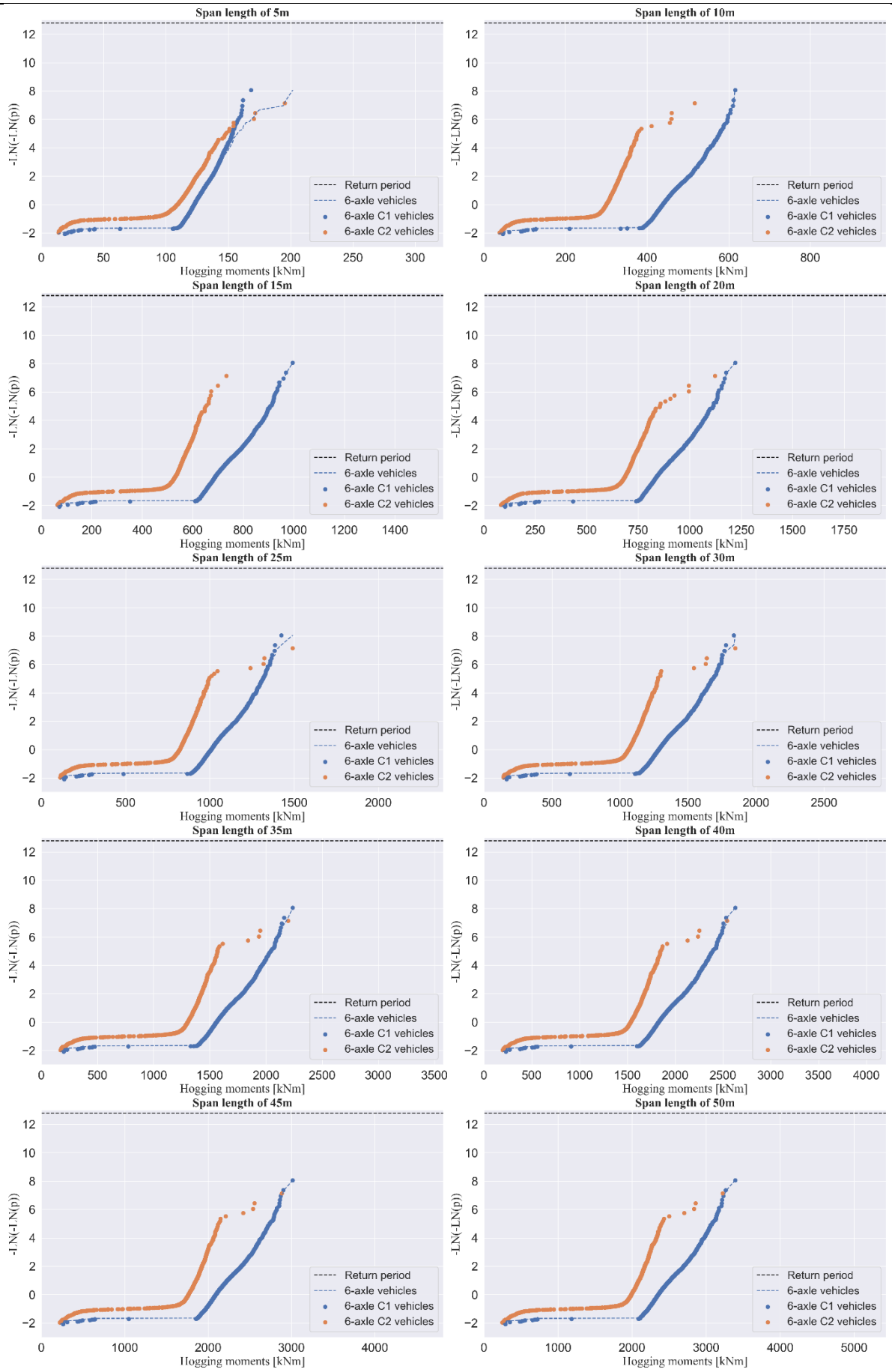

Figure F.4 Hogging moments GPP comparison for the sub-categories of 6- axle vehicles

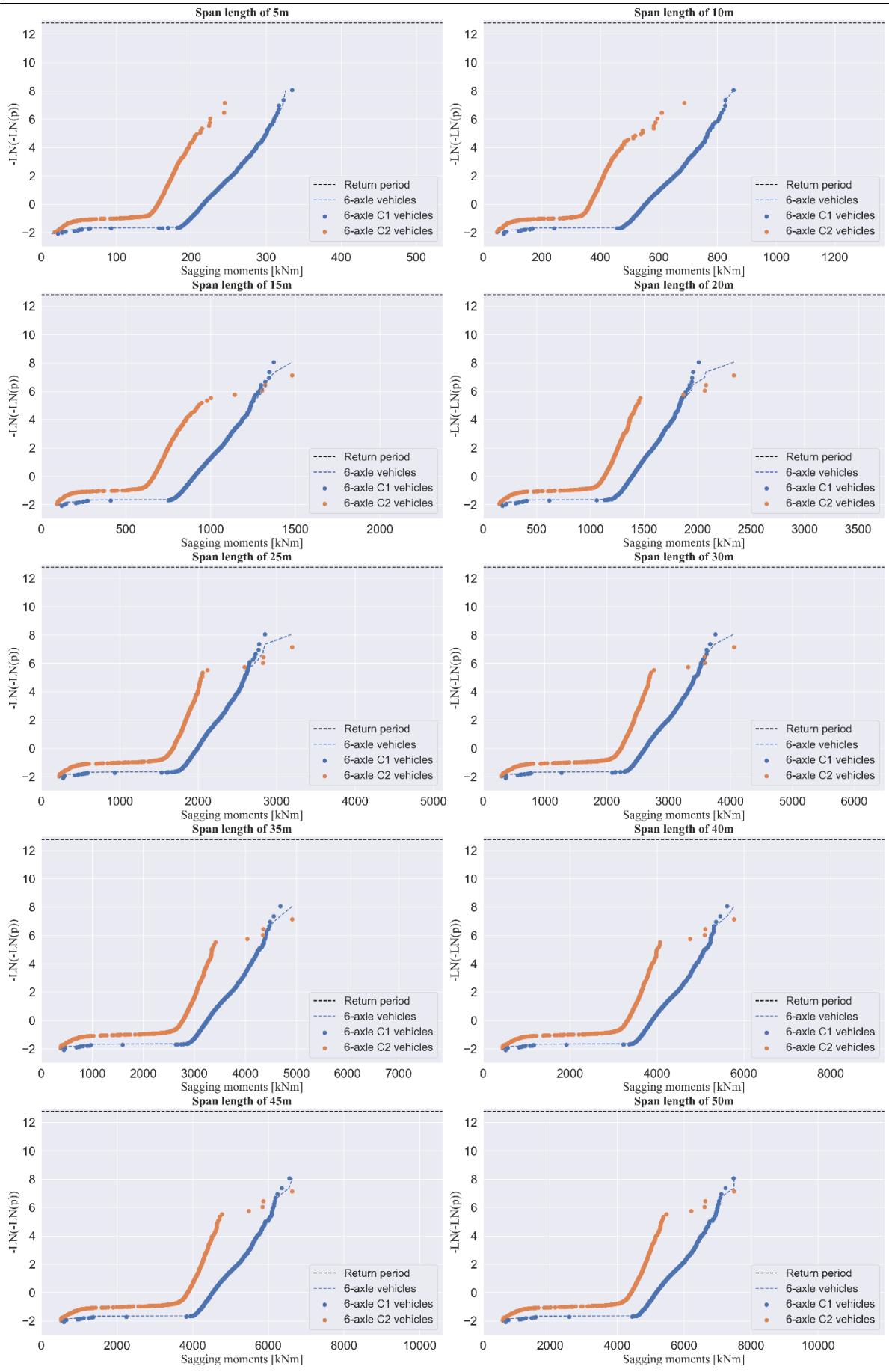

Figure F.5 Sagging moments GPP comparison for the sub-categories of 6- axle vehicles

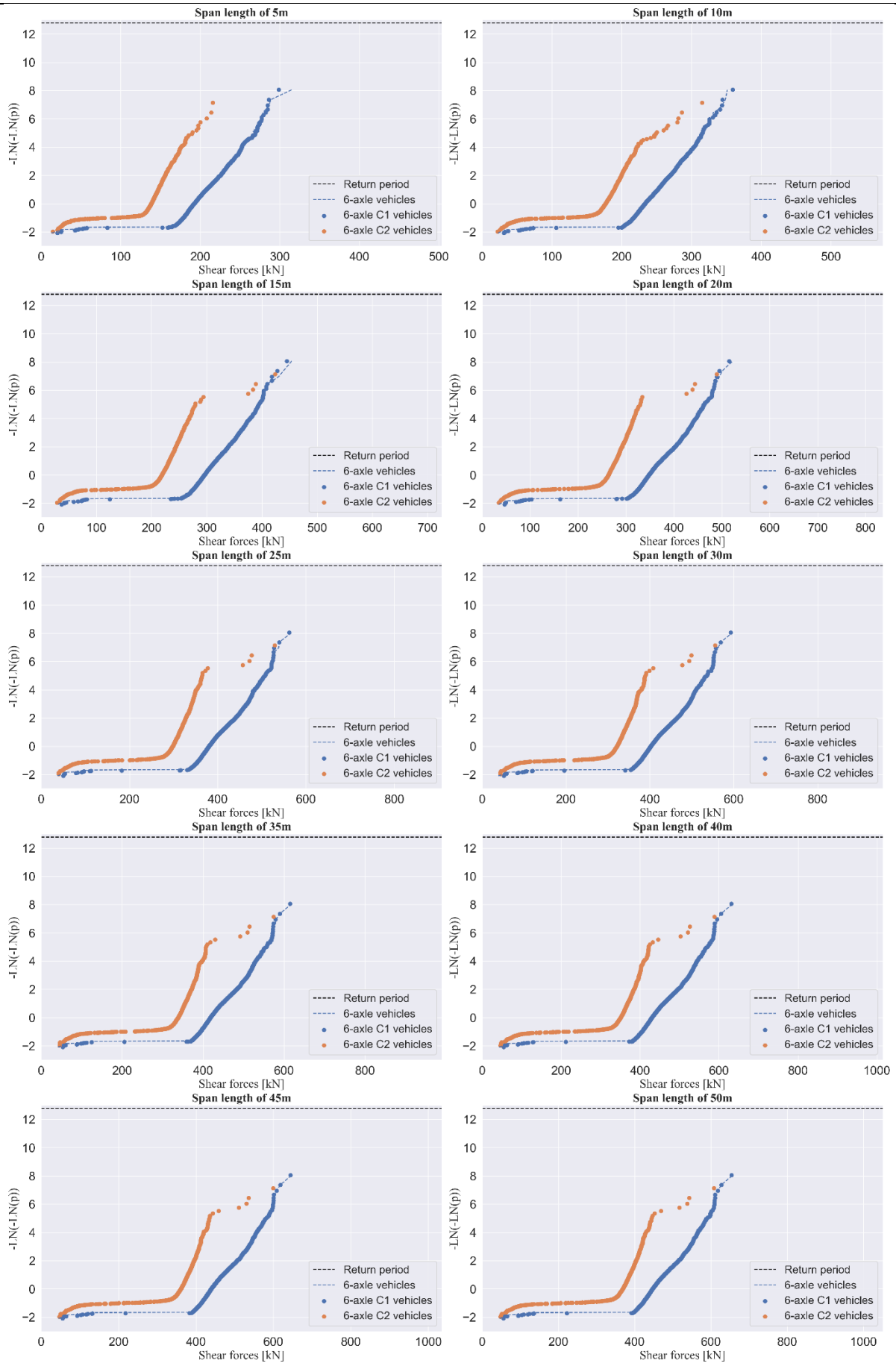

Figure F.6 Shear forces GPP comparison for the sub-categories of 6-axle vehicles

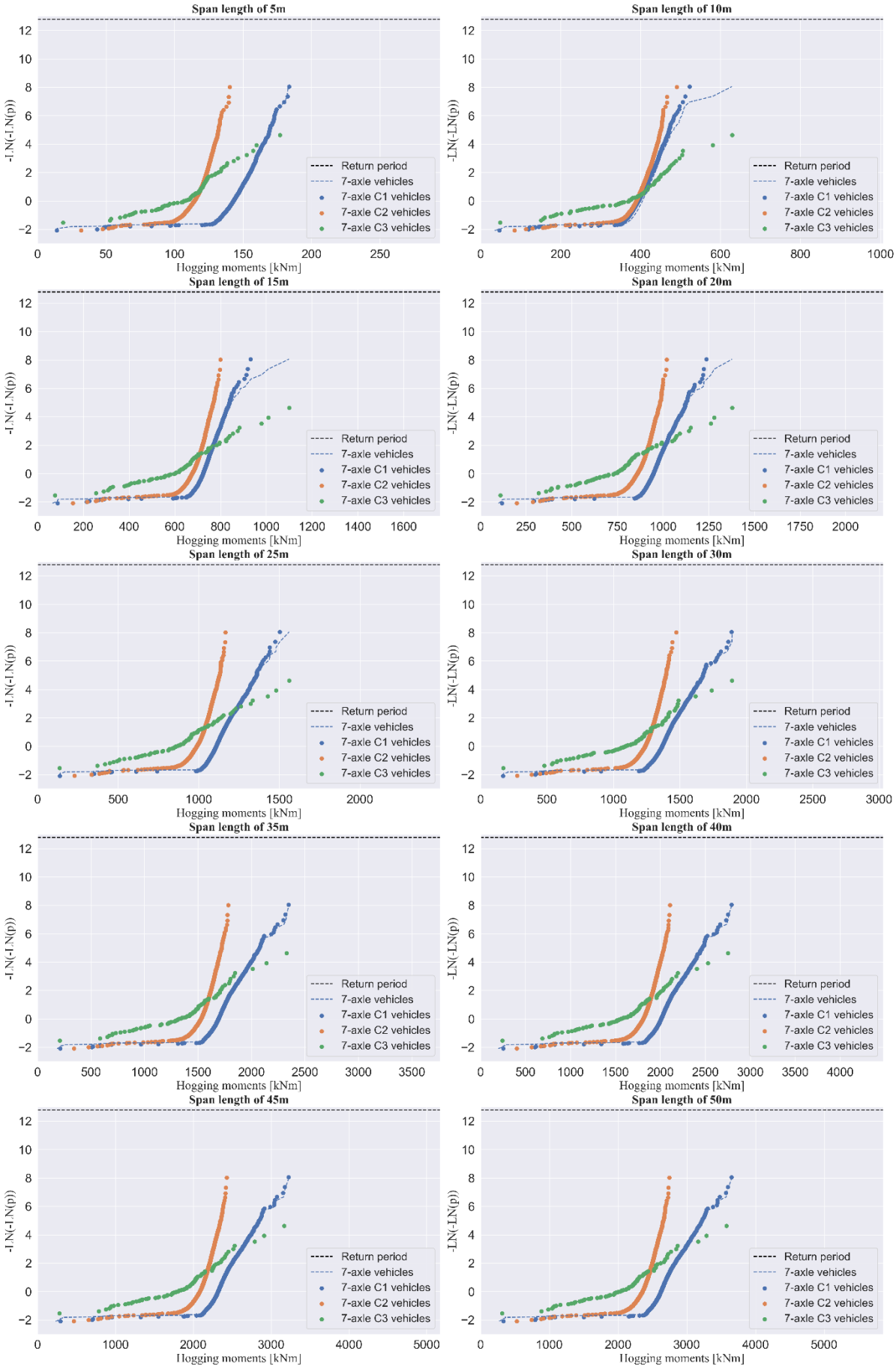

Figure F.7 Hogging moments GPP comparison for the sub-categories of 7-axle vehicles

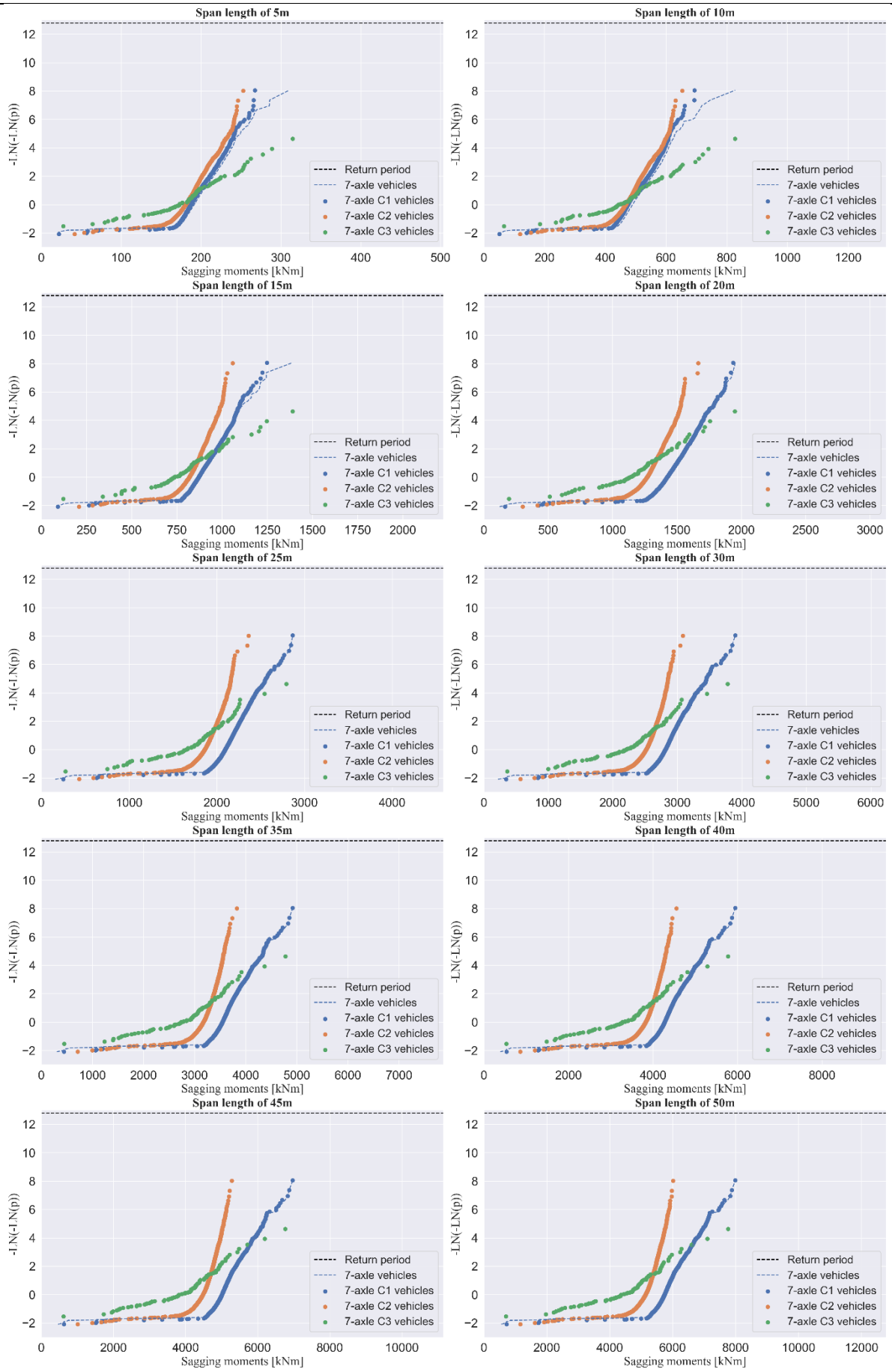

Figure F.8 Sagging moments GPP comparison for the sub-categories of 7- axle vehicles

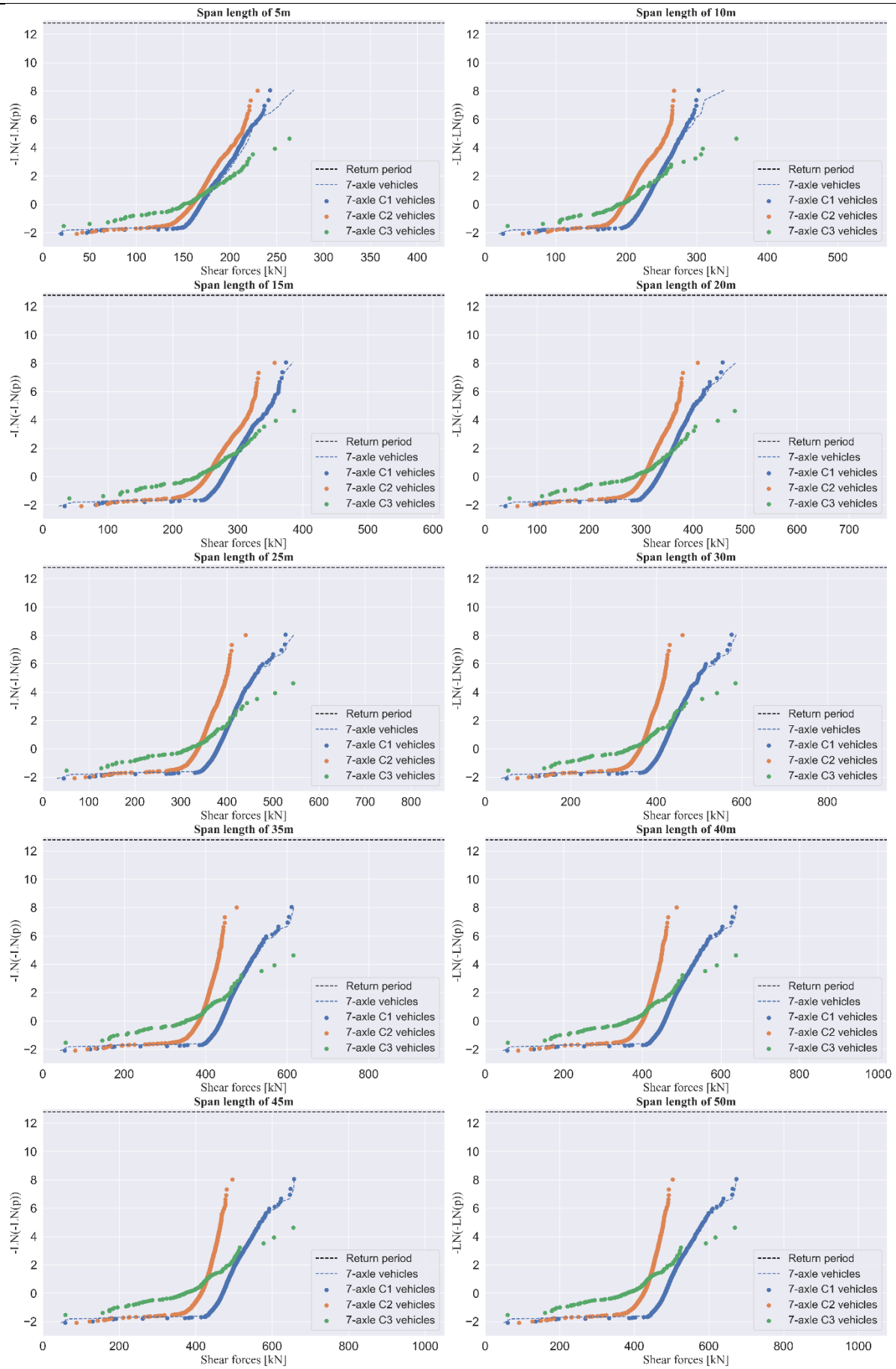

Figure F.9 Shear forces GPP comparison for the sub-categories of 7- axle vehicles

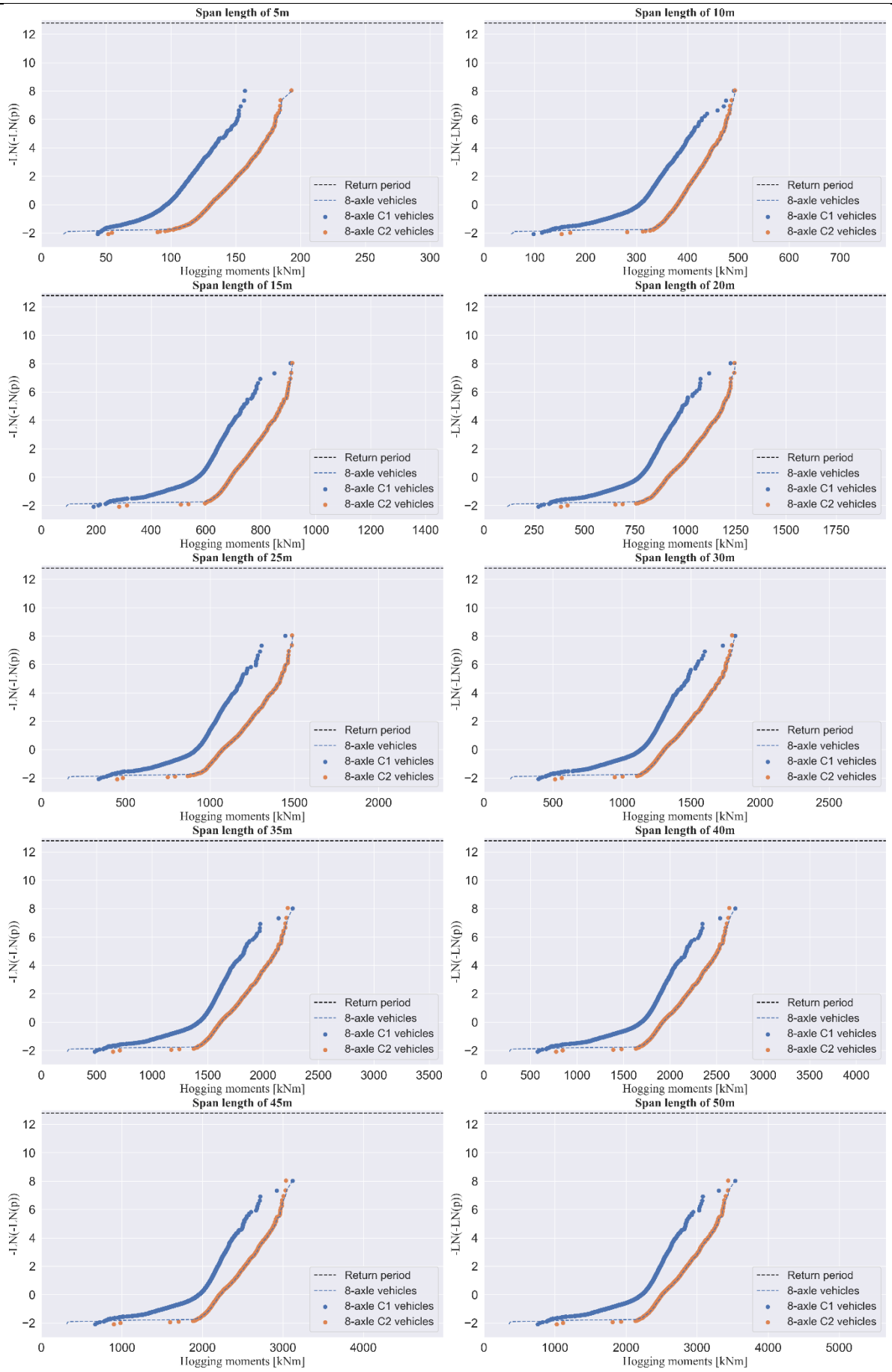

Figure F.10 Hogging moments GPP comparison for the sub-categories of 8- axle vehicles

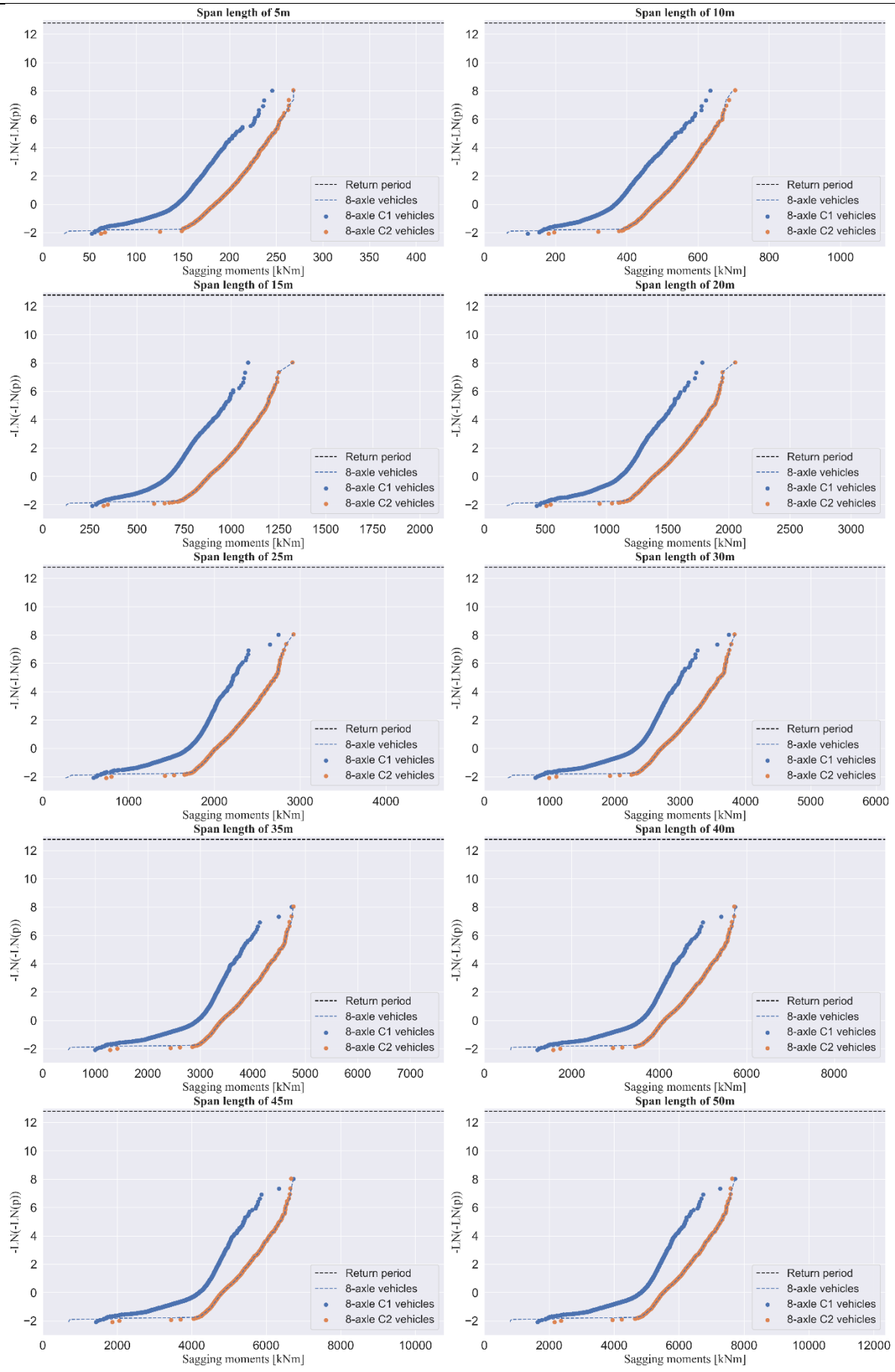

Figure F.11 Sagging moments GPP comparison for the sub-categories of 8- axle vehicles

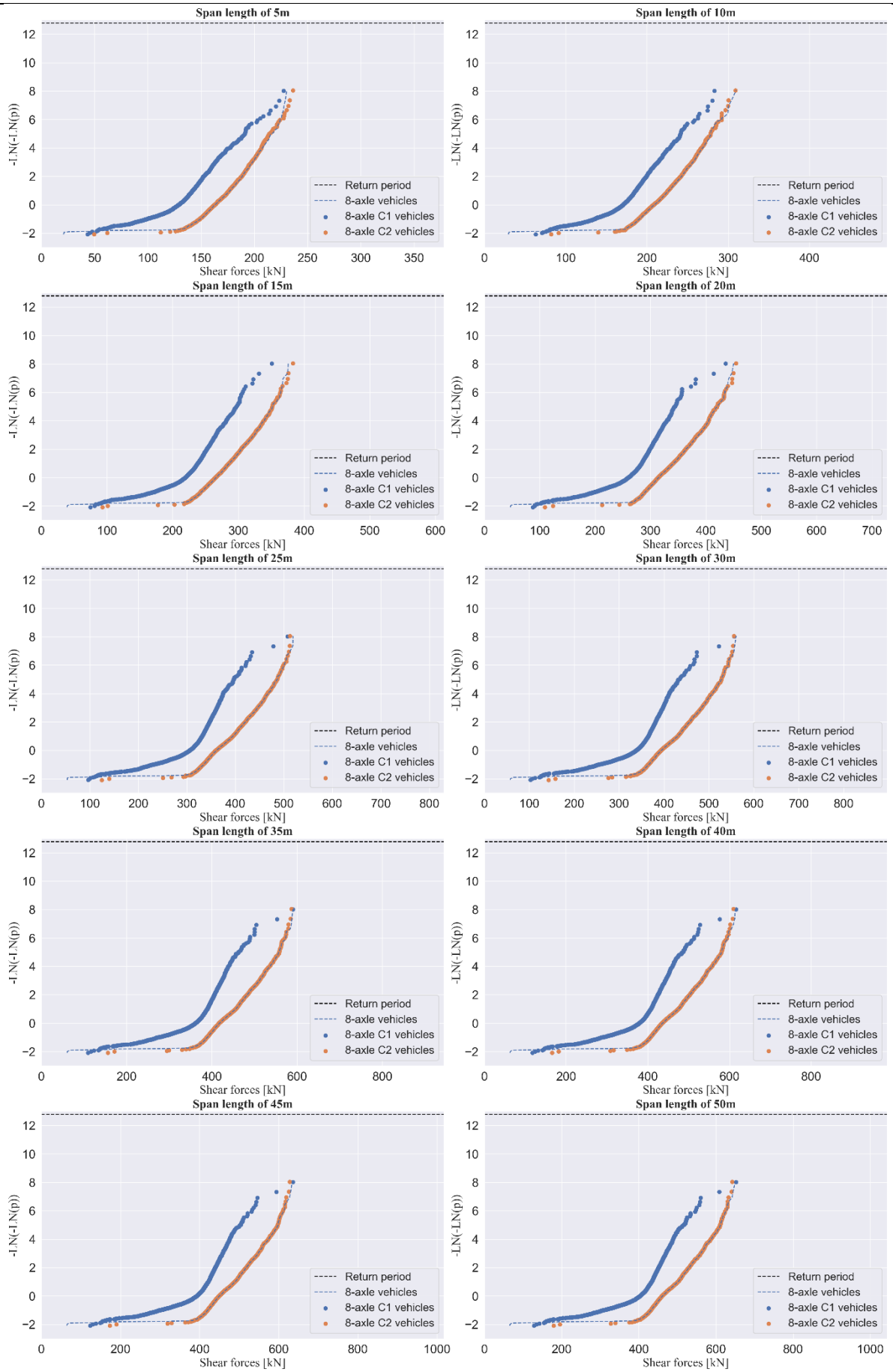

Figure F.12 Shear forces GPP comparison for the sub-categories of 8- axle vehicles